Sustained-Release Implants for Intraperitoneal Cisplatin Delivery

by
Aikaterini Mantzavinou

B.S. in Engineering Sciences
Harvard College, 2012

Submitted to the Harvard-MIT Program in Health Sciences and Technology in partial fulfillment of the requirements for the degree of

Doctorate of Philosophy in Medical Engineering
at the
MASSACHUSETTS INSTITUTE OF TECHNOLOGY

August 2018

Signature redacted

Signature of Author: _____
Harvard-MIT Program in Health Sciences and Technology
August 31, 2018

Signature redacted

Certified by: _____
Michael J. Cima, PhD
David H. Koch Professor of Engineering
Thesis Supervisor

Signature redacted

Accepted by: _____
Emery N. Brown, MD, PhD
Director, Harvard-MIT Program in Health Sciences and Technology
Professor of Computational Neuroscience and Health Sciences and Technology

THIS PAGE INTENTIONALLY LEFT BLANK

Sustained-Release Implants for Intraperitoneal Cisplatin Delivery

by

Aikaterini Mantzavinou

Submitted to the Harvard-MIT Program in Health Sciences and Technology
on August 31, 2018 in partial fulfillment of the requirements for the degree of
Doctorate of Philosophy in Medical Engineering

Abstract

The objective of this work was to develop materials for continuous low-dose delivery of cisplatin directly into the abdomen, also known as intraperitoneal (IP) chemotherapy. IP chemotherapy can help treat peritoneal metastasis in many advanced gynecologic and gastrointestinal cancers and has shown particular promise in treating advanced ovarian cancer. It is however tremendously underutilized because it requires a lot of resources and the current technology and maximum tolerated dose regimen cause complications and severe toxicity to patients.

We previously showed that continuous low-dose IP cisplatin delivery via an implanted diffusion-based reservoir device can be as effective as and less toxic than intermittent maximum tolerated dose IP injections. To translate this work to a clinically relevant implantable system, we developed composite materials that can deliver cisplatin at a continuous low dose that is tunable. The materials were mechanically well suited for placement in the abdomen and were evaluated for *in vitro* bioactivity, *in vivo* tolerability and *in vivo* ability to deliver platinum to key abdominal organs with promising results. Dosing studies with different material dimensions helped identify a dose to pilot treatment of ovarian cancer in human xenograft-bearing mice.

The implications of more accessible and affordable IP chemotherapy are especially important in countries with limited resources. Design reviews and a clinician survey in India reveal eagerness for early adoption of new technologies and dosing regimens to treat peritoneal metastasis and show promise for utilization of our implant in the developing world.

The work described in this thesis carries implications for the treatment of advanced ovarian cancer and peritoneal metastasis of other tumors affecting millions of patients worldwide and may help with the management of nonmalignant conditions with abdominal involvement.

Thesis Supervisor: Michael J. Cima, PhD
Title: David H. Koch Professor of Engineering

Acknowledgments

I would like to thank my advisor, Michael Cima, for giving me the opportunity to work in his lab the past five and a half years. Michael, thank you for trusting me to explore new ideas and directions in this project and for enabling me to join the community of Tata Fellows my last two years at MIT. Your guidance and mentorship were invaluable. Thank you also for your annual invitation to your gorgeous summer home in Maine.

I would like to thank my thesis committee chair, Jeff Karp, for his continuous enthusiasm and thoughtful insights that helped guide my research. Jeff, thank you for caring for my professional growth beyond the PhD and generously offering your advice and support. I would also like to thank my thesis reader, Marcela del Carmen, for lending her medical expertise and invaluable suggestions to this project from its early days before my time at MIT. Marcela, your dedication to helping your patients gave me inspiration and motivation to carry out this work.

I am grateful to my collaborators on this project at MIT, MGH and the Tata Memorial Cancer Center. Maple and Laura, thank you for everything you taught me. Kriti, thank you for your help and friendship the last two years – I am excited to see you continue this work! Lorenzo, Dr. Na, Giulia and Dr. Birrer, thank you for working with us on this project from across the river. Dr. Saklani, Dr. deSouza and Dr. Pramesh, thank you for welcoming me to Tata Memorial, introducing me to cancer care in India and helping me gain critical insights into ways that I can help with this technology.

Thank you to my lab mates for many thoughtful conversations and great laughs all these years. Special thanks to Alex, Brian, Greg and Max for their help with this project. Lenny, Barbara and Wendy, thank you for making sure the lab ran smoothly.

I had the privilege to receive a tremendous amount of advice and support throughout my years at MIT from many extremely talented and bright people. I would especially like to thank Tim O'Shea, Hok Hei Tam, Sid Jhunjhunwala, Owen Fenton, Suman Bose and Josh Doloff for their help and mentorship. I am thankful to Anne Deconinck, Tyler Jacks, Rob Stoner and Diane Rigos for their unwavering support. I feel privileged to have been able to work at the outstanding Koch Institute facilities and especially thank MIT DCM and the Histology Core for their expertise.

I am fortunate to have built a fantastic group of friends while at MIT. They provided me with the strength, happiness and drive necessary to get through the highs and lows of the past six years. Lina, Bryan, Santi, Carolin, Or, Sidney, Michela, Monica and Adrian: thank you for everything you have done to support me all these years. To the MEMP 2012 class: thank you for embarking on this unforgettable journey with me.

I am grateful to all my longtime friends from my years in Boston for their encouragement and love even when we were thousands of miles and many hours apart. Special shout-out to Sam, Zeina, Jovi, Colin, Sarah, Patty, Sri, Shawn, Mario and Kuong – thank you for cheering me on all this time.

I owe everything I have accomplished to my family. To my parents, thank you for empowering me to be the best I can and for sacrificing so much to give me all the opportunities in the world. To my brother, thank you for being my biggest champion and for always being there. I feel blessed to have a family like ours and love you all dearly.

To my life companion, Rajarshi: thank you for being my rock and urging me to aim higher and push harder. You make me a better person every day and I can't wait to see what awaits us next!

CONTENTS

List of Figures

List of Tables

List of Abbreviations

ANOVA	Analysis Of Variance
AUC	Area Under the Concentration-Time Curve
BLI	Bioluminescence Imaging
CBC	Complete Blood Count
CDDP	Cis-diamminedichloridoplatinum (cisplatin)
DDTC	Diethyldithiocarbamate trihydrate
D_H	Device High Dose
D_L	Device Low Dose
EDS	Energy Dispersive Spectroscopy
FBS	Fetal Bovine Serum
GOG	Gynecologic Oncology Group
H&E	Hematoxylin & Eosin
HIPEC	High-Temperature Intraperitoneal Chemotherapy
HPLC	High Performance Liquid Chromatography
ICP-MS	Inductively-Coupled Mass Spectrometry
IP	Intraperitoneal
IV	Intravenous
LAC	Lactose
LMICs	Low- and Middle-Income Countries
LY	Lymphocytes
MIT	Massachusetts Institute of Technology
MTD	Maximum Tolerated Dose
NE	Neutrophils
OS	Overall Survival
PBS	Phosphate-Buffered Saline
PCR	Polymerase Chain Reaction
PFS	Progression-Free Survival
PIPAC	Pressurized Intraperitoneal Aerosol Chemotherapy
PLT	Platelets
Pt	Platinum
RBC	Red Blood Cells
RPMI	Roswell Park Memorial Institute
SEM	Scanning Electron Microscopy
WBC	White Blood Cells

Chapter 1: Background

1.1 Intraperitoneal Drug Delivery

1.1.1 Background and Rationale

Intraperitoneal (IP) drug delivery is the administration of drugs directly into the peritoneal cavity. The peritoneal cavity is a potential space defined by the peritoneum – a serous membrane that surrounds the abdominal organs – that has been used widely for metabolite removal and drug administration because of its large surface area (~2 m^2 in adult humans) and the extensive blood flow through the tissues around it.[1,2] The peritoneal cavity of healthy individuals contains between 5 – 20 mL of serous exudate, which can reach up to 200 mL in women at different phases of the menstrual cycle.[3,4] Certain pathologic conditions may lead to excessive accumulation of peritoneal fluid, called ascites.

The peritoneal cavity is a frequent site of localized disease, is in intimate contact with many important abdominal organs and is an anatomically privileged compartment because the peritoneal–plasma barrier doesn't allow intracavitary partitioning of systemically administered drugs.[2] Solutes introduced intraperitoneally are metabolized in the cavity or leave it either via the lymphatics by bulk flow or via the tissue by convection and diffusion (Figure 1.1).[5] Solutes that leave the cavity via the visceral peritoneum that drains in the portal circulation may be inactivated by first-pass liver metabolism. This reduces systemic drug exposure while maximizing therapeutic advantage to treat localized disease. Solutes that reach the capillaries in the interstitium surrounding and supporting the peritoneum may enter the general circulation via

exchange with the plasma. The major resistances to transport are the capillary endothelium and cell-matrix system around the capillaries.[6] Water and low molecular weight solutes are absorbed mainly via diffusion from the peritoneum with convection becoming increasingly important as the solute molecular weight increases. Lymphatic flow is negligible for small molecules.[7] High molecular weight solutes are removed primarily via lymphatic drainage.[7]

IP drug delivery has been used to treat both localized and systemic diseases. Insulin is added to the dialysate of diabetic patients who undergo peritoneal dialysis while continuous IP insulin infusion has been found to be superior to subcutaneous insulin therapy in type 1 diabetes mellitus.[8,9] IP administration of antibiotics to combat dialysis–related peritonitis and IP chemotherapy to palliate malignant ascites are two of the earliest applications of IP therapy against regional disease.[10,11] IP drug delivery to treat peritoneal tumors received renewed interest in 1978 after Dedrick et al. published a paper presenting a pharmacokinetic rationale for the regional treatment of peritoneally metastasized ovarian cancer.[10,12]

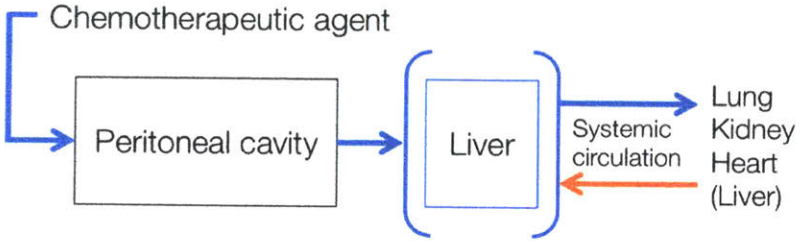

Figure 1.1: Pharmacologic rationale of IP chemotherapy administration. Adapted with permission.[12]

1.1.2 Intraperitoneal Chemotherapy for Ovarian Cancer Treatment

Peritoneal metastasis is the spread of cancer to the peritoneal cavity and can affect patients who suffer from cancers primarily of the abdomen and pelvis (e.g. ovarian, gastrointestinal) but also cancers of the breast, skin or lung.[13] Peritoneal metastasis seeds the cavity with tumors and fills it with malignant fluid called ascites (Figure 1.2). The prognosis of patients with peritoneal metastasis is very grim as it is usually a sign of terminal disease.

IP delivery of chemotherapy improves treatment outcome for patients with peritoneal metastasis and has found particular application in the management of ovarian cancer. Ovarian cancer is the main cause of gynecologic cancer death in the developed world.[14] The disease will affect an estimated 22,240 women and kill 14,070 women in the US in 2018.[15] Patients face an average five-year survival of 47.4% but survival statistics are a lot better when the disease is diagnosed early (stage I-II).[15] Only about 35% of ovarian cancer patients are however diagnosed at an early stage.[15] Advanced-stage ovarian cancer patients face a five-year relative survival lower than 30%.[16] IP treatment with platinum agents has been the single biggest breakthrough for more than 20 years.[10,12,17]

The superiority of ovarian cancer treatment with IP chemotherapy compared to intravenous (IV) chemotherapy alone has been demonstrated both in clinical trials (improving overall survival by 16 months)[18] and in clinical practice (improving 3-year survival by 10%).[19] This led the National Cancer Institute to make a clinical announcement in 2006 supporting IP chemotherapy to treat advanced ovarian cancer. More than a decade later, academic and media publications have repeatedly highlighted

extremely poor adoption statistics for IP chemotherapy against ovarian cancer despite evidence supporting its use.[19-22]

Adoption barriers facing IP chemotherapy stem primarily from the way that it is administered. The patient receives six cycles of high-dose chemotherapy infusions spaced three weeks apart to allow recovery from drug toxicity. The drug is dissolved in 2 L of saline and administered through an indwelling catheter that is connected to a port implanted on the patient's abdominal wall. More than 50% of ovarian cancer patients in clinical trials and 20% of ovarian cancer patients in clinical care discontinue IP therapy before completing all six cycles.[18,19] These patients drop out primarily because of toxicity from the high-dose infusions and complications from the catheter and port (infections, blockages, leaks among others).[18,19] IP chemotherapy is extremely underused as a result, despite its demonstrated advantage in clinical trials and in the clinic (Figure 1.3A). It was given to fewer than half of eligible ovarian cancer patients treated across six National Comprehensive Cancer Network centers from 2003 to 2012 (Figure 1.3B).[19] Adoption variability ranged from 4% to 67% of eligible patients between these centers.[19] Adoption statistics are expected to be worse in non-elite cancer centers. Most ovarian cancer patients receive care at such non-specialized facilities, and therefore lack access to IP chemotherapy even though they could benefit from it. Adoption statistics are also bound to be worse for cancers that have shown a smaller advantage with IP chemotherapy making it even less appealing as a treatment option given the toxicities and complications associated with its administration.

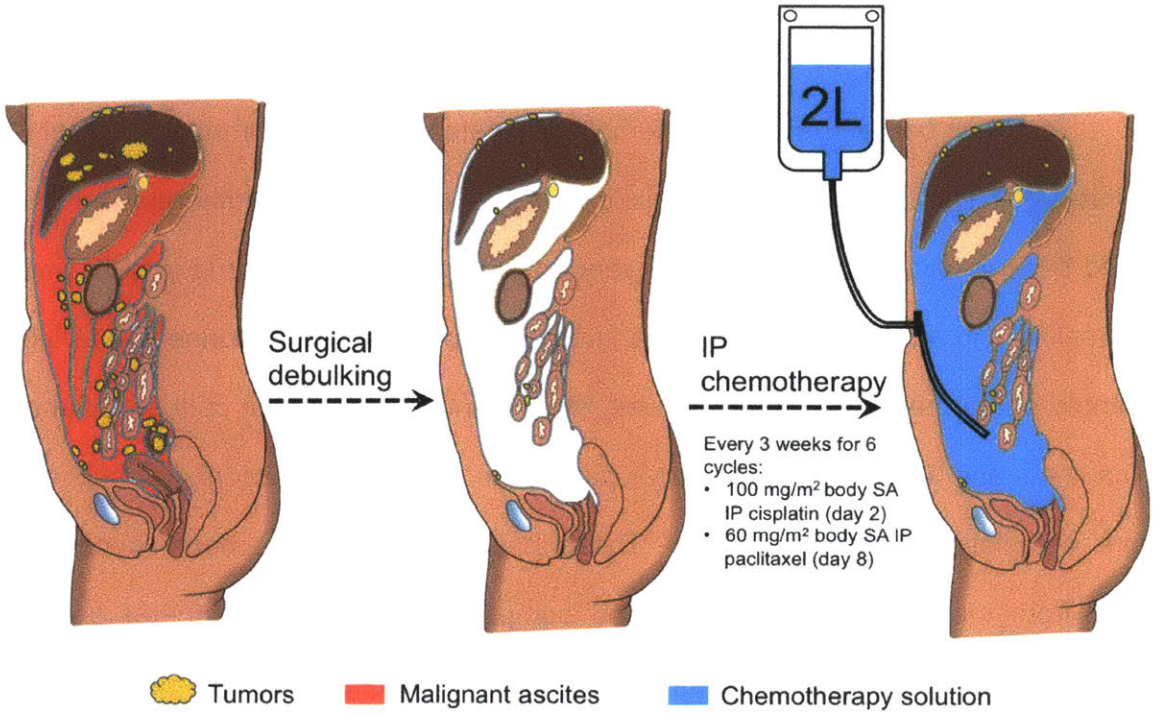

Figure 1.2: IP chemotherapy treatment regimen. The patient undergoes tumor debulking surgery to remove as much of the tumor burden as possible that commonly also removes the omentum, the ovaries and uterus, parts of the bowels and other affected organs that can be safely removed. A peritoneal catheter and port are also placed in the patient's abdomen to allow future access of the peritoneal cavity for IP chemotherapy administration. Surgery is followed by a break to allow the patient to recover and then six cycles of IP chemotherapy usually comprising a platinum and a taxane agent. The regimen shown here is the recommended dosing regimen following the Gynecologic Oncology Group (GOG) clinical trial 172. Modified dosing is frequently used to tailor the treatment to the patient's health status or when given in clinical trials evaluating dosing to maximize treatment while reducing toxicity. The chemotherapy is given as a two-liter infusion over the course of multiple hours and the patient is asked to change positions and rotate frequently to better distribute the drug solution. This regimen leads to many debilitating side effects including catheter and port infections, blockages or leaks, nausea and vomiting, tissue perforation and bowel obstruction.[11,23-25]

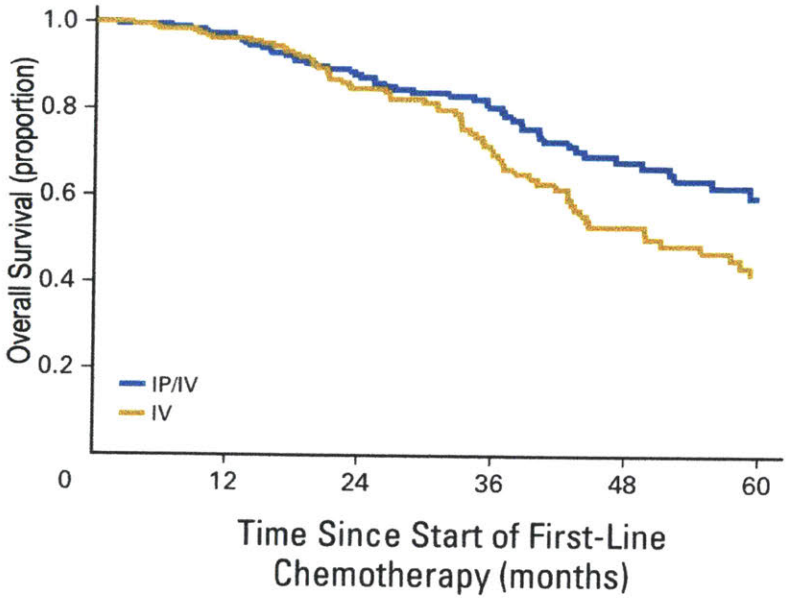

A

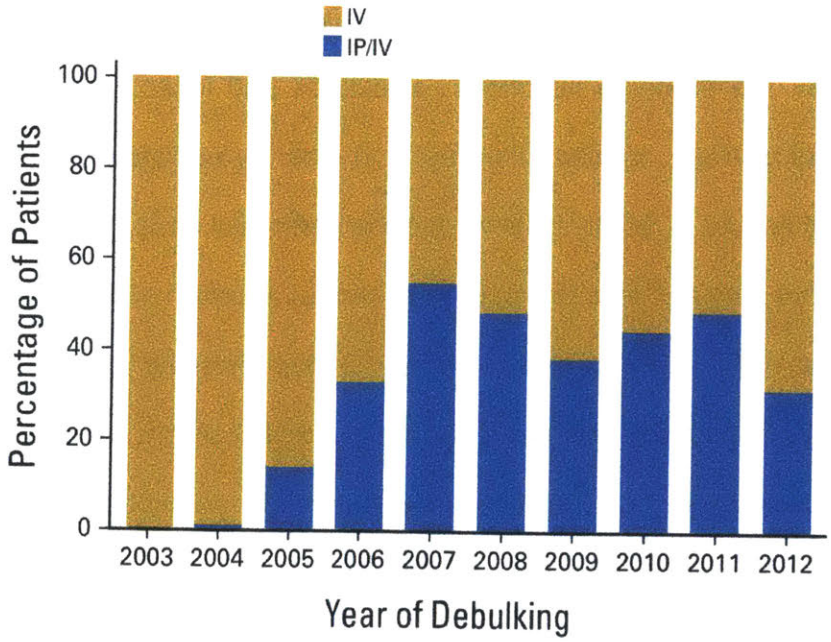

B

Figure 1.3: Use and outcomes of IP chemotherapy against ovarian cancer in the clinic. (A) Overall patient survival for ovarian cancer patients treated with a combination of IP and IV chemotherapy (blue line) or IV chemotherapy alone (yellow line) in six national cancer hospitals between 2003 and 2012. (B) Percentage of eligible ovarian cancer patients receiving combination IP/IV chemotherapy (blue) vs. IV chemotherapy alone (yellow) in the same hospitals between 2003 and 2012. Adapted with permission.[19]

1.1.3 Existing Tools and Other Solutions for Sustained IP Chemotherapy

The first peritoneal access systems were devices such as rubber catheters and sump drains that were borrowed from other fields like general surgery to use in peritoneal dialysis.[26] Serious complications resulting from those borrowed access systems and a growing interest in peritoneal dialysis led to the development of dedicated access tools, which improved patient outcomes and increased adoption of peritoneal dialysis.[27,28] Drug delivery to the peritoneal cavity has been employed for centuries but there exist no peritoneal access tools specifically designed for the purpose of IP drug administration, which is instead carried out using devices borrowed from peritoneal dialysis. The catheter and port used for IP chemotherapy require specially trained nursing staff for infusions.[29] They are prone to infections, blockages and leaks.[29] Every infusion can cause respiratory distress, nausea, diarrhea, and other immediate side effects because of the mutliliter fluid that is rapidly instilled into the peritoneal cavity.[29] The tools currently available therefore play a critical role in limiting clinical adoption of IP chemotherapy.

Sustained exposure to chemotherapy is hypothesized to improve antitumor efficacy by limiting treatment-free periods during which resistant tumor cells are given the opportunity to multiply.[30,31] There have been previous attempts to achieve localized and sustained chemotherapy delivery to the peritoneal cavity but they face several challenges related to the control of their drug release profile and the safety of their use in patients. The most notable examples are polymeric nanoparticles and microparticles as well as injectable gels and films that are placed at the desired site and release the contained drug over a period of time.[32-39] These modalities rely on bulk degradation to release drug and can therefore achieve only short-lasting, non-linear release.[40,41] They

also lose their mechanical integrity as they degrade, which would compromise the surgeon's ability to revise or remove them safely. Particles for targeted drug delivery face the additional challenge of achieving adequate concentrations near the site of disease often requiring local administration.[42] Nanoparticles are rapidly cleared from the peritoneal cavity via the lymphatics and so require frequent readministration.[39,43] Microparticles have longer retention times but suffer from documented material-associated toxicities.[35,39,43] Gels and films developed in the literature to date would scale up to dimensions that would be unrealistic for implantation in human patients in order to carry the required drug payload and often exhibit material properties like increased viscosity that make them untenable for injection.[31,37,44-46] Many of the existing studies of sustained-release IP chemotherapy systems have additionally limited the duration of treatment to 3 weeks or less making their findings less clinically relevant in comparison to the 18-week duration of the current IP chemotherapy standard of care.[45,46]

1.1.4 Proposed Solution

Nondegradable diffusion-based reservoir devices for controlled zero-order cisplatin release were previously created in our lab and used for continuous low-dose IP delivery of cisplatin in mouse models of ovarian cancer over a period of six weeks. The antitumor efficacy of the devices was comparable to that of periodic high-dose IP injections of cisplatin while toxicity was reduced.[45] Continuous chemotherapy is additionally thought to reduce the incidence of drug-resistant cancer clones by preventing their proliferation during treatment-free periods.[47]

The goal of this thesis was to translate these mouse findings to an implant for continuous low-dose IP cisplatin delivery in humans that is relevant to the clinical setting in specialized cancer centers as well as more resource-constrained facilities. The proposed solution is based on a composite nonresorbable material that can accomplish continuous low-dose cisplatin delivery to the peritoneal cavity while mechanically matching the properties of the surrounding tissues and maximizing the surface area for drug release to treat microscopic metastases left behind after surgical debulking. Solid drug is incorporated into the composite matrix without undergoing dissolution to maximize the payload while minimizing implant dimensions. A sacrificial excipient is added with the aim to create interconnected paths within the composite cross-section and so enable removal of the incorporated drug. The composite material is envisioned to form the basis for deployable thin sheets designed for IP placement by minimally invasive laparoscopy. The design of these deployable implants draws inspiration from origami tessellations (e.g. v-pleats, Miura ori) to create a drug-eluting collapsible sheet that can be placed and removed using laparoscopic tools. The sustained low-dose delivery of cisplatin from the implant is expected to maximize patient tolerability of the full course of IP chemotherapy due to the reduced morbidity expected from this dosing regimen and from eliminating catheter-and-port complications. The number of hospital visits required for treatment will be reduced to just two with no need for periodic infusions while full control of treatment will be given to clinicians in the operating room making the implant an attractive solution for resource-constrained settings. The clinical significance of the proposed solution may extend to treatment of peritoneal metastasis

of other cancers and even to peritoneal drug delivery for treatment of non-malignant conditions.

1.1.5 Selection of Intraperitoneal Chemotherapy Agent for Ovarian Cancer Treatment

The pharmacologic rationale behind IP drug administration is based on both drug uptake by the systemic circulation and drug intracavitary localization to achieve therapeutic concentrations at the site of regional disease. The antitumor effectiveness of IP chemotherapy to treat ovarian cancer is driven by: (1) the activity of the drug against ovarian cancer; (2) direct drug penetration into peritoneal tumors via the tumor surface; and (3) diffusion into the inner core of vascularized tumors as well as treatment of any distant metastases by entering the systemic circulation.[23] Drug absorption from the peritoneal cavity is faster with increasing lipophilicity while increasing molecular weight leads to intracavitary sequestration.[7,48] Drug inactivation by first-pass liver metabolism if absorbed into the systemic circulation via the visceral peritoneum may be problematic for treating distant metastases and for diffusing into the inner tumor core but beneficial for reducing systemic side effects. Drugs that are vesicants or major irritants when administered intraperitoneally can cause peritoneal inflammation with significant pain and adhesion formation that may affect intracavitary drug distribution and lead to more serious toxicity like bowel obstruction.[49] The ideal agent for IP chemotherapy has thus been described as one that: (1) is not toxic to the peritoneal lining; (2) has documented and concentration-dependent activity against the targeted malignancy; (3) is highly effective systemically against the malignancy; (4) can penetrate deep into the tumor;

and (5) is removed slowly from the peritoneal cavity but rapidly from the systemic circulation to maximize the IP pharmacologic advantage.[12,23,49]

High peritoneal-to-plasma concentration ratios can be achieved for many commonly used chemotherapeutics with IP administration. Table 1.1 summarizes the chemical properties and pharmacokinetic advantage of IP administration of commonly used chemotherapeutic agents. Selection of the drug to be incorporated into the composite matrix must take into account barriers to adoption of the proposed implant along with chances of success of the proposed dosing mechanism and regimen. The only agents currently approved for IP administration are cisplatin and paclitaxel.[46] Platinum chemotherapy is a cornerstone in ovarian cancer treatment and is one of the most extensively studied types of chemotherapy for IP administration. The platinum agents cisplatin and carboplatin both achieve a comparable pharmacokinetic advantage of 10-20-fold when given intraperitoneally but the bulk of data in support of superior treatment efficacy has come from trials using IP cisplatin.[50,51] An early study of IP carboplatin vs. IP cisplatin in rats by Los et al. found that the former required administration of a 6-10 – fold higher concentration than the latter to achieve comparable levels within peritoneal tumors.[52] Markman et al. then looked retrospectively at the response rate of patients with small-volume residual ovarian cancer treated on salvage cisplatin- or carboplatin-based IP chemotherapy regimens. They found that patients with microscopic residual tumors had an identical surgically documented complete response rate regardless of drug. Patients with small-volume residual macroscopic tumors (≤ 0.5 cm) in contrast responded significantly better to IP cisplatin (41% and 71% complete and overall response rate respectively) than to IP carboplatin

(11% and 32% complete and overall response rate respectively).[53] It has been pointed out however that the dose Markman and coauthors looked at may have been too low since they assumed dose equivalency between carboplatin and cisplatin that may have been erroneous, while the accuracy of the peritoneal tumor penetration in rats reported by Los et al. has been questioned and has not been replicated successfully.[49,51] It is also important to note that carboplatin has been found to cause less toxicity and side effects both via the IV and the IP route and the availability of encouraging clinical trial data for IP carboplatin has been increasing making it a promising candidate for future work in this project. Paclitaxel has a tremendous pharmacokinetic advantage of 1000-fold when given intraperitoneally but is water-insoluble requiring special formulations for IP administration and suffers from dose-limiting local side effects like abdominal pain that necessitate reduced systemic exposure compared to IV administration.[12]

Cisplatin was the chemotherapeutic agent previously used in our lab to demonstrate the viability of sustained low-dose IP chemotherapy as a treatment regimen in mouse ovarian cancer models. These previous data along with the extensive body of findings in support of IP cisplatin administration for ovarian cancer treatment and the fact that cisplatin has been approved for IP delivery make this drug an appropriate first choice for development of the proposed chemotherapy-eluting material for an IP implant. The implant is however intended to function as a platform that can be modified to release other chemotherapeutic agents as well. Table 1.1 illustrates that, beyond the potential of carboplatin for continuous low-dose IP delivery, the peritoneal-to-plasma concentration ratios for other common chemotherapeutics are even more striking than those for platinum agents suggesting an even greater potential

pharmacokinetic advantage. Some of these agents suffer from significant and obvious drawbacks making them less attractive for incorporation into the implant described in this thesis while others seem to hold promise for future studies expanding this work.

Agent	Molecular weight	Log P (T 25°C)	Water solubility	Peritoneal cavity / plasma drug level ratio	
				Peak	AUC
Cisplatin	300.05	-2.27	+	20	12
Carboplatin	371.25	-1.89 ± 0.41	+	24	10-18
Gemcitabine	263.20	-2.216 ± 0.487	+		759
Topotecan	421.45	0.318 ± 1.142	+		54
Mitomycin	334.33	-0.298 ± 0.542	±	71	-
Doxorubicin	543.53	0.239 ± 1.028	±	474	-
5-fluorouracil	130.08	-0.649 ± 0.237	±	298	367
Paclitaxel	853.92	3.950 ± 0.808	-	-	1000
Mitoxantrone	517.40	1.548 ± 1.475	-	-	1400
Melphalan	305.20	0.536 ± 0.428	-	93	65
Methotrexate	454.44	-0.446 ± 0.869	-	92	100
Docetaxel	807.88	2.456 ± 0.657	-		181

Table 1.1: Chemical properties and pharmacokinetic advantage of chemotherapeutic agents when delivered intraperitoneally. AUC = area under the concentration-time curve. Partition coefficient log P values are obtained using SciFinder. Water solubility indices and peritoneal cavity / plasma drug level ratios are adapted from Fujiwara et al. (2007).[23]

Doxorubicin, 5-fluorouracil, mitoxantrone, methotrexate and docetaxel are less attractive candidates for expansion of this work. Doxorubicin has showed limited penetration into the outermost four to six cell layers of peritoneal tumors in mice as well as into multicellular tumor spheroids *in vitro*.[23] Methotrexate similarly suffers from limited penetration into avascular tumors.[23] 5-fluorouracil has shown more promising data regarding penetration into tumor nodules but commonly causes chemical peritonitis.[54] Mitoxantrone has been reported to suffer from dose-limiting local toxicities similar to those seen with doxorubicin and paclitaxel while docetaxel has been found to cause gastrointestinal toxicity following IP administration.[55]

Gemcitabine, topotecan or perhaps even mitomycin may warrant further exploration to make the implant a platform for IP chemotherapy delivery. Gemcitabine demonstrated an impressive peritoneal/plasma AUC ratio of 759 in phase 1/2 studies and has a high total body clearance and little evidence of local toxicity in animals.[56,57] IP gemcitabine has already been used with success against peritoneal metastasis primarily of pancreatic and ovarian cancers although some have reported significant local toxicities including peritoneal irritation and adhesions in patients.[57-60] Topotecan is also an interesting candidate that has already been deemed tolerable for IP administration in ovarian cancer patients and tested as consolidation IP chemotherapy in phase 2 trials in ovarian and primary peritoneal cancer with good results.[61-63] A 2015 paper by Previs et al. highlighted promising preclinical findings of dual metronomic chemotherapy with IP nab-paclitaxel every other day and daily oral topotecan against ovarian cancer in mice.[64] Mitomycin is the most extensively used drug in the clinic as hyperthermic IP chemotherapy (HIPEC) to treat peritoneal spread of colorectal, appendiceal, ovarian and gastric cancer as well diffuse malignant peritoneal mesothelioma with good results but no data on its use as postoperative catheter-based IP chemotherapy without hyperthermia were found in the literature to-date.[65,66]

The choice of cisplatin as the first agent used in developing the sustained-release implants in this thesis is warranted given the body of findings in support of IP cisplatin to treat ovarian cancer both in the literature and in our lab. The future of this project however will likely involve exploration of other chemotherapeutic agents either as monotherapy or as combination therapy to maximize the anticancer efficacy of this IP treatment regimen.

1.2 Effect of Tumor Size on IP Chemotherapy Outcome*

1.2.1 Clinical Evidence

The majority of ovarian cancer patients are diagnosed with tumors spread throughout the peritoneal cavity. Debulking surgery to remove as many of these tumors as possible followed by chemotherapy is the clinical standard of treatment and a critical step to lengthen patient survival. The Gynecologic Oncology Group (GOG) has recommended that optimal debulking surgery translate to no residual tumors greater than 1 cm in size. There is however ongoing debate over the size of residual tumors required for good prognosis with suggested sizes ranging from 0.1 – 1.5 cm.[67,68] Skilled surgeons that can perform optimal debulking surgery can drastically improve patient survival but less than half of ovarian cancer patients have access to such care.[69] Microscopic residual tumors have regardless overall been shown to result in the best long-term treatment outcomes especially for patients receiving IP chemotherapy.[67,68,70]

The outcome of debulking surgery may have played a critical role in the most recent GOG 252 phase 3 clinical trial comparing IP and IV platinum chemotherapy. The trial released preliminary results in 2016 that have thrown the ovarian cancer community into renewed disagreement regarding the benefits of IP therapy. The GOG 252 preliminary results revealed no significant difference in progression-free survival (PFS) among patients receiving IV or IP chemotherapy and no significant increase in PFS in women with microscopic residual tumors.[71-73] Previous phase 3 GOG trials including GOG 172, GOG 114 and GOG 104 had found that IP chemotherapy led to longer PFS

---

* Parts of this chapter were reproduced or adapted from Tanenbaum and Mantzavinou et al. (2017).[7]

and overall survival (OS) when given to women with no visible residual tumors compared to women with visible residual tumors < 1 cm who received IP chemotherapy or to women who received IV chemotherapy.[18,70,74,75] The GOG 252 trial was intended to resolve the IP/IV debate by recruiting a larger number of patients and evaluating a lower IP cisplatin dose (75 mg/m^2 of patient surface area compared to the 100 mg/m^2 of patient surface area used in GOG 172). The GOG 252 trial also added bevacizumab 15 mg/kg IV to all treatment arms. It is these design parameters precisely that may ultimately have played a confounding role in its findings. [18,71,76] GOG 252 recruited 1560 patients from 500 sites compared to 415 eligible patients from 40 sites included in the GOG 172 analysis. Variability in subjective surgeon-reported debulking outcomes is bound to be greater with an order of magnitude more centers included in the GOG 252 trial compared to the GOG 172.[46] This variability makes it hard to determine with certainty the cases where optimal cytoreduction was actually achieved.[46,77] The trial authors themselves pointed out the importance of IP cisplatin dose reduction in interpreting the GOG 252 results.[78] The addition of bevacizumab modifying the overall treatment regimen is also regarded as a major confounding factor in the GOG 252 trial.[72] A more complete assessment of GOG 252 will have to wait for OS data that will become available in a few years but these confounding factors must be taken into consideration when attempting to interpret the GOG 252 findings to date.

1.2.2 Experimental Findings and Mechanism of Tumor Size-Dependent Response

Experimental findings in animal models of human ovarian cancer similarly support the notion that microscopic residual disease leads to better treatment outcomes. Jandial et

al. used mice with peritoneal tumor xenografts to show that platinum levels following IP cisplatin administration decrease significantly with increasing tumor size.[79] Helland et al. demonstrated that mice receiving debulking surgery followed by IP carboplatin/paclitaxel chemotherapy had longer average survival than those treated with either debulking surgery or chemotherapy alone.[80]

We were previously able to match the efficacy of high-dose weekly IP cisplatin injections in mice with human ovarian cancer xenografts using peritoneally implanted reservoir devices to continuously deliver low doses of cisplatin.[81] These devices caused lower toxicity than the injections but an average of 4.7 X more total cisplatin was needed to match the injection efficacy. There was no attempt to control the size of tumors in the mice before the start of treatment and it is very likely that multiple animals had tumors > 1 cm in their abdomen at the start of chemotherapy. This tumor size consideration may help explain the need for an increased total amount of cisplatin in the device treatment arm by looking at the mechanism of tumor kill by locally administered cisplatin.

Local exposure of tumors to intraperitoneally given chemotherapy aims to take advantage of direct chemotherapy penetration into the tumor. Penetration is affected by diffusion down the drug concentration gradient and by convection driven by fluid flow from vessels to the surrounding tissue and balanced by drainage into lymphatics.[82] Convection controls macromolecule transport as it affects fluid flow from blood vessels into the interstitium but transport of small molecules like cisplatin is primarily controlled by diffusion into tissue.[82] Diffusion depends on drug partitioning, drug diffusivity in the tissue and the diffusion length scale.[83] Cisplatin is a small molecule for which direct

diffusion into tumors appears to be limited to the outer 1.5 – 3 mm of the tumor.[5,84] This limitation of cisplatin diffusion may be improved by sustained exposure of tumors to cisplatin. The continuous presence of active cisplatin around a tumor may allow killing of each successive outer tumor cell layer and so enable the chemotherapy to reach deeper into the tumor.[84] This may however only be true up to a certain tumor size. Taking into account cisplatin toxicity the cisplatin concentration that can be safely maintained around tumors in a sustained-dosing regimen is necessarily going to be lower than that accomplished immediately after intermittent IP cisplatin administrations with breaks for recovery. This reduced concentration gradient between the peritoneal fluid and the tumor center may carry efficacy implications for larger tumors despite the fact that sustained exposure may allow layer-by-layer tumor cell kill.

Multicellular ovarian cancer aggregates called spheroids were used in *in vitro* studies in this project to help understand any relationship between tumor diameter and the efficacy of sustained low-dose cisplatin. The choice of spheroids for these studies was made on the basis of their relevance to both ovarian cancer metastatic potential and its response to treatment. Multicellular aggregates similar to spheroids are shed from the primary tumor in ovarian cancer patients and are carried by peritoneal fluid flow around the abdominal cavity seeding it with metastases.[85,86] These tumor spheroids are considered the greatest obstacle to effectively treating late-stage epithelial ovarian cancer.[86,87] The seeding process requires remodeling of surface proteins (e.g. integrins, cadherins) that is not recapitulated in traditional two-dimensional cultures of metastatic ovarian cancer cells.[85,88] Cells grown as spheroids *in vitro* not only express similar surface proteins as metastatic nodules *in vivo* but also develop extracellular matrix and

upregulate ovarian cancer biomarkers not observed in two-dimensional monolayer culture.[82,88-90] Poor response of unresected tumors to chemotherapy is attributed to limited drug penetration into the tumors and the ability of cells at the tumor core to develop resistance.[87] Multiple studies have shown that both *in vitro* and *in vivo* ovarian cancer spheroids require higher chemotherapy doses than those same cells grown in a monolayer to accomplish a similar response.[85-87,89] Loessner *et al.* found that ovarian cancer cell spheroids exhibited a 50% greater survival compared to their monolayer counterpart when exposed to the same treatment regimen with paclitaxel.[88] These finding support the use of spheroids *in vitro* to better model the structure, biological markers and predicted *in vivo* treatment response of metastatic ovarian cancer and so reach conclusions that are more clinically relevant.[91,92]

1.2.3 Implications for Animal Model Appropriateness to Study Treatment Efficacy

The implications of tumor size for assessing drug penetration extend beyond *in vitro* models to affect the preclinical animal models of disease used to study the response of human ovarian cancer to various dosing agents and regimens. Preclinical drug screening in ovarian cancer is predominantly performed in immunocompromised mice with orthotopic human cancer xenografts, as those are most clinically relevant to study the chemosensitivity of new agents and replicate the early stages of tumor development.[80] The mice are inoculated with large numbers of cancer cells (order of magnitude of 10^6 – 10^7 cells/animal) that are free-floating in solution. Investigators usually wait for a sufficiently long period after cell inoculation before start of treatment.[38,80] Generation of mouse models with this technique in this project has resulted in diffuse and massive tumor nodules of irregular size throughout the peritoneal cavity. Helland et al. pointedly emphasized the obvious disconnect between such mouse models and the actual clinical presentation of debulked ovarian cancer patients before the start of adjuvant chemotherapy.[80]

Surgical debulking to leave minimal residual disease behind is one of the most critical components of ovarian cancer treatment. The benefit of IP chemotherapy has been demonstrated in patients after optimal debulking, and there is ongoing debate around (i) the benefit, if any, of IP chemotherapy in patients with larger residual disease and (ii) the impact of experience and performance in surgical debulking on the outcome of ovarian cancer treatment. It is difficult to rationalize dose-finding studies in mice with enormous tumors bearing no resemblance to residual disease in a debulked patient, especially when exploring low-dose therapy. Surgical debulking in mice has been

attempted but the procedure is highly invasive and very challenging for animal survival.[80] Laparoscopic debulking in mice is not possible due to size limitations and back-to-back larger incisions would result in confounding loss of many animals.

Creation of a novel xenograft mouse model inoculated with ovarian cancer cell spheroids of specific dimensions instead of free cells is likely to offer two benefits: (i) better control of tumor nodule size and spatial nodule distribution; and (ii) more accurate representation of the human disease by three-dimensional cell growth that mimics the tumor microenvironment and promotes peritoneal metastasis.[93] It remains to be understood whether tumor size affects chemosensitivity via drug transport through larger tumor nodules or via surface area-to-volume ratio for drug exposure. The *in vivo* spheroid model studies along with the *in vitro* spheroid cisplatin exposure studies described in this thesis may help shed light into this issue.

1.3 Application of This Technology to Cancer Care in Low- and Middle-Income Countries

The global cancer burden has shifted, and most new cancer cases and deaths now occur in low- and middle-income countries (LMICs).[94] Gynecologic and gastrointestinal cancers are two of the most prevalent cancer types in LMICs estimated to affect more than 2 million individuals and to kill more than 1 million patients every year.[95] The overall objective of this project is to develop implants for sustained delivery of IP chemotherapy to treat peritoneal metastasis of cancer. Peritoneal metastasis is a primary cause of morbidity and mortality in advanced-stage gynecologic and gastrointestinal cancers and approximately 60-80% of cancer patients present with advanced- or end-stage disease in LMICs.[96] The burden of disease of peritoneal metastasis in those countries is therefore high. Management of advanced cancer is largely unfeasible in the LMIC setting due to high cost, treatment unavailability, poor infrastructure, and personnel limitations.[96] Management of advanced gynecologic and gastrointestinal malignancies with peritoneal metastasis is even grimmer as it requires costly, technologically advanced or resource-heavy modalities such as surgical tumor removal and frequent rounds of radiation therapy or chemotherapy to kill the remaining cancer cells. IP chemotherapy has shown promise for better patient outcomes but has faced limited clinical adoption in high-income countries in large part driven by the complications and toxicities of the current infusion system and dosing regimen.[19] Adoption statistics are bound to be direr in non-elite cancer centers that are not well equipped to handle the resource- and expertise-intensive technology currently used for IP chemotherapy in the US and abroad.[20,21]

A collaboration with the MIT Tata Center for Technology and Design was established to explore the potential of bringing the sustained-release chemotherapy implants developed in this project to the Indian setting. Drugs such as platinum-based agents used in IP chemotherapy for peritoneal metastasis are on the WHO list of essential medicines and are currently off-patent, making them more available and affordable in LMICs.[96] Metronomic chemotherapy — chronic and frequent chemotherapy administration at low, minimally toxic doses with no prolonged drug-free breaks — has been championed as a cancer treatment strategy in resource-limited settings because of its low cost, ease of access, and potential for improved cancer control.[94,97] Informal interviews with physicians throughout India were conducted as preliminary research and revealed that catheter-based IP chemotherapy use, which never really took off in the first place, has now dropped to almost zero in specialized cancer centers. Indian physicians faced with the need to provide care to vast numbers of cancer patients flocking to central hospitals from across the country are instead performing high-temperature IP chemotherapy (HIPEC) and piloting pressurized IP aerosol chemotherapy (PIPAC) during debulking surgery in the operating room. HIPEC and PIPAC are getting embraced by Indian providers because they give them full control of the treatment in the operating room with no infusion system maintenance and no associated complications and have no loss to follow-up. The costs of HIPEC and PIPAC are tremendously high compared to catheter- based IP or systemic chemotherapy and very few patients are eligible to go through their extremely aggressive regimens. Chemotherapy rarely ends at the HIPEC or PIPAC stage and the patient will most likely require further treatment at a later point.

These considerations create a vacuum for care of patients with peritoneal metastasis that presents itself as a potential opportunity to affect the lives of millions of patients globally by using fully implantable sustained-release systems for localized chemotherapy. A clinician survey was distributed to centers across India using the Indian National Cancer Grid to collect information on the current state of peritoneal metastasis care in India, the use of surgical debulking, IP chemotherapy and metronomic dosing, and the potential for adoption of the sustained-release implants developed in this project by Indian physicians. The results show promise for use of this technology in resource-constrained settings to give physicians autonomy of treatment and help relieve the burden of follow-up care and of debilitating toxicity affecting patient livelihood particularly for cancer patients seeking care from remote regions of the country.

Chapter 2: Ovarian Cancer Treatment with an Intraperitoneally Implantable Cisplatin-Eluting Composite Material

2.1 Introduction

Ovarian cancer patients commonly present with peritoneal metastasis and can benefit from IP delivery of chemotherapy after optimal surgical debulking. IP chemotherapy is tremendously underused because it must be delivered as periodic high-dose infusions through a catheter, causing severe toxicity and catheter complications. A better way to perform IP chemotherapy is urgently needed. A supersoft silicone elastomer was impregnated with cisplatin and lactose as a sacrificial excipient at different proportions to create nonresorbable composite materials that mechanically match the properties of abdominal tissues. Cisplatin and lactose crystals were uniformly distributed throughout the composite materials and no crystal dissolution was apparent. Cisplatin was released from the materials *in vitro* at a sustained rate over a period greater than three months and following a triphasic linear release profile. A formulation was selected for further development based on its *in vitro* cisplatin release profile and the bioactivity of the released cisplatin against ovarian cancer cells was confirmed *in vitro*. The ability of material samples to deliver cisplatin throughout the abdomen after intraperitoneal implantation was confirmed *in vivo* in mice. Preliminary tolerability assessment of the material *in vivo* in mice showed promising results. These findings suggest that this cisplatin-eluting composite material is a good candidate to create implants for sustained, controlled IP chemotherapy delivery against ovarian cancer.

2.2 Materials and Methods

2.2.1 Chemicals and materials

Ecoflex 00-30 was purchased from Smooth-On Inc. (Macungie, PA, USA). Phosphate-buffered saline (PBS) was purchased from VWR (Radnor, PA, USA). Diethyldithiocarbamate trihydrate (DDTC), nickel (II) chloride, sodium hydroxide, high-performance liquid chromatography (HPLC)-grade water, HPLC-grade methanol, 70% nitric acid, cisplatin powder and lactose monohydrate powder were purchased from Sigma-Aldrich (St. Louis, MO, USA). Erbium 1,000 µg/mL standard solution was purchased from Agilent Technologies (Santa Clara, CA, USA). Platinum 1,000 µg/mL standard solution in nitric acid was purchased from Inorganic Ventures (Christiansburg, VA, USA). Roswell Park Memorial Institute (RPMI) 1640 medium, McCoy's 5A medium, 0.25% trypsin-EDTA, 100X penicillin-streptomycin-glutamine and fetal bovine serum (FBS) were purchased from Thermo Fisher Scientific (Waltham, MA, USA). MTT formazan powder was purchased from Santa Cruz Biotechnology (Dallas, TX, USA). Medical injection-grade cisplatin solution (100 mg/100 mL) for bolus injections was purchased from McKesson Medical-Surgical (Richmond, VA, USA).

2.2.2 Composite material fabrication

A matrix-type cisplatin-eluting composite biomaterial was fabricated by mixing cisplatin and lactose powders with a supersoft silicone elastomer. Ecoflex 00-30, a two-part platinum-catalyzed supersoft silicone elastomer, was manually mixed with cisplatin powder and lactose monohydrate powder to create a composition containing 50% w/w_{total} powder. The 50% w/w_{total} final solid powder content was determined based on

preliminary experiments to achieve a matrix with interconnected pore paths allowing for continuous release of its contents in an aqueous environment over a period of multiple weeks. Ecoflex 00-30 was selected because of its mechanical properties that closely resemble those of soft tissue. Lactose monohydrate was selected as a sacrificial excipient to help create interconnected paths in the composite matrix and modulate the rate of cisplatin release because it is a commonly used excipient with no adverse side effects in the pharmaceutical industry, is readily available off-the-shelf, is very soluble in water (lactose solubility in water = 100 mg/mL) and its molecular weight (360.31 g/mol) is close to that of cisplatin (300.01 g/mol). Four different formulations containing different proportions of cisplatin and lactose powders were tested to assess their *in vitro* cisplatin release profile and determine the best candidate for sustained zero-order cisplatin release: (1) CDDP5: 5% w/w_{total} cisplatin – 45% w/w_{total} lactose; (2) CDDP10: 10% w/w_{total} cisplatin – 40% w/w_{total} lactose; (3) CDDP25: 25% w/w_{total} cisplatin – 25% w/w_{total} lactose; (4) CDDP40: 40% w/w_{total} cisplatin – 10% w/w_{total} lactose. A mass of 1.5-2 g of the cisplatin-lactose-silicone mixture was poured into circular plasma-treated polystyrene molds measuring approximately 35 mm in diameter and 18 mm in depth. The mixture was spread evenly across the surface of the circular molds and allowed to degas completely in vacuum for 15 min followed by overnight curing at room temperature and pressure. This yielded composite material pieces measuring 35 mm in diameter and approximately 1.2-1.7 mm in height, depending on the mass of material poured in the mold. Cisplatin-containing samples were kept away from light for all experiments. An additional composite formulation containing only lactose 50% w/w_{total} (LAC50) was prepared to use in *in vitro* cytotoxicity studies and for mechanical testing,

where material porosity was the critical parameter. The LAC50 formulation was prepared in the same way as the cisplatin-containing formulations. A 5 mm-diameter disposable biopsy punch was used to punch out disks from the cured material pieces for *in vitro* cisplatin release quantification, *in vitro* cytotoxicity assessment and *in vivo* implantation. The resulting disks measured 5 mm in diameter and 1-1.5 mm in thickness. All disks used for cytotoxicity assessment and *in vivo* implantation were sterilized by ethylene oxide gas and allowed to degas for 48 hours in a hood before use. Ecoflex 00-30 and LAC50 samples for mechanical testing were prepared by pouring uncured Ecoflex 00-30 or uncured LAC50 respectively into dog bone-shaped Teflon molds measuring 1.5 mm in depth then allowed to degas completely in vacuum for 15 min and cure overnight at room temperature and pressure.

2.2.3 Chemical and structural characterization

Ecoflex 0030, LAC50, CDDP5, CDDP10, CDDP25 and CDDP40 disks were sectioned through the axis of the disk using a razor to create lateral cross-sections of the disk thickness. The cross-sections were examined by scanning electron microscopy (SEM; Zeiss Merlin SEM, Jeol 5910 SEM and Jeol 5600LV SEM) and energy-dispersive X-ray spectroscopy (EDS; Bruker) to study the presence and distribution of cisplatin and lactose in the silicone matrix. A 10-μm gold-palladium coating was applied to the cross-sections prior to SEM imaging to prevent charging of the sample.

2.2.4 Mechanical characterization

Tensile testing of dog bone-shaped Ecoflex 00-30 and LAC50 samples was performed on an Instron 5943 testing machine with a 500 N load cell and steel grip platens.

Specimens were subjected to elongation at a rate of 15 mm/min until failure. To examine the mechanical properties of the composite material after prolonged release of impregnated solid powder, dog bone-shaped LAC50 samples were immersed in PBS for 6 weeks, allowed to fully dry in an oven at 80°C for 48 hr and subsequently underwent the same tensile test. Force was converted to stress using the cross-sectional surface area of the sample and elongation was converted to strain using the initial length of the sample. Stress-strain diagrams were plotted and the modulus of elasticity, ultimate tensile stress and elongation at break were calculated and compared to those of Ecoflex 00-30 and of representative tissues in the human abdominal cavity.

2.2.5 *In vitro* cisplatin release

CDDP5, CDDP10, CDDP25 and CDDP40 disks were immersed in PBS in scintillation vials and incubated at 37°C on a shaker oscillating at 60 cycles/min to quantify the amount of cisplatin released *in vitro* at regular intervals for a total period of 109 days. Each disk was lodged within the turns of a thin stainless steel spring similar to the method described by Keskar et al. (McMaster-Carr, Elmhurst, IL, USA) to prevent the disk from settling on the bottom of the vial or floating to the top of the liquid.[98] A piece of thin nickel wire was threaded through the spring and brought near the top of the vial to allow movement of the setup to a new vial containing fresh PBS at regular time intervals. The PBS was renewed at an amount equivalent to 2 mL of fresh PBS every 24 hours to maintain sink conditions for the dissolution of lactose (lactose solubility in water = 100 mg/mL) and cisplatin (cisplatin solubility in water = 2.53 mg/mL). The interval between PBS renewals was kept to 6 days or shorter to minimize cisplatin

degradation. The amount of cisplatin present in the solution was measured at each prescribed time point by HPLC with a nickel (II) chloride internal standard and the method described previously by our group.[45] A solution containing lactose alone was also assessed by HPLC to confirm that lactose-associated peaks did not interfere with the cisplatin peak and so their presence would not affect the perceived measured amount of cisplatin in the sample, to ensure that the HPLC method would be cisplatin-specific.

2.2.6 Cell culture

The cisplatin-sensitive UCI101 human ovarian cancer cell line (Dr. G. Scott Rose, University of California, Irvine) and cisplatin-resistant SKOV3 human ovarian cancer cell line (ATCC, Manassas, VA, USA) were used. Cells were pathogen tested in 2015 by the Comparative Pathology Laboratory at MIT and in 2018 by the High-Throughput Screening Core at the MIT David H. Koch Institute for Integrative Cancer Research and tested negative for mycoplasma. The UCI101 cell line was authenticated in 2012 using whole-genome copy number variation analysis comparing the pattern of variants to those of other serous ovarian cancer cell lines. UCI101 cells were grown and maintained in RPMI 1640 medium supplemented with 10% fetal bovine serum (FBS) and 1% penicillin-streptomycin-glutamine. SKOV3 cells were grown and maintained in McCoy's 5A medium supplemented with 10% FBS and 1% penicillin-streptomycin-glutamine. Cells were grown as monolayers at 37°C with 5% CO_2 and were subcultured with 0.25% trypsin-EDTA at regular time intervals to maintain cell densities below 80% confluence. Cells were not used after passage number 13.

2.2.7 *In vitro* material cytotoxicity

The CDDP25 formulation was deemed the most appropriate for use as the material for a human implant based on its *in vitro* cisplatin release profile. The *in vitro* cytotoxicity of the CDDP25 formulation was evaluated against both UCI101 cisplatin-sensitive cells and SKOV3 cisplatin-resistant cells. The LAC50 formulation and Ecoflex 00-30 alone were also tested as controls to evaluate any cytotoxic effect of the lactose excipient or the silicone elastomer. Sterile CDDP25, LAC50 and Ecoflex 00-30 disks were incubated for 24 hours in 2 mL of PBS at 37°C on a shaker oscillating at 60 cycles/min prior to cell culture use. This allowed elimination of the cisplatin burst observed in the first 24 hours of CDDP25 release and use of the disks during their near-zero-order release phase. The five treatment groups tested *in vitro* were: (1) untreated control; (2) CDDP25 disk; (3) equivalent cisplatin solution; (4) LAC50 disk; (5) Ecoflex 00-30 disk. The equivalent cisplatin solution group exposed the cells to the amount of cisplatin released by a CDDP25 disk over 24 hours, calculated using the average *in vitro* cisplatin release rate from the cisplatin release profile of the four different composite formulations. Cells were seeded as a monolayer in 24-well plates at a density of 2×10^4 cells/well one day before the start of the *in vitro* cytotoxicity study and allowed to adhere to the well bottom overnight. The disks for groups 2, 4 and 5 were subsequently placed in Transwell cell culture inserts featuring polyester membranes with an 8.0 µm pore size (Corning, Corning, NY, USA) and immersed in the cell culture medium within each well without coming in contact with the cell monolayer at the bottom of the well. Cisplatin at the 24-hour equivalent amount was added as a solution in PBS in the cell culture medium of each of the group 3 wells at that time. The cell culture medium in each well across all five groups was refreshed every 24 hours, including the cisplatin-containing medium in

group 3 wells to prevent any cisplatin degradation. Cell viability was evaluated using the MTT assay after 24, 48 and 72 hours of treatment read at 570 nm (measurement) and 720 nm (background) using a BioTek Synergy 4 plate reader (BioTek, Winooski, VT). All chemicals and materials for the *in vitro* cytotoxicity studies were sterile and maintained under sterile conditions.

2.2.8 Surgical and euthanasia procedures for *in vivo* experiments

All listed procedures were in accordance with the Massachusetts Institute of Technology Committee on Animal Care guidelines, as well as the NIH Guide for the Care and Use of Laboratory Animals. Animal surgeries to implant CDDP25 and Ecoflex 00-30 disks were performed within a sterile field and all surgical equipment was autoclaved. Inhalation anesthesia was maintained throughout surgeries with isoflurane. Slow-release buprenorphine was used as pre- and post-surgical analgesia per recommendation by the animal care committee. The incision site was sterilized with iodine and isopropyl alcohol. A small abdominal incision of about 5 mm was made through the skin and peritoneum to implant the disks. The disks once implanted were allowed to freely move within the peritoneal cavity. Mice were weighed regularly to monitor overall health and euthanized upon weight loss greater than 20% or poor body condition. Euthanasia was carried out by carbon dioxide inhalation at a steadily increasing flow rate to minimize distress.

2.2.9 *In vivo* composite toxicity study

The *in vivo* toxicity of the CDDP25 formulation was assessed in healthy immunocompetent mice and compared to the toxicity of a single IP cisplatin injection. All chemicals and materials for this study were sterile and maintained under sterile conditions. Female BALB/c immunocompetent mice bearing no tumors and weighing 20-25 g were used (Charles River Laboratories, Wilmington, MA, USA). Blood was sampled via the saphenous vein of all mice prior to the start of the experiment to obtain baseline complete blood count (CBC) values with auto differential. The mice were allocated in three different treatment groups: (1) intraperitoneal (IP) implantation of a single CDDP25 5 mm-diameter disk (n=2); (2) IP administration of a single 4 mg/kg cisplatin injection (n=2); or (3) untreated control (n=1). The single animal of group 3 was included in the study to serve as a healthy control in the blood workup and histological examination of the two treatment groups. Sterile CDDP25 disks were incubated in 2 mL of PBS at 37°C on a shaker oscillating at 60 cycles/min for 24 hours to eliminate their cisplatin burst. The disks were then implanted intraperitoneally in the mice of group 1. The mice of group 2 received a 4 mg/kg IP cisplatin injection at the same time as the implantation surgery given as a 1 mL injection using 0.9% w/v saline as a diluent and injected via a 28G needle. The mice of group 2 were euthanized 48 hours after the start of treatment. The mice of groups 1 and 3 were euthanized 15 days after the start of treatment. Blood was collected from all mice at euthanasia by cardiac puncture for CBC with auto differential and serum platinum quantification. Blood samples for CBC with auto differential were collected in EDTA-coated 100 µL microvettes (Sarstedt, Nümbrecht, Germany) as per manufacturer instructions to prevent clotting and were processed on a Hemavet 950FS Auto Blood Analyzer (Drew Scientific, Miami Lakes,

FL, USA) within 24 hrs after collection. Samples that were not processed immediately after collection were stored in the refrigerator to maintain sample integrity. Blood samples for serum platinum quantification were collected in 1.1 mL Z-Gel microtubes (Sarstedt, Nümbrecht, Germany) containing serum gel with clotting activator and were centrifuged at 13,000 g for 5 minutes. The serum was collected following blood centrifugation and ultrafiltered using an Amicon Ultra-0.5 mL centrifugal filter (MilliporeSigma, Burlington, MA, USA) as per manufacturer instructions to collect both the serum ultrafiltrate and the serum concentrate. The serum ultrafiltrate is free of proteins, primarily albumin, and therefore does not contain protein-bound cisplatin that is no longer therapeutic. Serum ultrafiltrate and concentrate samples were stored at -80^{o}C until further processing. The platinum concentration in serum ultrafiltrate was measured by inductively coupled plasma mass spectroscopy (ICP-MS) on an Agilent 7900 ICP-MS (Agilent, Santa Clara, CA, USA). The liver, spleen, kidneys, stomach, sections of the small and large intestine, ovaries, uterus, femurs, fat pad tissue – if present – and implant along with any surrounding fibrous capsule were harvested from the euthanized mice. All harvested tissues were prepared for histological analysis to assess toxicity using the following protocol. The implant and tissues with the exception of the femurs were placed in 10% neutral buffered formalin immediately after harvesting and allowed to fix for 48-72 hours. The femurs were placed in Bouin's solution and allowed to decalcify for at least two weeks and until they could be bent by applying a small amount of force to each end of the bone. The fixed tissues with the exception of the femurs were sectioned with a razor blade and half of each sample was placed in histology cassettes. The femurs were placed in histology cassettes without any

sectioning. The implants were carefully sectioned with a razor blade along their axis to ensure any fibrous capsule remained on the sample and placed in histology cassettes such that the implant cross-section and capsule would be visible on the paraffin section. Care was taken to ensure that all five liver lobes and half of each kidney as well as different representative sections of the small and large intestines were included in the respective cassette. The cassettes were placed in 70% ethanol followed by paraffin embedding and hematoxylin & eosin (H&E) staining of slides for pathology review with a veterinary pathologist consultant at the Hope Babette Tang Koch Institute Histology Core.

2.2.10 *In vivo* abdominal platinum distribution study

The abdominal platinum distribution accomplished by intraperitoneally implanting a single CDDP25 disk was assessed in healthy immunocompetent mice and compared to that achieved with a single IP cisplatin injection. Any platinum leaching of Ecoflex 00-30 disks after intraperitoneal implantation was also assessed since the elastomer is platinum-catalyzed. All chemicals and materials for the *in vivo* platinum distribution study were sterile and maintained under sterile conditions. Female BALB/c immunocompetent mice bearing no tumors and weighing 20-25 g were used (Charles River Laboratories, Wilmington, MA, USA). The mice were allocated in three different treatment groups: (1) intraperitoneal (IP) implantation of a single CDDP25 5 mm-diameter disk (n=6); (2) IP administration of a single 4 mg/kg cisplatin injection (n=12); or (3) IP implantation of a single Ecoflex 00-30 5 mm-diameter disk (n=3). Sterile CDDP25 and Ecoflex 00-30 disks were incubated in 2 mL of PBS at 37°C on a shaker

oscillating at 60 cycles/min for 24 hours to eliminate the cisplatin burst from the CDDP25 disks. The disks were then implanted intraperitoneally in the mice of groups 1 and 3. The mice of group 2 received their IP cisplatin injection at the same time given as a 1 mL injection using 0.9% w/v saline as a diluent and injected via a 28G needle. The euthanasia time points were as follows: group 1 – two mice euthanized at each of days 3, 8 and 15 after implantation; group 2 – two mice euthanized at each of 0.5hr, 1hr, 2hr, 3 days, 8 days and 15 days after injection; and group 3 – one mouse euthanized each of 3, 8 and 15 days after implantation. The earlier time points at 1.5hr, 1hr and 2hr after injection were added for group 2 to ensure that the cisplatin levels in serum and tissue would be adequately quantified at the peak following injection and before the drug was cleared from the systemic circulation and peritoneal cavity. The liver, spleen, kidneys, stomach, small and large intestine, ovaries, uterus and fat pad tissue – if present – of the euthanized mice were harvested. The harvested tissues were prepared for platinum quantification using the following protocol. The tissues were collected in Eppendorf tubes and placed immediately on dry ice followed by storage at -80°C until further processing. To quantify the amount of platinum in the harvested tissues, the organs were homogenized using a Bertin Precellys CK14 soft tissue homogenization kit (VWR, Radnor, PA, USA) and digested using 70% nitric acid. Briefly, each organ was weighed and then divided into pieces weighing at most 200 mg. Each piece was placed in a tissue homogenization tube containing inert 1.4 mm zirconium oxide beads and 1 mL of RIPA lysis and extraction buffer (Invitrogen, Carlsbad, CA, USA) was added. The tubes were placed in a Precellys 24 homogenizer (Bertin, Montigny le Bretonneux, France) and the samples were homogenized at 6,000 RPM for 4 x 20 s cycles. The tubes were

then centrifuged at 10,000 g for 10 min to remove any foam buildup and placed uncapped on a thermoblock at 95°C for at least 48 hours until all the supernatant had evaporated. The lysed tissue pellets were digested by adding 1 mL of 70% nitric acid to each tube, loosely capping it and placing it in the hood on a hot plate at 55°C for 24 hours. The platinum concentration of the digested samples was quantified by ICP-MS. Samples were serially diluted to a final dilution of 10^{-3} using 2% nitric acid before ICP-MS measurement. An internal erbium standard was used to monitor the performance of the ICP-MS run for any drift and the bounds for rejecting readings were defined at +/- 20% of the erbium internal standard recovery. A platinum calibration curve was prepared using eight platinum concentrations ranging from 0 to 500 ppb to convert the ICP-MS platinum-to-erbium count ratio to a platinum concentration for each sample. The platinum calibration curved was a straight line through the origin with $R^2 = 0.9999$. The platinum concentration values obtained for each sample were multiplied by the dilution factor to obtain the platinum concentration in the original sample and the calculated platinum mass was divided by the tissue sample mass in each tube to obtain a normalized µg Pt / g tissue content for each sample.

2.2.11 Data analysis

All data are expressed as a mean +/- standard deviation. All error bars represent standard deviations from the mean. All samples were examined in triplicate unless if otherwise noted. The GraphPad Prism software was used for all statistical analyses (GraphPad Software, CA, USA). *In vitro* cytotoxicity results were compared across the five groups (CDDP25 disk, equivalent cisplatin solution, LAC50 disk, Ecoflex 00-30 disk, untreated control) using a one-way ANOVA with Tukey's multiple comparisons test. The

two cisplatin treatment groups 'CDP25 implant' and 'Equivalent cisplatin solution' were further compared using an unpaired student's t-test. Tissue platinum content values were compared for each organ across the two treatment groups (IP injection, CDDP25 implant) using an unpaired student's t-test. Differences with p-value < 0.05 were considered to be statistically significant. Statistical significance is indicated as: ns $p >= 0.05$; * $p < 0.05$; ** $p < 0.01$; *** $p < 0.001$; **** $p < 0.0001$.

2.3 Results

2.3.1 Chemical and structural characterization

Secondary electron SEM imaging of the Ecoflex 00-30, LAC50, CDDP5, CDDP10, CDDP25 and CDDP40 disk cross-sections was performed to assess the topography of the cross-sections and confirmed the presence of two distinct phases, with the minor phase appearing as crystals of various shapes and sizes dispersed homogeneously within a flat-appearing major phase across the height of the cross-section (Figure 2.1A-C). Backscatter electron SEM imaging of the CDDP25 disk cross-section was performed to assess the composition of the cross-sections. Cisplatin crystals were expected to appear as brighter on backscatter electron SEM due to the higher atomic number of platinum that backscatters electrons more strongly than the other elements. Backscatter SEM of the CDDP25 disk cross sections confirmed the presence of brighter and darker crystals across the silicone matrix thickness attributed to cisplatin and lactose respectively and appearing homogeneously distributed throughout the thickness with no apparent dissolution (Figure 2.1D). EDS spectra of the CDDP25 disk cross-section revealed that the flat-appearing major phase comprised mainly silicon while the crystal-appearing minor phase contained crystals with either the presence of carbon corresponding to lactose or the presence of platinum and chlorine corresponding to cisplatin (Figure 2.2A-B).

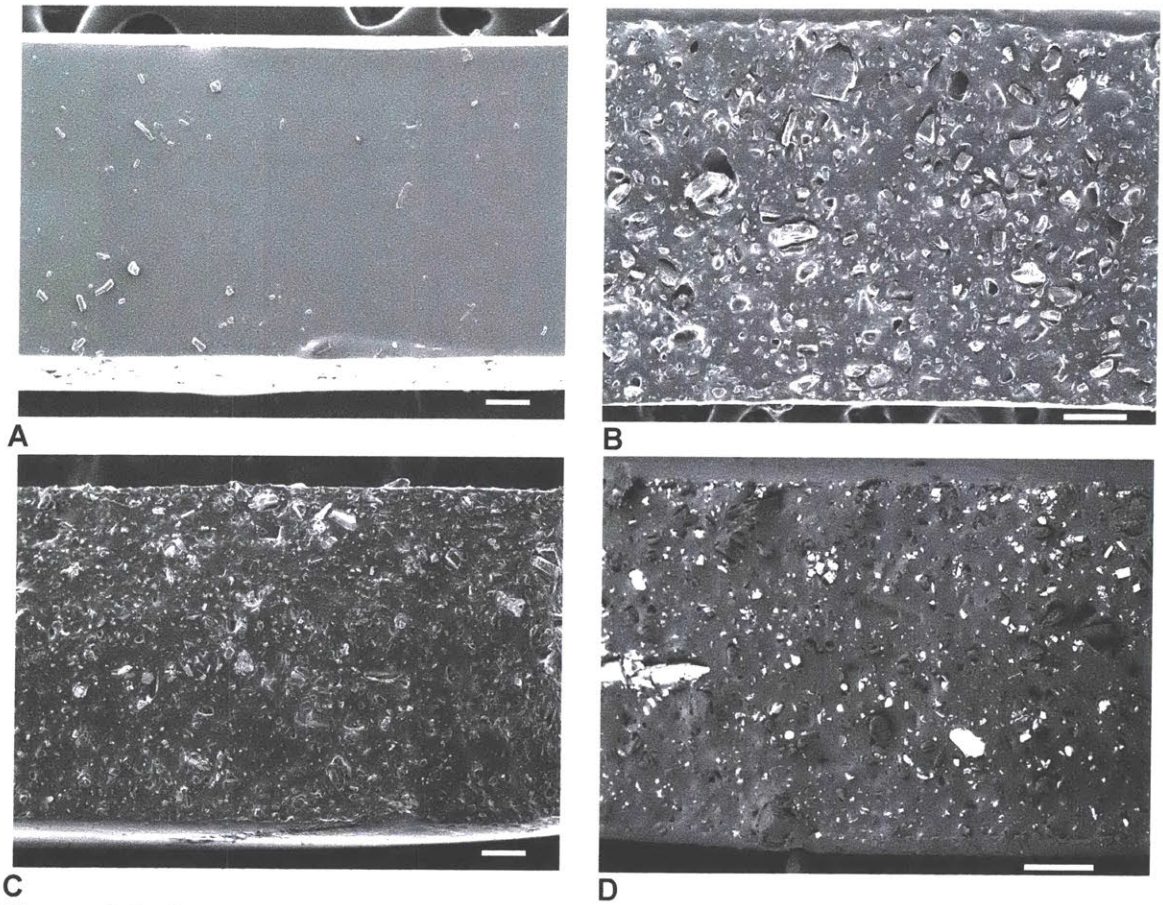

Figure 2.1: SEM images of composite cross sections. (A)-(C) Secondary electron SEM images of cross-sections of (A) Ecoflex 00-30; (B) LAC50; and (C) CDDP25; (D) Backscatter SEM image of cross-section of CDDP25. The cross-sections are oriented such that the top surface of the cast sample is at the top of the SEM image and the bottom surface that is in contact with the mold is at the bottom. A uniform distribution of crystals throughout the Ecoflex 00-30 matrix is seen in both LAC50 and CDDP25 cross-sections. Cisplatin crystals are expected to appear brighter in the backscatter electron SEM than lactose crystals because of the heavier Pt nuclei that more effectively scatter electrons compared to low-atomic-number elements. Scale bars are 200 μm.

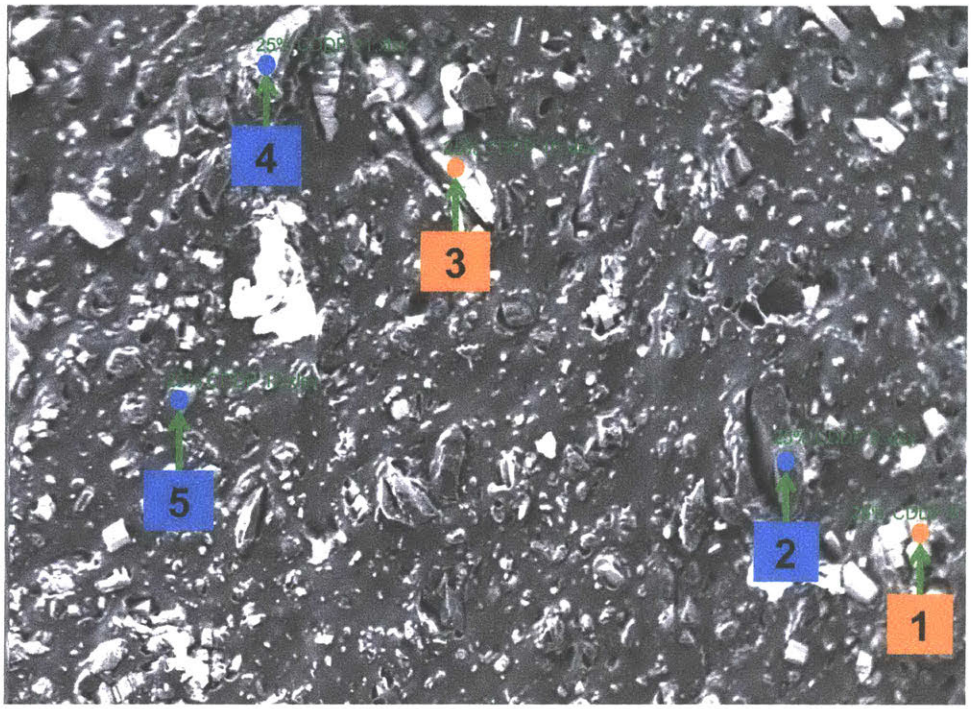

A

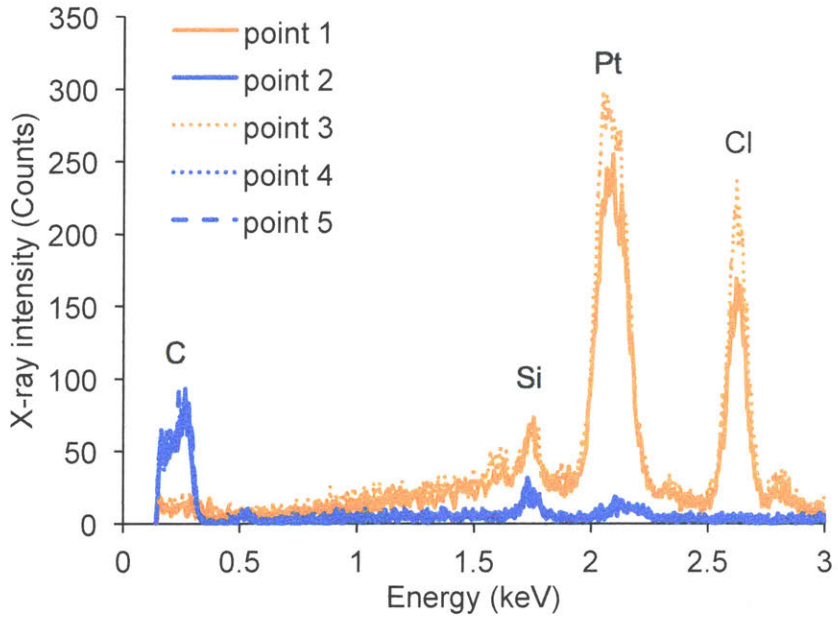

B

Figure 2.2: EDS analysis of CDDP25 cross section. (A) CDDP25 cross-section with points # 1-5 analyzed by EDS marked. (B) Plot of the EDS spectrum of the points indicated in (A). Intensity of the measured X-rays emitted from each point is plotted against X-ray energy. Peaks corresponding to the elements of interest are identified. Pt and Cl were used to identify cisplatin in the sample while Si was used to identify the Ecoflex 00-30 matrix and C was used as an indicator of the

presence of lactose. The colors in (A) and (B) are matched to help visualize which line in the EDS spectrum corresponds to which point in the cross-section. Points #1 and 3 were identified as cisplatin crystal while points #2,4 and 5 were identified as lactose crystals. Slight peaks corresponding to Si were present in all points analyzed and this is reasonable given that all crystals are encased in a silicone matrix. The EDS spectrum confirmed that cisplatin and lactose crystals are present and randomly distributed throughout the material.

2.3.2 Mechanical characterization

Ecoflex 00-30 and LAC50 dog bone-shaped samples underwent tension testing to evaluate their elastic modulus, ultimate tensile strength and elongation at break and compare them to the values reported by the Ecoflex manufacturer as well as those of tissues commonly found in the abdominal cavity. This mechanical characterization was used as a metric of the composite material's mechanical appropriateness for intraperitoneal placement. Two types of LAC50 samples were tested to fully recapitulate the intended multi-week composite implantation for *in vivo* cisplatin release: (1) fully cured LAC50 samples after production and (2) fully cured LAC50 samples entirely immersed in PBS for six weeks followed by drying completely in an oven. The complete results along with values obtained from the literature for Ecoflex 00-30 and representative human tissues found in the abdomen (esophagus, stomach, liver, small and large bowel and colon) are shown in Table 2.1.

Material	Elastic modulus (MPa)	Ultimate tensile strength (MPa)	Elongation at break (%)
Ecoflex 00-30 (literature)	0.027-0.125[99-101]	1.379[102]	900[102]
Ecoflex 00-30 (experimental)	0.031	0.550	832
LAC50	0.226	0.356	590
LAC50 after 42 days in PBS	0.128	0.401	317
Esophagus	0.018[103]	1.2[104]	140[104]
Stomach	0.002[105]	0.7[104]	190[104]
Liver	0.006[105] – 0.27[106]	0.023[107]	46[107]
Small bowel	0.0029[108]	0.5[104]	140[104]
Large bowel	0.0029[108]	0.9[104]	180[104]
Colon	5.18[109]	0.87[109]	62.81[109]

Table 2.1: Mechanical properties of Ecoflex 00-30, LAC50 and representative abdominal tissues.

The elastic modulus of Ecoflex 00-30 was found experimentally to lie within the range reported in the scientific literature (0.031 MPa compared to 0.027 – 0.125 MPa respectively). The ultimate tensile strength of Ecoflex 00-30 was found to be approximately 40% of the value reported by the manufacturer (0.550 MPa compared to 1.379 MPa respectively) meaning that the material was actually 60% less strong than the manufacturer-reported specification. The Ecoflex 00-30 elongation at break was found to be approximately 92% of the value reported by the manufacturer (832% compared to 900% respectively), meaning that the material tolerated a strain almost as high as expected according to the manufacturer specifications.

The elastic modulus of LAC50 samples after 42 days of leaching in PBS was found to be approximately 40% smaller than that of LAC50 samples tested without further manipulation after curing (0.128 MPa compared to 0.226 MPa respectively), suggesting a less stiff material. This is expected since the material has at this point lost lactose content and the increased porosity should lead to a decrease in its modulus.[110-112] The ultimate tensile strength of LAC50 samples was found to be approximately 65% of that calculated for Ecoflex 00-30 alone experimentally (0.356 MPa compared to 0.550 MPa respectively), while the ultimate tensile strength of LAC50 samples after 42 days of leaching in PBS was found to exceed 70% of the ultimate tensile strength calculated for Ecoflex 00-30 alone (0.401 MPa compared to 0.550 MPa respectively). These values suggest that the LAC50 composite material maintains the majority of the strength seen with Ecoflex 00-30 despite being impregnated with 50% powder w/w_{total} and its strength is not compromised by releasing its powder content over six weeks immersed in PBS. LAC50 in fact contained only lactose powder, which is much more readily soluble in water compared to cisplatin powder. The amount of powder that leached out of the LAC50 dog bone-shaped samples in the six-week leaching period is therefore expected to be larger than the amount of powder expected to leach out of samples made of the CDDP25 composite material, creating a more porous material at 42 days. The ultimate tensile strength of CDDP25 after leaching would be expected to be larger than that determined experimentally for LAC50 after leaching, and so any change in the ultimate tensile strength of CDDP25 after six weeks of immersion in an aqueous environment is anticipated to be even smaller than that seen with LAC50. The elongation at break of LAC50 was found to be approximately 71% of that of Ecoflex 00-30 alone (570%

compared to 832% respectively), but it markedly decreased after six weeks of leaching. The elongation at break of LAC50 after six weeks in PBS was less than 60% of the value for LAC50 without further manipulation after curing (317% compared to 590% respectively), meaning that the composite material is able to withstand much less stretching after the start of plastic deformation before it breaks once it has been immersed in an aqueous solution and leached lactose powder over six weeks. This effect is similarly expected to be less dramatic with CDDP25 compared to LAC50 because of cisplatin's lower water solubility.

The elastic modulus of Ecoflex 00-30 was confirmed comparable to the elastic modulus of key organs in the abdominal cavity like the liver and bowels based on values reported in the literature.[99-109] The elastic modulus of LAC50 both intact (0.226 MPa) and after the 42-day leaching period (0.128 MPa) was larger than that reported for all abdominal organs examined with the exception of the colon (5.18 MPa), suggesting a stiffer material than those tissues. The modulus values however fall within 1-2 orders of magnitude of the modulus reported for the softest tissues (liver, stomach) and are an order of magnitude smaller than the modulus of colon. The ultimate tensile strength and elongation at break of the LAC50 formulation both before and after leaching are both comparable to the values reported in the literature for the examined abdominal organs. The LAC50 composite material, both before and after leaching, can thus be considered mechanically matched to key organs in the abdominal cavity and is therefore expected to be mechanically well tolerated *in vivo* upon contact with abdominal tissues. These mechanical properties also suggest that routine surgical manipulation of the composite material *in vivo* will be safe since it will involve forces similar to those used when

manipulating surrounding tissues. Further assessment of the composite material's response to forces specifically experienced during laparoscopic placement, removal and more extreme manipulation is necessary to ensure implantation safety and should be carried out as a next step in material development.

2.3.3 *In vitro* cisplatin release

A multiphasic cisplatin release profile was observed for the CDDP5, CDDP10, CDDP25 and CDDP40 samples *in vitro* over the 109-day release period. An initial burst during the first 24 hours of release was followed by three phases of near-linear cisplatin release that were distinct and occupying the same time intervals for all formulations. The time intervals for each phase were as follows: Phase 0 (burst) on day 0; Phase 1 on days 1-12; Phase 2 on days 17-44; Phase 3 on days 49-109. The intermediate days between the end and start of phases 1-3 were not sampled for all release studies, and so cannot be assigned to either the preceding or succeeding phase with confidence. No peaks attributed to lactose were found to interfere with the peak attributed to cisplatin in the HPLC method, ensuring its specificity to quantifying active cisplatin in solution.

The cisplatin release profiles for the four composite material formulations are shown in Figure 2.3. Cisplatin release for each formulation during each phase 1-3 can be approximated by a distinct zero-order release profile. Linear best-fit trendlines having $R^2 > 0.98$ were therefore used to quantify the average cisplatin release rates during each of the phases 1-3 for each of the four formulations, and the results are shown in Figure 2.4 and Table 2.2. Two methods were used to calculate an average *in vitro* cisplatin release rate for each formulation for the entire duration of the 109-day release

period. The first method fit a linear trendline to the entire data set for each formulation without forcing the line to pass through the origin ($R^2 > 0.9$ for all trendlines fitted to the data) and used the slope of the resulting line as an estimate for the average cisplatin release rate for each formulation. The second method calculated a weighted average of the release rates of phases 1-3 for each formulation using the relative duration of each phase in comparison to the total period of release as a weight. The average and weighted average *in vitro* release rates are shown in Table 2. The values for each formulation were similar overall for the average and weighted average *in vitro* release rates, with the largest difference observed for the CDDP40 formulation (8.6% faster *in vitro* release rate computed when using a weighted average) and the smallest difference observed for the CDDP25 formulation (0.9% slower *in vitro* release rate computed when using a weighted average). The initial 24-hr burst was not taken into account in calculating *in vitro* release rates as it was eliminated for all formulations after 24 hours. The initial 24-hour burst could similarly be eliminated in the actual clinical embodiment of these composite materials for an intraperitoneal implant, for instance by pre-treating the implant before placement in the patient.

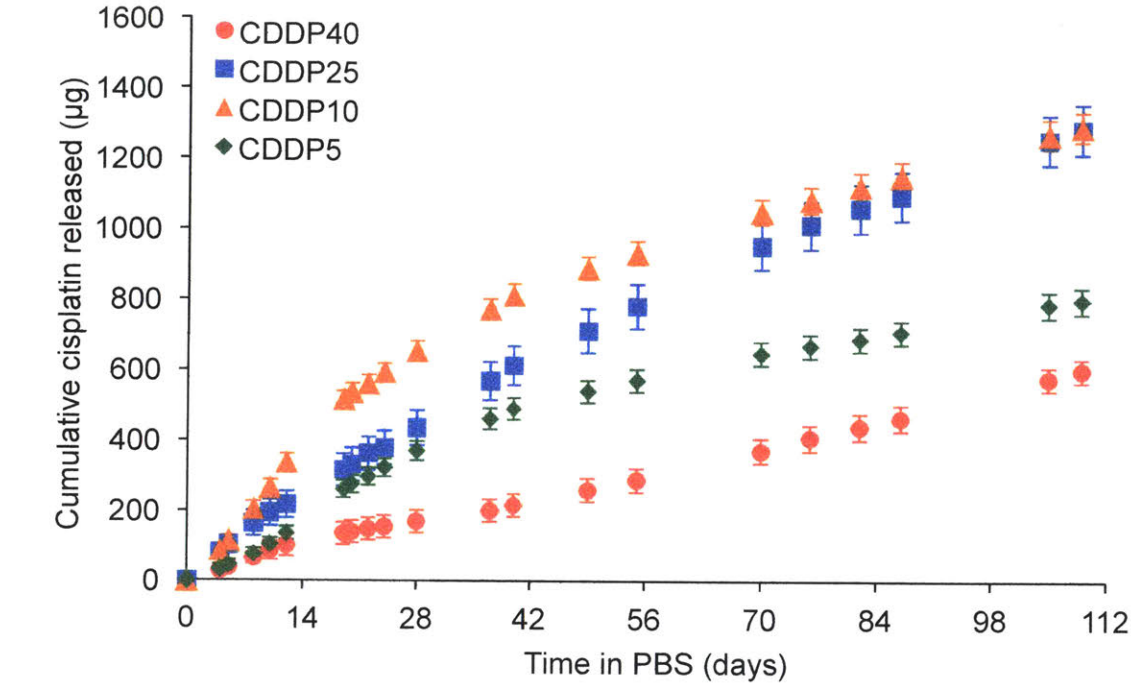

A

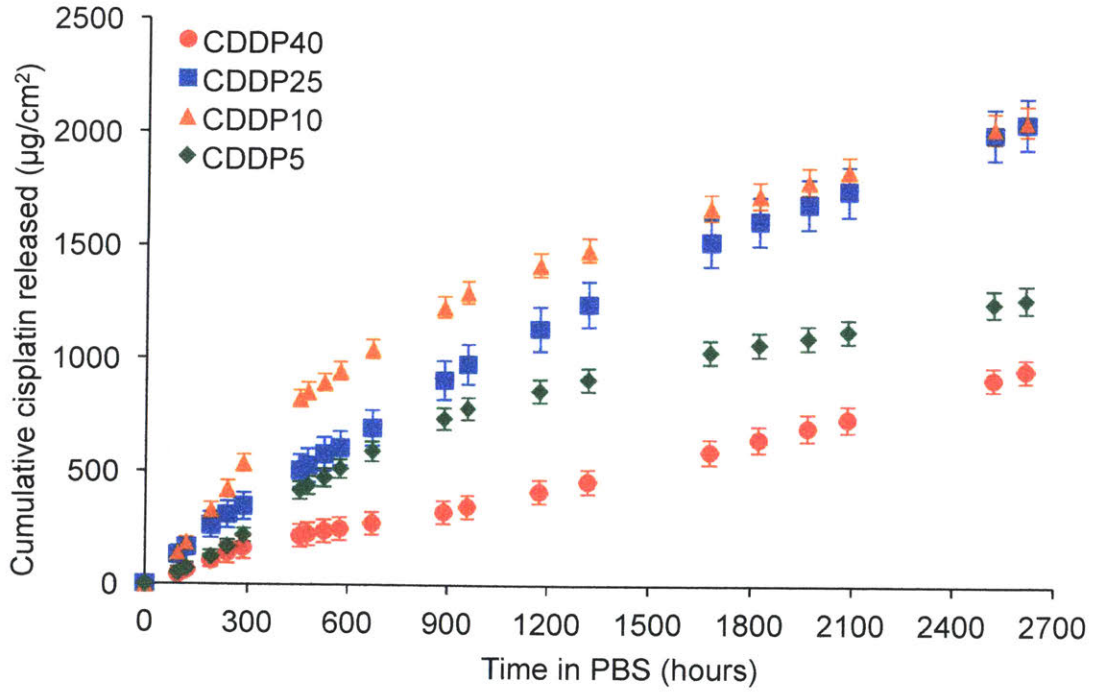

B

Figure 2.3: *In vitro* cisplatin release from various composite formulations. (A) *In vitro* cisplatin release rate over time in days and (B) normalized *in vitro* cisplatin release rate per square centimeter of sample area over time in hours. Values are average of four studies with n=2 each. Error bars represent standard deviation from the mean.

The initial cisplatin burst displayed by all four formulations is attributed to the dissolution of cisplatin crystals found on the surface of the composite samples. The dissolution of these readily accessible cisplatin crystals by the aqueous solvent, PBS, is governed exclusively by the solubility and dissolution rate of cisplatin in the solvent. The three-phase zero-order release profiles displayed by all four formulations after this initial burst are hypothesized to arise from the swelling process happening in the composite samples, similar to the mechanism of cisplatin release from ureasil-poly(ethylene oxide)-cisplatin matrices proposed by Molina et al. and to the swelling and potassium dichromate release from silicone matrices described by Golomb et al.[113-115] The swelling is driven by the influx of the aqueous solvent in which a composite sample is immersed both through pores generated by dissolution of the excipient crystals and through the polymer backbone rendered more hydrophilic by the hydrophilic excipients incorporated in the silicone matrix.[115]

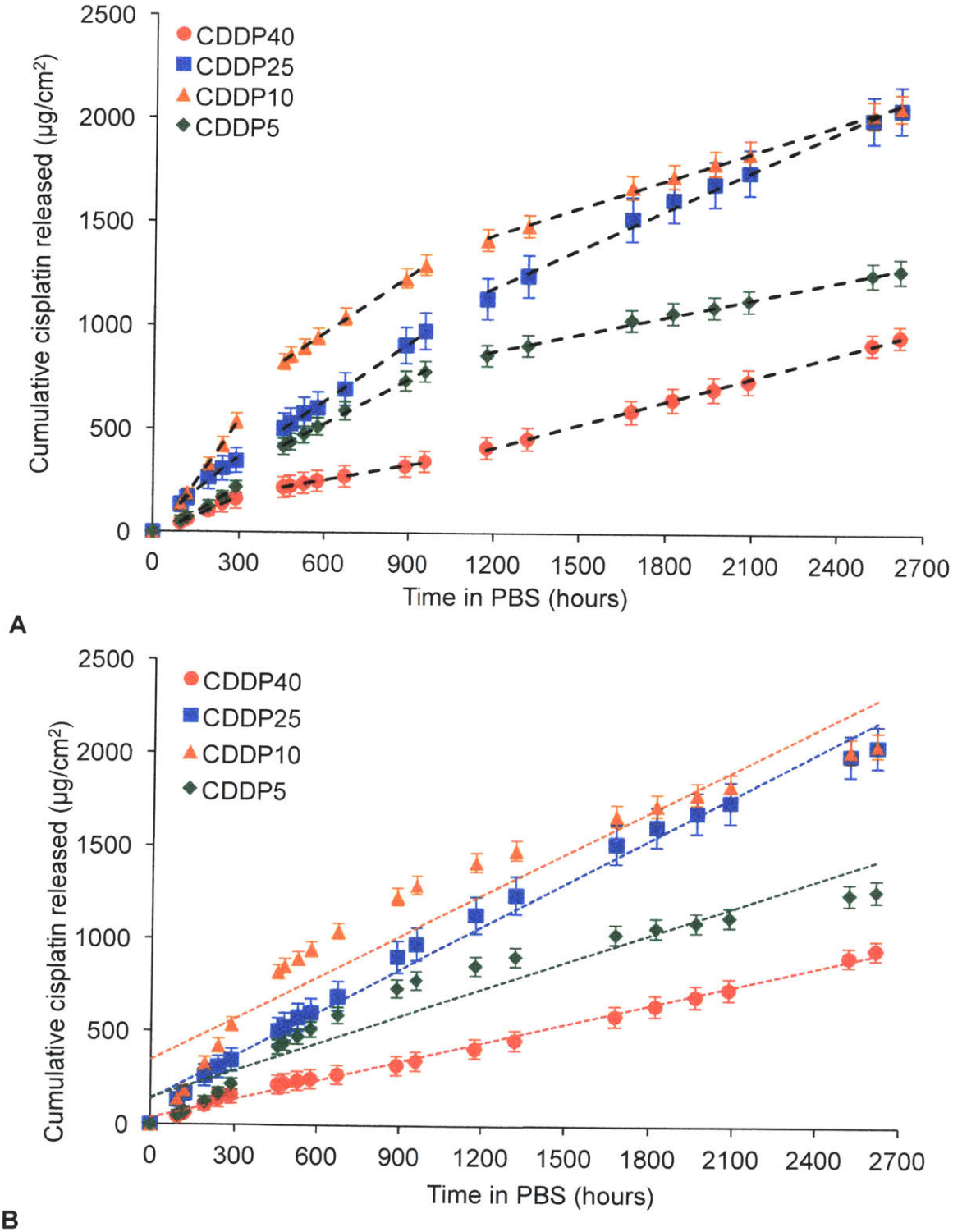

Figure 2.4: *In vitro* cisplatin release rate estimation for various composite formulations. Linear best-fit trendlines for (A) phases 1-3 and (B) the entire 109-day release for each formulation used as two different methods to estimate the average *in*

vitro cisplatin release rate. Trendline equations and R^2 values tabulated in Table 2.

Formulation	Phase	Cisplatin release rate (μg/cm²/hr)	R^2
CDDP5	1	0.855	0.995
	2	0.719	0.998
	3	0.282	0.995
	Entire release (linear best-fit trendline)	0.492	0.930
	Entire release (phase 1-3 weighted average)	0.471	-
CDDP10	1	2.058	0.999
	2	0.924	0.999
	3	0.446	0.997
	Entire release (linear best-fit trendline)	0.746	0.917
	Entire release (phase 1-3 weighted average)	0.772	-
CDDP25	1	1.143	0.988
	2	0.932	0.999
	3	0.628	0.993
	Entire release (linear best-fit trendline)	0.780	0.989
	Entire release (phase 1-3 weighted average)	0.773	-
CDDP40	1	0.625	0.998
	2	0.249	0.998
	3	0.376	0.999
	Entire release (linear best-fit trendline)	0.342	0.995
	Entire release (phase 1-3 weighted average)	0.372	-

Table 2.2: *In vitro* cisplatin release rates for CDDP5, CDDP10, CDDP25 and CDDP40 formulations. The rates are calculated using zero-order models based on linear best-fit trendlines for phases 1-3 for each formulation or for the entire 109-day release period.

Dissolution of the cisplatin crystals on the surface of the composite sample creates a high cisplatin concentration near the sample surface. The dissolved cisplatin is extracted away from the surface and toward the solution, driving an inverse PBS flux into the composite.[113] This flux is thought to be the driver behind phase 1 in the *in vitro* cisplatin release profile of all four formulations. The passage of PBS into the composite is aided both by the creation of pores by excipient dissolution as well as by PBS diffusion directly into the polymer backbone. Plain silicone is highly hydrophobic and does not swell when immersed in an aqueous solvent. The addition of lactose and cisplatin (both hydrophilic) likely alters the hydrophobicity of the composite material, allowing passage of PBS through the polymer backbone and subsequent swelling.[115] The presence of excipient crystals inside the composite matrix is necessary to act as the driving force for water uptake into the composite generating an osmotic pressure. The more lactose a sample contains the faster it is expected to release cisplatin in phase 1. Lactose is readily soluble in aqueous solvents and so a network of interconnected pores will form sooner in samples containing a greater proportion of lactose. Lactose is also significantly more hydrophilic than cisplatin (logP -5.4 vs. -2.27 respectively) and so a composite containing a larger proportion of lactose is likely rendered more hydrophilic and allows passage of PBS into its polymer backbone faster. This rate dependence on lactose content is indeed observed in the phase 1 cisplatin release profile of the CDDP10, CDDP25 and CDDP40 formulations: the less cisplatin (and so more lactose) the sample contained, the faster it released the drug. The CDDP5 formulation however did not follow the trend, its phase 1 rate falling in between those of

CDDP40 and CDDP25. This may be attributed to the fact that CDDP5 contains too little cisplatin and the availability of the drug is what causes this formulation's slower release.

As excipient crystals – both lactose and cisplatin – are dissolved away from the composite, the hydrophobic nature of the silicone matrix encourages the composite surface to try and shrink in order to minimize exposure to the aqueous solvent.[113] This shrinking force opposes the PBS flux into the matrix, but the osmotic pressure between the cisplatin- and lactose-rich composite and the surrounding PBS allows the solvent to continue entering the composite, swelling it and dissolving more cisplatin and lactose.[113] The cisplatin release rate however slows down due to the shrinking of the composite surface, the increasing swelling of the sample and resulting elastic contraction forces and the osmotic flow of solute into the matrix, giving rise to the slower phase 2 for all four formulations. Phase 2 corresponds to the intermediate stage described by Molina et al.[113] The trend is now reversed in terms of cisplatin release rate vs. lactose content for CDDP5, CDDP10 and CDDP25: the higher the lactose content the slower the cisplatin release in phase 2. This is attributed to an increased swelling of the composite with increased lactose content that results in increased elastic contraction forces within the composite opposing the osmotic pressure generated by the undissolved excipients.

Osmotic solvent flow into the composite and further cisplatin and lactose dissolution continues in phase 3, the last phase evident in the 109-day release. Phase 3 is expected to last until the expanded network inside the swollen composite is able to exert an elastic contraction force equivalent to the osmotic pressure and so hinder further solute diffusion.[113] The CDDP5, CDDP10 and CDDP25 formulations all displayed a decreased cisplatin release rate during phase 3 as compared to the release

rate during phase 2, and the rate decrease was more dramatic with decreasing cisplatin content. The CDDP40 formulation on the contrary displayed a slight acceleration in cisplatin release during phase 3. The behavior of the four formulations during phase 3 can be explained as follows. The total solid powder content in all formulations was constant at 50% w/w_{total} and so the formulations with lower cisplatin content had higher lactose content. Lactose is readily soluble in water and its dissolution upon exposure to an aqueous solvent like PBS is not rate limiting. The rate of swelling across formulations upon immersion in PBS is expected to increase with increasing lactose content as a result. The elastic contraction force and subsequent network rigidity occurring during swelling as described previously will follow a similar trend, becoming effective at hindering cisplatin diffusion and counterbalancing the osmotic gradient earlier on in the *in vitro* release process as the lactose-to-cisplatin proportion is increased across formulations. The CDDP40 formulation, containing more cisplatin than lactose, is most likely accelerating cisplatin release during phase 3 because the swelling of the sample is not sufficient to fully counterbalance the osmotic solute gradient and diffusion of the now-dissolved cisplatin from within the pores of the composite to the outside solution. The cisplatin release rates during each phase are plotted as a function of lactose content in Figure 2.5 to illustrate this point further.

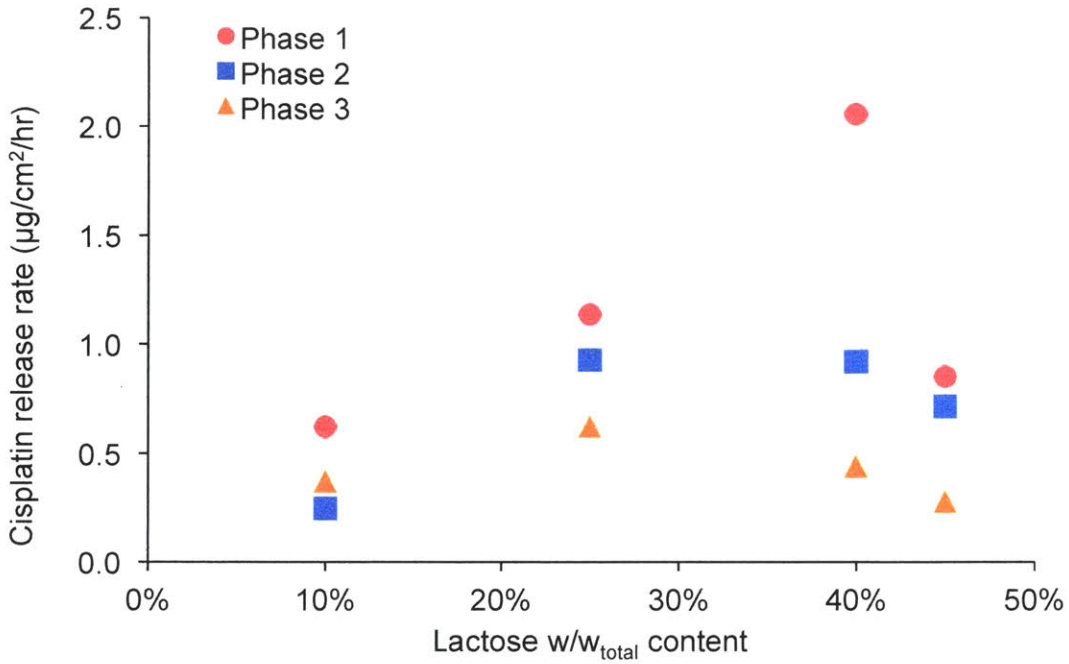

Figure 2.5: Cisplatin release rate plotted as a function of formulation lactose content. As the lactose content increases the phase 1 release rate (pink circles) increases until a certain percentage of lactose after which the amount of cisplatin in the sample is too little to continue the trend and the cisplatin release rate drops (CDDP5 formulation at 45% lactose content). This observation is due to the fact that the total solid powder content in each formulation is kept constant while ratios of cisplatin and lactose are varied. A similar trend is observed for phases 2 (blue rectangle) and 3 (yellow triangle) although less pronounced than in phase 1 likely due to the fact that sample swelling is counteracting aqueous solution entry into the matrix and slowing down cisplatin release universally. The release rate consistently drops from phase 1 to phase 3 for all but the CDDP40 formulation. The CDDP40 formulation instead exhibits a slightly faster release rate in phase 3 compared to phase 2. This formulation contains more cisplatin than lactose and so during phase 3 the swelling of the sample is likely no longer sufficient to counteract the osmotic solute gradient and diffusion of the now-dissolved cisplatin from within the pores of the composite.

It is important to note that the total excipient content of 50% w/w$_{total}$ was selected based on preliminary experiments as well as the existing literature in an effort to create interconnected pores throughout the thickness of a composite sample. Having such a network of interconnected pores would theoretically allow the entire excipient load to be released once immersed in an aqueous solvent assuming sink conditions are maintained around the sample. It may be however that the excipient content is not

enough to fully connect all the excipient crystals to each other, leaving some crystals undissolved inside the sample. This is not expected to be an issue as long as enough crystals are in contact to sustain cisplatin release at the desired rate for the desired amount of time and so deliver the intended cumulative cisplatin dose to the patient. The porosity and pore interconnectivity of the composite material could be assessed quantitatively by various methods including analysis of z-stacks of SEM images, mercury porosimetry, permeability tests based on Darcy's law, gas adsorption and the Brunauer-Emmett-Teller equation as well as three-dimensional imaging such as micro-computed tomography, magnetic resonance imaging and confocal or multiphoton microscopy.[116]

The *in vitro* cisplatin release data were used to determine which of the four formulations would be best suited to use as the basis for a clinically relevant implant, including material fine-tuning, *in vitro* anticancer toxicity assessment and *in vivo* evaluation in animal models. The CDDP25 formulation was selected for further development based on (i) its near-zero-order cisplatin release profile for the entire duration of the 109-day release studies that exhibited small changes in release rate from one phase to the next and (ii) its average cisplatin release rate (0.780 $\mu g/hr/cm^2$, weighted average 0.773 $\mu g/hr/cm^2$) that was the largest of the four initial formulations.

The average disk sample mass and estimated cisplatin content for each formulation tested in these *in vitro* release studies are listed in Table 3, along with the amount of cisplatin released over 109 days *in vitro* calculated as a percentage of the sample payload. These calculations illustrate that only a fraction of the total cisplatin

payload was released over 109 days, suggesting that these composites can continue releasing drug for a much longer period of time if necessary.

Formulation	Average sample mass (mg)	Estimated cisplatin content (mg)	Total cisplatin released after 109 days (mg)	Fraction released (%)
CDDP5	27.82	1.39	0.797	57
CDDP10	31.64	3.16	1.292	41
CDDP25	34.10	8.53	1.286	15
CDDP40	25.95	10.38	0.598	6

Table 2.3: Cisplatin content release characteristics for the four composite formulations over 109 days *in vitro*. Average sample mass, estimated cisplatin content per sample based on the % $w_{cisplatin}/w_{total}$ formulation ratio, average total cisplatin released as determined quantitatively by HPLC in studies 1-4 of Figure 6 and calculated fraction of total cisplatin content per sample that was released over the 109-day *in vitro* release period are given for each of the four formulations. All formulations released less than 60% of their estimated cisplatin content with CDDP5 releasing the most (57%) and CDDP40 releasing the least (6%) of their respective payloads. CDDP40 contains primarily cisplatin that dissolves over a much longer timescale in aqueous solvents compared to lactose and therefore is expected to be the slowest-releasing formulation. These values suggest that all formulations could continue release past the 109 days until they had released their entire payload or until the only cisplatin remaining was trapped in spots not accessible to the interconnected network of pores created through dissolution of cisplatin and lactose by PBS.

2.3.4 *In vitro* cytotoxicity

CDDP25 samples were as effective as an equivalent *in vitro* cisplatin solution in killing both cisplatin-sensitive and cisplatin-resistant human ovarian cancer cells *in vitro*. No cytotoxicity was observed as a result of exposure to Ecoflex 00-30 alone or the lactose-only composite LAC50. Cells treated with cisplatin were exposed to either a single 5 mm-diameter CDDP25 disk (total surface area 0.628 cm^2, average release rate 0.777 $\mu g/cm^2/hr$) or a cisplatin solution containing 11.7 µg of cisplatin (the equivalent amount of drug released over 24 hours). Cell viability for each group is plotted in Figure 2.6. It is important to note that the CDDP25 disk released cisplatin gradually while the equivalent

cisplatin solution group was exposed to the entire 24-hour cisplatin amount from the start of treatment. The CDDP25 disk was still able to accomplish greater cell toxicity against both the cisplatin-sensitive UCI101 cell line and the cisplatin-resistant SKOV3 cell line compared to the equivalent cisplatin solution. The difference was not statistically significant when compared across all groups with a one-way ANOVA with Tukey's multiple comparisons test. This difference in cell kill may however be explained in part by the fact that cisplatin loses its activity over time in solution.[117,118] The drug's half-life *in vitro* at 37°C has been reported to range from less than 2 hours (in human blood, plasma or ultrafiltrate)[119] to almost 12 hours (in RPMI 1640 cell culture medium supplemented with 10% FBS)[120]. Media changes in this study were performed every 24 hours. The CDDP25 disk releases freshly dissolved drug steadily over the 24-hour period. The equivalent cisplatin dose accomplishes a high-dose cisplatin exposure that may then start to diminish after a few hours as the drug degrades whereas the disk continues to release fresh, active cisplatin over time. The drug more readily kills cisplatin-sensitive cells and so this effect of a high transient dose vs. a low continuous dose is more dramatic with cisplatin-resistant cell lines like SKOV3 that are harder to kill with cisplatin. Dose-dense chemotherapy has been championed as an approach to help address drug resistance in many types of cancers including ovarian cancer and this phenomenon may be attributed to a similar mechanism.[121-123] The findings of the *in vitro* cytotoxicity studies confirm .that the drug released from the CDDP25 composites is active against both cisplatin-sensitive and cisplatin-resistant cancer cells as expected and that no other component of the composite material (the silicone matrix or the lactose sacrificial excipient) is causing any of the observed cytotoxicity.

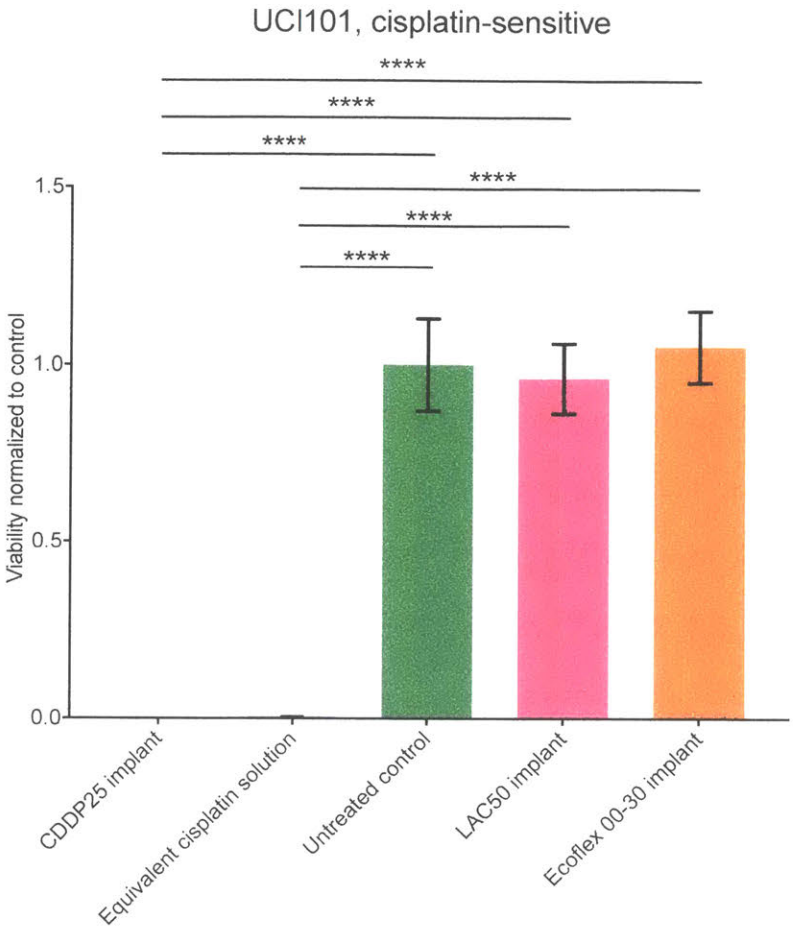
UCI101, cisplatin-sensitive
****
****
****
****
****
****
1.5
1.0
0.5
0.0
Viability normalized to control
CDDP25 implant
Equivalent cisplatin solution
Untreated control
LAC50 implant
Ecoflex 00-30 implant

A

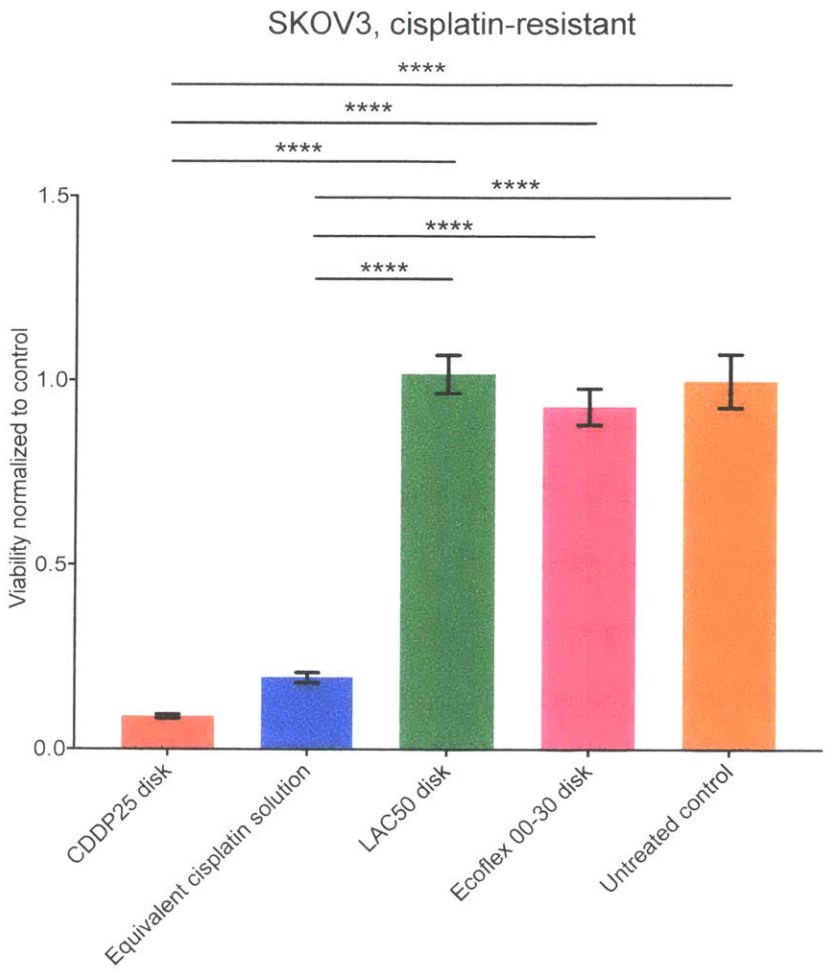

B

Figure 2.6: Cytotoxicity of the CDDP25 composite formulation against cisplatin-sensitive (UCI101) and cisplatin-resistant (SKOV3) human ovarian cancer cell lines. Cells were cultured as monolayers. (A) and (B) present the normalized viability after 72hrs of exposure to either a CDDP25 disk in a Transwell insert (red, n=3), an equivalent cisplatin solution in cell culture media (blue, n=3), regular cell culture media (green, n=3), a LAC50 disk in a Transwell insert (pink, n=2) or an Ecoflex 00-30 disk in a Transwell insert (yellow, n=2). LAC50 and Ecoflex 00-30 caused no cytotoxicity to either cell line while the CDDP25 disk resulted in greater cell kill compared to an equivalent cisplatin dose but the difference was not statistically significant based on one-way ANOVA with Tukey's multiple comparisons test across all groups.

2.3.5 *In vivo* composite toxicity

CDDP25 5 mm-diameter disks implanted intraperitoneally in mice were well tolerated and did not cause any toxicity as confirmed by animal weight tracking, CBC and histological examination of key abdominal organs known to suffer toxicity as a result of cisplatin treatment (liver, kidneys, spleen, small and large intestine, bone marrow) (Figure 2.7). All examined organs appeared normal and a thin capsule was seen around the CDDP25 implant displaying very little fibrosis after 15 days of implantation (Figure 2.8), which helps address any concern about fibrous capsule formation around the implant hampering cisplatin release from its surface. No remarkable histological differences were noted in any of the organs examined in the IP injection group. CBC with differential showed that the white blood cell (WBC), lymphocyte (LY) and red blood cell (RBC) counts were largely within normal bounds (dashed lines in Figure 2.7B-D) for all mice at euthanasia. Platelet (PLT) count was within normal bounds for mice implanted with the CDDP25 formulation but was slightly below normal for mice that received a single 4 mg/kg IP injection of cisplatin, suggesting possible thrombocytopenia (Figure 2.7E). Thrombocytopenia is a known side effect of platinum chemotherapy that is commonly addressed by supplementing with thrombopoietic agents like thrombopoietin, reducing the chemotherapy dose or, in extreme cases, stopping chemotherapy altogether.[124] The reduction in platelet count in the IP group is small and the value is still close to the normal lower bound. It is possible that 48 hours are not enough to actually see meaningful changes in platelet survival based on the cell half-life (7-10 days in human patients).[124] This finding however may be indicative of hematopoietic toxicity caused by the bolus IP cisplatin injection that is absent when treating with the CDDP25 formulation.

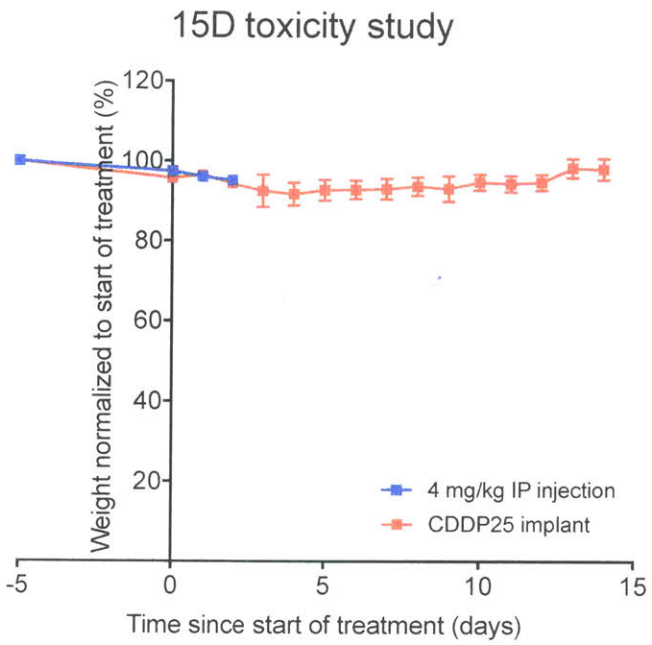
15D toxicity study
Weight normalized to start of treatment (%)
120
100
80
60
40
20
4 mg/kg IP injection
CDDP25 implant
-5
0
5
10
15
Time since start of treatment (days)

A

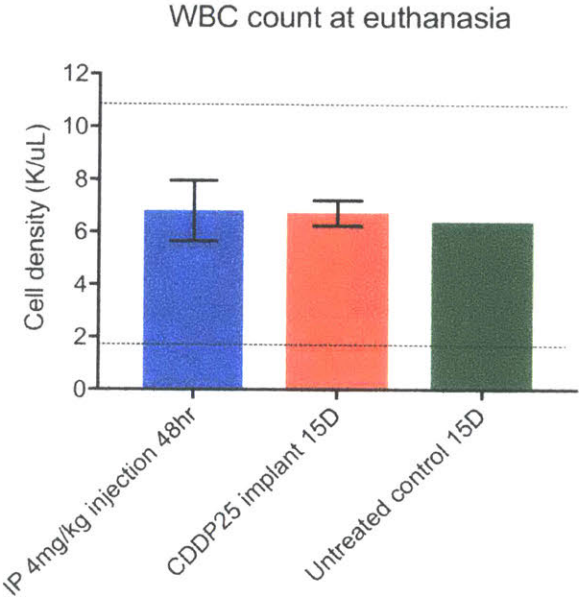
WBC count at euthanasia
Cell density (K/uL)
12
10
8
6
4
2
0
IP 4mg/kg injection 48hr
CDDP25 implant 15D
Untreated control 15D

B

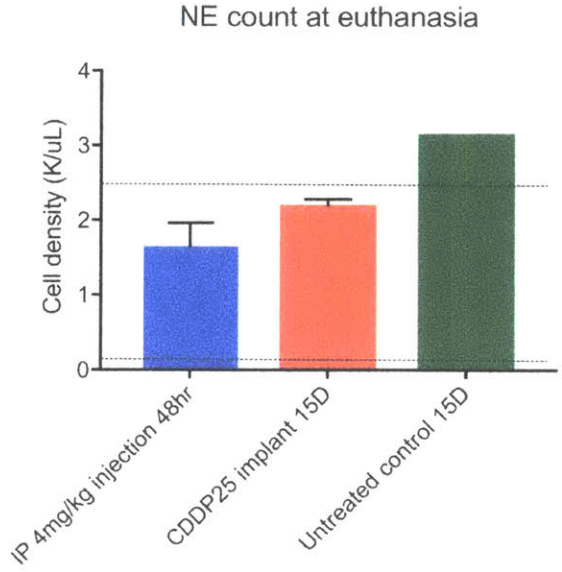
NE count at euthanasia
Cell density (K/uL)
0
1
2
3
4
IP 4mg/kg injection 48hr
CDDP25 implant 15D
Untreated control 15D

C

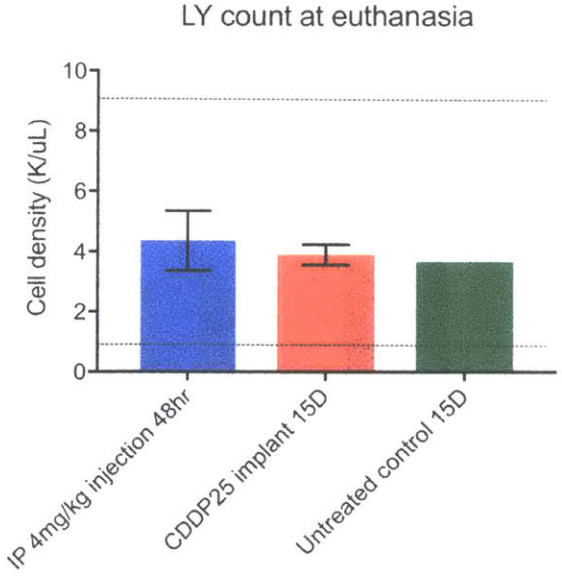
LY count at euthanasia
Cell density (K/uL)
0
2
4
6
8
10
IP 4mg/kg injection 48hr
CDDP25 implant 15D
Untreated control 15D

D

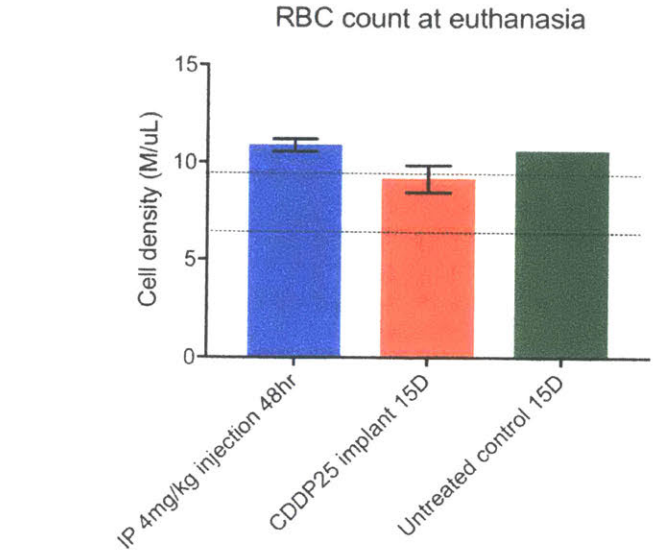

E

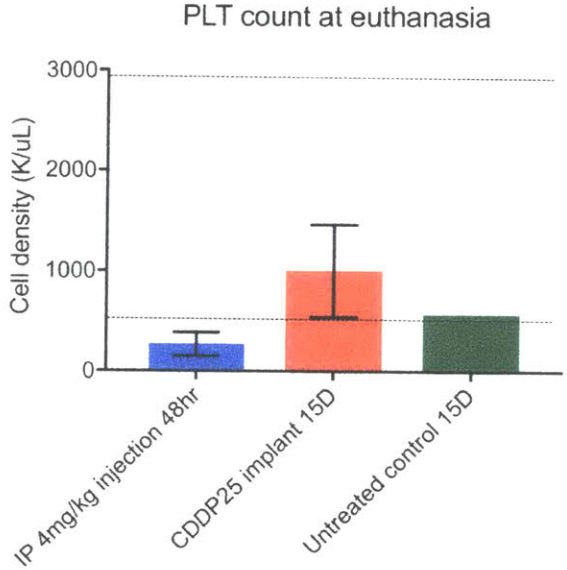

F

Figure 2.7: *In vivo* toxicity results of 15-day implantation with a CDDP25 disk. (A) is a plot of average mouse weight normalized to its value at the start of treatment and tracked starting five days before start of treatment and through the treatment period for CDDP25-implanted mice (red line) and mice receiving a single 4 mg/kg IP cisplatin injection (blue line). The latter group was euthanized 48 hours after injection to observe any toxicity caused by the cisplatin before the tissues had a chance to regenerate so weight tracking stops on day 2, the last day of the group's treatment period. Both groups showed relatively stable weights with the CDDP25 group animals experiencing a slight weight loss after surgery,

which is expected, and recovering from it by day 7. (B)-(F) are plots of the average cell density of white blood cells, neutrophils, lymphocytes, red blood cells and platelets respectively for each of the two treatment groups. Values were obtained by CBC with auto-differential from samples collected at euthanasia. A healthy animal was included to provide a normal control as an extra security check against the normal bounds given by the CBC analysis software. All values were within normal bounds for all groups with the exception of platelet counts for the mice receiving a singe 4mg/kg IP injection, which were low. Dashed lines indicate normal value bounds.

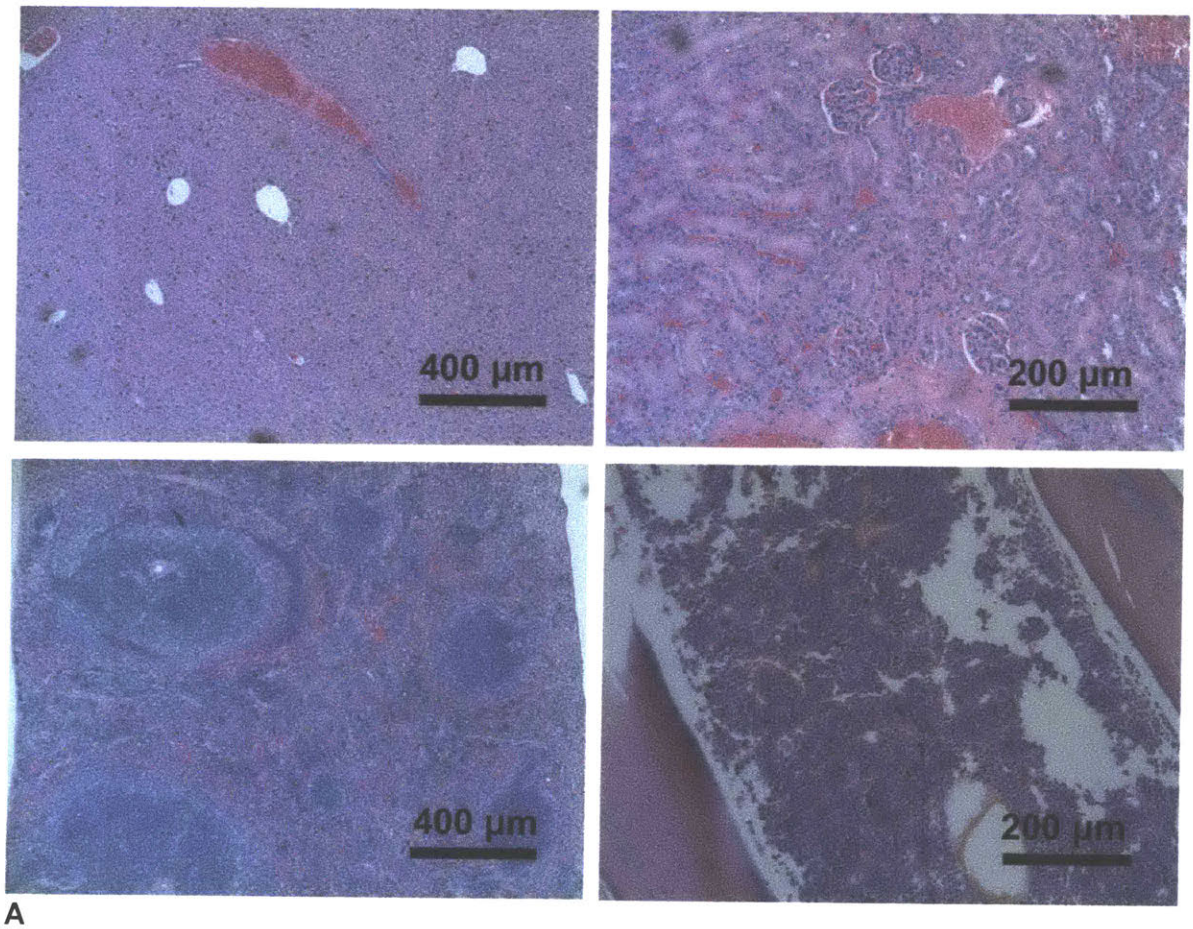

A

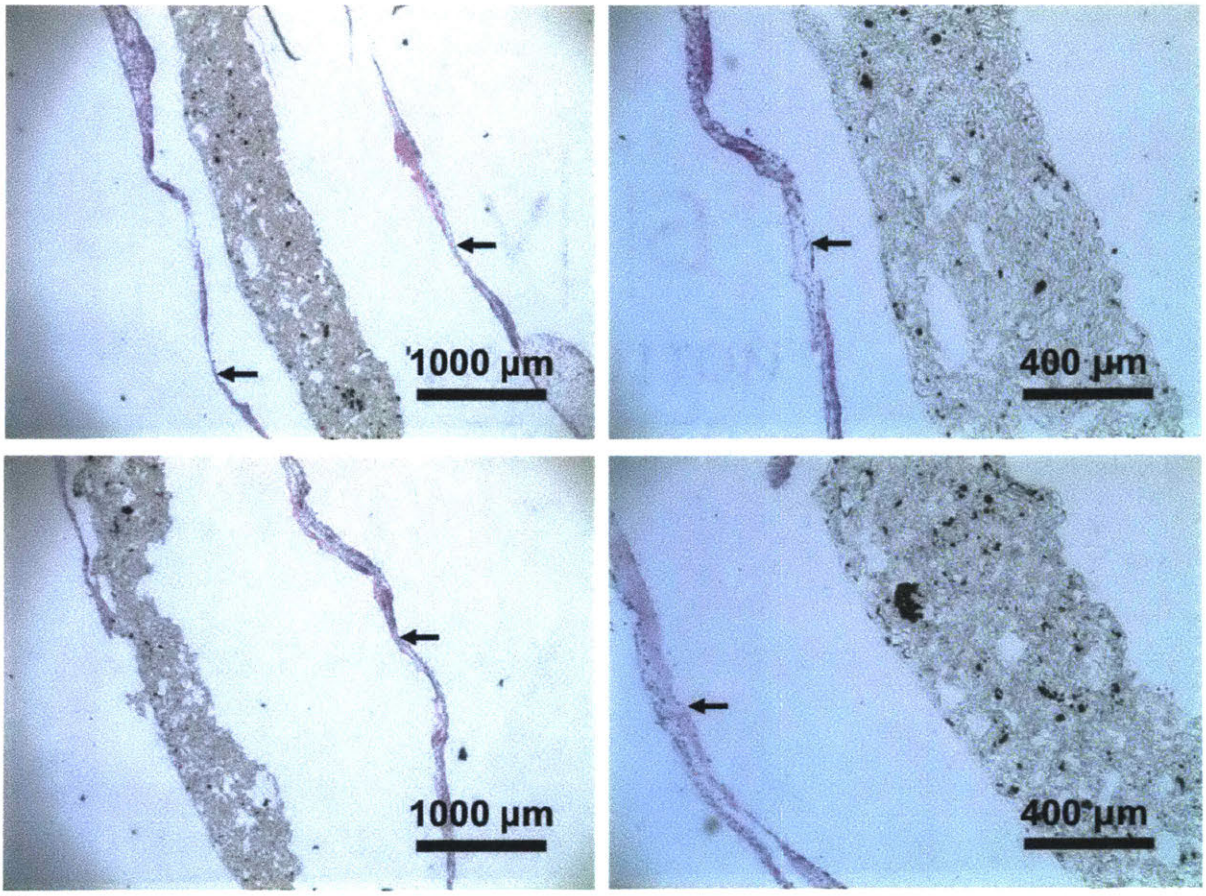

B

Figure 2.8: Representative histology with H&E staining from mice implanted with a CDDP25 disk for 15 days. (A) Clockwise from top left: liver, kidney, bone marrow and spleen sections showed no tissue pathology. (B) Representative implant and surrounding capsule sections from the two mice in the toxicity study. A thin capsule was noted around the implant displaying a very small amount of fibrosis. Arrows point to capsule.

2.3.5 *In vivo* abdominal platinum distribution

The CDDP25 disks resulted in a higher concentration of platinum (Pt) in μg Pt/g tissue compared to a 4 mg/kg IP injection of cisplatin after 15 days of implantation in all organs examined while the blank Ecoflex 00-30 implants resulted in a negligible concentration of Pt in all organs examined (Figure 2.9). The difference in Pt concentration was statistically significant for the liver (3.265 μg/g vs. 0.313 μg/g, $p < 0.0001$), the kidneys (5.247 μg/g vs. 0.403 μg/g, $p < 0.0001$), the small intestine (0.970 μg/g vs. 0.170 μg/g, $p < 0.0001$), the large intestine (1.198 μg/g vs. 0.145 μg/g, $p = 0.006$) and the ovaries and uterus (1.320 μg/g vs. 0.191 μg/g, $p = 0.0118$). There was no statistical significant difference in Pt levels for any tissue between the single IP injection and blank Ecoflex 00-30 implant groups. All the values for all organs across the three groups are tabulated in Table 2.4.

The average *in vitro* cisplatin release rate for the CDDP25 implant was 0.488 μg/hr (using an average of 0.777 $\mu g/cm^2/hr$ from Table 2 and multiplying by the implant surface area). This translates to a weekly cisplatin dose of approximately 82 μg. A 4 mg/kg IP cisplatin injection delivers approximately 80-100 μg of cisplatin to an average mouse weighing 20-25 g. The total amount of cisplatin delivered by an implant over a two-week period would therefore be approximately 1.6-2X the amount delivered by a single 4 mg/kg IP injection based on *in vitro* release data. The *in vivo* release rate, even though not quantified yet, is expected to be lower due to any small amount of fibrosis encasing the implant, the presence of tissues and in particular of fat in direct contact with the implant surface as well as due to the higher protein content of the peritoneal fluid compared to PBS that is likely to slow down fluid uptake into the implant and cisplatin dissolution. The difference, if any, in total cisplatin delivered over the intended

treatment period for each group is nevertheless not sufficient to explain the significantly higher levels of platinum in all abdominal tissues after implantation with the CDDP25 sample compared to an IP cisplatin injection. This difference points to the fundamental issue of drug clearance from the peritoneal cavity following bolus administration that results in a transient drug concentration spike that may not necessarily translate to elevated penetration of the drug into the tissues of interest in the abdomen. A continuous low-dose releasing implant can however accomplish such an elevated platinum content in these tissues and may thus be able to more effectively and consistently expose microscopic metastases throughout the peritoneal cavity to cisplatin.

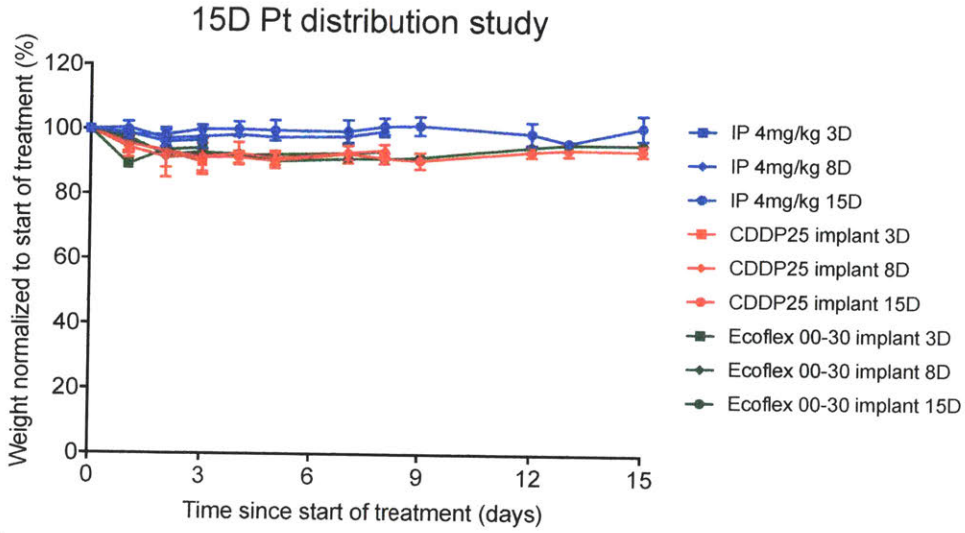
15D Pt distribution study
Weight normalized to start of treatment (%)
120
100
80
60
40
20
0
0
3
6
9
12
15
Time since start of treatment (days)
IP 4mg/kg 3D
IP 4mg/kg 8D
IP 4mg/kg 15D
CDDP25 implant 3D
CDDP25 implant 8D
CDDP25 implant 15D
Ecoflex 00-30 implant 3D
Ecoflex 00-30 implant 8D
Ecoflex 00-30 implant 15D

A

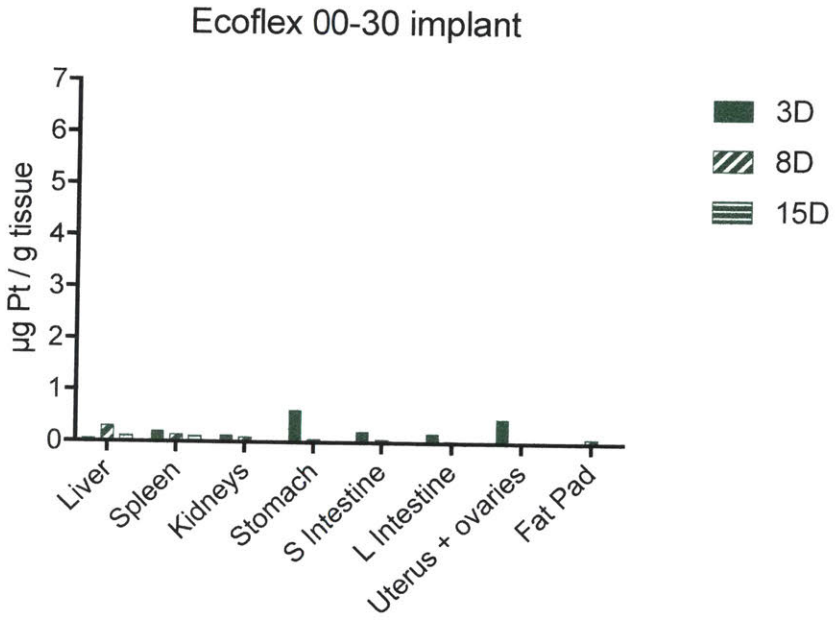
Ecoflex 00-30 implant
µg Pt / g tissue
7
6
5
4
3
2
1
0
Liver
Spleen
Kidneys
Stomach
S Intestine
L Intestine
Uterus + ovaries
Fat Pad
3D
8D
15D

B

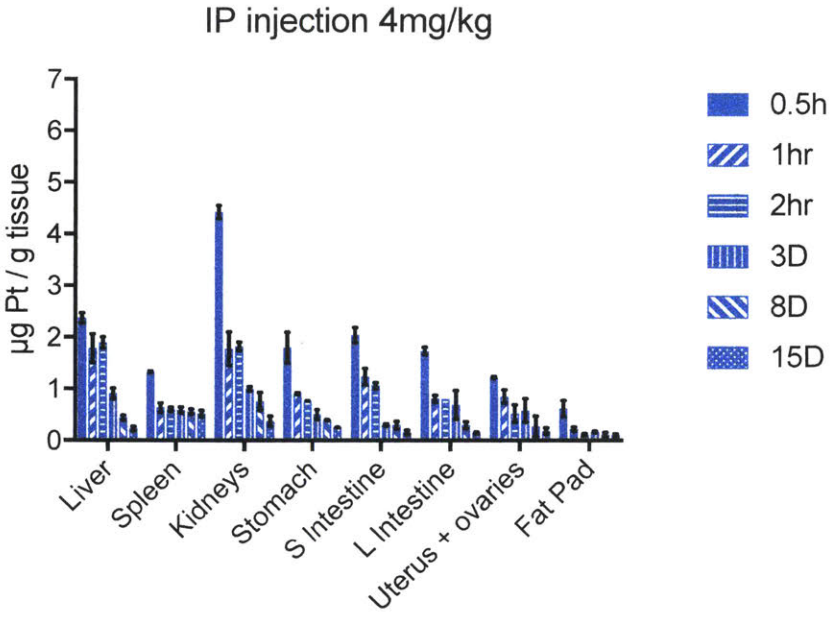
IP injection 4mg/kg
µg Pt / g tissue
0
1
2
3
4
5
6
7
Liver
Spleen
Kidneys
Stomach
S Intestine
L Intestine
Uterus + ovaries
Fat Pad
0.5h
1hr
2hr
3D
8D
15D

C

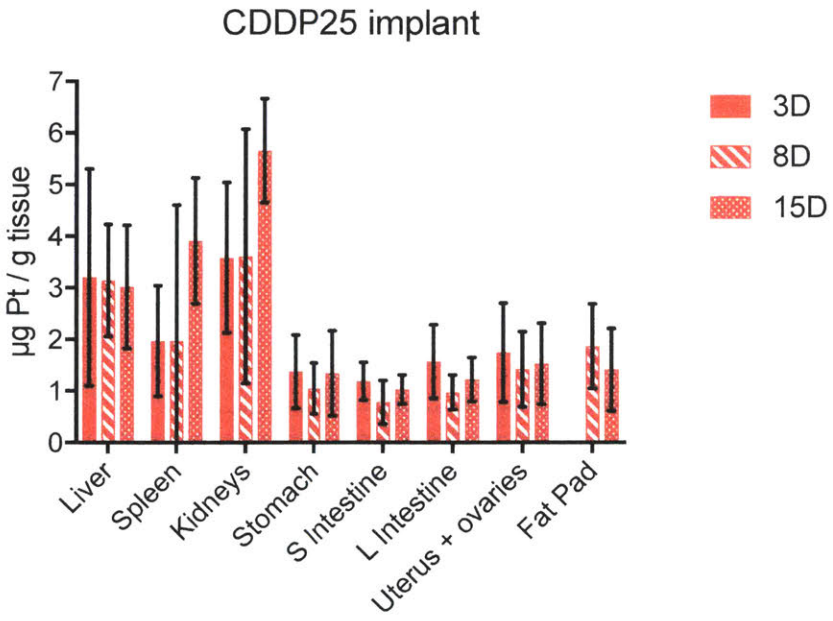
CDDP25 implant
µg Pt / g tissue
0
1
2
3
4
5
6
7
Liver
Spleen
Kidneys
Stomach
S Intestine
L Intestine
Uterus + ovaries
Fat Pad
3D
8D
15D

D

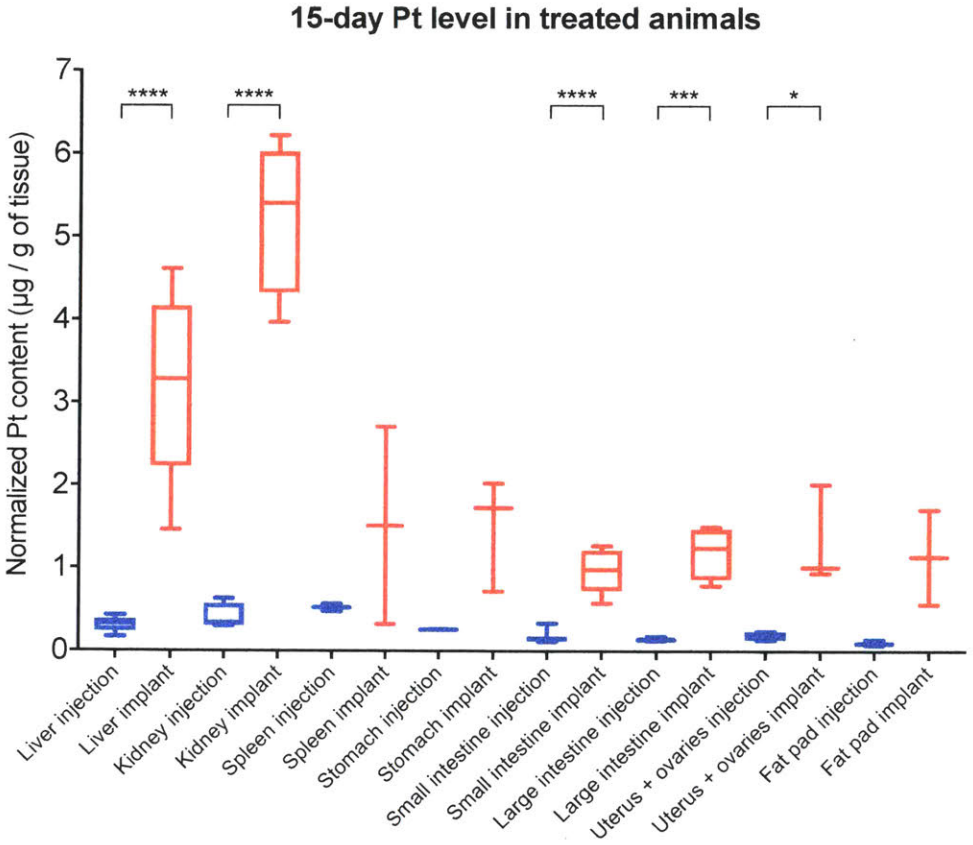

E

Figure 2.9 Platinum distribution results of *in vivo* 15-day CDDP25 disk implantation. (A) Average mouse weight normalized to its value at the start of treatment for each treatment group and each time point. Weights are not included for the ½ hr, 1hr and 2hr IP injection time points since their weight did not change from the start of treatment. None of the groups experienced any dramatic loss in weight suggesting that their overall health remained good throughout the treatment period. Error bars indicate standard deviation from the mean. (B)-(D) Normalized tissue platinum (Pt) content in ppb for each of the abdominal organs examined in the Ecoflex 00-30, single 4mg/kg IP injection and CDDP25 implant group respectively. The Ecoflex 00-30 group exhibited almost negligible Pt content as expected while the IP injection group exhibited a spike in Pt content soon after injection that wore off to almost negligible levels for all organs by 15 days after injection. The CDDP25 implant group exhibited Pt content that was higher than that of the IP injection group on all time points examined for the liver and spleen and was higher than the IP injection group for all organs on the 15-day time point. Error bars indicate standard deviation from the mean. (E) Box-and-whiskers plots of the average normalized tissue Pt content in ppm for the two cisplatin treatment groups only (IP injection and CDDP25 implant) 15 days after the start of treatment. The ends of the box in plot E are the upper and lower quartiles of the data, the lines outside the box indicate the highest and lowest values and the median is marked by the vertical line inside the box. The CDDP25 group had higher normalized Pt content in all organs compared to the IP injection group. The difference was statistically

significant for the liver, kidneys, small intestine, large intestine and ovaries/uterus/fallopian tubes when compared with an unpaired student's t-test. These data support the hypothesis that the CDDP25 implant, even though releasing cisplatin at a much lower dose than that accomplished briefly by the 4 mg/kg IP injection can achieve a higher total exposure of tissue to platinum. The high levels of Pt in the liver, kidneys, spleen and intestines achieved by the CDDP25 implant may however also be cause for concern for toxicity even though mouse weight remained relatively constant throughout the study. A follow-up toxicity study was carried out to confirm that these ppm values were not toxic to the tissues.

Tissue	**Pt level (µg / g tissue)**			**Comparison p-value**		
	CDDP25 implant	IP injection	Ecoflex 00-30 implant	CDDP25 vs. injection	CDDP25 vs. Ecoflex 00-30	Injection vs. Ecoflex 00-30
Liver	3.265	0.313	0.139	<0.0001	<0.0001	0.841
Kidneys	5.247	0.403	0.018	<0.0001	<0.0001	0.764
Spleen	1.514	0.522	0.049	0.724	0.643	0.945
Stomach	1.491	0.259	0.035	0.181	0.207	0.944
S Intestine	0.970	0.170	0.015	<0.0001	<0.0001	0.298
L Intestine	1.198	0.145	0.013	0.0005	0.0009	0.758
Ovaries + Uterus	1.32	0.191	0	0.013	0.014	0.809
Fat pad	1.136	0.104	0.037	0.181	0.279	0.992

Table 2.4: Platinum levels in tissues for all animal groups in the 15-day Pt distribution study. The p-values of comparing the mean of each group to the mean of every other group using one-way ANOVA with Tukey's multiple comparisons test are also tabulated.

2.4 Discussion

The objective of this work was to develop a material as the basis for an IP implant that could release cisplatin in a controlled, sustained manner while being safe for implantation and effective against ovarian cancer *in vitro*. A matrix-type drug delivery system was created to take advantage of the high level of control in drug release that it allows and load the drug in solid form to minimize implant dimensions and preserve drug activity.[2,45,98] The implant is intended for placement in the peritoneal cavity, a complex space that may change in volume depending on the amount of accumulated peritoneal fluid that fluctuates with time and with a person's health status. The peritoneal cavity is also in intimate contact with critical organs of the abdominal viscera like the liver, kidneys, spleen and part of the digestive tract, which can be injured upon contact with a mechanically mismatched implant. A matrix-type system is preferred over a reservoir-type system because it can lead to smaller implant dimensions and offers more tunable mechanical properties than a reservoir filled with solid drug powder.

Mechanical matching to surrounding tissue is a critical component of what makes an implant safe and well tolerated *in vivo*. Mechanically mismatched implants can trigger a foreign body response: an immune response to the implant that attempts to encapsulate it in a fibrous sheath and therefore isolate it from the surrounding tissues and the rest of the body. Mechanically mismatched implants may, beyond the foreign body response, directly irritate and traumatize tissues that they come in contact with inside the abdominal cavity. This can lead to the formation of adhesions – fibrous tissue bands bonding abdominal organs and tissues together and causing side effects that range from pain and discomfort to potentially life-threatening complications like bowel

obstruction.[125-127] Adhesions not only reduce a patient's quality of life but have also been stipulated to affect effectiveness of IP-delivered chemotherapy in cancer treatment due to the obstructive effect of the scar tissue in the distribution of the chemotherapy solution in the peritoneal cavity.[128,129] A silicone elastomer was used to create composite cisplatin-eluting materials because silicone elastomers have well-documented biocompatibility and minimized fibrotic response as long-term implants.[130-133] Ecoflex 00-30 was used in particular because it is readily available off-the-shelf, has mechanical properties similar to those of soft tissue, has been certified as safe for skin contact and has previously been implanted *in vivo* in animals over the course of multiple weeks with no adverse biocompatibility findings.[99,102,134]

Cisplatin was used as the chemotherapeutic agent of choice because it is part of the first-line standard of treatment for many cancers that metastasize to the peritoneal cavity including ovarian cancer. Cisplatin is slightly hydrophilic (logP -2.27)[135] while Ecoflex 00-30 is hydrophobic being a silicone elastomer. Lactose was used as the sacrificial pore-generating excipient of choice because it is an excipient commonly found in the pharmaceutical industry that poses very low risk of adverse patient side effects, is readily soluble in water and has a molecular weight similar to that of cisplatin.

Structural examination of the composite materials developed in this work confirmed that they comprised a polymer matrix with solid powder crystals uniformly distributed throughout the sample thickness. EDS examination confirmed that the solid powder crystals comprised lactose and cisplatin randomly distributed in the silicone matrix with no evidence of dissolution or partition.

Preparation of the composite materials developed in this work involves a straightforward and simple mixing and casting method that ensures ease of fabrication and of scale-up to produce both larger-sized implants and batches of multiple implants at a time. The pot life of Ecoflex 00-30 is 45 minutes according to the manufacturer but it becomes much shorter for Ecoflex 00-30-based composites with 50% w_{powder}/w_{total}. No attempt was made to measure the pot life of these composites per se but experience casting them places their pot life closer to 15 minutes. This is a disadvantage of using Ecoflex 00-30 that can complicate implant fabrication as it imposes a limit on the amount of working time from combining the two parts of the silicone elastomer to casting and degassing the sample before it starts to cure. Other silicone candidates like ExSil 100 or ExSil 50 (Gelest, Inc., Morrisville, PA, USA), whose curing time can be highly controlled with temperature, have been identified and preliminary tests have shown that CDDP25 and LAC50 composites can be manufactured using them in place of Ecoflex 00-30. Further testing and development is warranted to confirm controlled, sustained cisplatin release and cytotoxicity *in vitro* as well as tolerability and *in vivo* functionality of these composites.

The mechanical properties of the LAC50 composites produced in this study, measured both after production with no further processing and after a 42-day leaching period in PBS that simulated a 6-week IP implantation, were found to fall within the range of values typical of organs in the abdominal cavity. Histological examination of CDDP25 disks implanted *in vivo* in the peritoneal cavity of healthy, immunocompetent mice that can mount a foreign body response with subsequent fibrous capsule formation showed minimal signs of fibrosis after 15 days of implantation. The overall body

condition of the animals implanted with Ecoflex 00-30 disks or CDDP25 disks was good and they were able to return to their pre-surgery weight soon after implantation, suggesting that their overall health status was good while being implanted with the disks (Figures 2.6A, 2.7A). These data combined provide evidence that the composite implants developed in this study are mechanically well matched to the surrounding tissues in the abdominal cavity and can be implanted safely from a mechanical properties perspective. They can therefore form the basis for a peritoneal implant of appropriate dimensions to achieve the desired cisplatin dose and surface area for drug delivery for ovarian cancer patients with microscopic peritoneal metastases left behind after surgical debulking.

The four different composite formulations developed were found to release cisplatin in a controlled, sustained manner over a period greater than 100 days *in vitro* under physiologic temperature and pressure. Their cisplatin release profiles are in accordance with a matrix-type drug delivery system driven by drug dissolution and diffusion through the pores generated throughout the polymer matrix by the leached solid powder. A brief 24-hour burst period is followed by three distinct phases of near-zero-order release for all formulations. All formulations released only a fraction of their total payload after 109 days *in vitro*, indicating that they could sustain cisplatin release for a longer period of time. The total duration of treatment for ovarian cancer patients receiving IP chemotherapy is 18 weeks (6 chemotherapy cycles x 3 weeks/cycle).[18,23,136] Each cycle lasts 3 weeks because it includes a 2-week drug-free break to allow the patient to recover from the severe toxicity and side effects caused by the bolus maximum-tolerated-dose chemotherapy infusion. A treatment regimen like the

one proposed in this work that relies on continuous low-dose chemotherapy instead of periodic maximum-tolerated-dose chemotherapy would presumably last shorter than 18 weeks. The composites developed here are however expected to sustain treatment over 18 weeks or even longer if necessary.

The CDDP25 formulation, selected for further testing and development based on its *in vitro* cisplatin release rate, showed cytotoxic activity *in vitro* against both cisplatin-sensitive and cisplatin-resistant human ovarian cancer cells. Its cytotoxic activity was at least as effective as that of an equivalent cisplatin solution and no cytotoxic effect could be attributed to the sacrificial lactose excipient or the Ecoflex 00-30 matrix alone. The CDDP25 formulation was in fact found to be more effective against the cisplatin-resistant SKOV3 cells than an equivalent cisplatin solution. This may be attributed to the continuous release of freshly dissolved, active cisplatin from CDDP25 contrasted with the cisplatin degradation occurring over time in the equivalent cisplatin solution. Degradation of cisplatin due to temperature, pH or exposure to light is an important consideration that may affect a solution's therapeutic potency.[117,118]

CDDP25 disks were able to release cisplatin *in vivo* after IP implantation in mice and they resulted in higher tissue platinum content at the 15-day time point in all harvested abdominal organs compared to a single 4 mg/kg IP cisplatin injection. The statistically significant higher platinum levels found in the liver, kidneys and spleen of the mice implanted with CDDP25 disks along with the fact that cisplatin has known toxicity against these organs warranted further confirmation that these elevated values were not associated with organ toxicity. It was also important to assess whether the cisplatin dose released by the CDDP25 disks *in vivo* was well tolerated overall. Neither

the physical presence of the CDDP25 disks nor the cisplatin dose that they released *in vivo* caused toxicity as tracked by weight loss, histologic examination of abdominal organs or CBC values. H&E-stained slides of the liver, spleen, kidneys, small and large intestine and bone marrow of the animals did not show any histologic abnormalities. The white blood cell, lymphocyte, neutrophil, red blood cell and platelet counts of the mice were all within normal values throughout the implantation period. These data taken together provide evidence for the *in vivo* functionality of the CDDP25 disks in delivering cisplatin in the peritoneal cavity at a dose that was well tolerated and at the same time resulted in higher platinum concentration in key abdominal organs compared to a bolus cisplatin IP injection. An implant releasing low-dose cisplatin continuously in the peritoneal cavity can thus accomplish higher platinum levels in target organs compared to bolus dosing without causing toxicity. These platinum levels however may be due to tissue accumulation of both cisplatin and its inactive degradation products. A way to differentiate between these sources of platinum in the tissue or an assessment of antitumor efficacy in addition to platinum accumulation will help answer whether these higher platinum levels seen with the CDDP25 implants translate into tumoritoxic advantage. This platinum distribution study additionally did not differentiate between tissue close to the edge of organs and deeper tissue when quantifying tissue platinum concentration. The penetration depth of IP platinum chemotherapy is a cornerstone of its benefit over systemic chemotherapy administration and various methods including heat and pressure have been explored to enhance it further.[118,137-142] The size of tumors left behind after cytoreductive debulking surgery in fact critically affects the outcome of

IP chemotherapy in patients and so understanding how deep inside a tissue mass can continuous low-dose cisplatin penetrate will be a critical next step.[11,18,23]

Chapter 3: Development of Spheroid-based Ovarian Cancer Models to Capture the Impact of Residual Tumor Size on the Effectiveness of Intraperitoneal Chemotherapy*

3.1 Introduction

Surgical tumor debulking is one of the most important components of treating advanced ovarian cancer that has metastasized to the peritoneal cavity. The current standard of care calls for optimal cytoreduction whenever possible leaving behind sub-centimeter tumors.[14,68,69,143-145] Residual tumor size affects tumor response to subsequent chemotherapy particularly for IP administration but the mechanism that controls drug transport into residual tumors is debated. Ovarian cancer tumor models with controlled dimensions were developed *in vitro* using spheroids. They were then exposed to different cisplatin dosing regimens mimicking intermittent high-dose and continuous low-dose treatment in order to better understand how spheroid size affects response to the drug. Small spheroids were found to respond the same way to intermittent high-dose and continuous low-dose cisplatin. Large spheroids were found to shrink most effectively after exposure to a continuous cisplatin regimen delivering the largest cumulative dose.[83] These findings support the diffusion-controlled theory regarding drug penetration into subcentimeter residual tumors and underscore the importance of optimal surgical debulking for treating ovarian cancer patients with IP chemotherapy. Continuous low-dose IP cisplatin has previously been shown to be as effective in treating mice with human ovarian tumor xenografts as intermittent high-dose IP cisplatin while causing less toxicity.[45] Ovarian cancer mouse models based on spheroids were

* Parts of this chapter were reproduced or adapted from Tanenbaum and Mantzavinou et al. (2017).[7]

piloted to attempt tighter control of tumor size at the start of treatment and more diffuse dissemination of nodules throughout the peritoneal cavity in efforts to more closely recapitulate the clinical appearance of advanced ovarian cancer after optimal surgical cytoreduction. These models hold promise to more accurately assess the efficacy of continuous low-dose vs. intermittent high-dose IP cisplatin as a follow-up to this work. The *in vitro* and *in vivo* findings of this work illustrate the critical role that debulking surgery plays in affecting the prognosis of ovarian cancer patients, the need to better standardize the outcome of debulking surgery in terms of residual disease, the urgency to develop animal models that more closely resemble patients after debulking surgery when assessing the efficacy of new treatment regimens particularly for IP delivery and the promise of adjuvant IP chemotherapy for superior outcomes in ovarian cancer patients with microscopic residual tumors after surgery.

3.2 Materials and Methods

3.2.1 Chemicals and materials

AggreWell 400 and AggreWell 800 24-well plates containing 1200 (AggreWell 400) or 300 (AggreWell 800) microwells per well with a 400-μm (AggreWell 400) or 800-μm (AggreWell 800) microwell diameter were purchased from StemCell Technologies (Vancouver, Canada). RPMI 1640 cell culture medium with no added L-glutamine, 0.25% trypsin-EDTA, FBS and 100x penicillin-streptomycin-glutamine were purchased from Thermo Fisher Scientific (Cambridge, MA, USA). Pluronic F-127 was purchased from Sigma-Aldrich (St. Louis, MO, USA). Sterile cell culture grade water, sterile phosphate-buffered saline (PBS) and Becton-Dickinson ultra-fine U-100 insulin syringes 3/10 cc 31G were purchased from VWR International (Radnor, PA, USA). Medical injection-grade cisplatin solution (100 mg/100 mL) for use in the spheroid cisplatin exposure studies was purchased from McKesson Medical-Surgical (Richmond, VA, USA). Sterile, non-tissue culture treated 24-well polystyrene plates were purchased from Thermo Fisher Scientific (Waltham, MA, USA). Luciferin was purchased from PerkinElmer (Waltham, MA, USA).

3.2.2 Cell culture

The UCI101 cell line expressing the firefly luciferase gene was provided by Dr. G. Scott Rose (University of California, Irvine, CA, USA). The A2780 cell line expressing the firefly luciferase gene was purchased from Sigma-Aldrich (St. Louis, MO, USA). Cells were pathogen tested in 2015 by the Comparative Pathology Laboratory at MIT and in 2018 by the High-Throughput Screening Core at the MIT David H. Koch Institute for

Integrative Cancer Research and tested negative for mycoplasma. Cells were grown as monolayers at 37°C with 5% CO_2 using RPMI 1640 medium containing 10% FBS and 1% pen-strep-glut and were subcultured with 0.25% trypsin-EDTA at regular time intervals to maintain cell densities below 80% confluence. Cell monolayers were trypsinized at approximately 80% confluence for the creation of spheroids. Cells were not used after passage number 13.

3.2.3 Spheroid formation

AggreWell 400 plates were used to generate (i) UCI101 spheroids of approximately 100- or 200- µm diameter comprising 100 or 2000 cells per microwell and (ii) A2780 spheroids of approximately 100-, 150-, 175- or 200-µm diameter comprising 100, 500, 1000 or 2000 cells per microwell for in the *in vitro* cisplatin exposure and shrinkage evaluation studies. AggreWell 400 and AggreWell 800 plates were used to generate UCI101 spheroids of approximately 190-, 200- or 300-µm diameter respectively comprising 1250, 2000 or 10000 cells per microwell for the *in vivo* spheroid model pilot studies. Each well of an AggreWell 400 or 800 plate was filled with 500 µL of 5% sterile pluronic F-127 in cell culture-grade water to create a coating that prevents cell adhesion to the microwell wall. Plates were centrifuged at 3500 RPM for 5 minutes to fill the microwells within each well with the pluronic solution (5810R Centrifuge, Eppendorf, Hamburg, Germany). Plates were examined under a microscope to confirm that no air bubbles remained in the microwells. A second centrifugation step was carried out if air bubbles were present in order to eliminate them. Plates with wells containing the pluronic solution were subsequently incubated at room temperature for 30 minutes and

then washed twice with sterile cell culture-grade water and twice with FBS-free cell culture medium (500 µL per wash). The last culture medium wash was not removed from the wells until immediately before adding the cell suspension for spheroid formation. The cell suspension for spheroid formation was prepared in FBS-free cell culture medium to prevent cell division overnight during spheroid formation and thus achieve greater accuracy at estimating cell number per spheroid. To add the cell suspension, each well was aspirated but not fully to prevent formation of air bubbles in the microwells. 500 µL of homogeneously mixed cell suspension were added to each well at a specific cell density to accomplish a desired spheroid diameter. Spheroids of approximately 100-, 150-, 175-, 190-, 200- or 300-µm diameter comprising 100, 500, 1000, 1250, 2000 or 10000 cells per microwell translated to 1.2×10^5, 6×10^5, 1.2×10^6, 1.5×10^6, 2.4×10^6 or 3×10^6 cells per well respectively. Plates were then centrifuged at 1000 RPM for 5 minutes to distribute cells within the microwells and incubated at 37°C with 5% CO_2 for 24 hours to allow the cells to form spheroids. Spheroids were imaged *in situ* in the AggreWell plates using transmitted light microscopy (Invitrogen EVOS FL Auto Cell Imaging System, Thermo Fisher Scientific).

3.2.4 Spheroid cisplatin treatment and shrinkage evaluation

Only spheroids measuring 100 or 200 µm in diameter (comprising approximately 100 or 2000 cells respectively) were used in the cisplatin treatment and shrinkage assessment studies. Spheroids were harvested from AggreWell plates after formation and transferred to non-tissue culture treated 24-well plates for cisplatin exposure. Spheroids were harvested by adding 500 µL of culture media to each well of the AggreWell plate

and using a 1000 µL pipet to gently pipet up and down 2-3 times and dislodge the spheroids from the microwells. Each well was subsequently washed three times with an additional 1000 µL of media per wash to collect remaining spheroids. Spheroids of the same size were collected in a 50 mL conical tube for each cell line and allowed to settle to the bottom of the tube. The FBS-free cell culture medium was aspirated taking care to not aspirate any spheroids and complete cell culture medium was added to a volume that diluted the original spheroid suspension to prevent well overpopulation and minimize spheroid aggregation. The dilutions were as follows: (i) UCI101: 1:2 dilution for 100-µm spheroids and 1:4 dilution for 200-µm spheroids; (ii) A2780: 1:1 dilution for 100-µm spheroids and 1:2 dilution for 200-µm spheroids. 1000 µL of the dilute suspension were added to each well of the non-tissue culture treated 24-well plate.

Four cisplatin treatment conditions were applied to 100-µm and 200-µm spheroids from each cell line by incubating them with cisplatin-containing media at predetermined concentrations for specific amounts of time (Figure 3.1). The four cisplatin treatment groups for UCI101 spheroids were: (i) Untreated control for 72 hours; (ii) IP cisplatin (5 µg/mL) for 2 hours; (iii) Device Low D_L cisplatin (0.14 µg/mL) for 72 hours; and (iv) Device High D_H cisplatin (0.5 µg/mL) for 72 hours. The four treatment groups for A2780 spheroids were: (i) Untreated control for 72 hours; (ii) IP cisplatin (10 µg/mL) for 2 hours; (iii) Device Low D_L cisplatin (0.28 µg/mL) for 72 hours; and (iv) Device High D_H cisplatin (1.0 µg/mL) for 72 hours. The IP cisplatin concentrations for each cell line were chosen based on prior *in vitro* cytotoxicity data using cell monolayers.[45] The D_L cisplatin concentrations for each cell line were chosen to match the total area under the concentration-time curve (AUC) of the IP concentrations

(UCI01: AUC_L = 10 μg-hr/mL; A2780: AUC_L = 20 μg-hr/mL). The D_H cisplatin concentrations were chosen to deliver a higher AUC than the IP dose (UCI101: AUC_H = 36 μg-hr/mL; A2780: AUC_H = 72 μg-hr/mL). Cisplatin dosing varied between the two cell lines to account for previously observed cisplatin sensitivity differences between UCI101 and A2780 monolayers.[45] Doses were additionally increased from those previously used against monolayers to account for the increased chemoresistance reported with three-dimensional ovarian cancer cell spheroids.[85-87,89] Fresh cisplatin solutions were prepared and media changes in the spheroid plates were performed every 12 hours to maintain cisplatin activity throughout the 72-hour treatment period.[120] Media changes were performed in all four treatment groups to account for any handling-induced damage to spheroids not attributed to cisplatin. Spheroids were imaged after 6, 24, 48, and 72 hours of treatment and the ImageJ software was used to measure the length and width of non-aggregated spheroids to calculate average spheroid diameter at each time point. Unless noted otherwise, a total of fifteen spheroids were measured for each spheroid size at each treatment condition and time point for each cell line to calculate an average spheroid diameter.

3.2.5 *In vivo* spheroid model pilot studies

Female Nu/Nu immunodeficient mice (Charles River Laboratories, Wilmington, MA, USA) were used for the *in vivo* spheroid pilot studies. Nu/Nu mice lack a thymus and are therefore unable to produce T-cells making them appropriate for xenograft research. The UCI101 cell line was used to generate spheroids as described previously.

The first pilot study compared orthotopic human ovarian cancer xenografts

generated by IP injection of 3 x 10^6 UCI101 cells as a suspension of 188-μm diameter spheroids to xenografts generated by IP injection of 3 x 10^6 UCI101 cells as a free cell suspension (n=3 mice per group). The second pilot study compared orthotopic human ovarian cancer xenografts generated by IP injection of 3 x 10^6 UCI101 cells as a suspension of 188-μm diameter spheroids to xenografts generated by IP injection of 3 x 10^6 UCI101 cells as a suspension of 301-μm diameter spheroids (n=6 mice per group). For spheroid injections, spheroids were generated as described previously and allowed to settle to the bottom of a 50 mL conical tube after collection from the AggreWell plates. For free cell injections, UCI101 cells were grown as a monolayer, harvested in 50 mL conical tubes when they reached ~80% confluence and centrifuged at 100 g for 5 minutes to create a pellet. The culture medium was aspirated and cold sterile PBS (stored at 4°C) was added to the spheroid or free cell suspension to create a cell density of 3 x 10^6 UCI101 cells / mL of PBS. 1 mL of the spheroid or free cell suspension was loaded into 1 cc syringes using 18G blunt tip needles to prevent spheroid or cell shearing. The blunt tip needles were replaced with 25G or 21G bevel tip needles for *in vivo* injection of 188-μm spheroids/free cells or 301-μm spheroids respectively. Loaded syringes were stored in ice until injection. UCI101 cells grown as monolayers were harvested to create spheroids over 24 hrs as well as prepare the free cell injections for tumor inoculation. Mice receiving free cell injections were injected a day prior to mice receiving spheroid injections as a result in order to use cells of the same passage number in both groups. The rate of tumor uptake and distribution of tumors throughout the mouse abdomen were evaluated noninvasively via bioluminescence imaging (BLI) at regular time points after cell injection using the IVIS

Spectrul Pre-Clinical Trial *In Vivo* Imaging System from PerkinElmer (PerkinElmer, Waltham, MA, USA). Mice were injected intraperitoneally with 5 µL of 30 mg/mL luciferin solution per g of body weight using BD ultra-fine U-100 insulin syringes and imaged 10 minutes after injection. Mice in the first study (188-µm spheroids vs. free cells) were imaged using the two-dimensional modality of the imaging system. Mice in the second study (188-µm spheroids vs. 301-µm spheroids) were imaged using both the two-dimensional and the three-dimensional modality of the imaging system in an attempt to evaluate the size and location of individual tumor nodules more accurately. Both studies continued until all mice required euthanasia. Mice were weighed regularly to monitor overall health and euthanized upon weight loss greater than 20% or poor body condition. Euthanasia was carried out by carbon dioxide inhalation at a steadily increasing flow rate to minimize distress. Tumors and any ascites were collected at euthanasia and their mass was recorded as a direct measurement of tumor burden.

3.2.6 Statistical analysis

A one-way ANOVA with Tukey's multiple comparisons test (InStat GraphPad Software, San Diego, CA, USA) was used to compare average spheroid diameter across treatment groups for each cell line and each spheroid size at each time point. Experiments were done in triplicate for each cell line. Reported results are expressed as mean ± standard deviation from the mean. Differences with p-value < 0.05 were considered to be statistically significant. Statistical significance is indicated as: ns $p >= 0.05$; * $p < 0.05$; ** $p < 0.01$; *** $p < 0.001$; **** $p < 0.0001$.

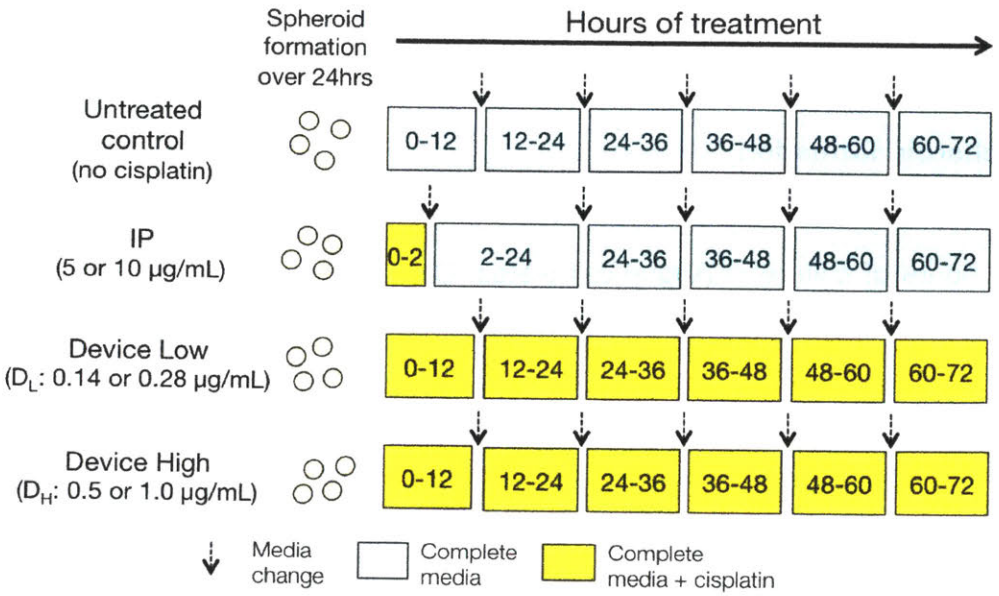

Figure 3.1: Experimental design for spheroid exposure to cisplatin *in vitro*. Adapted from original schematic by L. M. Tanenbaum.[83]

3.3 Results

3.3.1 Spheroid formation

The UCI101 and A2780 human ovarian cancer cell lines were able to form spheroids after 24 hours of culture in AggreWell plates. Different spheroid sizes were formed by adding different cell concentrations in each microwell of the plate (Figure 3.2). The cell number – spheroid diameter range generated for UCI101 and A2780 cells is tabulated in Table 3.1 along with data for 500 and 1000 UCI101 cells per microwell previously collected by L.M. Tanenbaum.

Cells in microwell	Resulting average spheroid diameter (μm)	
	UCI101	**A2780**
100	87.8 ± 10.9	91.8 ± 6.5
500	154.2 ± 4.1	137.3 ± 4.3
1000	173.1 ± 5.2	171.6 ± 5.0
2000	205.7 ± 9.7	197.7 ± 7.1

Table 3.1: Average diameter of spheroids produced with various numbers of cells for the human ovarian cancer cell lines UCI101 and A2780. Diameter is measured using the length and width of each spheroid on ImageJ (n=10 spheroids per group). Data for 500 and 1000 UCI101 cells per microwell collected by L.M. Tanenbaum and reproduced.[46]

The relationship between spheroid diameter D and cell number per spheroid N previously described by Tanenbaum was confirmed by plotting spheroid diameter as a function of the cube root of the number of cells in the microwell:

$$D \propto \mathrm{N}^{1/3}$$

Both cell lines displayed a strong linear relationship with linear best-fit trendlines through the data displaying $R^2 = 0.97$ for UCI101 and $R^2 = 0.99$ for A2780 (Fig. 3.2B,D). The spheroid diameters generated by both cell lines in these studies are clinically relevant because they are similar in size to typical multicellular aggregates present in malignant ascites *in vivo* (30 – 200 μm)[146] and are comparable to the subcentimeter- to submillimeter-sized tumor nodules left behind after optimal surgical cytoreduction.[67,68]

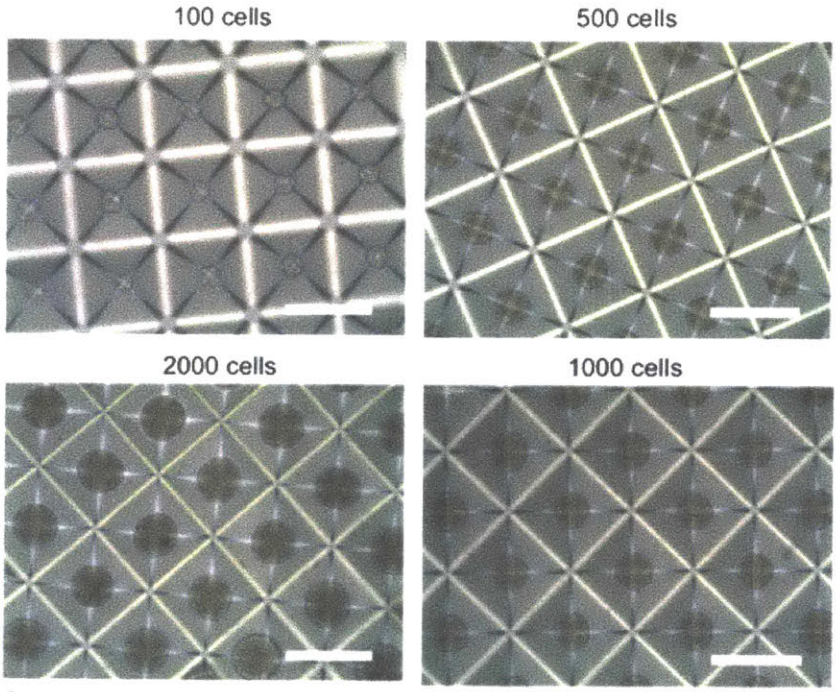

A

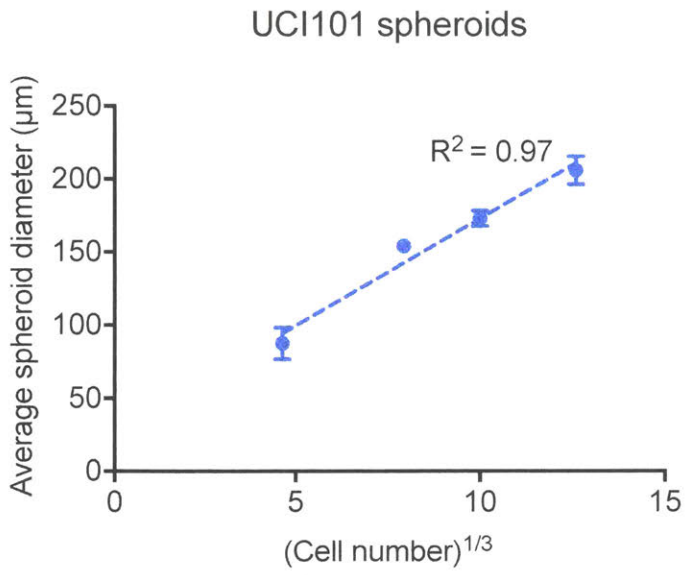
UCI101 spheroids
Average spheroid diameter (µm)
250
200
150
100
50
0
0
5
10
15
$R^2 = 0.97$
$(\text{Cell number})^{1/3}$

B

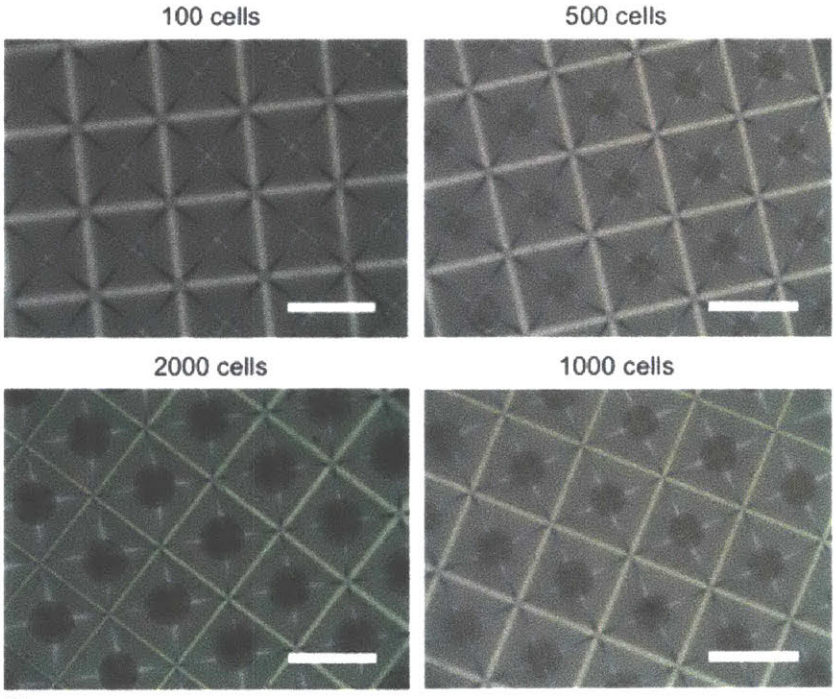
100 cells
500 cells
2000 cells
1000 cells

C

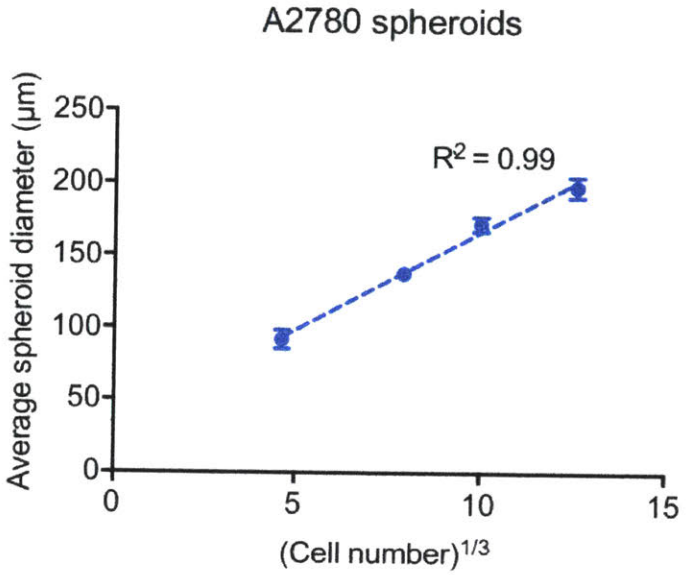

D

Figure 3.2: Relationship between cell number and spheroid size in UCI101 and A2780 spheroids. (A) and (C): UCI101 and A2780 spheroids respectively grown with various cells per AggreWell microwell ranging from 100 to 2000. Spheroid size increased with increasing cell number and the spheroids of all sizes displayed a high degree of sphericity and compactness. Scale bar is 400 µm. 500- and 1000-cell per spheroid data collected by L.M. Tanenbaum and reproduced. (B) and (D): Average spheroid diameter for UCI101 and A2780 cells respectively correlated strongly to the cube root of the cell number for each spheroid size (n=10, R^2=0.97-0.99). Error bars represent standard deviation. Adapted.[83]

3.3.2 Spheroid cisplatin treatment and shrinkage evaluation

Cisplatin treatment of 200-μm spheroids was compared to the treatment of 100-μm spheroids for both cell lines following the treatment regimen outlined in Figure 3.1. Cisplatin works by crosslinking DNA during mitosis, interfering with cell division and causing the cell to become apoptotic after failing to repair the damaged DNA. No spheroid shrinkage is therefore expected until the amount of time the spheroid has been exposed to cisplatin has allowed for cell divisions to occur and for affected cells to become apoptotic. UCI101 cells divide approximately every 24 hours while A2780 cells divide every 13-22 hours. Spheroid shrinkage started becoming apparent at 48 hours after the start of cisplatin exposure for both cell lines (Figures 3.3A, D and 3.4A, D). Average spheroid diameter over time is plotted in Figure 3.3B, E (100-μm spheroids) and Figure 3.4B, E (200-μm spheroids).

Exposure to any cisplatin dosing regimen led to significantly smaller spheroid diameters for both cell lines and both spheroid sizes compared to untreated spheroids at the 72-hour time point ($p < 0.0001$, Figure 3.3 and 3.4 C, F). Both UCI101 and A2780 small spheroids shrunk similarly after exposure to the IP and D_H or D_L cisplatin regimen ($p > 0.05$, Figure 3.3C, F). Both UCI101 and A2780 large spheroids shrunk significantly more after exposure to the IP cisplatin regimen compared to the D_L regimen with the same AUC ($p < 0.001$ for UCI101 and $p < 0.05$ for A2780, Fig. 3.4C, F). Both UCI101 and A2780 large spheroids shrunk significantly more after exposure to the D_H cisplatin regimen with a higher AUC compared to the IP regimen ($p < 0.01$ for UCI101 and $p < 0.001$ for A2780, Fig. 3.4C, F). The D_H dose, in addition to spheroid shrinkage, markedly reduced A2780 spheroid density and spheroid border definition after 72 hours (Figure 3.5). This was especially noticeable in large A2780 spheroids and so diameter

quantification excluded cell debris around the spheroid. The visibly reduced spheroid density of large A2780 spheroids in the D_H group after 72 hours compared to the IP and D_L groups further emphasizes the improved efficacy of this treatment regimen. Average spheroid diameter ± standard deviation for all treatment arms and both cell lines after 72 hours is listed in Table 2. The D_H dosing regimen resulted in an additional reduction of large spheroid diameter by 35.7 µm (UCI101) and 46.3 µm (A2780) compared to the IP regimen translating to a reduction in spheroid volume by 41.0% and 64.4% respectively.

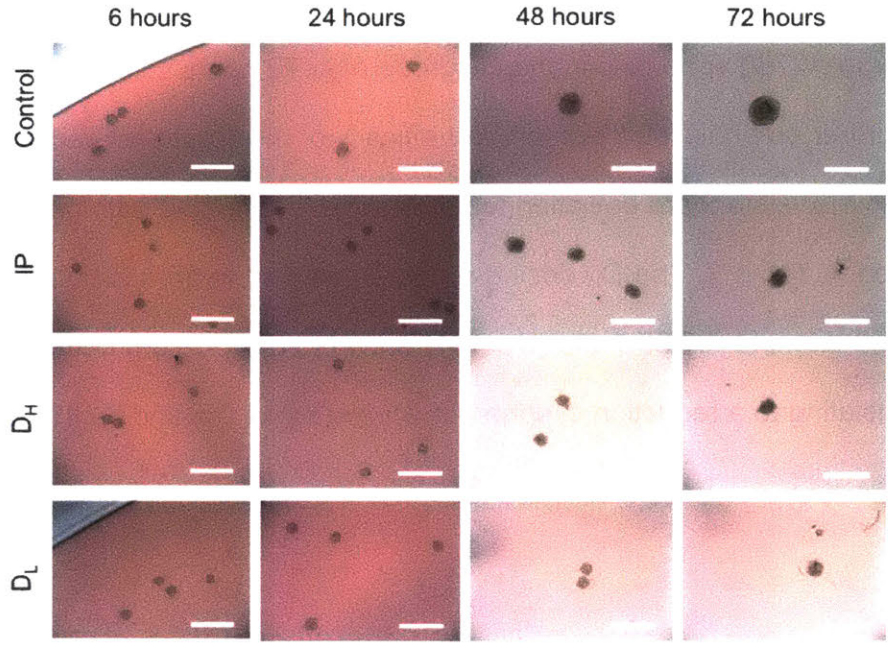
6 hours
24 hours
48 hours
72 hours
Control
IP
D_H
D_L

A

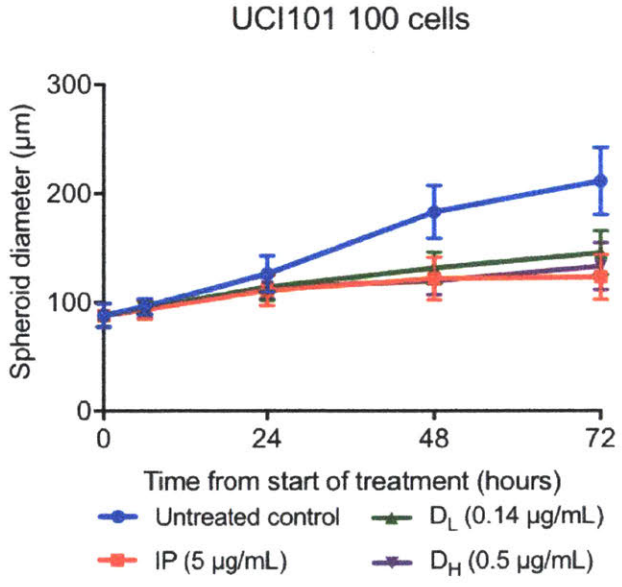
UCI101 100 cells
Spheroid diameter (µm)
300
200
100
0
0
24
48
72
Time from start of treatment (hours)
Untreated control
D_L (0.14 µg/mL)
IP (5 µg/mL)
D_H (0.5 µg/mL)

B

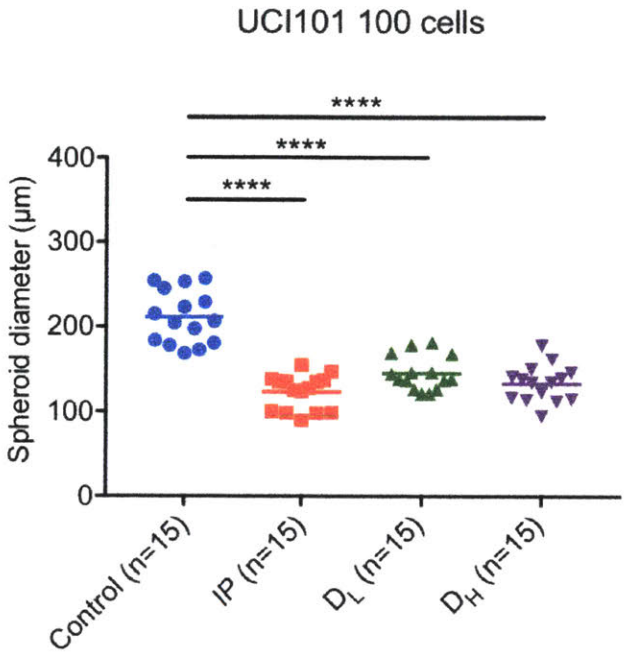
UCI101 100 cells
****
****
****
Spheroid diameter (µm)
400
300
200
100
0
Control (n=15)
IP (n=15)
D_L (n=15)
D_H (n=15)

C

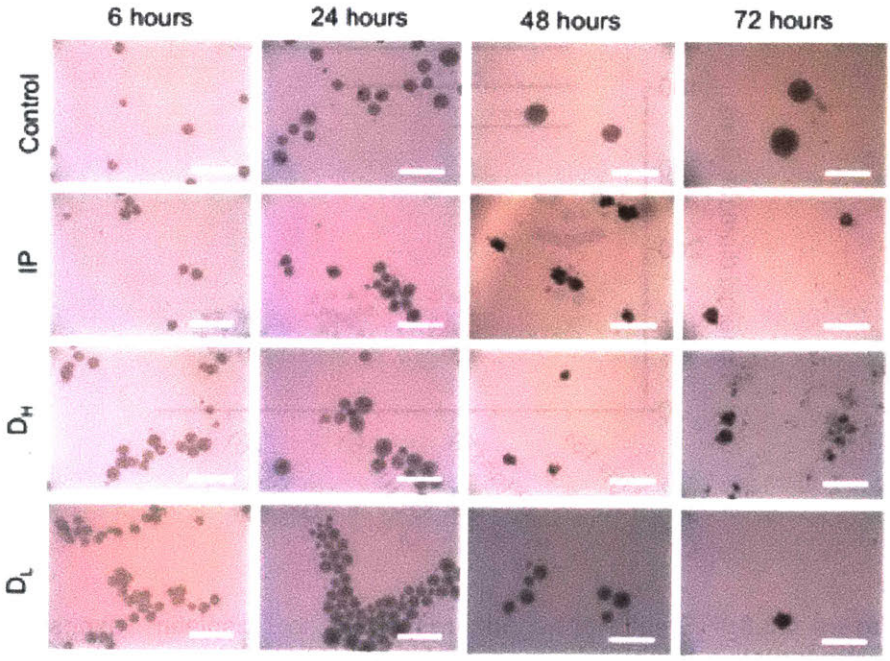
6 hours
24 hours
48 hours
72 hours
Control
IP
D_H
D_L

D

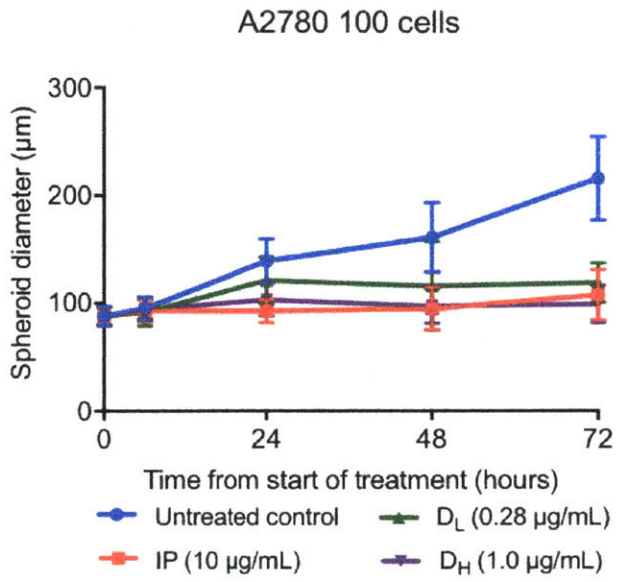

E

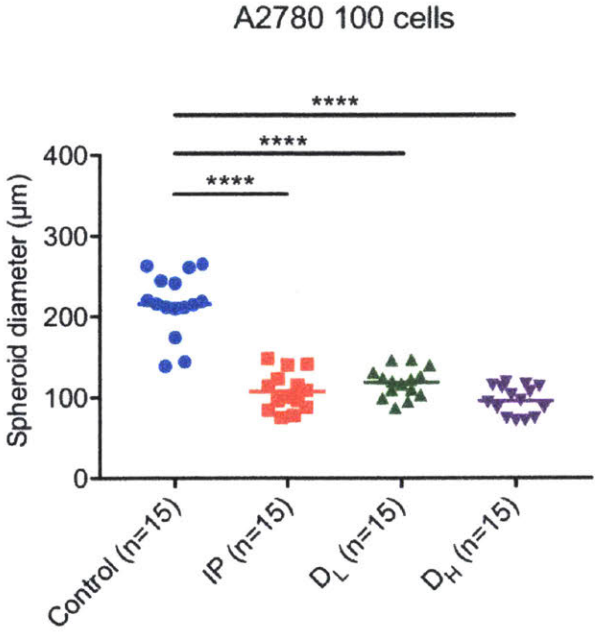

F

Figure 3.3: Small spheroid response to cisplatin exposure. Representative bright field images of small (A) UCI101 and (D) A2780 spheroids at regular time intervals (6, 24, 48, and 72 h) after the start of treatment for all treatment groups (control, IP, device low, device high). Small spheroids had a starting diameter of approximately 100 µm. Scale bars are 400 µm. (B),(E): Average small spheroid diameter throughout the 72- hour treatment period was quantified at regular intervals for untreated control, IP, D_L, and D_H groups for each cell line. (C),(F): Scatter plot of spheroid diameters after 72 h of treatment

showing the mean for each treatment group for small UCI101 and A2780 spheroids. All treated spheroids were significantly smaller than untreated controls after 72 h ($p < 0.0001$). D_L doses with the same AUC as the IP group caused the same degree of shrinkage ($p > 0.05$), and D_H also matched the spheroid shrinkage of the IP group ($p > 0.05$). Only significant comparisons are highlighted in the figure; all other statistical comparisons among treatment groups were not significant ($p > 0.05$). Reported results are expressed as mean ± standard deviation of the mean and n = 15 spheroids for each group. Adapted.[83]

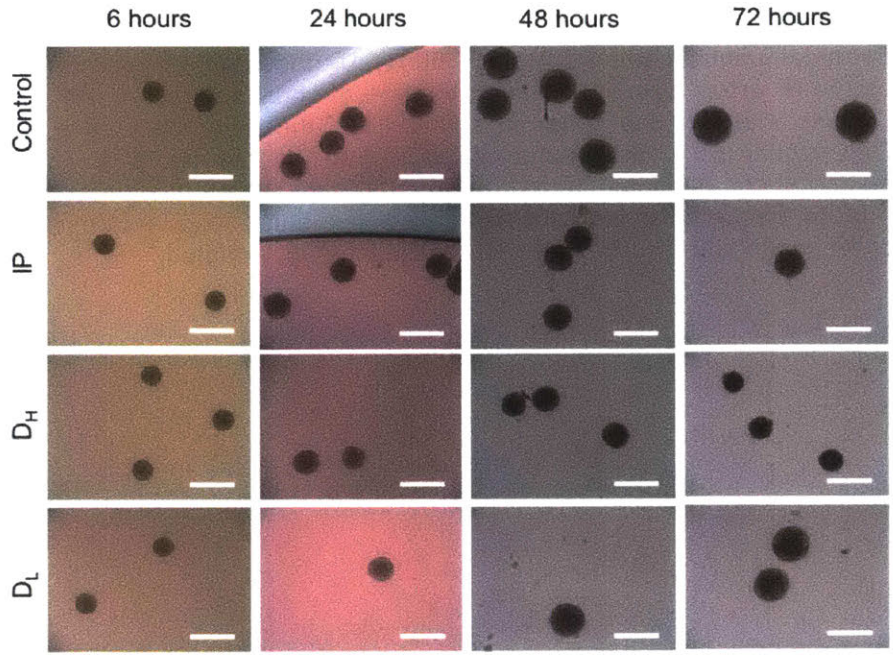
6 hours
24 hours
48 hours
72 hours
Control
IP
D_H
D_L

A

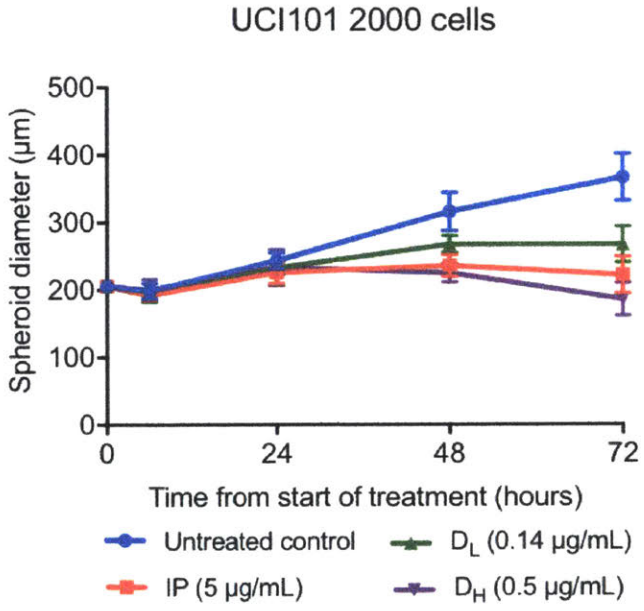
UCI101 2000 cells
Spheroid diameter (µm)
500
400
300
200
100
0
0
24
48
72
Time from start of treatment (hours)
Untreated control
D_L (0.14 µg/mL)
IP (5 µg/mL)
D_H (0.5 µg/mL)

B

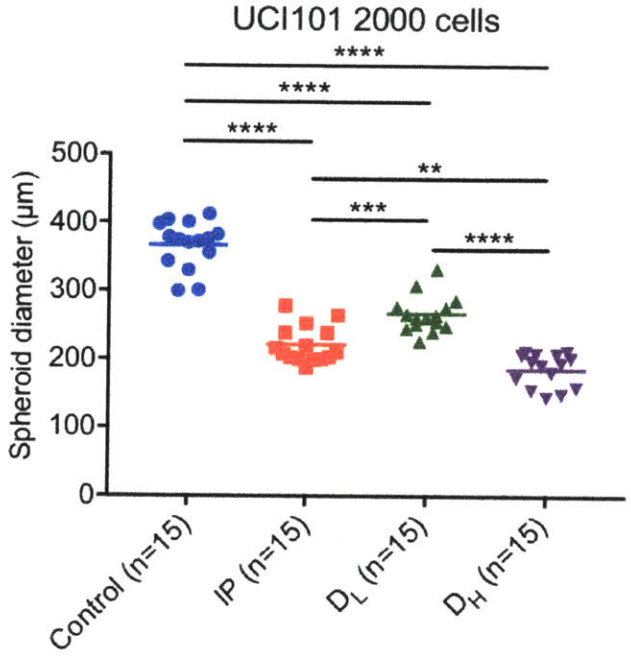
UCI101 2000 cells
****
****
****
**
***
****
Spheroid diameter (µm)
500
400
300
200
100
0
Control (n=15)
IP (n=15)
D_L (n=15)
D_H (n=15)

C

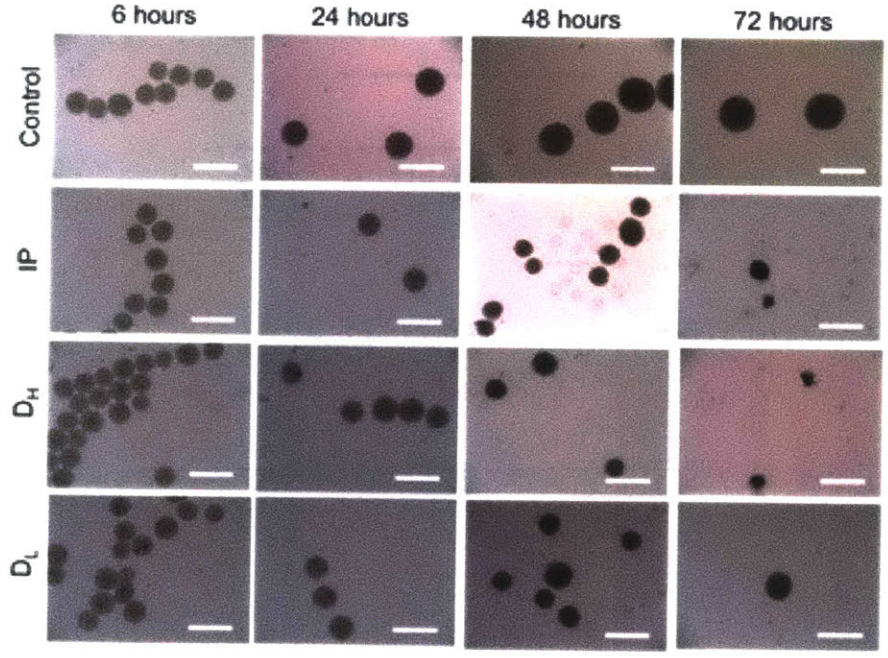
6 hours
24 hours
48 hours
72 hours
Control
IP
D_H
D_L

D

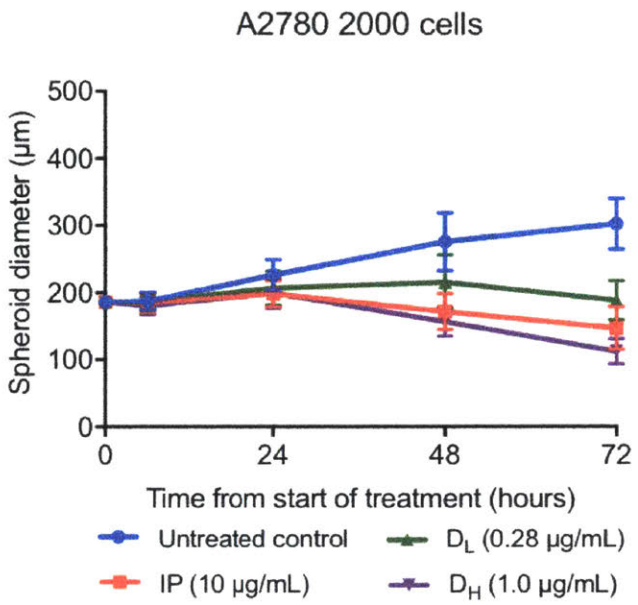

E

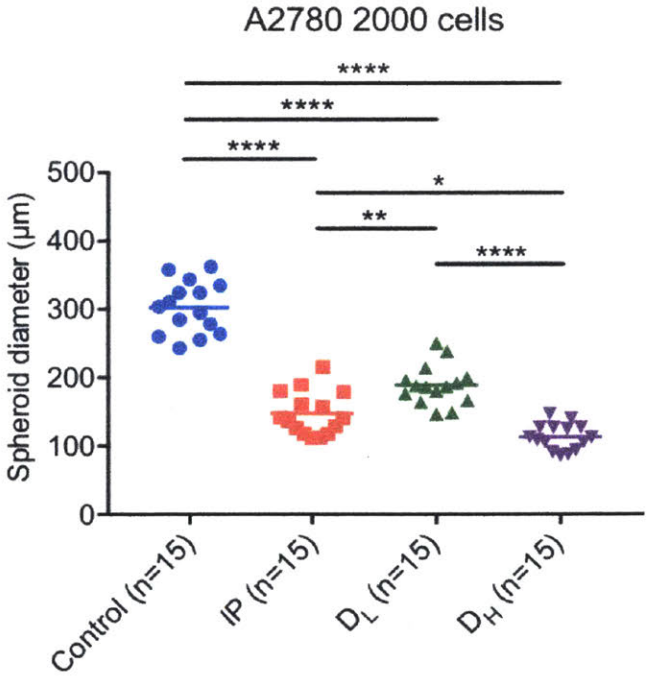

F

Figure 3.4: Large spheroid response to cisplatin exposure. Representative bright field images of large (A) UCI101 and (D) A2780 spheroids at regular time intervals (6, 24, 48, and 72 h) after the start of treatment for all treatment groups (control, IP, device low, device high). Large spheroids had a starting diameter of approximately 200 µm. Scale bars are 400 µm. (B),(E) Average large spheroid diameter throughout the 72- hour treatment period was quantified at regular

intervals for control, IP, device low and device high groups for each cell line. (C),(F) Scatter plot of spheroid diameters after 72 h of treatment showing the mean for each treatment group for large UCI101 and A2780 spheroids. All treated spheroids were significantly smaller than untreated controls after 72 h ($p < 0.0001$). D_L doses with the same AUC as the IP group caused less shrinkage than IP treatment in both cell lines ($p < 0.001$ for UCI101 and $p < 0.01$ for A2780), but high device doses caused more shrinkage than the IP regimen in both cell lines ($p < 0.01$ for UCI101 and $p < 0.05$ for A2780). Only significant comparisons are highlighted in the figure; all other statistical comparisons among treatment groups were not significant ($p > 0.05$). Reported results are expressed as mean ± standard deviation from the mean and n = 15 spheroids for each group. Adapted.[83]

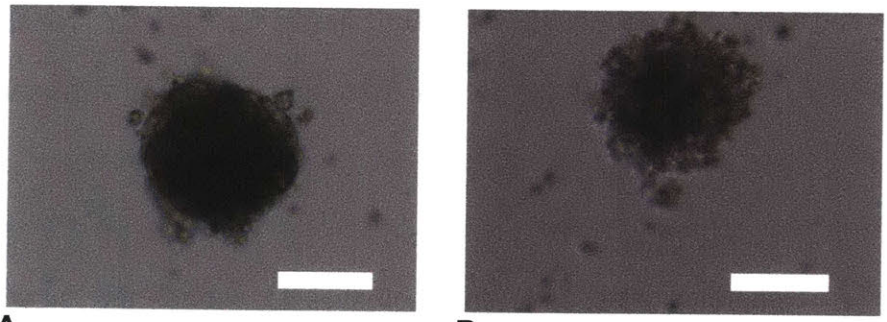

A B

Figure 3.5: Effect of cisplatin exposure on spheroid compactness and border definition. Representative bright field images of A2780 spheroids after a 72-hr cisplatin exposure to either (A) the IP (10 μg/mL for 2hr followed by cisplatin-free media) or (B) the D_H (1.0 μg/mL for 72hr) treatment regimen. Spheroid density and compactness are visibly reduced in the D_H-treated spheroid compared to the IP-treated one. This is an edded indicator of the superior efficacy of this dosing regimen against the A2780 lage spheroids beyond spheroid diameter. Scale bar is 100 μm. Adapted.[83]

	Average spheroid diameter after 72 hours (μm)			
	UCI101		A2780	
Treatment group	**100 cells**	**2000 cells**	**100 cells**	**2000 cells**
Untreated control	211.4 ± 31.1	366.4 ± 34.9	215.7 ± 38.9	302.5 ± 38.1
IP	122.8 ± 20.8	221.3 ± 27.0	107.3 ± 23.2	147.3 ± 31.7
D_L	145.2 ± 20.3	266.8 ± 26.7	118.6 ± 18.2	188.7 ± 29.2
D_H	132.9 ± 21.6	185.6 ± 24.3	95.7 ± 17.8	112.8 ± 18.8

Table 3.2: Average spheroid diameter ± standard deviation for both cell lines after exposure to each type of treatment over a 72-hr period. Adapted.[83]

3.3.3 *In vivo* spheroid model pilot study 1: feasibility

The UCI101 cell line was selected to pilot an *in vivo* orthotopic human ovarian cancer model based on injecting cell spheroids intraperitoneally and compare it to the model previously used in this project that relied on IP inoculation with free UCI101 cells. The goal of this work was to assess whether spheroids could offer a viable tumor inoculation platform to replace free cell injections.

A spheroid-based *in vivo* model is of great interest to this work. Spheroids are expected to seed the peritoneal cavity with disseminated tumors more readily than free cells since they are (i) more robust due to their compactness[147] and extracellular matrix formation[82] (ii) more metastatically aggressive similar to multicellular aggregates shedding from the primary tumor and circulating in the peritoneal fluid of patients.[85,86,88,89] Spheroids also offer the potential to control the size of seeded peritoneal tumors since spheroid size can be accurately determined immediately prior to injection and assuming that they remain relatively non-aggregated when flowing inside the mouse peritoneal cavity and seeding it with tumors. UCI101 spheroids measuring approximately 188 μm in diameter and comprising approximately 1250 cells each resulted in an increase in bioluminescence signal faster than free cells when injected intraperitoneally in Nu/Nu female mice (Figures 3.6 and 3.7). The bioluminescence flux color map also suggested a more widely disseminated disease in the peritoneal cavity, with hot spots of maximum flux (shown in red) appearing as high up in the abdomen as the mouse diaphragm and as low down as the bladder (Figure 3.6).

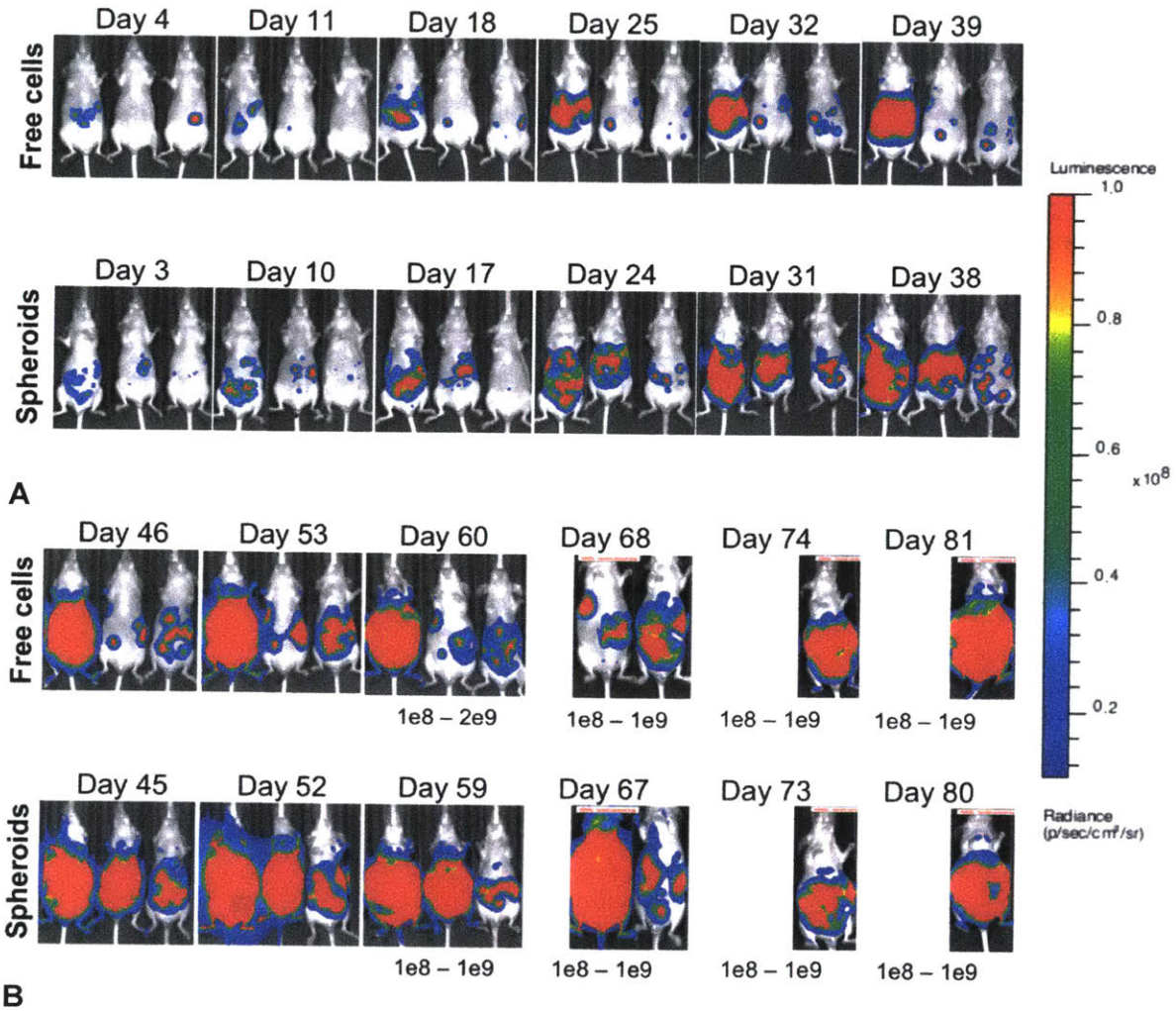

Figure 3.6: BLI flux sequence over 80 days for mice injected with UCI101 free cells or spheroids. Mice received a 3 x 10^6 cell injection either as (A) a free cell suspension or (B) a suspension of spheroids with diameter approximately measuring 186 µm. Mice injected with spheroids developed BLI signal faster and appear to have more diffuse disease throughout the peritoneal cavity compared to those injected with free cells. The color map range is $1e^7$-$1e^8$ for all images until day 60 and range is otherwise noted under the image. With L.M. Tanenbaum.

The average signal over the course of the study was plotted as total flux over time for each group and the results are shown in Figure 3.7. The spheroid group consistently had higher flux values compared to the free cell group especially taking into account the fact that the mice in the spheroid group were imaged a day closer to inoculation day

compared to the mice in the free cell group. The spheroid group also increased their average flux signal more dramatically over the same amount of time compared to the free cell group. The standard deviation from the mean for both groups was however high especially on time points when flux was very high for some of the mice in each group. This variability in the signal prevents any meaningful statistical conclusions to be drawn from this pilot dataset in terms of differences in total flux at comparable time points in the inoculation period.

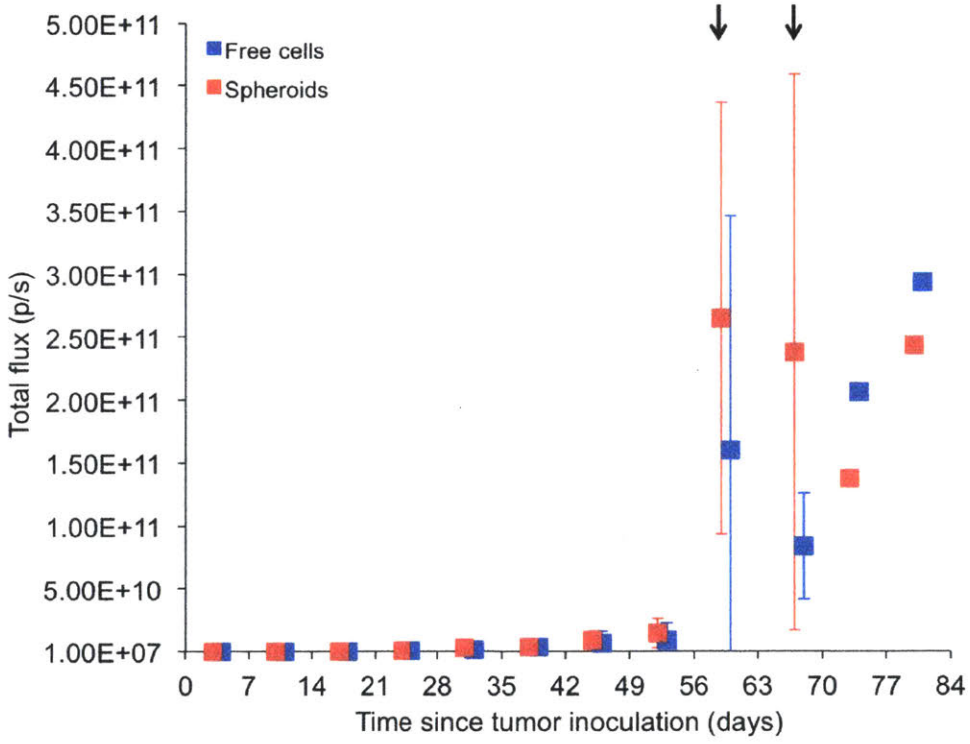

A

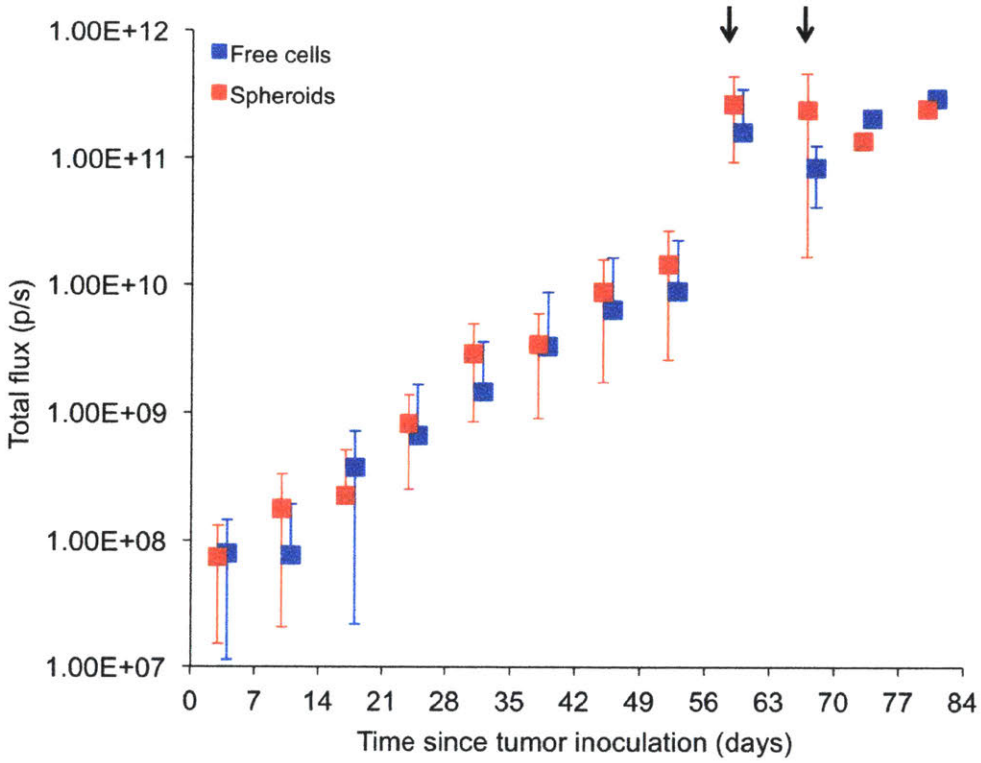

B

Figure 3.7: Bioluminescence flux over time for the free cell and spheroid mouse groups. Flux values are plotted on a (A) linear and (B) logarithmic scale. Arrows indicate days when mice with highest signal had to be euthanized. The spheroid group had higher flux than the free cell group on almost all imaged time points indicating faster tumor growth in these animals. The study started with n=3 animals in each group and mice were euthanized when they were moribund.

3.3.5 *In vivo* spheroid model pilot study 2: optimization

The UCI101 cell line was used to generate an *in vivo* orthotopic human ovarian cancer model in mice that more closely resembled residual tumors left behind in patients after debulking surgery and to develop methods for noninvasive tumor tracking that would enable use of this model to assess the effectiveness of continuous low-dose IP cisplatin treatment *in vivo*. Two larger spheroid sizes were produced in an attempt to inoculate mice with spheroids closer in size to the subcentimeter tumors commonly left behind after optimal debulking. They comprised 10000 and 20000 cells per spheroid respectively and were expected to have a diameter of approximately 300 and 400 μm based on the diameter-cell number correlation established previously for the UCI101 cell line. Spheroid shape, border definition and robustness allowing removal from the plates without disintegration were evaluated qualitatively based on spheroid microscopy photos (Figure 3.8). Spheroids comprising 20000 cells each were not considered further for *in vivo* injection because they more closely resembled cubes instead of spheres, had poor border definition and disintegrated upon attempting to collect them from the plates. Spheroids comprising 10000 cells each were more spherical and had an average diameter of 341.8 ± 9.8 μm (n=15 spheroids). Spheroid diameter after collection from the plate (301.01 ± 22.06 μm) was approximately 86% of the diameter measured while in the plate suggesting that the spheroids experienced a limited degree of disintegration during harvesting and were therefore viable for *in vivo* IP injection in mice. Two different spheroid sizes were therefore injected intraperitoneally in mice for tumor inoculation: spheroids measuring approximately 188 μm or 301 μm in diameter.

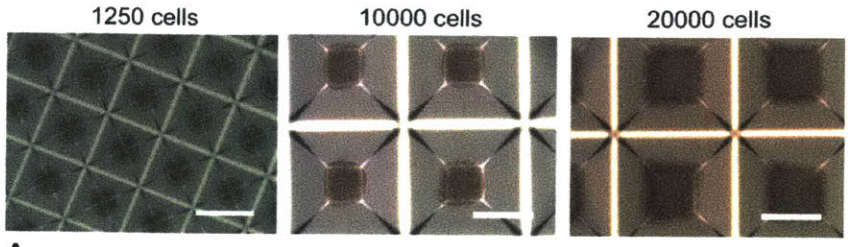

A

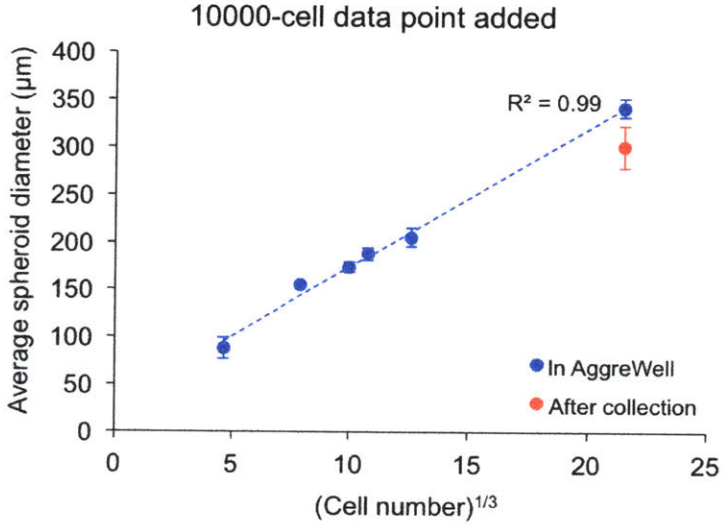

B

Figure 3.8: Spheroid size scale-up for *in vivo* ovarian cancer model development. (A) Representative images of UCI101 spheroids comprising 1250, 10000 and 20000 cells each respectively. The 1250-cell spheroids with an average diameter of 188 µm displayed the most sphericity and compactness. The 10000-cell spheroids with an average diameter of 342 µm were spherical and compact. The 20000-cell spheroids had a shape resembling a cube rather than a sphere and were not compact enough to allow diameter quantification and successful removal from the AggreWell plate. Scale bar is 400 µm. (B) The UCI101 spheroid diameter-cube root of cell number plot is updated to include measurements for the 10000-cell spheroids both before (blue) and after (red) collection from the AggreWell plate. The 10000-cell spheroid diameter maintained the strong linear correlation seen previously when added to the plot (before-collection value, R^2=0.99).

The 301-µm spheroids were deemed problematic even prior to injection since they were prone to settling to the bottom and along the walls of the loaded syringe and required agitation to bring them back to suspension, which can presumably negatively

affect spheroid integrity and lead to inadvertent spheroid aggregation due to contact. A larger-gauge needle had to be used for IP injections of these larger spheroids to ensure they would not shear during passage through the needle (needle inner diameter > spheroid diameter). A 21G needle was selected as a compromise between spheroid shearing risk and risk of adverse effects to the animal due to injection with a large-gauge needle. The injection site did not appear to leak any spheroid suspension after injection and no peritoneal fluid leakage-related infections were noted in any of the mice but 5 of 6 mice in the group grew subcutaneous tumors at the injection site.

Three-dimensional reconstructions of the bioluminescence flux for all six mice in each group on day 21 after spheroid injection are shown in Figure 3.9. This time point was chosen because previous work with this animal model and UCI101 free cell injections allowed a 21-day tumor inoculation period before the start of treatment. Both spheroid groups show sources of bioluminescence signal suggestive of tumor nodules in the mouse abdomen at this time point. The 301-μm spheroid group however appears to have signal more localized near the site of injection (lower left quadrant of mouse abdomen) compared to the 188-μm spheroid group. 4 out of 6 animals in the 188-μm spheroid group and 3 out of 6 animals in the 301-μm spheroid group appear to have a more dispersed distribution of signal sources in the abdomen. This may indicate a more widespread metastatic pattern in the abdominal cavity similar to the microscopic metastases remaining in patients after debulking surgery.

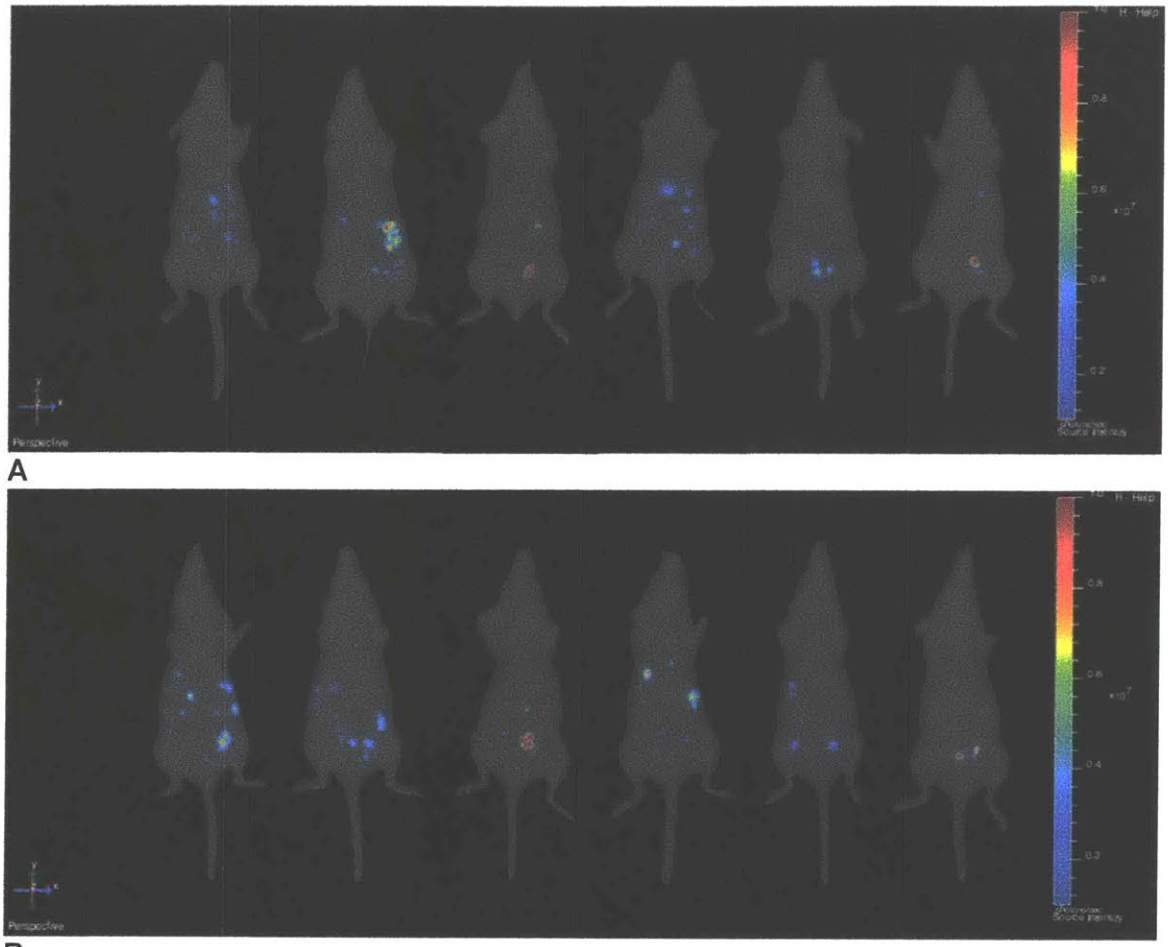

Figure 3.9: Three-dimensional diffused luminescent imaging tomography reconstruction of bioluminescent sources in mice 21 days after injection with UCI101 spheroids of different sizes. Mice were injected with either (A) 301-µm or (B) 188-µm spheroids. The mouse is positioned so that its ventral surface is facing up and the mouse surface has been reconstructed using the IVIS software built-in tools. Flux cutoffs for the color map are $1e^6$-$1e^7$. More mice in the smaller spheroid group appear to have diffuse sources of bioluminescence throughout their abdomen compared to the large-spheroid group relative to the injection site (lower left quadrant of the mouse abdomen).

The two-dimensional total flux at euthanasia is plotted as a function of total tumor burden (solid peritoneal tumor, ascites and any subcutaneous tumors) for all animals in Figure 3.10. Logarithmic trendlines have been added to both the 188-µm and the 301-µm dataset. Neither trendline fit the data very well, with $R^2 = 0.53$ for 188-µm spheroids and $R^2 = 0.64$ for 301-µm spheroids. This can be attributed to certain outliers –

particularly mice with a large tumor burden. The larger size of tumors observed in animals with increased tumor load can help explain the existence of these outliers. Many of the tumors at this point have become necrotic, adding to the gross tumor mass at euthanasia but not contributing to the flux since the cells in the necrotic tumor core are not producing any bioluminescence. The luciferase reaction is oxygen-dependent, so the varying degree of hypoxia within the tumor may also account for the inaccuracies observed.[148] The presence of vasculature within these tumors can play a role in hypoxia and necrosis as well as accessibility of deeper parts of the tumor for delivery of active agents.[148] Larger tumors with inhomogeneous blood vessel presence within their mass may not be accessible to the IP-injected luciferin that enters the systemic circulation.[148] Diffusion of luciferin from the peritoneal cavity directly into tumors may additionally be hindered in the case of larger tumors preventing live cells deeper into the tumor from emitting a signal. The depth at which cancer cells lie within the mouse abdominal cavity affects the intensity of the signal they emit – it was observed that a number of mice in both spheroid groups had subcutaneous tumors at euthanasia that likely contributed a bioluminescence signal that was greater in proportion to their mass compared to that of tumors deeper inside the abdomen, whose signal may be dampened by surrounding tissues.

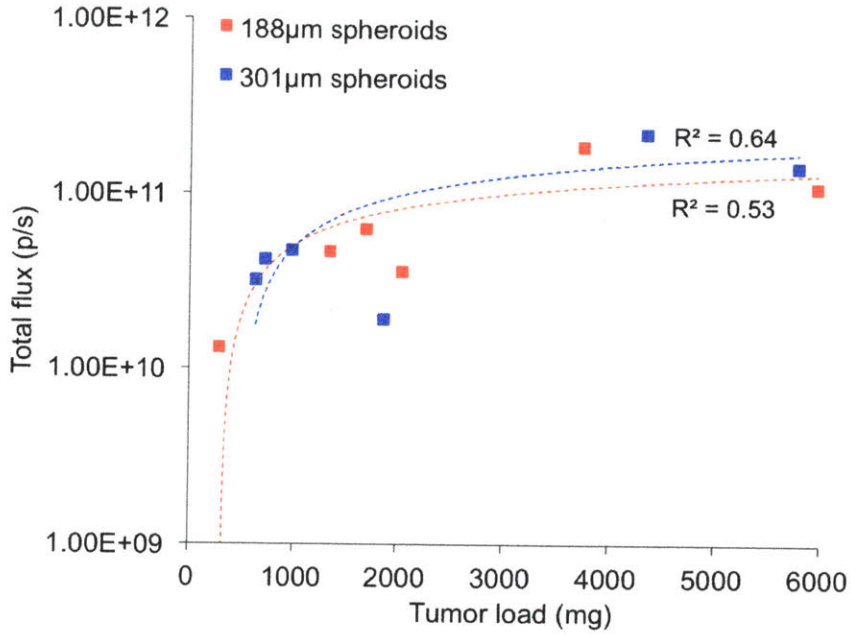

A

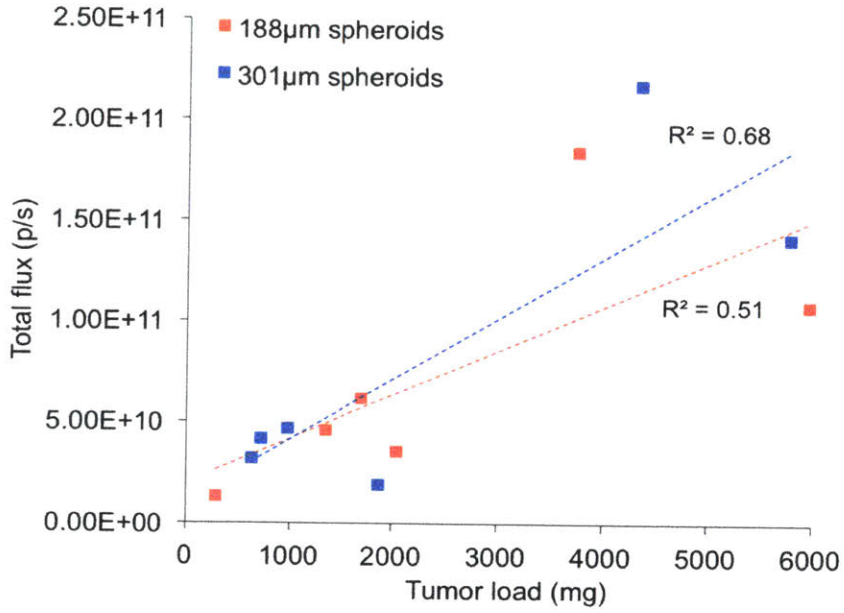

B

Figure 3.10: Bioluminescence of tumors in mice injected with 188-µm or 301-µm spheroids plotted as total flux over tumor mass measured at necropsy following euthanasia. Flux is plotted on (A) a logarithmic or (B) a linear scale and data is fitted with (A) logarithmic or (B) linear best-fit trendlines. The R^2 values are given next to the trendlines. The flux-tumor load data appear to be correlated although the correlation is not as good as those commonly reported in the literature. Others like Black et al. have pointed out poor correlation between BLI and other measures of tumor like MRI. BLI nevertheless remains a relevant noninvasive way of measuring tumor burden progression in this model.[148]

3.4 Discussion

Multiple clinical trials and experience in the clinic have established that the success of tumor debulking surgery in reaching optimal cytoreduction (leaving behind subcentimeter tumors only) heavily influences the treatment outcome of advanced-stage ovarian cancer patients. We have previously also shown that replacing maximum-tolerated-dose intermittent cisplatin IP injections – akin to the infusions currently used in the clinic – with continuous low-dose IP cisplatin delivered via fully implanted reservoir devices can be as effective and less toxic in mouse models of ovarian cancer.[45] The total amount of cisplatin delivered by these devices however was 4.7 times that delivered by the IP injections to accomplish a comparable extent of tumor kill. The effect of tumor size on the efficacy of continuous IP cisplatin treatment has not yet been established and it is a critical part of the puzzle when trying to determine the populations of patients that may benefit the most from a continuous low-dose IP cisplatin regimen. The optimal cisplatin dose of such a continuous regimen is also a key component of developing a successful treatment alternative to the currently used periodic IP infusions.

In vitro and in vivo models of ovarian cancer that closely recapitulate the clinical picture of an optimally debulked patient before the start of adjuvant chemotherapy would ideally be used to establish this optimum continuous dose – one that maximizes tumor kill while maintaining tolerable toxicity. The use of ovarian cancer cell spheroids to explore the impact of tumor size on the tumoritoxic effectiveness of continuous low-dose cisplatin was previously established in our lab by L.M. Tanenbaum and expanded in this project.[46] The work described here uses ovarian cancer cell spheroids from two different cell lines as models of subcentimeter tumor nodules *in vitro* to demonstrate

that: (i) smaller nodules are treated as effectively by continuous low-dose cisplatin as by a brief bolus dose of cisplatin with the same AUC; and (ii) larger nodules require exposure to continuous cisplatin at a dose delivering a larger AUC for effective treatment. The work then proceeds to develop spheroid-based *in vivo* models of ovarian cancer to demonstrate that: (iii) spheroids are a viable platform to inoculate *in vivo* mouse models of ovarian cancer with precise control of nodule size on injection and faster tumor growth compared to free cell injections; and (iv) spheroid-inoculated mouse models exhibit a diffuse pattern of nodular disease throughout the abdomen but there exists a limit to the starting size of spheroids that can successfully be injected intraperitoneally to create such lesions.

The barrier of drug distribution into larger tumor nodules is a known hindrance to effective treatment.[148] It has been shown *in vitro* that tumor cell layers as thin as 200 μm dramatically affect cisplatin penetration.[149] A low-dose cisplatin regimen further reduces drug penetration into tumors since the cisplatin concentration gradient between the surrounding fluid and the center of the tumor is smaller. This affects cisplatin diffusion into the tumor. Continuous exposure to cisplatin can kill cells in each successive outer layer of a spheroid but, as Tanenbaum points out, the surface-area-to-volume ratio of a spheroid decreases with increasing spheroid radius and so a smaller proportion of cells in the spheroid are exposed to cisplatin.[46]

Drug penetration into tumors is not the only mechanism limiting cisplatin cell kill. Cisplatin effectively binds DNA within both actively dividing and non-dividing (quiescent) cells but the apoptotic pathways ultimately leading to cell death are only activated as a result of failed repair of this bound DNA during cell division. Quiescent cells will

therefore not be killed by cisplatin. Solid tumors are known to contain necrotic cores as well as quiescent cells due to limited oxygen, nutrients and metabolites. Similar chemical gradients (oxygen, nutrients, metabolites / catabolites) have been observed in spheroids starting at approximately 200-μm diameters and necrotic cores have been observed in spheroids with larger diameters (> 500μm).[150,151] The spheroids used in this work are too small to anticipate a necrotic core *in vitro* but smaller spheroids are expected to contain fewer quiescent cells than larger spheroids and this may help explain their more dramatic shrinkage in response to cisplatin exposure.[46] Larger spheroids are likely responding differently to continuous high-AUC cisplatin (D_H) compared to a brief bolus exposure to lower-AUC cisplatin (IP) primarily due to limited drug penetration into the spheroid.

The *in vitro* portion of this work showed that continuous low-dose IP cisplatin can effectively treat small tumors causing the same degree of shrinkage as an AUC-matched brief IP bolus dose. This is not the case for larger tumors: continuous cisplatin doses that result in a greater total AUC are needed in order to match or surpass shrinkage by a brief IP bolus dose. These findings are in accordance with clinical data showing improved IP chemotherapy outcomes in women with microscopic to no residual tumors. These findings can also help shed some light on the results of the GOG 252 trial to date both in terms of a cisplatin dose reduction in the IP arm and in terms of the variability in outcome of debulking surgery.

These *in vitro* findings emphasize the urgency to use animal models that are clinically relevant and representative of optimally debulked patients to assess continuous low-dose IP cisplatin regimens. Clinical relevance encompasses both the

size of tumor nodules in the models as well as their distribution throughout the abdomen. Helland et al. attempted to perform cytoreductive surgery on mice bearing orthotopic SKOV3 human ovarian cancer xenografts prior to start of a carboplatin-paclitaxel combination IP chemotherapy and found that the group receiving surgery followed by chemotherapy had the longest mean survival similar to clinical experience with ovarian cancer patients.[80] The technical challenges associated with successfully performing optimal cytoreduction on mice with no adverse survival outcomes make this approach less attractive. Such an approach is additionally expected to maintain a degree of subjectivity on determining surgical outcome that has been criticized in the clinic and may help explain in part the findings to date of the GOG 252 trial – at least until imaging tools that precisely guide lesion removal during debulking are readily available. Spheroids have previously been used extensively as *in vitro* three-dimensional models of cancer. Nishikawa et al. used spheroids to inoculate mice intravenously with lung adenocarcinoma and found that spheroids were more effective than a cell suspension at generating lung lesions and that smaller spheroids led to greater tumor load than larger spheroids.[152] The use of spheroids to inoculate mice orthotopically with UCI101 xenografts was found to result in faster tumor growth and a more widely distributed disease pattern compared to an equivalent inoculation with free cells in suspension (Figure 3.6 and 3.7). This observation is in accordance with the findings of Nishikawa et al. in their lung adenocarcinoma spheroid model.

The size of spheroids used for *in vivo* inoculation was varied as a next step in developing this model in an attempt to get even closer to the clinical picture of an optimally debulked patient. The 301-μm spheroids produced were at the limit of

sphericity and compactness needed for spheroid size quantification and viable transfer from the spheroid formation plate to syringes for *in vivo* injection. They were however found to noticeably disintegrate upon agitation to mix the spheroid suspension in the syringe immediately prior to injection. Their size posed a challenge for safe injection in mice due to the large-gauge needle required. The large-gauge needle was additionally found to likely promote spheroid suspension backflow into the subcutaneous space at the injection site and thus cause growth of subcutaneous tumors that negatively affect the orthotopic aspect of this model. The 188-μm spheroids were not only free of these limitations but were also found to exhibit a relatively more dispersed nodule pattern throughout the peritoneal cavity on BLI imaging (Figure 3.9B). The 188-μm spheroids exhibited a greater degree of compactness and sphericity compared to the 301-μm spheroids *in vitro* (Figure 3.8A) and can presumably sustain a greater amount of shear during passage through the injection needle before breaking apart. They also exhibited limited to no visible aggregation while resting in the syringe prior to injection and were easily resuspended in the injection solution by gentle agitation of the syringe with no disintegration observed by naked eye. These characteristics may help explain the relatively more diffuse pattern of disease observed qualitatively in the three-dimensional BLI sequence shown in Figure 3.9B (188-μm spheroids) compared to Figure 3.9A (301-μm spheroids).

Both spheroid sizes resulted in a similar pattern of flux-tumor mass correlation at euthanasia (Figure 3.10). The aggregates of either spheroid size that remained viable and seeded the peritoneal cavity thus ultimately gave rise to tumors that grew to comparable dimensions when the disease was allowed to reach advanced stage. These

tumors likely suffered from similar limitations related to their necrotic core and other considerations described previously that affect the flux-tumor mass correlation (R^2=0.51 and R^2=0.68 for linear-fit trendlines in the flux-tumor mass data of 188-μm and 301-μm spheroids respectively, Figure 3.10A).

Chapter 4: Material Optimization, Efficacy Pilot and Origami-Inspired Proof-of-Concept Shapes for the *In Vivo* Translation of a Composite Material for Intraperitoneal Cisplatin Delivery

4.1 Introduction

A CDDP25 composite material was previously developed as the basis of an implant for sustained low-dose release of cisplatin in the peritoneal cavity for the treatment of advanced ovarian cancer. A thinner version of this composite was developed, reducing its thickness by more than 50% to a 0.4-0.45 mm thick sheet. The structural and mechanical properties of this thinner CDDP25 material were examined and its similarity to the previously developed thicker CDDP25 material was confirmed. Disks of various diameters were cut out of the thinner sheet to serve as individual implants for use in mice for intraperitoneal cisplatin delivery. The disks allowed modulation of the total cisplatin release rate of the implant and behaved as expected when releasing cisplatin *in vitro*. Disks measuring 1.0 cm, 1.5 cm or 2.0 cm in diameter were implanted intraperitoneally in healthy mice in two dosing studies and their cisplatin dose tolerability, biocompatibility and ability to deliver platinum effectively to tissues of interest in the abdomen were assessed. The 1.5-cm diameter disks were deemed likely to deliver the maximum tolerated cisplatin dose for this CDDP25 formulation and are good candidates for implantation in mice bearing ovarian cancer xenografts for assessment of their antitumor efficacy. An antitumor efficacy pilot was conducted in tandem with the dosing studies using CDDP25 disks measuring 0.4 mm in thickness and 1.0 cm in diameter or 1.0 mm in thickness and 0.5 cm or 0.8 cm in diameter. The pilot suffered serious drawbacks related to an acquired bacterial infection and the number of animals

used was too small to draw any statistically significant conclusions but a degree of response to treatment was seen in all implant groups. Proof-of-concept origami-inspired shapes were prototyped using the previously developed LAC50 formulation to assess the feasibility of this approach for designing sheet-like implants that can be deployed laparoscopically into the abdomen.

4.2 Materials and Methods

4.2.1 Chemicals and materials

Ecoflex 00-30 was purchased from Smooth-On Inc. (Macungie, PA, USA). Phosphate-buffered saline (PBS) was purchased from VWR (Radnor, PA, USA). Diethyldithiocarbamate trihydrate (DDTC), nickel (II) chloride, sodium hydroxide, high-performance liquid chromatography (HPLC)-grade water, HPLC-grade methanol, 70% nitric acid, cisplatin powder and lactose monohydrate powder were purchased from Sigma-Aldrich (St. Louis, MO, USA). Erbium 1,000 µg/mL standard solution was purchased from Agilent Technologies (Santa Clara, CA, USA). Platinum 1,000 µg/mL standard solution in nitric acid was purchased from Inorganic Ventures (Christiansburg, VA, USA). Medical injection-grade cisplatin solution (100 mg/100 mL) for bolus injections was purchased from McKesson Medical-Surgical (Richmond, VA, USA).

4.2.2 Composite material fabrication

A matrix-type cisplatin-eluting composite material formulation (CDDP25) was fabricated as previously described by mixing cisplatin and lactose powders with Ecoflex 00-30 supersoft silicone elastomer. Ecoflex 00-30 was mixed with cisplatin powder and lactose

monohydrate powder using a dual asymmetric centrifugal lab mixer (SpeedMixer, Flacktek Inc., Landrum, SC, USA) to create a composition containing 25% $w_{cisplatin}/w_{total}$ and 25% $w_{lactose}/w_{total}$. A mass of 1.0-1.5 g of the cisplatin-lactose-silicone mixture was poured into a rectangular mold measuring 30 mm length by 70 mm width and 0.5 mm depth that was machined in-house from Delrin black acetal using a micro CNC router (Cameron Micro Drill Presses, Sonora, CA, USA). A razor blade was used to spread the mixture evenly throughout the mold by sweeping the mixture along the mold length in both directions. The mold was then placed in vacuum for 15 min to allow the mixture to degas fully followed by overnight curing at room temperature and pressure. This yielded composite material sheets measuring approximately 30 mm in length and 70 mm in width and having a thickness of approximately 0.4-0.45 mm. Metal punches of various diameters (1.0 cm, 1.5 cm, 2.0 cm) were used to punch out disks from the cured material pieces for *in vitro* cisplatin release quantification and *in vivo* implantation in mice. The resulting disks measured 1.0-2.0 cm in diameter and 0.4-0.45 mm in thickness. All disks used for *in vivo* implantation were sterilized by ethylene oxide gas and allowed to degas for 48 hours in a hood before use. An additional composite formulation containing only lactose 50% w/w_{total} (LAC50) was prepared to use for mechanical testing, where material porosity was the critical parameter. The LAC50 formulation was prepared in the same way as the CDDP25 formulation except that dog bone-shaped Delrin black acetal molds measuring 0.5 mm in depth were used for casting the material into shapes appropriate for carrying out tensile testing. Cisplatin-containing samples were kept away from light for all experiments.

4.2.3 Miura v-pleat shape prototyping

Two-part molds were created for casting sheets of Ecoflex 00-30 and LAC50 to cure with a partially pre-folded Miura v-pleat origami shape. The first Miura v-pleat origami sheet proof-of-concept prototype was cast in a mold designed using SolidWorks (Dassault Systèmes, Vélizy-Villacoublay, France) and machined out of a white Teflon block in-house using a micro CNC router and the appropriate twist drill bit. The second Miura v-pleat sheet prototype was intended to more closely resemble the dimensions of an implant for human patients and was therefore cast in a mold designed using SoldiWorks and 3D-printed using ABS*plus* proprietary thermoplastic material on a Dimension Elite 3D printer with a 178-µm layer thickness (Stratasys, Eden Prairie, MN, USA). The two molds were used to cast Ecoflex 00-30 and LAC50 Miura v-pleat sheets following the same casting protocol previously described with the exception of filling the mold bottom part with an excess of material and then firmly securing the top mold part in place before degassing the closed mold in vacuum for 15 min.

4.2.4 Structural characterization

A razor was used to create lateral cross-sections of the CDDP25 sheet through the sheet thickness. The cross-sections were examined by secondary and backscatter scanning electron microscopy (SEM; 5600LV SEM) to study the composition of the CDDP25 sheet and the topography of cisplatin and lactose crystals in the silicone matrix and compare them to those of thicker CDDP25 samples prepared previously by manual mixing and casting in different molds. A 10-µm gold-palladium coating was applied to the cross-sections prior to SEM imaging to prevent charging of the sample.

4.2.5 Mechanical characterization

Tensile testing of dog bone-shaped LAC50 samples was performed on an Instron 5943 testing machine with a 500 N load cell and steel grip platens. Specimens were subjected to elongation at a rate of 15 mm/min until failure. Force was converted to stress using the cross-sectional surface area of the sample and elongation was converted to strain using the initial length of the sample. Stress-strain diagrams were plotted and the modulus of elasticity, ultimate tensile stress and elongation at break were calculated and compared to those of LAC50 samples with thickness 1-1.5 mm and of representative tissues in the human abdominal cavity.

4.2.6 *In vitro* cisplatin release

CDDP25 disks measuring 0.4-0.45 mm in thickness and either (i) 0.5 cm, (ii) 1.0 cm or (iii) 1.5 cm in diameter (Figure 2) were immersed in 50 mL of PBS in amber glass jars and incubated at 37°C on a shaker oscillating at 60 cycles/min to quantify the amount of cisplatin released *in vitro* at regular intervals for a total period of 49 days. Each disk was lodged within the turns of a thin stainless steel spring similar to the method described by Keskar et al. (McMaster-Carr, Elmhurst, IL, USA) to prevent the disk from settling on the bottom of the vial or floating to the top of the liquid.[98] The disks were transferred to jars containing fresh PBS at regular time intervals to maintain sink conditions for the dissolution of lactose (lactose solubility in water = 100 mg/mL) and cisplatin (cisplatin solubility in water = 2.53 mg/mL). The interval between PBS renewals was kept to 6 days or shorter to minimize cisplatin degradation. The PBS solution was sampled frequently on the periods when the disks remained in the same jar by removing 1 mL of PBS at regular time points. The amount of cisplatin present in the solution was

measured at each prescribed time point by HPLC with a nickel (II) chloride internal standard and the method described previously by our group.[45]

4.2.7 Surgical and euthanasia procedures for *in vivo* experiments

All listed procedures were in accordance with the Massachusetts Institute of Technology Committee on Animal Care guidelines, as well as the NIH Guide for the Care and Use of Laboratory Animals. Animal surgeries to implant CDDP25 disks were performed within a sterile field and all surgical equipment was autoclaved. Inhalation anesthesia was maintained throughout surgeries with isoflurane. Slow-release buprenorphine was used as pre- and post-surgical analgesia per recommendation by the animal care committee. The incision site was sterilized with iodine and isopropyl alcohol. A small abdominal incision of about 5 mm was made through the skin and peritoneum to implant the disks. The disks were rolled up for placement inside the abdomen. The disks once implanted were unfolded flat and allowed to freely move within the peritoneal cavity. Mice were weighed regularly to monitor overall health and euthanized upon weight loss greater than 20% or poor body condition. Euthanasia was carried out by carbon dioxide inhalation at a steadily increasing flow rate to minimize distress.

4.2.8 Inductively coupled plasma mass spectroscopy protocol for platinum quantification in tissue and blood serum

The platinum concentration in blood serum ultrafiltrate and nitric acid-digested mouse tissue was measured by inductively coupled plasma mass spectroscopy (ICP-MS) on an Agilent 7900 ICP-MS (Agilent, Santa Clara, CA, USA). Samples were serially diluted to a final dilution of 10^{-3} using 2% nitric acid before ICP-MS measurement. An internal

erbium standard was used to monitor the performance of the ICP-MS run for any drift and the bounds for rejecting readings were defined at +/- 20% of the erbium internal standard recovery. A platinum calibration curve was prepared using eight platinum concentrations ranging from 0 to 500 ppb to convert the ICP-MS platinum-to-erbium count ratio to a platinum concentration for each sample. The platinum calibration curved was a straight line through the origin with R^2 = 0.9999. The platinum concentration values obtained for each sample were multiplied by the dilution factor used when preparing the sample to obtain the platinum concentration in the original sample. The calculated platinum concentration for blood serum ultrafiltrate samples was used to express the serum platinum content in µg Pt / L serum. The calculated platinum concentration for digested tissue samples was multiplied by the sample volume after acid digestion to obtain the total platinum mass in each sample. This total platinum mass was then divided by the tissue mass in each tube to obtain a normalized µg Pt / g tissue content for each sample.

4.2.9 *In vivo* CDDP25 implant dosing studies

The *in vivo* tolerability and platinum delivery of three CDDP25 disk sizes with thickness of 0.4-0.45 mm and either (i) 1.0-cm diameter, (ii) 1.5-cm diameter or (iii) 2.0-cm diameter were assessed over six weeks in tumor-free mice and compared to those of weekly 4 mg/kg intraperitoneal (IP) cisplatin injections. The different CDDP25 disk sizes were evaluated as a way to escalate the cisplatin dose delivered by the CDDP25 implant and so identify a maximum tolerated dose (MTD) for treatment with the implant. All chemicals and materials for the *in vivo* portions of these studies were sterile and

maintained under sterile conditions. Two separate dosing studies were carried out: the first compared CDDP25 disks of 1.5-cm or 2.0-cm diameter to weekly 4 mg/kg IP cisplatin injections. The second compared CDDP25 disks of 1.0-cm diameter to weekly 4 mg/kg IP cisplatin injections. The two studies were performed on different dates and different batches of mice were used so IP cisplatin injection groups were included in both studies to provide an unbiased comparison to the CDDP25 implant treatment groups. Female Nu/Nu athymic mice bearing no tumors and weighing 20-25 g were used in both studies (Charles River Laboratories, Wilmington, MA, USA) because they are well-suited for growth of human tumor xenografts due to their deficient immune system and are expected to serve as the animal model for antitumor efficacy studies using the CDDP25 material. Blood was sampled via the saphenous vein of all mice prior to the start of the experiment to obtain baseline complete blood count (CBC) values with auto differential. The mice in the first dosing study were allocated in four different treatment groups: (1a) IP implantation of a single CDDP25 2.0-cm diameter disk (n=3 mice); (2a) IP implantation of a single CDDP25 1.5-cm diameter disk (n=3 mice); or (3a) IP administration of weekly 4 mg/kg IP cisplatin injections (six total injections, n=3). The mice in the second dosing study were allocated in two different treatment groups: (1b) IP implantation of a single CDDP25 1.0-cm diameter disk (n=3 mice); or (2b) IP administration of weekly 4 mg/kg IP cisplatin injections (six total injections, n=3). Sterile CDDP25 disks were incubated in 50 mL of PBS at 37°C on a shaker oscillating at 60 cycles/min for 24-48 hours prior to implantation to eliminate their cisplatin burst. The disks were then implanted intraperitoneally in the mice of groups 1a, 2a and 1b. The mice of groups 3a and 2b received a 4 mg/kg IP cisplatin injection at the same time as

the implantation surgery given as a 1 mL injection using 0.9% w/v saline as a diluent and injected via a 28G needle. All mice in the first study were euthanized 42 days after the start of treatment or whenever their body condition required euthanasia, whichever came first. Mice in group 1b in the second study were euthanized 42 days after the start of treatment and mice in group 2b in the second study were euthanized 48 hours after administration of their 6^{th} cisplatin injection to capture any cisplatin toxicity before they had time to recover. The liver, spleen, kidneys, stomach, sections of the small and large intestine, ovaries, uterus, femurs, implant with any surrounding fibrous capsule and fat pad tissue – if present – of the euthanized mice were harvested. The implant and any associated capsule were placed intact in 10% neutral buffered formalin immediately after harvesting and processed for histological analysis. All harvested tissues with the exception of the femurs were cut in half using a razor blade. One half of each tissue was processed for histological analysis to assess toxicity and the other half was processed for platinum quantification as an indirect measurement of the *in vivo* cisplatin dosing capability of the different-size CDDP25 disks and 4 mg/kg IP injections. The femurs were entirely processed for histological analysis.

4.2.10 CDDP25 implant tolerability evaluation – in vivo dosing studies

Approximately 100 µL of blood were collected weekly from all mice in both dosing studies by saphenous vein puncture for CBC with auto differential unless if their body condition made them unfit for safe blood collection. Blood was also collected from all mice at euthanasia by cardiac puncture for CBC with auto differential and serum platinum quantification. Blood samples for CBC with auto differential were collected in

EDTA-coated 100 µL microvettes (Sarstedt, Nümbrecht, Germany) as per manufacturer instructions to prevent clotting and were processed on a Hemavet 950FS Auto Blood Analyzer (Drew Scientific, Miami Lakes, FL, USA) within 24 hrs after collection. Samples that were not processed immediately after collection were stored in the refrigerator to maintain sample integrity. The tissue halves for histological analysis with the exception of the femurs were placed in 10% neutral buffered formalin immediately after harvesting and allowed to fix for 48-72 hours. The femurs were placed in Bouin's solution and allowed to decalcify for at least two weeks and until they could be bent by applying a small amount of force to each end of the bone. The fixed tissues with the exception of the femurs were sectioned with a razor blade and half of each sample was placed in histology cassettes. The femurs were placed in histology cassettes without any sectioning. The implants were carefully sectioned with a razor blade along their axis to ensure any fibrous capsule remained on the sample and placed in histology cassettes such that the implant cross-section and capsule would be visible on the paraffin section. Care was taken to ensure that all five liver lobes and half of each kidney as well as different representative sections of the small and large intestines were included in the respective cassette. The cassettes were placed in 70% ethanol followed by paraffin embedding and hematoxylin & eosin (H&E) staining of slides for pathology review with a veterinary pathologist consultant at the Hope Babette Tang Koch Institute Histology Core.

4.2.11 CDDP25 implant platinum delivery to systemic circulation and tissues – *in vivo* dosing studies

Blood samples for serum platinum quantification were collected on euthanasia in 1.1 mL Z-Gel microtubes (Sarstedt, Nümbrecht, Germany) containing serum gel with clotting activator and were centrifuged at 13,000 g for 5 minutes. The serum was collected following blood centrifugation and ultrafiltered using an Amicon Ultra-0.5 mL centrifugal filter (MilliporeSigma, Burlington, MA, USA) as per manufacturer instructions to collect both the serum ultrafiltrate and the serum concentrate. Serum ultrafiltrate and concentrate samples were stored at -80°C until further processing. The serum ultrafiltrate is free of proteins, primarily albumin, and therefore does not contain protein-bound cisplatin that is no longer therapeutic. The platinum levels in serum ultrafiltrate were measured by ICP-MS using the method described previously. The tissue halves for platinum quantification were collected in Eppendorf tubes on euthanasia and placed immediately on dry ice followed by storage at -80°C until further processing. To quantify the amount of platinum in the harvested tissues, the organs were homogenized using a Bertin Precellys CK14 soft tissue homogenization kit (VWR, Radnor, PA, USA) and digested using 70% nitric acid. Briefly, each organ was weighed and then divided into pieces weighing at most 200 mg. Each piece was placed in a tissue homogenization tube containing inert 1.4 mm zirconium oxide beads and 1 mL of RIPA lysis and extraction buffer (Invitrogen, Carlsbad, CA, USA) was added. The tubes were placed in a Precellys 24 homogenizer (Bertin, Montigny le Bretonneux, France) and the samples were homogenized at 6,000 RPM for 4 x 20 s cycles. The tubes were then centrifuged at 10,000 g for 10 min to remove any foam buildup and placed uncapped on a thermoblock at 95°C for at least 48 hours until all the supernatant had evaporated. The

lysed tissue pellets were digested by adding 1 mL of 70% nitric acid to each tube, loosely capping it and placing it in the hood on a hot plate at 55°C for 24 hours. The platinum concentration of the digested samples was quantified by ICP-MS using the protocol described previously.

4.2.12 *In vivo* CDDP25 antitumor efficacy pilot

The *in vivo* antitumor efficacy of three different CDDP25 disk types was evaluated in a small pilot study using female athymic Nu/Nu mice weighing 20-25g (Charles River Laboratories, Wilmington, MA, USA) and bearing UCI101 human ovarian cancer orthotopic xenografts. All chemicals and materials for the *in vivo* portion of the efficacy pilot were sterile and maintained under sterile conditions. The antitumor efficacy pilot occurred in parallel with the thin CDDP25 dosing studies and so the three different CDDP25 disk types evaluated were chosen based on data that had been collected previously in the project. The three disk types evaluated were: (i) 0.5-cm diameter, ~1.0-mm thickness (n=6); (ii) 0.8-cm diameter, ~1.0-mm thickness (n=6); and (iii) 1.0-cm diameter, ~0.4-mm thickness (n=5). Disk type (i) represented the original CDDP25 composite material and thickness previously evaluated over a 15-day platinum distribution and toxicity study *in vivo* in mice (Chapter 1). Disk type (iii) represented the 1.0-cm (i.e. 'small') thin implant used in the thin CDDP25 dosing studies that had been well tolerated *in vivo* at the point of starting the efficacy pilot. Disk type (ii) was chosen as an intermediate dose between the expected dose by disk type (i) and that expected by disk type (iii). The remaining three treatment groups in the efficacy pilot were: (iv) mice receiving 6 weekly 4 mg/kg IP cisplatin injections (n=5); (v) mice receiving 6

weekly 10 mg/kg IP cisplatin injections (n=6); and (vi) untreated control mice (n=5). The IP injection dose used in group (v) was selected because it was calculated to be the mouse equivalent to the recommended dose used in ovarian cancer care for IP cisplatin infusions (100 mg/m^2). The IP injection dose used in group (iv) was selected because it had previously been used in this project and had been found to effectively treat tumors without causing intolerable toxicity.[45] Animals were weighed multiple times every week following inoculation with tumor cells and throughout the duration of the pilot as a marker of their overall health status. Methods for tumor cell inoculation and noninvasive tumor monitoring by BLI are described in greater detail in Chapter 2. Briefly, all mice were inoculated with 3 x 10^6 UCI101 cells / mouse injected intraperitoneally as a free cell suspension in 1 mL of cold PBS using a 26G needle. The UCI101 cells used in this study bear the luciferase gene and so all mice were imaged with BLI twice weekly as a noninvasive measure of their tumor load starting one day after tumor cell inoculation and throughout the duration of the study following the protocol described in Chapter 2. The mice were imaged both on the dorsal and on the ventral side to ensure that the maximum bioluminescence intensity was captured at each time point in case of uneven tumor growth. There was BLI signal variability across animals on each imaging time point that is expected given the variable rate of tumor rejection and growth *in* vivo. BLI signal on day 23 after tumor cell inoculation was used to randomize animal assignment to the six different treatment groups. Treatment with either IP implantation of a CDDP25 disk or administration of weekly IP cisplatin injections was started for mice in groups (i)-(v). The duration of the efficacy pilot was 41 days to allow administration of 6 weekly cisplatin injections bringing the total duration of the efficacy pilot to 64 days. Mice were

euthanized either on day 64 or whenever their body condition required euthanasia. Methods for blood sampling for CBC and platinum quantification in serum as well as for organ harvesting for histology and platinum quantification in tissues are described in greater detail in Chapter 1 and earlier in Chapter 3. Briefly, blood was sampled from the saphenous vein of all mice before the start of treatment to establish a baseline CBC and then again on week 2 and 5 after the start of treatment. Blood was sampled from the facial vein of all mice on week 3 after the start of treatment and the serum was separated, filtered and stored at -80°C for future systemic platinum level quantification by ICP-MS. The liver, kidneys, spleen, stomach, small and large intestine, ovaries and uterus and femurs of each mouse were harvested at euthanasia and prepared as described previously for platinum quantification by ICP-MS and histologic evaluation of toxicity. The implants of mice in groups (i)-(iii) were collected along with any surrounding fibrous capsule and prepared for histologic evaluation. All visible solid tumors and any ascites were collected from each mouse and weighed to quantify the tumor mass at euthanasia. Methods for *in vitro* cisplatin release from CDDP25 are described in detail in Chapter 1 and earlier in Chapter 3. Briefly, extra CDDP25 disks that were prepared as backup but not implanted in animals were placed in PBS at 37°C on a shaker oscillating at 60 RPM to quantify their cisplatin release profile over 42 days. This release profile served as an indirect measurement of the expected *in vivo* cisplatin release profile of the CDDP25 disks used in this pilot.

4.2.13 Data analysis

All data are expressed as a mean +/- standard deviation. All error bars represent standard deviations from the mean. All samples were examined in triplicate unless if otherwise noted. The GraphPad Prism software was used for all statistical analyses (GraphPad Software, CA, USA). Tissue platinum content values were compared for each organ across treatment groups in the two thin CDDP25 dosing studies using a one-way ANOVA with Tukey's multiple comparisons test. Tumor mass values at euthanasia were compared across treatment groups in the antitumor efficacy pilot using a one-way ANOVA with Tukey's multiple comparisons test. Differences with p-value < 0.05 were considered to be statistically significant. Statistical significance is indicated as: ns $p >= 0.05$; * $p < 0.05$; ** $p < 0.01$; *** $p < 0.001$; **** $p < 0.0001$.

4.3 Results

4.3.1 Structural characterization

Secondary electron SEM imaging of the thin (~0.4 mm) CDDP25 sheet cross-section was performed to assess its topography and compare it to that of the thicker (~1.5 mm) CDDP25 composite material developed previously. Two distinct phases were seen in the thin sheet similar to what was previously seen in the thicker composite, with the minor phase similarly appearing as crystals of various shapes and sizes dispersed homogeneously within a flat-appearing major phase across the height of the cross-section (Figure 4.1A-B). Backscatter electron SEM imaging of the thin CDDP25 sheet cross-section was performed to assess its composition and confirmed the presence of brighter and darker crystals across the silicone matrix thickness attributed to cisplatin and lactose respectively and appearing homogeneously distributed throughout the thickness (Figure 4.1C-D).

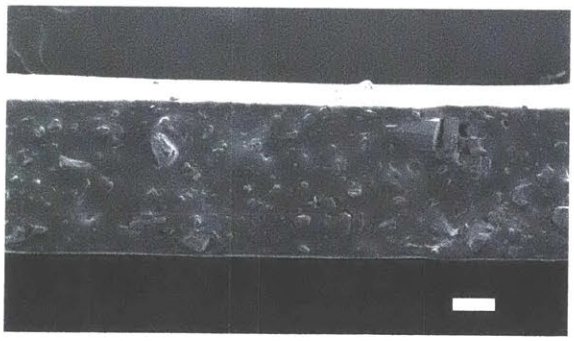

A

B

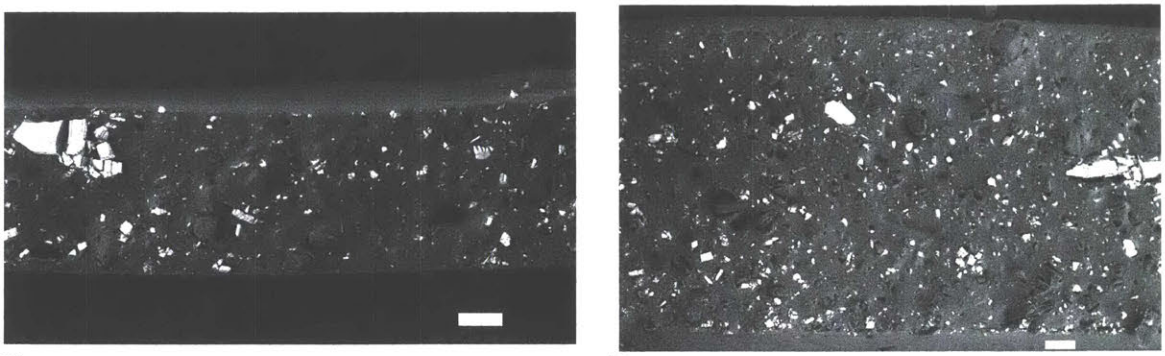

C D

Figure 4.1: SEM images of thin CDDP25 cross-sections. (A)-(B) secondary electron SEM images of cross-sections of (A) thin CDDP25 sheet and (B) thicker CDDP25 disk; (C)-(D) backscatter SEM images (C) thin CDDP25 sheet and (D) thicker CDDP25 disk. The cross-sections are oriented such that the top surface of the cast sample is at the top of the SEM image and the bottom surface that is in contact with the mold is at the bottom. A uniform distribution of crystals throughout the Ecoflex 00-30 matrix is seen in both thin and thick CDDP25 cross-sections. Cisplatin crystals are expected to appear brighter in the backscatter electron SEM than lactose crystals because of the heavier Pt nuclei that more effectively scatter electrons compared to low-atomic-number elements. Scale bars are 100 μm.

4.3.2 Mechanical characterization

LAC50 dog bone-shaped samples with thickness measuring 0.4-0.45 mm underwent tension testing to evaluate their elastic modulus, ultimate tensile strength and elongation at break and compare them to the values previously calculated for thicker LAC50 samples measuring 1-1.5 mm in thickness. The thicker LAC50 material had been deemed appropriate for peritoneal implantation based on its mechanical performance compared to the properties of representative tissues in the abdomen. This mechanical characterization of the thinner LAC50 composite was similarly used as a metric its mechanical appropriateness for intraperitoneal placement. The complete results are shown in Table 4.1.

Material	Elastic modulus (MPa)	Ultimate tensile strength (MPa)	Elongation at break (%)
LAC50 thin	0.186	0.277	454
LAC50 thick	0.226	0.356	590

Table 4.1: Mechanical properties of thin LAC50 samples (0.4-0.45 mm thickness) compared to thick LAC50 samples previously developed (1-1.5 mm thickness). The thinner version of the LAC50 composite is almost 18% less stiff, 22% less strong and 23% less stretchy than the thicker version previously developed. Values are the mean of three measurements from identical samples

The elastic modulus of the thin LAC50 material was 18% lower than that of the thicker material (0.186 MPa compared to 0.226 MPa respectively). The elastic modulus is a material property so no difference in its value would be expected with sample dimension changes for the same material. The difference observed here /is relatively small but not negligible. This difference could be the result of batch-to-batch manufacturing variability since the thicker samples were made and evaluated previously. It could also be the result of defects in the composite structure made more prominent in the thinner

material. The ultimate tensile strength of the thinner LAC50 material was found to be almost 80% of the value calculated for the thicker samples (0.277 MPa compared to 0.356 MPa respectively) meaning that the thinner material is approximately 20% less strong than its thicker counterpart. The thin LAC50 elongation at break finally was found to be approximately 77% of the value calculated for the thicker LAC50 samples (454% compared to 590% respectively) making it slightly less stretchy. The differences in these mechanical properties between the two thickness versions of LAC50 were relatively small. The thinner material was still within the same value ranges as those previously considered for relevance to tissues found in the abdominal cavity like the liver, stomach and intestines suggesting that it would be safe for peritoneal placement. Further assessment of the response of both LAC50 thicknesses to forces specifically experienced during laparoscopic placement, removal and more extreme manipulation is necessary to ensure implantation safety and should be carried out as a next step in material development.

4.3.3 *In vitro* cisplatin release of thin CDDP25

The thickness and diameter of the three CDDP25 disk sizes used for the *in vitro* release studies are shown in Figure 4.2. The cisplatin release profile of the three CDDP25 disk sizes over the 49-day *in vitro* release period is shown in Figure 4.3 as a rate per day (A) and per hour (B). The shape of the release profiles suggests three discrete phases with different rates of release occurring during the same time intervals for all three diameters. The difference in release rate between phases becomes more prominent as disk diameter increases. Linear best-fit trendlines were added to each phase and their slopes used to calculate a weighted average cisplatin release rate taking into account the relative duration of each phase. This weighted average was used as an estimate of a zero-order constant release rate for each disk size for the entire 49-day *in vitro* release period.

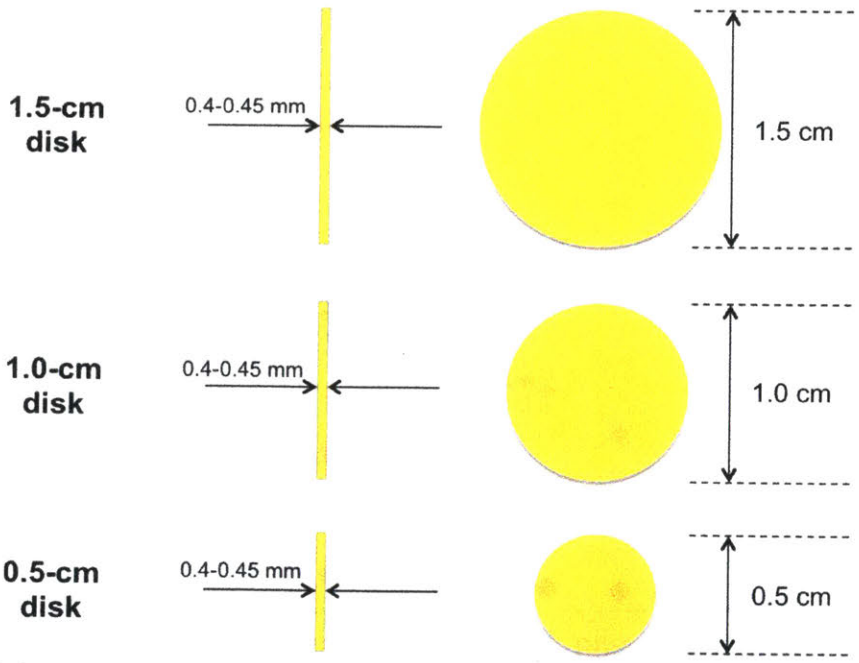

Figure 4.2: Schematic representation of the three thin CDDP25 disk sizes used for *in vitro* release studies. The schematic indicates average thickness and diameter values.

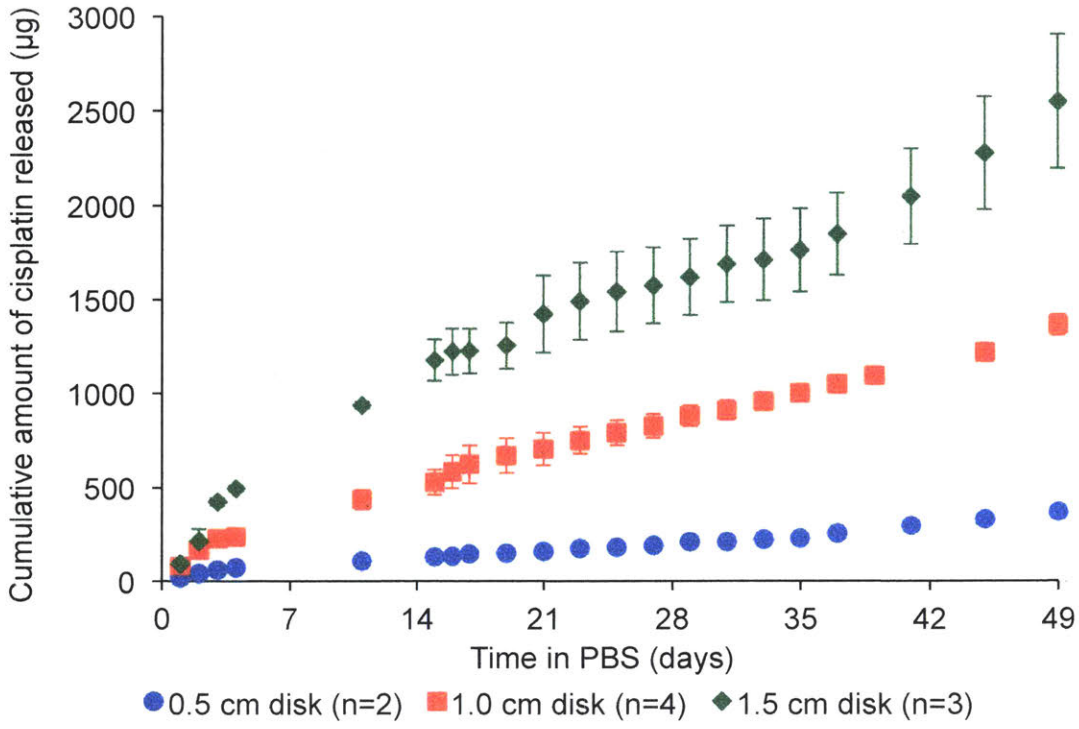
Cumulative amount of cisplatin released (µg)
3000
2500
2000
1500
1000
500
0
0
7
14
21
28
35
42
49
Time in PBS (days)
0.5 cm disk (n=2)
1.0 cm disk (n=4)
1.5 cm disk (n=3)

A

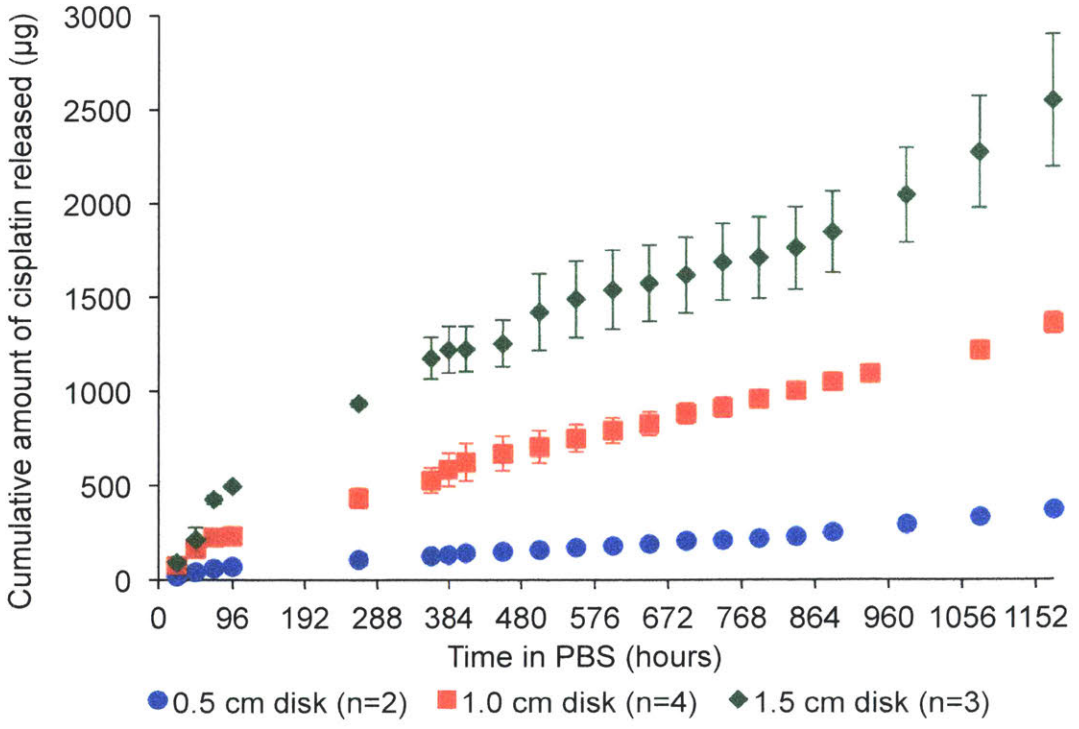
Cumulative amount of cisplatin released (µg)
3000
2500
2000
1500
1000
500
0
0
96
192
288
384
480
576
672
768
864
960
1056
1152
Time in PBS (hours)
0.5 cm disk (n=2)
1.0 cm disk (n=4)
1.5 cm disk (n=3)

B

Figure 4.3: *In vitro* cisplatin release for the 0.5-cm, 1.0-cm and 1.5-cm diameter CDDP25 thin disks over a 49-day period. Time on the x-axis is measured in (A) days or (B) hours. Error bars represent standard deviation from the mean.

The *in vitro* cisplatin release rate for each disk size normalized by the average surface area for release of the sample is plotted in Figure 4.4 as a function of time expressed in hours. The premise behind prototyping a thinner version of the previously developed CDDP25 composite material and using disk surface area to modify cisplatin release rate was the assumption that this new, thinner material will behave similarly to the thicker version of CDDP25 characterized previously. This implies that the thin CDDP material must have a surface area-normalized release rate that is similar to the one calculated for the thick CDDP25 composite (0.773-0.780 $\mu g/cm^2/hr$ calculated using linear best-fit trendlines or weighted average of release rates in each of three distinct phases respectively). An average release rate of 0.777 $\mu g/cm^2/hr$ can be assumed for the thick CDDP25 formulation as the middle value of this range. The normalized release rates for each disk size and their performance against the thick CDDP25 average normalized release rate are found in Table 4.2. The 0.5-cm and 1.0-cm disk sizes were closest to the expected release rate (0.656 $\mu g/cm^2/hr$ and 0.657 $\mu g/cm^2/hr$ compared to 0.777 $\mu g/cm^2/hr$) at 84% and 85% of the expected value respectively. The 1.5-cm disk size was the least close (0.579 $\mu g/cm^2/hr$ compared to 0.777 $\mu g/cm^2/hr$) at 75% of the expected value. The normalized release rates were nevertheless overall close to their expected values. These findings illustrate that the CDDP25 formulation is consistently releasing cisplatin in a predictable manner. The findings also illustrate that the CDDP25 formulation can be scaled both in terms of thickness – which is very important for designing a laparoscopically deployable implant – and in terms of surface area for

release – which provides a way to modulate the cisplatin dose that can be delivered from an implant made out of CDDP25 without altering the formulation itself.

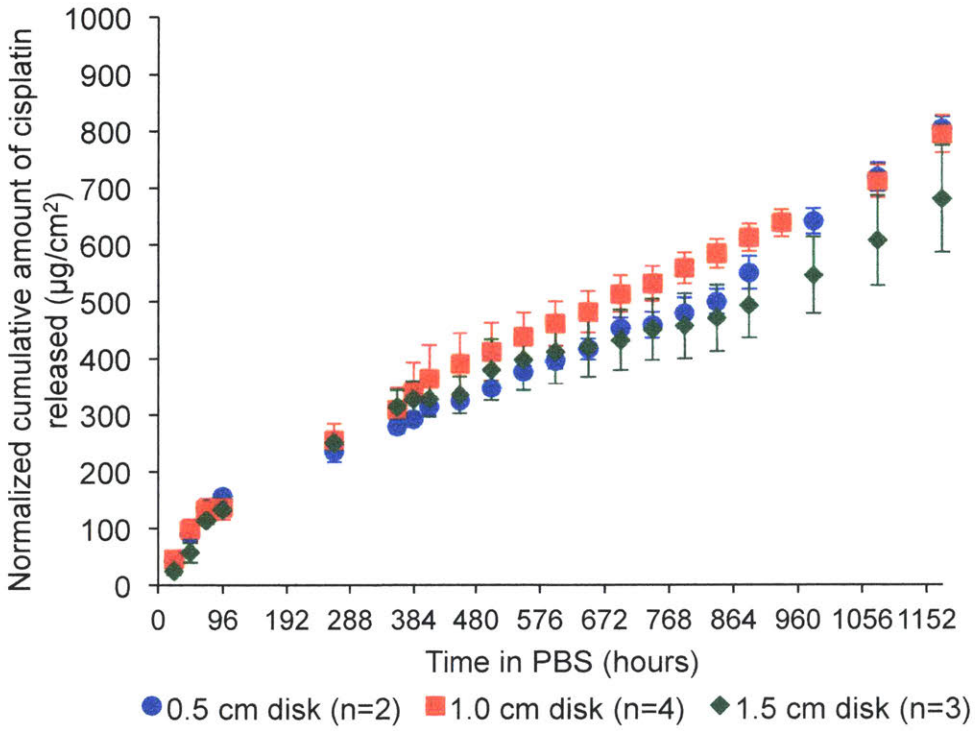

Figure 4.4: *In vitro* cisplatin release normalized to disk surface area for the 0.5-cm, 1.0-cm and 1.5-cm diameter CDDP25 thin disks over a 49-day period. Time on the x-axis is given in hours. The surface area-normalized release profiles were expected to be very similar for all three disk sizes since they comprise the same material. The data are in good accordance with this expectation although there exists some variability in the release profiles that can likely be attributed to human error during manufacturing or cisplatin quantification. The normalized release rates should be close to the normalized *in vitro* cisplatin release rate previously calculated for the CDDP25 thicker version of the composite (0.773-0.780 µg/cm^2/hr). Taking 0.777 µg/cm^2/hr as the average thick CDDP25 release rate, the release rate of the 0.5-cm and 1.0-cm disks (0.656 and 0.657 µg/cm^2/hr respectively) were 84 and 85% of the expected value respectively The release rate of the 1.5-cm disk (0.579 µg/cm^2/hr) was 75% of the expected value. Values in the plot are the mean of results from identical samples (sample number indicated in graph label). Error bars correspond to standard deviation from the mean.

The initial 24-hr burst was not taken into account in calculating *in vitro* release rates as it was eliminated for all disk sizes after 24 hours. The initial 24-hour burst could similarly be eliminated in the actual clinical embodiment of these composite materials

for an intraperitoneal implant, for instance by pre-treating the implant before placement in the patient.

Disk diameter (cm)	Expected *in vitro* release rate (µg/day)	Actual average *in vitro* release rate (µg/day)	Proportion of expected rate achieved (%)
0.5	8.6	7.2	84
1.0	31.7	26.9	85
1.5	70.1	52.5	75

Table 4.2: *In vitro* cisplatin release rate estimation for thin CDDP25 disks of various diameters. A constant *in vitro* release rate for each disk size was estimated over the 49-day period using the duration-weighted average of the slopes of the linear best-fit trendlines through each phase for each size. This rate is compared to the expected release rate based on the disk surface area and normalized release rate of the thicker CDDP25 composite previously developed. The three disk sizes overall performed reasonably well with the worst performing one (1.5 cm) still achieving 75% of its expected release rate.

4.3.4 *In vivo* dosing studies with CDDP25 implants

The first dosing study focused on mice implanted with medium (1.5-cm diameter, n=3 mice) or large (2.0-cm diameter, n=2 mice) CDDP25 disks while the second dosing study focused on mice implanted with small (1.0-cm diameter, n=3 mice) CDDP25 disks (Figure 4.5). The first dosing study lasted 42 days to allow administration of 6 weekly IP cisplatin injections to the injection-treated group and a full week of recovery after the 6th injection. The IP injection group in the second dosing study was euthanized on day 37, 48 hours after receiving their 6th injection to collect data on acute toxicity before the mice had a chance to recover and also quantify tissue platinum levels in the first two days after an injection.

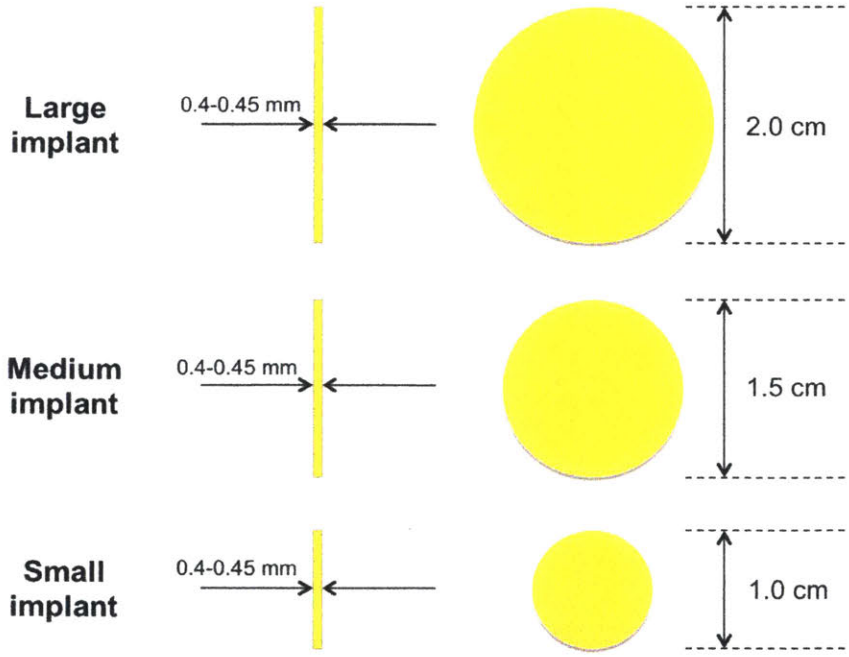

Figure 4.5: Schematic representation of the three CDDP25 disk sizes used for the two *in vivo* dose escalation studies. The schematic indicates average thickness and diameter values. The large and medium implants were used in the first study while the small implant was used in the second study.

Expected *in vitro* cisplatin release rates for each implant size on a daily and weekly basis are given in Table 4.3 along with an average weekly cisplatin dose administered by a 4 mg/kg IP injection to an average-sized mouse weighing 22.5 g. These values allow a comparison of the total weekly cisplatin dose administered with the different treatments, although the implant values are estimates based on *in vitro* release data and not on actual *in vivo* release data. It is therefore expected that the cisplatin dose values for all implant groups are likely to be lower *in vivo* than the estimates in Table 4.3. Many factors can affect implant release inside the peritoneal cavity including: (i) implant contact with connective tissues like fat that may affect the implant surface area available for cisplatin release; (ii) any fibrotic response to the implant that may encase it in a fibrous sheath affecting cisplatin transport through it and to the surrounding peritoneal cavity; and (iii) the protein-rich environment of the peritoneal fluid compared to PBS used for *in vitro* release. The table values however still provide a means of comparison of estimated weekly doses for each treatment as a ballpark.

Dosing Study	Implant diameter (cm)	Estimated *in vitro* release rate (µg/week)	Ratio to weekly 4 mg/kg IP cisplatin injection
2	1.0	182.2	2.0
1	1.5	397.2	4.4
1	2.0	695.9	7.7

Table 4.3: Comparison of the estimated weekly cisplatin dose released by each implant size used in the two dose escalation studies to the amount of cisplatin delivered once weekly by a 4 mg/kg IP injection. An average mouse mass of 22.5 g was used for calculating the IP injection dose administered since the mice used in these two studies weighed 20-25 g. The estimated weekly cisplatin dose released by the implants is calculated based on a 15.13 $\mu g/cm^2$/day average cisplatin release rate calculated from multiple *in vitro* release studies of various sample diameters. The actual *in vivo* cisplatin dose achieved with each implant size has not yet been quantified so this is providing an estimate that is expected to be higher than what can actually be accomplished *in vivo* due to any fibrosis of the implant, contact with tissues like the fat pad obstructing release from parts of its surface and the higher protein content of the peritoneal fluid compared to PBS.

The amount of platinum (Pt) present in different tissues of the peritoneal cavity was quantified for the small- and medium-implant and IP injection groups and is shown in Figure 4.6A. The large-implant group was not included in the analysis because the animals had to be euthanized just 3 days after implantation due to toxicity. The medium implant achieved a higher concentration of Pt in all tissues examined compared to either the small implant or to six 4 mg/kg IP cisplatin injections at the 42-day time point. The difference between the medium implant and the six injections was statistically significant for the liver ($p = 0.0008$), kidney ($p = 0.0095$), small intestine ($p = 0.0007$) and large intestine ($p = 0.0143$). The medium CDDP25 implant, even though releasing cisplatin continuously at a much lower dose than that achieved instantaneously by each 4 mg/kg IP injection, is able to accomplish more Pt delivery to key tissues of interest in the abdominal cavity that are frequently sites of metastasis in ovarian cancer. The medium implant was expected to deliver a total cisplatin dose 4.4X larger than the total dose delivered by the IP cisplatin injections and so this may in part explain the difference in Pt content seen in the tissues. The small implant on the other hand achieved a lower Pt content in all organs compared to either the medium implant or the 6 injections at the 42-day time point even though it is expected to release a total cisplatin dose that is 2.0X

larger than the total injection dose. The difference between the small and medium implant was statistically significant for the liver ($p < 0.0001$), the spleen ($p = 0.0097$), the kidney ($p = 0.0020$), the small intestine ($p = 0.0001$) and the large intestine ($p = 0.0017$). There was no statistical significant difference between the small implant and the IP injection group at the 42-day time point.

The amount of Pt in blood serum ultrafiltrate from the small- and medium-implant mice and corresponding IP injection mice measured by ICP-MS is plotted on a logarithmic scale in Figure 4.6B. Three different time points were sampled in the IP injection group, at 2 hours, 48 hours and 7 days after the 6th cisplatin injection (blue squares). The 2-hr and 48-hr samples come from a different batch of animals than the 7-day samples (IP injection group of second and first dose escalation study respectively). The Pt content values in the IP injection group illustrate a spike in serum Pt content reaching 583 µg/L 2 hours after injection and dropping to approximately 11 µg/L 7 days later. The small-implant group time points all correspond to the intended euthanasia point 42 days after surgical implantation and illustrate a serum Pt content of approximately 19 µg/L. The medium-implant group contains two Pt serum values, one from the two mice euthanized on the intended date at 42 days after implantation (~66.5 µg/L) and one from the single mouse that had to be euthanized early 10 days after implantation (~163 µg/L). The serum Pt value of the medium-implant mouse that had to be euthanized is more than twice the value of the other two mice in the same group that survived. This can be explained by revisiting the *in vitro* release profile of the medium implants shown in Figure 4.3. The profile displayed a faster release phase in the first two weeks that then dropped to a lower release rate for more than 20 days and

appeared to accelerate again on day 37. The medium-implant mouse euthanized early may have still been experiencing the steep accelerated release of those first few days, which may in part explain its demise and also the elevated Pt serum value. It could be plausible that the medium implant assigned to this mouse released cisplatin at an even faster rate than that expected due to sample-to-sample variability. This possibility was ruled out by resuming *in vitro* cisplatin release for this implant after it was explanted from the euthanized mouse and comparing the profile to that of an extra medium implant from the same batch that had been prepared as a backup for this study. The release profile for these two medium implants is plotted in Figure 4.6C and shows a similar release profile for the two samples. The Pt serum levels measured for the two implant groups were all detectable but well below the maximum Pt serum level measured for the IP injection groups, with the maximum Pt serum level measured in an implant-bearing mouse being less than 30% of the maximum Pt serum level measured in IP-injected mice (162.96 µg/L vs. 582.87 µg/L respectively).

The fact that a higher total cisplatin dose can be delivered with a CDDP25 implant compared to periodic bolus IP injections raises a critical question regarding the tolerability and toxicity of such an implant. Answering this question is key to assessing the potential of this continuous low-dose approach for optimizing maximum tolerated dosing. The weights, CBC and histology of harvested tissues were all evaluated for the two dosing studies to determine whether the dose delivered by each implant size was toxic to the mice.

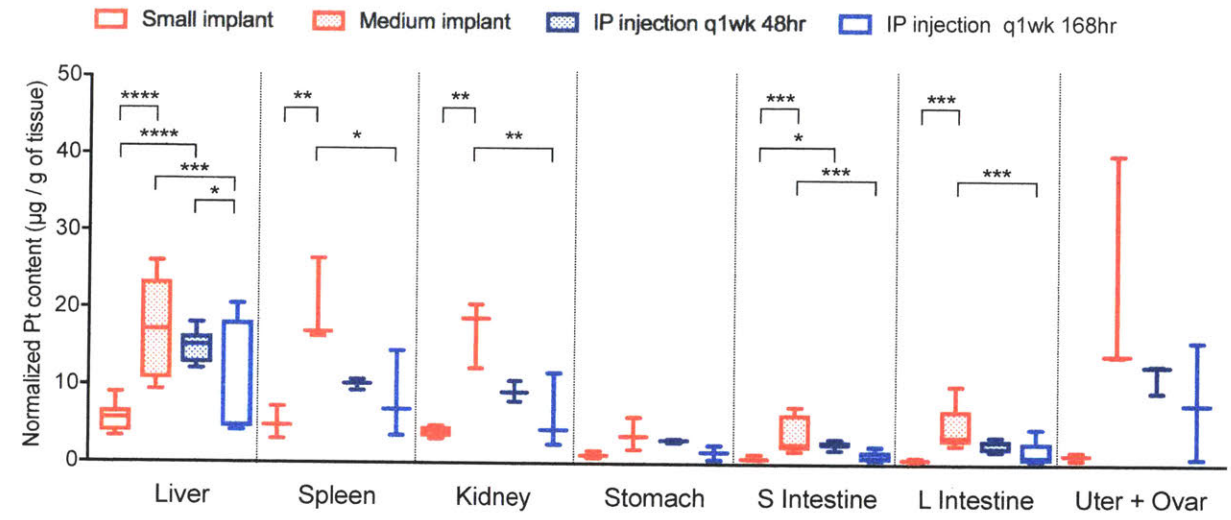
Small implant
Medium implant
IP injection q1wk 48hr
IP injection q1wk 168hr
Normalized Pt content (µg / g of tissue)
50
40
30
20
10
0
****
****
***
*
**
*
**
**
***
*
***
***
***
Liver
Spleen
Kidney
Stomach
S Intestine
L Intestine
Uter + Ovar

A

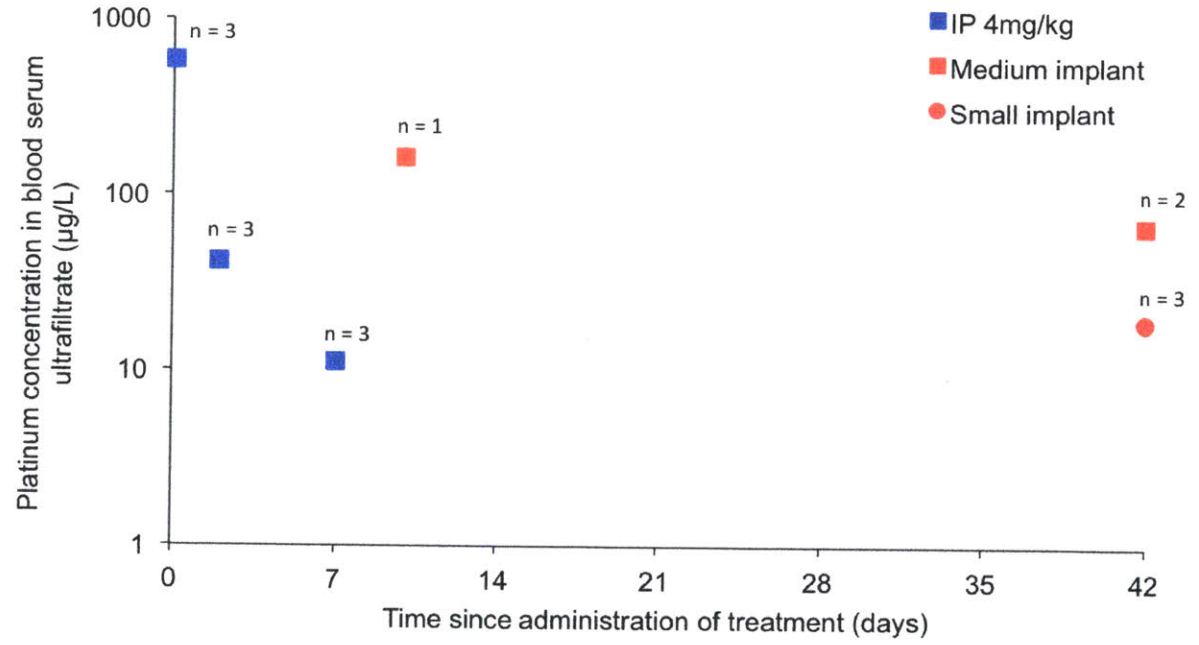
IP 4mg/kg
Medium implant
Small implant
Platinum concentration in blood serum ultrafiltrate (µg/L)
1000
100
10
1
n = 3
n = 3
n = 3
n = 1
n = 2
n = 3
0
7
14
21
28
35
42
Time since administration of treatment (days)

B

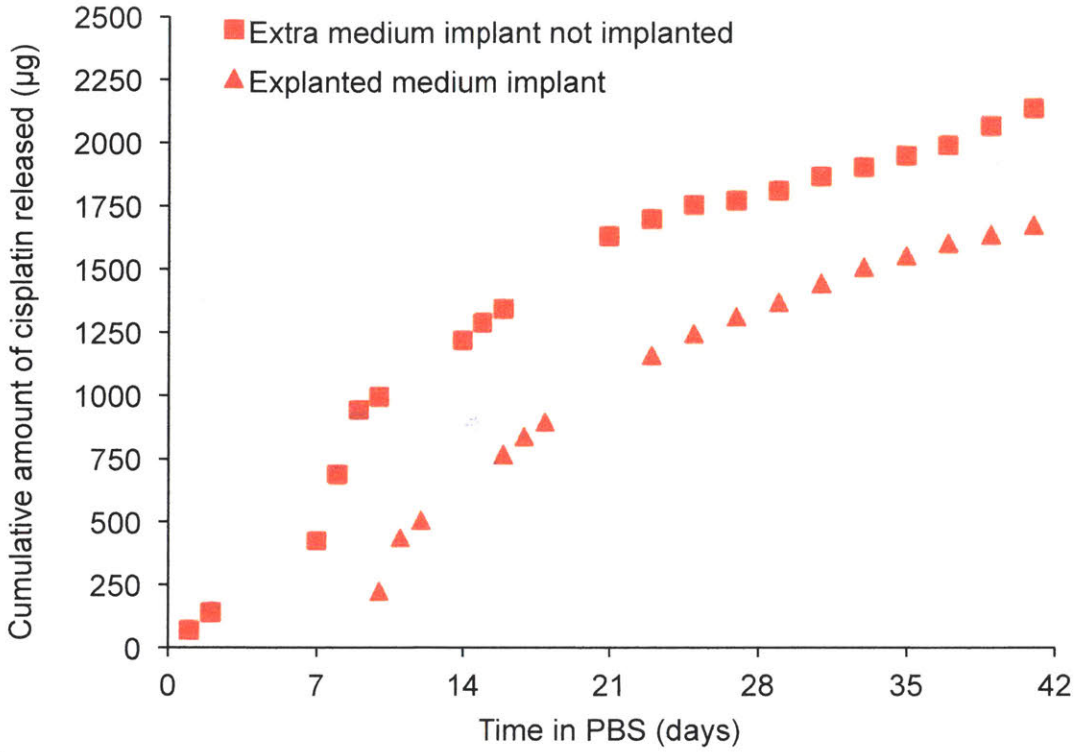

C

Figure 4.6: Platinum quantification and cisplatin release results from the two thin CDDP25 *in vivo* dosing studies. (A) Box-and-whiskers plots of the average normalized tissue platinum (Pt) content in ppm for the small- and medium-implant and IP injection groups quantified at euthanasia. The IP injection mice in study 1 were euthanized 7 days after the 6th injection while the IP injection mice in study 2 were euthanized 48 hours after the 6th injection. The ends of the box are the upper and lower quartiles of the data, the lines outside the box indicate the highest and lowest values and the median is marked by the vertical line inside the box. The medium-implant group had higher normalized Pt content in all organs compared to the IP injection and small-implant groups. The difference between the medium implant and six injections was statistically significant for the liver, kidneys, small intestine and large intestine when compared with a one-way ANOVA. The difference between the medium implant and the small implant was statistically significant for all organs except for the stomach and the reproductive system (ovaries, uterus). There was no statistically significant difference between the small implant group and the six IP injections. These data support the hypothesis that the medium CDDP25 implant, even though releasing cisplatin continuously at a much lower dose than that achieved instantaneously by each 4 mg/kg IP injection, is able to achieve more Pt delivery to key tissues of interest in the abdominal cavity. The medium implant was expected to deliver a total cisplatin dose 4.4X that delivered by the 6 combined IP cisplatin injections and so this may in part explain the difference in Pt content seen with this data. (B) Blood serum ultrafiltrate Pt levels in samples from mice implanted with a small or medium implant or receiving weekly 4 mg/kg IP cisplatin injections. The time since administration of treatment is measured starting on surgery day for implant-bearing mice and starting on the day of the last injection for injection-treated mice. The number of animals sampled at each point is indicated above the data point. Both small and medium implants resulted in detectable Pt levels in the serum that were nevertheless orders of magnitude lower than the maximum Pt serum level in the IP injection group, measured

2hr after injection. Not enough blood could be collected by the large-implant mice at euthanasia for serum ultrafiltration and isolation of unbound cisplatin for quantification by ICP-MS. (C) *In vitro* cisplatin release was tracked for an extra medium implant produced with those implanted in mice but not used *in vivo* (red squares) as well as the medium implant explanted from the mouse that had to be euthanized early 10 days after implantation (red triangles). Both release profiles were similar to that expected from other medium-implant *in vitro* release studies and the original release studies of the CDDP25 formulation using thicker samples. This confirmed that the implants were behaving as expected in terms of cisplatin release, to help address the cause behind the early demise of a medium-implant mouse.

4.3.5 CDDP25 implant tolerability evaluation – *in vivo* dosing study 1

Animal survival for the first dosing study is plotted in Figure 4.7A. The mice implanted with large disks (large-implant) had to be euthanized 3 days after undergoing surgery for disk implantation because of poor body condition (signs of respiratory distress). One of the mice implanted with medium disks (medium-implant) had to be euthanized on day 10 after surgery because of exceeding 20% weight loss despite supportive measures even though it was alert and behaviorally otherwise appeared healthy. The remaining two medium-implant mice and three IP-injection mice were followed over the intended 42-day (6-week) period.

Average animal weights tracked over the study duration are plotted in Figure 4.7B. The mice receiving a weekly 4 mg/kg IP injection of cisplatin (blue rectangles) exhibited weight fluctuations that aligned with their injection schedule: their weight dropped visibly soon after receiving an injection and eventually started recovering only to plummet again with the next injection. They appeared to stabilize at a weight that was approximately 90% of their original pre-treatment weight by the 5^{th} injection although the standard deviation of the weight measurements is high and increasing over time, suggesting significant animal variability within the group. The two remaining medium-implant mice also experienced a marked drop in their weight after surgery that eventually brought them down to approximately 80% of their pre-treatment weight. The two mice remained stable at this reduced weight but were alert and responsive throughout the 42-day study despite their weight loss.

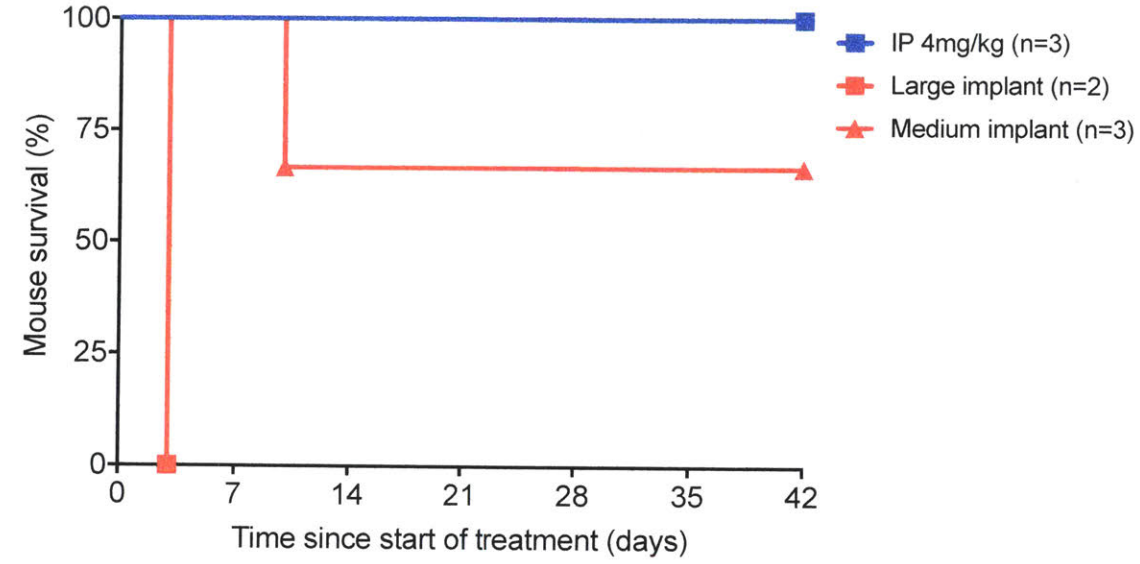

A

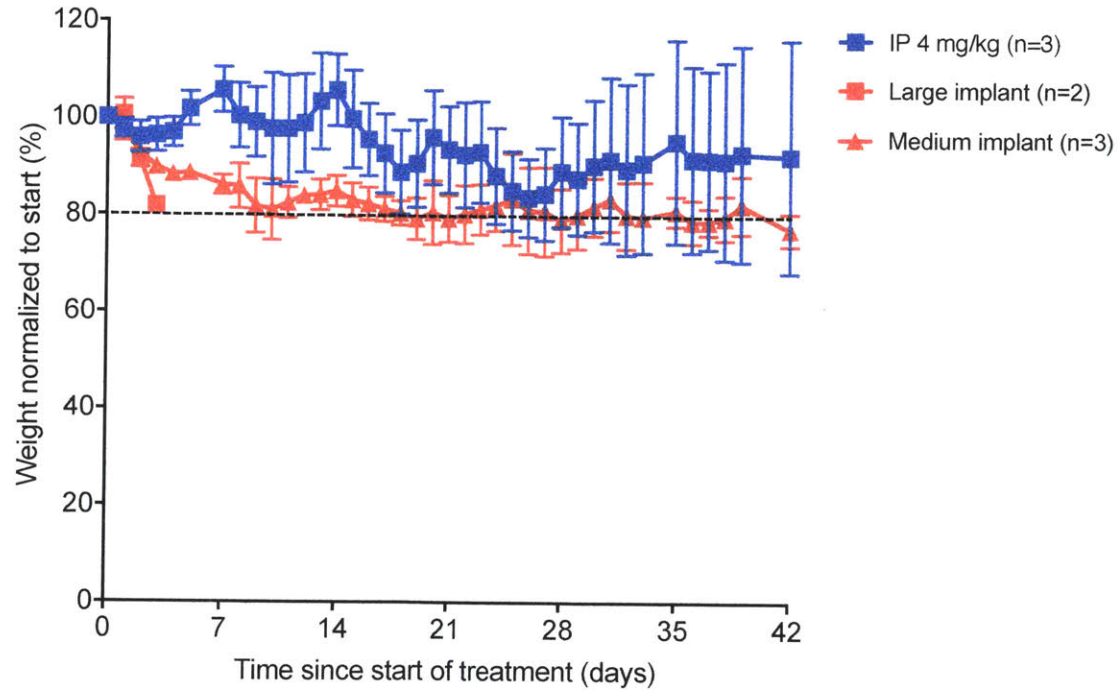

B

Figure 4.7: Tolerability of the thin CDDP25 implants in the first dosing study. (A) Survival plot and (B) average animal weight plot for the three treatment groups in the first dose escalation study. Large-implant animals had to be euthanized three days after the start of treatment due to toxicity and poor body condition. One of the medium-implant mice also had to be euthanized early at ten days after the start of treatment because of rapid weight loss that did not recover even though it appeared otherwise healthy. The mice receiving a weekly 4 mg/kg IP cisplatin injection displayed a seesaw weight loss pattern matching their injection schedule, with each injection resulting in a weight plummet and an eventual recovery to about 90% of their pre-treatment weight and stabilization after the last injection.

The standard deviation from the mean weight in this group was however quite large indicating that some animals dropped a lot more weight with each injection while others tolerated the treatment better. The medium-implant mice experienced a weight loss following surgery that reached approximately 20% of their pre-surgery weight and remained relatively stable around the 80% weight value throughout the rest of the treatment period. The standard deviation from the mean weight in the medium-implant group was much smaller compared to the IP injection group, suggesting that these mice more consistently responded to treatment with the medium implant in terms of weight fluctuation. The values plotted are the mean weight of the mice in each group surviving at each time point and the error bars correspond to standard deviation from the mean. The dashed line indicates the 20% weight loss point that is commonly used as a criterion for euthanasia alongside the rest of the clinical picture of the animal.

The average CBC values at euthanasia for all treatment groups in the study are plotted in Figure 4.8. Dashed lines have been added to indicate normal range bounds for each cell type. All values were within normal bounds for all treatment groups with the lymphocyte count (Figure 4.8C) being borderline low for large-implant mice and the platelet count for similarly being borderline low IP-injection and large-implant mice (Figure 4.8E), which suggests the possible start of bone marrow depletion due to the cisplatin dose received.

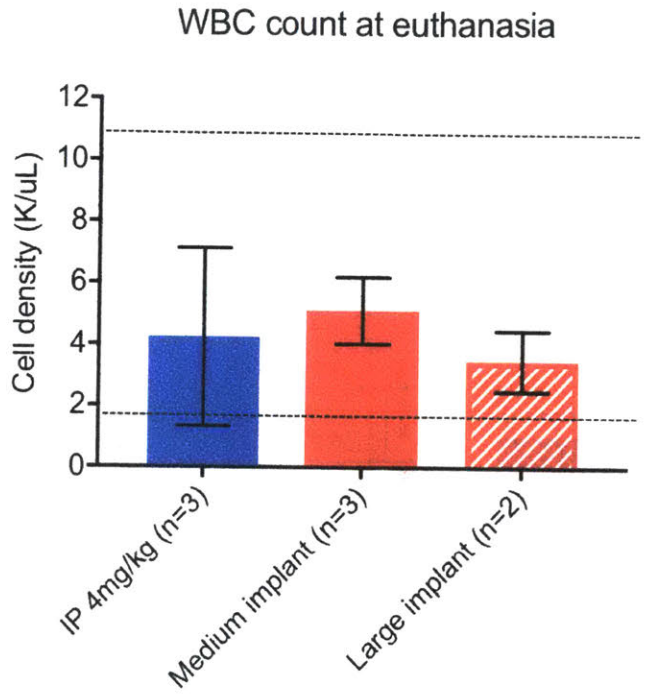
WBC count at euthanasia
Cell density (K/uL)
12
10
8
6
4
2
0
IP 4mg/kg (n=3)
Medium implant (n=3)
Large implant (n=2)

A

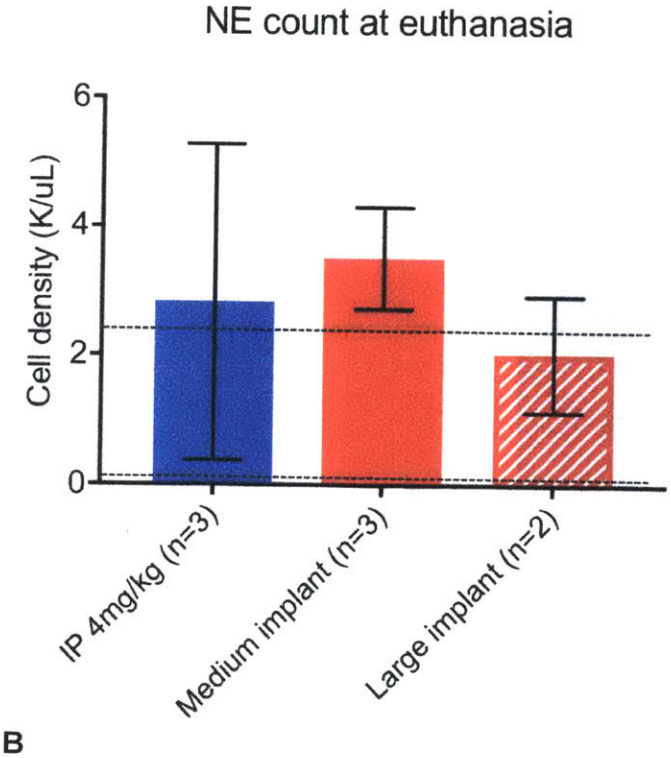
NE count at euthanasia
Cell density (K/uL)
6
4
2
0
IP 4mg/kg (n=3)
Medium implant (n=3)
Large implant (n=2)

B

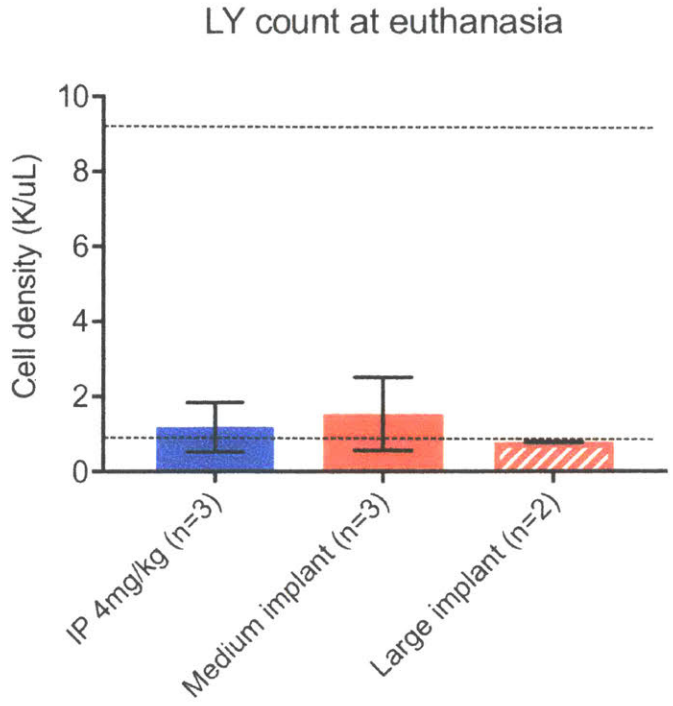
LY count at euthanasia
Cell density (K/uL)
10
8
6
4
2
0
IP 4mg/kg (n=3)
Medium implant (n=3)
Large implant (n=2)

C

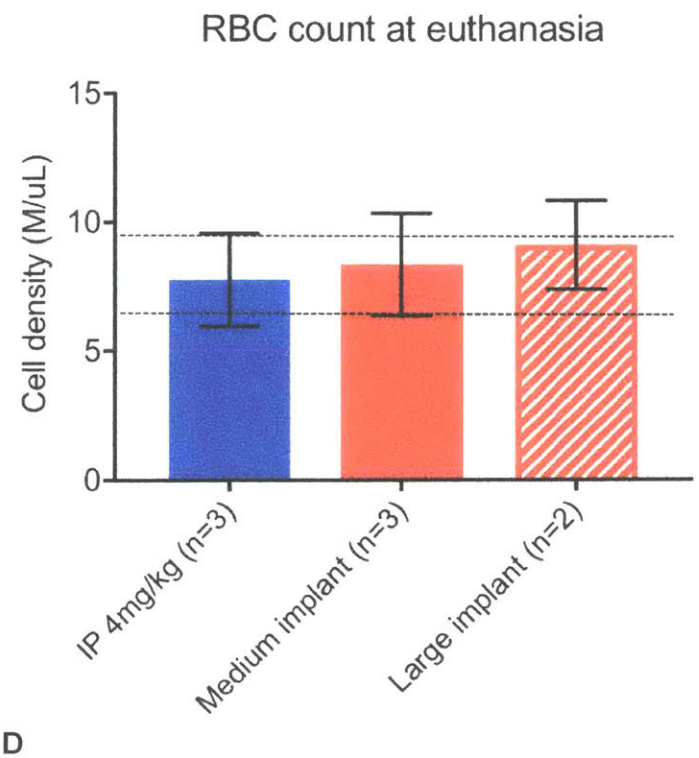
RBC count at euthanasia
Cell density (M/uL)
15
10
5
0
IP 4mg/kg (n=3)
Medium implant (n=3)
Large implant (n=2)

D

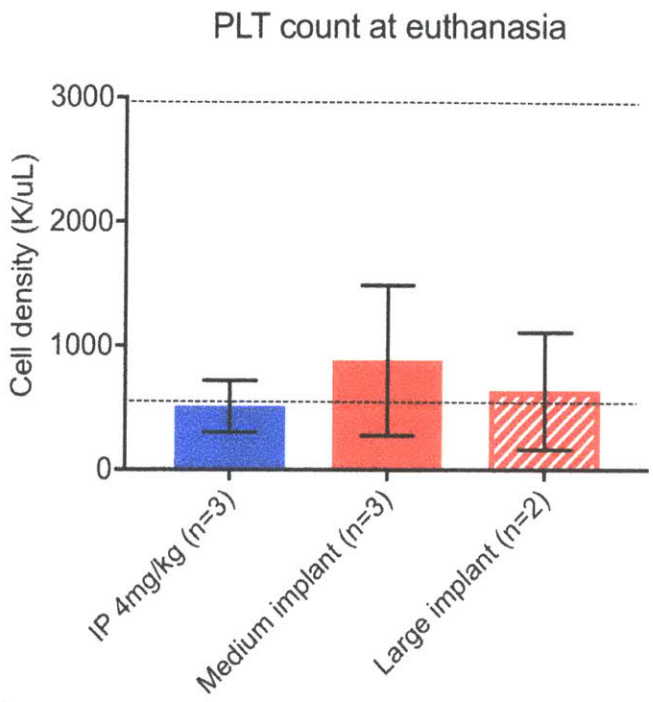

E

Figure 4.8: Plots of the average cell density of different blood cell populations for each of the three treatment groups in the first thin CDDP25 dosing study. The populations assessed are: (A) white blood cells, (B) neutrophils, (C) lymphocytes, (D) red blood cells and (E) platelets. Values were obtained by CBC with auto-differential from samples collected at euthanasia. All values were within normal bounds for all groups with the exception of lymphocyte counts for the large-implant group (borderline low). Lymphocyte counts were at the lower end of the normal range for all three groups but the Nu/Nu mice lack a thymus and display reduced lymphocyte counts in general. The platelet counts for the mice receiving weekly 4mg/kg IP injections and those with a large implant were also at the lower end of the normal range, suggesting platelet depletion possibly as a result of the cisplatin dose given. Platelet counts are an important indicator in cancer treatment since patients will be taken off chemotherapy when their platelets drop to dangerously low numbers and put them at risk for uncontrollable bleeding. The fact that the platelet counts for the medium-implant mice are the highest in this group suggests that this treatment is best tolerated from that safety perspective. It is important to note that the medium-implant mouse that required euthanasia early due to rapid weight loss had an elevated red blood cell count of 10.58 M cells / µL (upper normal bound is 9.42 M cells / µL) suggesting that it was dehydrated and this may have caused its rapid weight loss. Dashed lines indicate normal value bounds.

Histologic examination of the liver, kidneys, spleen, small and large intestine and explanted implant – for implant treatment groups – of the mice in this study showed extensive kidney and gut damage in large-implant mice (Figure 4.9A) and no fibrotic response to the implant as well as minimal tissue toxicity in medium-implant mice (Figure 4.9B). This included the medium-implant mouse that had to be euthanized early 10 days after surgical implantation. This mouse suffered rapid dehydration whose cause could not be identified on necropsy. The *in vitro* cisplatin release profile of an extra medium implant prepared for this study but not implanted in an animal displayed very rapid release on days 7-9 (Figure 4.6C). It is possible that the health deterioration of the animal leading to its euthanasia was the result of a similar faster cisplatin release happening in those first 10 days that this particular mouse tolerated less well than the two that survived the entire 42-day study period. The large implants explanted from the two mice in this study were not submitted for histology because they were removed after only three days of implantation and were saved instead for future cisplatin *in vitro* release studies and cisplatin quantification analysis.

The weight, CBC and histologic findings taken together indicate that the large implant (2.0-cm diameter) caused intolerable toxicity due to its cisplatin release rate and that the medium implant (1.5-cm diameter) resulted in borderline tolerable toxicity and therefore may be indicative of the maximum tolerated dose for the cisplatin-eluting CDDP25 composite material.

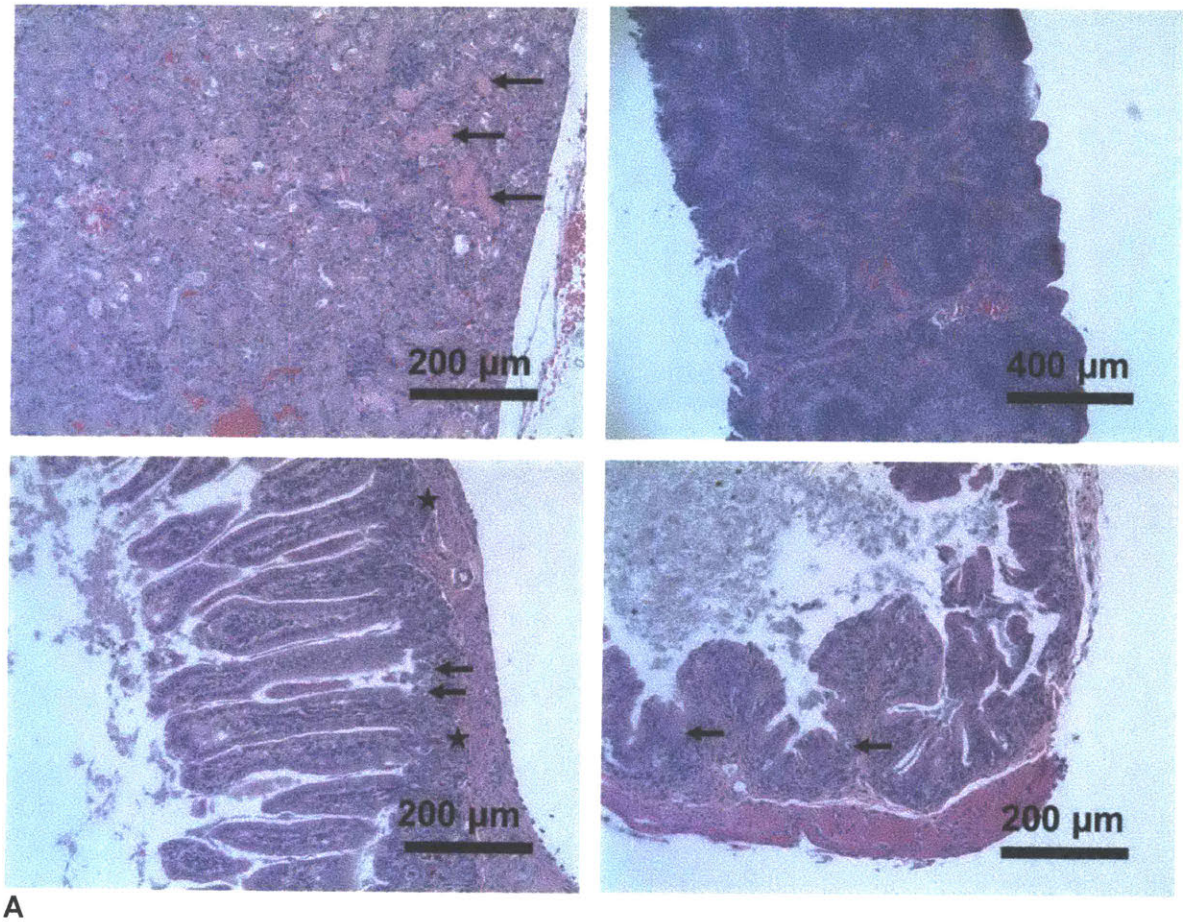

A

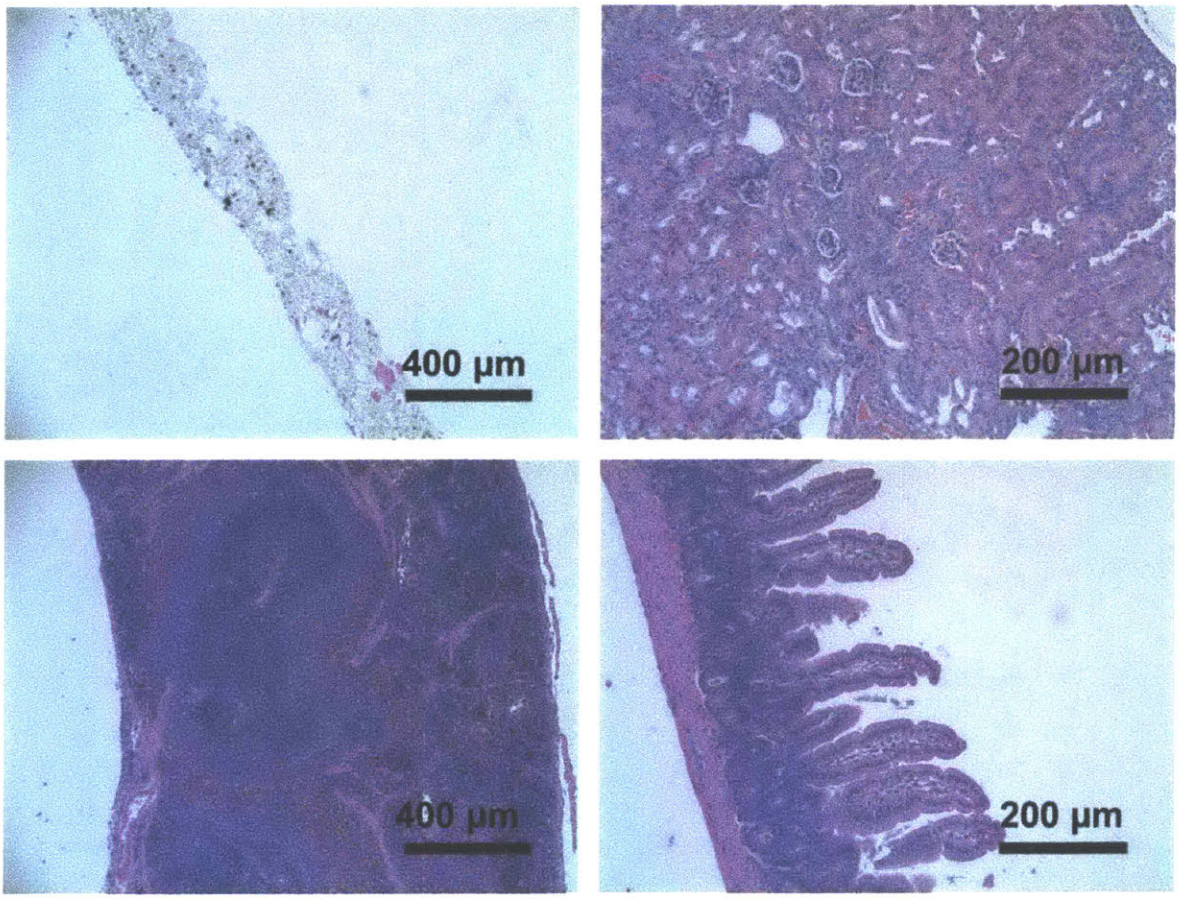

B

Figure 4.9: Representative histology with H&E staining from mice implanted with thin CDDP25 disks in the first dosing study. Mice received (A) large or (B) medium implants. (A) Clockwise from top left: kidney, spleen, small intestine and colon sections. There was marked tubular epithelium apoptosis and protein accumulation (arrows) in the renal cortex and a lot of apoptosis in the spleen. Paneth cells in the small intestine had very red granules and an abnormally large number of them had released their granules out of the cytoplasm (star). There were apoptotic cells near the base of the villi (arrows). The colon displayed an uneven crypt border and apoptotic cells (arrows) as well. (B) Clockwise from top left: implant, kidney, spleen and small intestine cross sections. No fibrosis or other signs of an inflammatory response were visible in the implant histology. The kidney showed no signs of acute damage but a small amount of tubular regeneration was evident. The spleen and small intestine both appeared normal.

4.3.6 CDDP25 implant tolerability evaluation – *in vivo* dosing study 2

Animal survival for the second dose escalation study is plotted in Figure 4.10A. All mice survived and were followed over the intended treatment period (37 days to include 48 hours after the 6th injection for the IP injection group and 42 days for the small-implant group).

Average animal weights tracked over the study duration are plotted in Figure 4.10B. The mice receiving a weekly 4 mg/kg IP injection of cisplatin (blue rectangles) again exhibit weight fluctuations that align with their injection schedule: their weight drops visibly soon after receiving an injection and eventually starts recovering only to plummet again with the next injection. They lost 20% of their weight following the first injection to recover almost fully by day 21. They then experienced consistent weight loss until their euthanasia on day 37 at which point they had reached almost 70% of their pre-treatment weight. These mice appear to have tolerated the weekly IP cisplatin injection regimen less well than the equivalent IP injection group in the first dosing study (Figure 4.7B). The small-implant mice lost approximately 20% of their pre-surgery weight by the first week after implantation but had returned to almost 95% of their pre-surgery weight by day 28 of the study. The error bars in the small-implant group were smaller than those in the weekly IP injection group similarly to what was observed in the first *in vivo* dosing study of the thin CDDP25 material suggestive of less animal-to-animal variability in tolerating this dosing regimen.

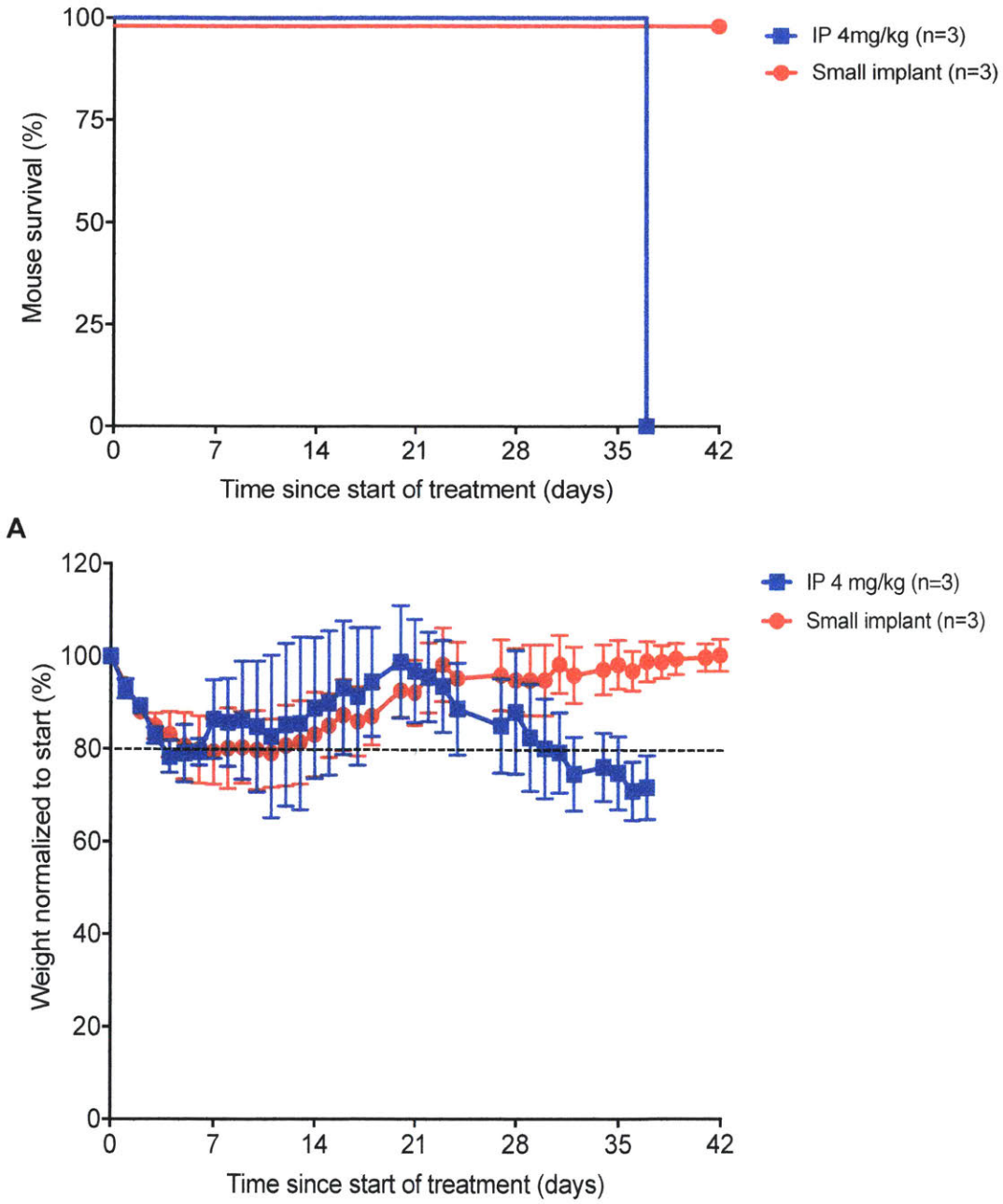

Figure 4.10: Tolerability of the thin CDDP25 implants in the second dosing study. (A) Survival plot and (B) average animal weight plot for the two treatment groups in the second dosing study. All mice survived to the intended euthanasia time point (48 hours after the 6th injection for IP injection mice and 42 days after implantation for small-implant mice). The mice receiving a weekly 4 mg/kg IP cisplatin injection (blue squares) displayed a seesaw weight loss pattern matching their injection schedule, with each injection resulting in a weight plummet. These animals experienced a more dramatic weight loss compared to the same treatment group in the first dose escalation study, losing more than 80% of their weight after the first injection,

recovering slightly and eventually undergoing weight loss without recovery after the 5th injection that brought them well below the 20% weight loss cutoff commonly used as an indicator for euthanasia. The small-implant mice (red circles) experienced weight loss following surgery that reached approximately 20% of their pre-surgery weight, remained relatively stable at this reduced weight until approximately 14 days after implantation and then recovered to almost 95% of their pre-surgery weight by day 28. The values plotted are the mean weight of the mice in each group surviving at each time point and the error bars correspond to standard deviation from the mean.

The average CBC values at euthanasia for both treatment groups in the study are plotted in Figure 4.11. Dashed lines have been added to indicate normal range bounds for each cell type. All values were within normal bounds for all treatment groups with the exception of the platelet count (Figure 4.11E) being low for IP-injection mice, which is reasonable given their weight loss and suggests toxicity to the bone marrow likely as a result of the repeated cisplatin injections.

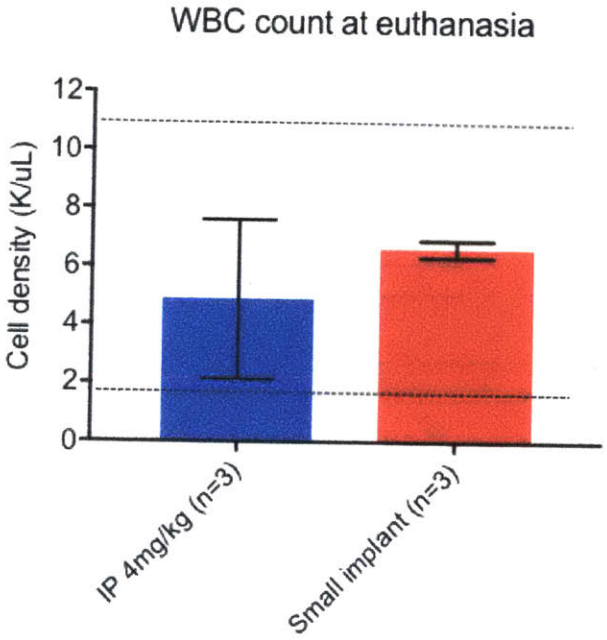

A

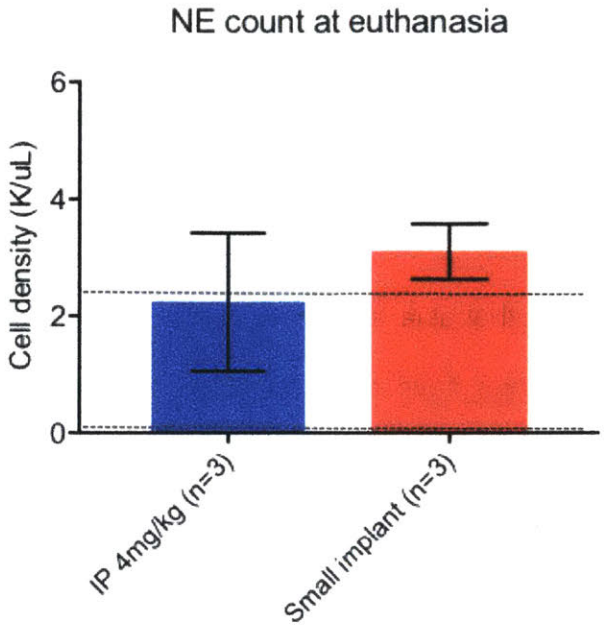
NE count at euthanasia
Cell density (K/uL)
6
4
2
0
IP 4mg/kg (n=3)
Small implant (n=3)

B

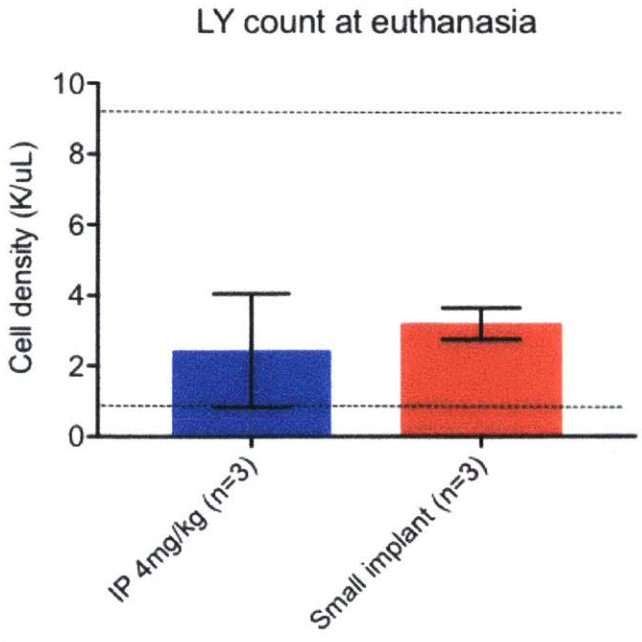
LY count at euthanasia
Cell density (K/uL)
10
8
6
4
2
0
IP 4mg/kg (n=3)
Small implant (n=3)

C

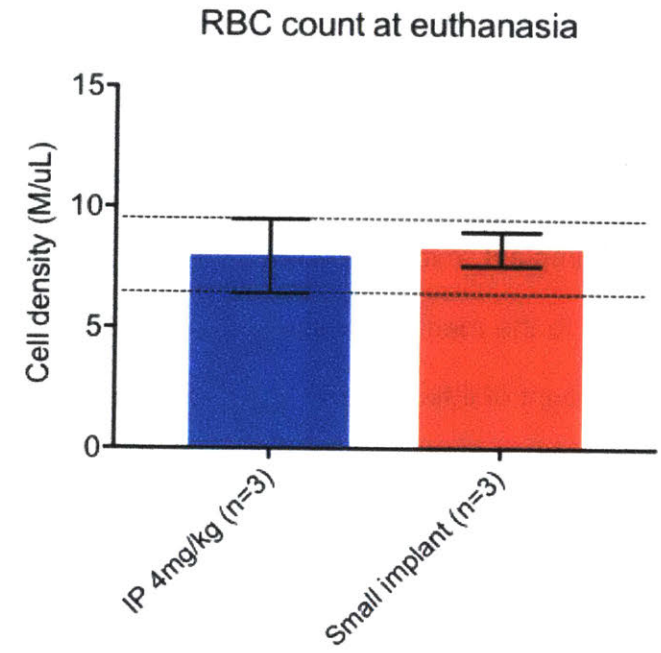

D

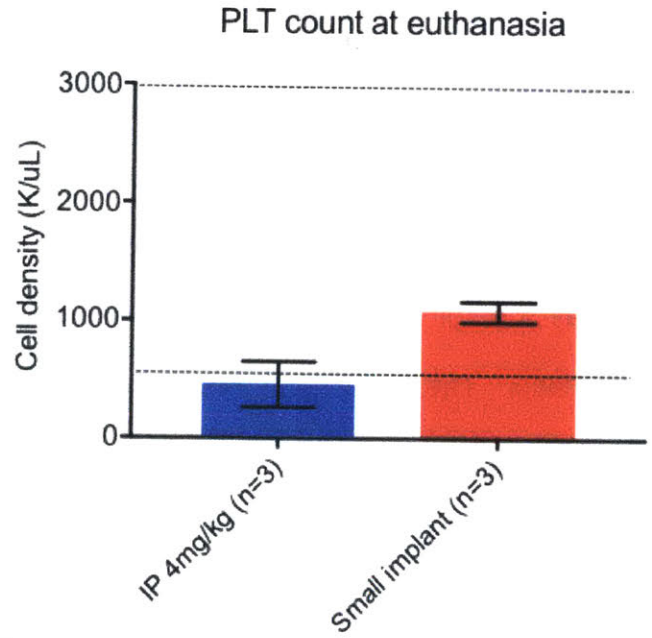

E

Figure 4.11: Plots of the average cell density of different blood cell populations for each of the two treatment groups in the second thin CDDP25 dosing study. The populations assessed are: (A) white blood cells, (B) neutrophils, (C) lymphocytes, (D) red blood cells and (E) platelets. Values were obtained by CBC with auto-differential from samples collected at euthanasia. All values were within normal bounds for all groups with the exception of platelet counts for the IP injection

group that were low. Dashed lines indicate normal value bounds.

Histologic examination of the liver, kidneys, spleen, small and large intestine of the mice in this study showed no signs of toxicity in either treatment group. The explanted implants of the small-implant mice showed however a greater fibrotic response to the implants compared to the medium-implant mice in the first dosing study (Figure 4.12). A more extensive amount of inflammation and deposition of fibrous tissue were noted in these histologic sections. The small implants were found to be more mobile inside the abdomen after implantation compared to the medium implants: two of the three implants had migrated to distant locations from the site of placement on surgery, one being found at the back of the animal pushing against its spine and the other enveloping one of the liver lobes. Only one small implant was found close to the site of placement on surgery. All three medium implants were found near the site of placement on surgery for comparison. This implant migration *in vivo* displayed by the small-implant group may help explain the more extensive inflammatory response and fibrosis caused by these implants as a result of movement of the implants inside the abdomen and subsequent tissue irritation. The small implant that had enveloped a liver lobe was found to have created a thin layer of inflammatory fibrotic tissue at the boundary between the implant and the liver but no tissue damage further inside the liver was noted. This suggests that the cisplatin dose delivered by the small implants was not in itself toxic.

The small-implant mice in this second dosing study tested positive by polymerase chain reaction for corynebacterium bovis (C. bovis), a pathogenic bacterium that causes scaly skin lesions in mice and is highly contagious. It is possible that any

bacteria that crossed to the mouse systemic circulation localized themselves to the implant forming a biofilm and exacerbated any inflammatory response already mounting against it.

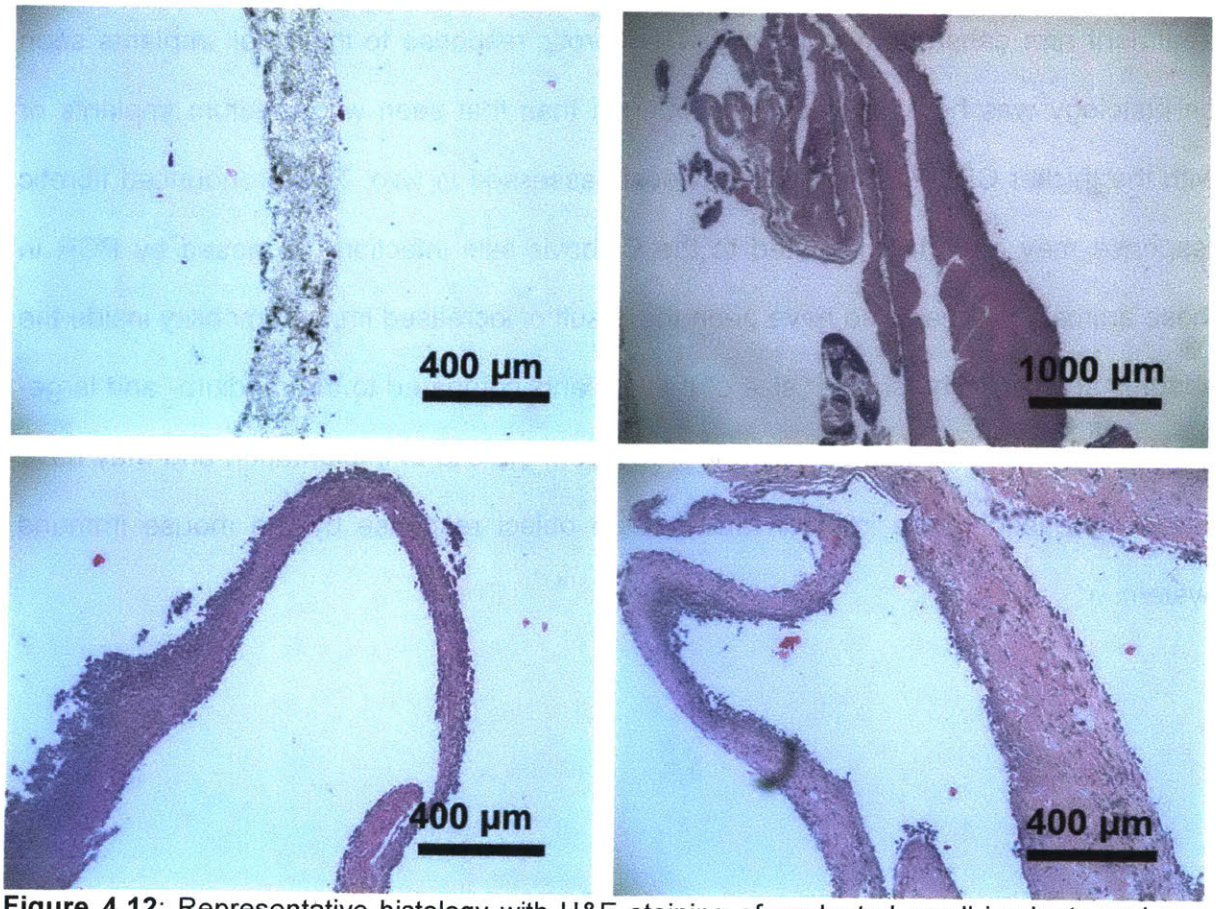

Figure 4.12: Representative histology with H&E staining of explanted small implants and any surrounding fibrotic response. Clockwise from top left: cross-section of a small implant after explantation; fibrotic tissue from all three small-implant mice. The first and second fibrotic tissue panels at the top right and bottom right respectively show the response to the small implant that migrated to the back and the implant that enveloped a liver lobe respectively. The last fibrotic tissue panel at bottom left shows the response to the small implant that stayed close to the site of placement at surgery. The fibrotic response was least pronounced for the implant that did not migrate far from the site of placement at surgery, suggesting that implant movement within the abdominal cavity may be problematic for implant tolerability and functionality.

The weight and CBC findings taken together suggest that the small implant was well tolerated by the animals in terms of systemic toxicity while the 4 mg/kg IP injections led to toxicity that met the requirements for animal euthanasia before the end of the study. The histologic findings regarding abdominal organs similarly suggest that neither treatment arm caused organ toxicity. The fibrotic response to the small implants seen on histology was however more pronounced than that seen with medium implants or with the thicker CDDP25 material previously assessed *in vivo*. This pronounced fibrotic response may have been related to the C. bovis skin infection diagnosed by PCR in these animals but may also have been the result of increased implant mobility inside the abdominal cavity. The smaller size of the implants compared to the medium- and large-implant sizes allowed them to migrate away from the site of implantation and may have led to increased tissue irritation and foreign object response by the mouse immune system.

4.3.7 *In vivo* antitumor efficacy pilot

Multiple animals (9 out of 34) in different treatment groups of the efficacy pilot randomly selected for screening tested positive by PCR for C. bovis bacterial infection. This bacterium is highly contagious and the animals were housed in different cages before being assigned to treatment groups so it is highly unlikely that any mice were not infected by C. bovis. This bacterium has been associated with suppressed growth of implanted tumors, changes in immune cell activity (especially affecting natural killer cells) and increased toxicity of chemotherapeutic agents.[153] Mice that were implanted with CDDP25 disks were additionally found to have a 60% incidence of abscesses at the site of subcutaneous analgesia injection on their neck, often resulting in significant swelling and purulent discharge. These abscesses had not been observed previously in animals that had not tested positive for C. bovis. The infected abscesses are likely linked to this bacterial infection after consultation with the veterinarians of the MIT Division of Comparative Medicine. The C. bovis and abscess findings are expected to have affected the outcome of the efficacy pilot and so analysis of the harvested tissues and blood serum filtrate samples were halted in light of these findings. Average *in vitro* cisplatin release rates and their comparison to expected values for each sample type are tabulated in Table 4.4. The *in vitro* cisplatin release profile, animal survival, animal weight and bioluminescence normalized to the start of treatment and the tumor mass at euthanasia were averaged within each treatment group and are plotted in Figure 4.13.

Linear best-fit trendlines for each of the three periods of near-zero-order release evident in the Figure 4.13A release profiles for each disk type (period 1: day 1-6, period 2: day 7-30, period 3: day 31-42) were used to calculate a weighted average *in vitro* cisplatin release rate over the 42-day period. The values are compared to those

expected based on previous *in vitro* release studies in Table 4.4. A lower average *in vitro* cisplatin release rate and larger-than-anticipated variability were observed in the *in vitro* cisplatin release profile of all three CDDP25 disk types (Table 4.4, Figure 4.13A) based on the *in vitro* cisplatin release data previously exhibited by CDDP25 samples (Chapters 2 and 4). All three disk types had a cisplatin release profile that accelerated after day 30 and was less linear than expected. Possible reasons for the lower cisplatin release rate, larger variability and less linear release include inconsistencies with the batch of Ecoflex 00-30 used for these implants as well as a different cisplatin crystal size distribution compared to previous vials of cisplatin powder used in CDDP25 manufacturing. The size of drug crystals affects drug release kinetics from silicone matrices as described by Golomb et al. and can either accelerate or decelerate release depending on the matrix and its preparation.[115] Better control of cisplatin and lactose crystal size during composite manufacturing is needed moving forward to ensure such discrepancies are addressed.

Animal survival in the efficacy pilot is plotted in Figure 4.13B. Multiple animals had to be euthanized before the end of study leaving three mice in the 0.5 cm group (i), one mouse in the 0.8 cm group (ii), four mice in the 1.0 cm group (iii), five mice in the 4 mg/kg IP injection group (iv), three mice in the 10 mg/kg IP injection group (v) and three mice in the untreated control group (vi) by day 41. All but the three mice of group (v) were euthanized due to excessive tumor burden. The three mice of group (v) were euthanized due to excessive weight loss and poor body condition associated with their cisplatin injections.

Disk diameter (cm)	Disk thickness (mm)	*In vitro* release rate (µg/day)	Proportion of expected *in vitro* release rate achieved (%)
0.5	1.0	8.48	83
0.8	1.0	17.87	76
1.0	0.4	25.15	87

Table 4.4: Comparison of the weighted average daily cisplatin dose released *in vitro* by each disk type used in the efficacy pilot to the expected daily *in vitro* release from previous studies. All disk types released cisplatin at a lower rate than expected (76-87% of expected). All disk types displayed greater standard deviation than that seen in previous *in vitro* release studies. These discrepancies may be the result of CDDP25 composite manufacturing for this particular batch and specifically cisplatin crystal size distribution.

Mouse weights plotted in Figure 4.13C normalized to the value at the start of treatment further illustrate the toxicity of the 10 mg/kg weekly IP injections given to group (v). A dashed line has been added as a visual guide to mark the point of 20% weight loss commonly used as a criterion for animal euthanasia due to poor body condition. The animals in group (v) reached this degree of weight loss by day 11 of treatment following two weekly injections. Their weight continued to drop reaching less than 70% of its initial value by day 35 of treatment. Special permission was obtained from the veterinarians to allow continuation of the study in this treatment group until day 41.

There was large variability in bioluminescence across all mice in this pilot study before the start of any treatment, as seen by the large standard deviation error bars in the BLI plot (Figure 4.13D). This suggests that some animals were less likely to reject the xenografts and showed a faster tumor growth rate compared to others. The number of mice in this pilot was small and so all animals were randomized to treatment groups

even though previous experience with this animal model suggested that those with a lower BLI signal (<1E8) were at risk for xenograft rejection.

The average BLI in each treatment group plotted in Figure 4.13D suggests tumor response to treatment for all five cisplatin treatment groups. The normalized BLI signal is lower after CDDP25 disk implantation in groups (i) and (ii) compared to the untreated control group (vi). This pattern continues until the euthanasia of two untreated control mice that had high tumor burden and did not recover from isoflurane anesthesia on day 4.14. The BLI signal at later time points is affected by successive animal euthanasias in groups (i), (ii) and (vi) and it becomes hard to make across-group comparisons using the average BLI signal of the remaining mice. The normalized BLI signal is lower after CDDP25 disk implantation in group (iii) compared to the untreated control group (vi) as well and this trend continues until the end of the study on day 41. Only one animal was euthanized early in group (iii) making the BLI signal series more representative of the true average tumor response to treatment throughout the 41-day pilot. Both IP injection groups (iv) and (v) reduced their BLI signal by day 41 to < 5% of its value at the start of treatment. These groups responded the best to treatment as tracked noninvasively by BLI.

Tumor mass at euthanasia is plotted in Figure 4.13E as box-and-whiskers plots from the minimum to the maximum value and showing all points. Multiple mice had tumors that developed both an intraperitoneal and a subcutaneous portion, penetrating the abdominal wall. Only intraperitoneal tumors and ascites were weighed and included in this quantification. A one-way ANOVA with Tukey's multiple comparisons test was used to compare the average tumor mass of each treatment group to the others. The

only statistically significant differences were between the 0.8-cm diameter disk (group (ii)) and the 4 mg/kg and 10 mg/kg weekly IP cisplatin injection regimens (groups (iv) and (v)) with p-values of 0.0260 and 0.0177 respectively. The large variability in tumor rejection and growth between animals resulted in lack of any significant difference between the two extreme control groups: group (v) receiving 10 mg/kg IP cisplatin injections equivalent to the current standard of care and group (vi) receiving no treatment. The fact that the two extreme controls (clinically-treated and entirely untreated) did not have a statistically significant difference in tumor mass at euthanasia means that the results of this efficacy pilot are not reliable. Better approaches to the mouse model used and the tumor burden cutoff applied for treatment group randomization should be implemented in the next efficacy studies to avoid such an issue.

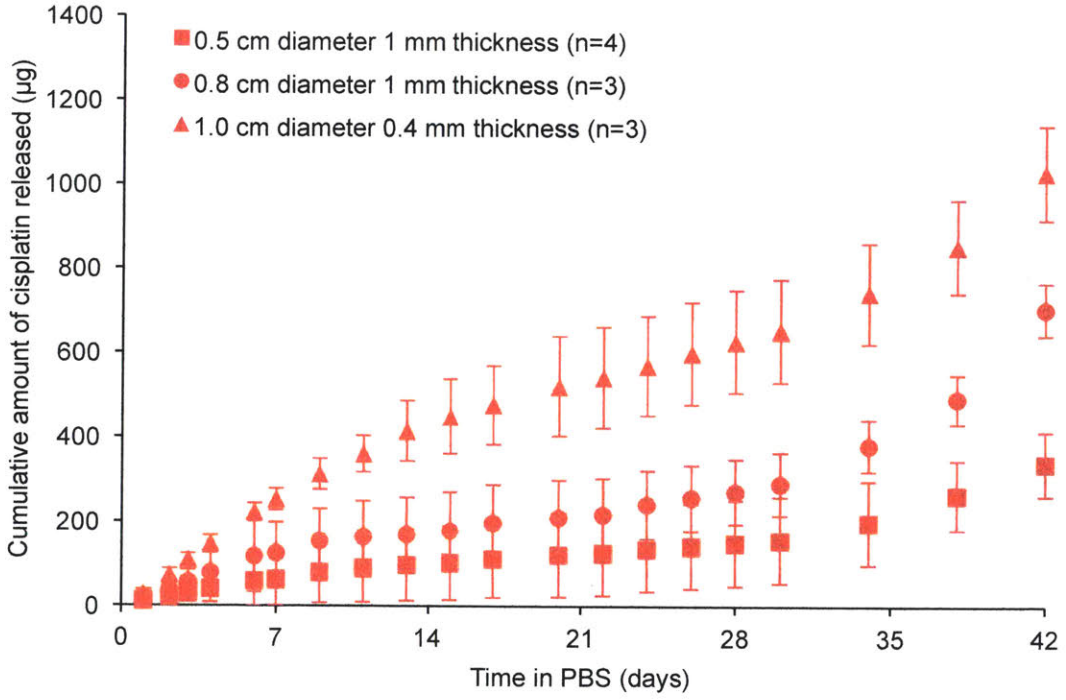

A

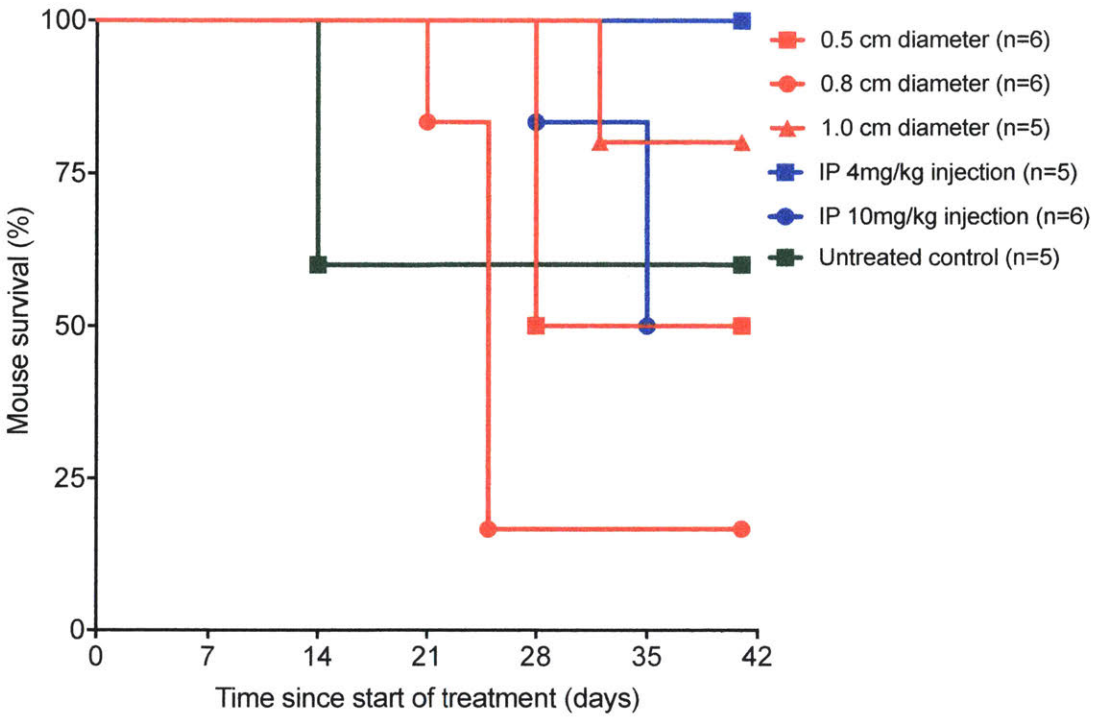
100
75
50
25
0
Mouse survival (%)
0
7
14
21
28
35
42
Time since start of treatment (days)
0.5 cm diameter (n=6)
0.8 cm diameter (n=6)
1.0 cm diameter (n=5)
IP 4mg/kg injection (n=5)
IP 10mg/kg injection (n=6)
Untreated control (n=5)

B

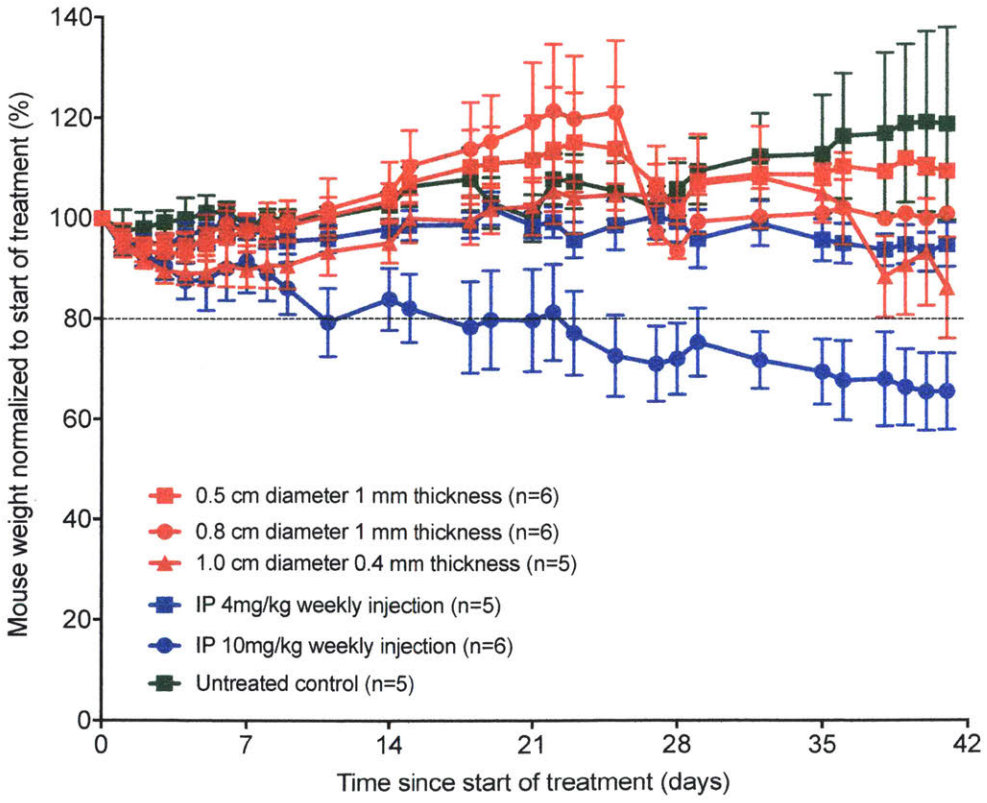
140
120
100
80
60
40
20
0
Mouse weight normalized to start of treatment (%)
0
7
14
21
28
35
42
Time since start of treatment (days)
0.5 cm diameter 1 mm thickness (n=6)
0.8 cm diameter 1 mm thickness (n=6)
1.0 cm diameter 0.4 mm thickness (n=5)
IP 4mg/kg weekly injection (n=5)
IP 10mg/kg weekly injection (n=6)
Untreated control (n=5)

C

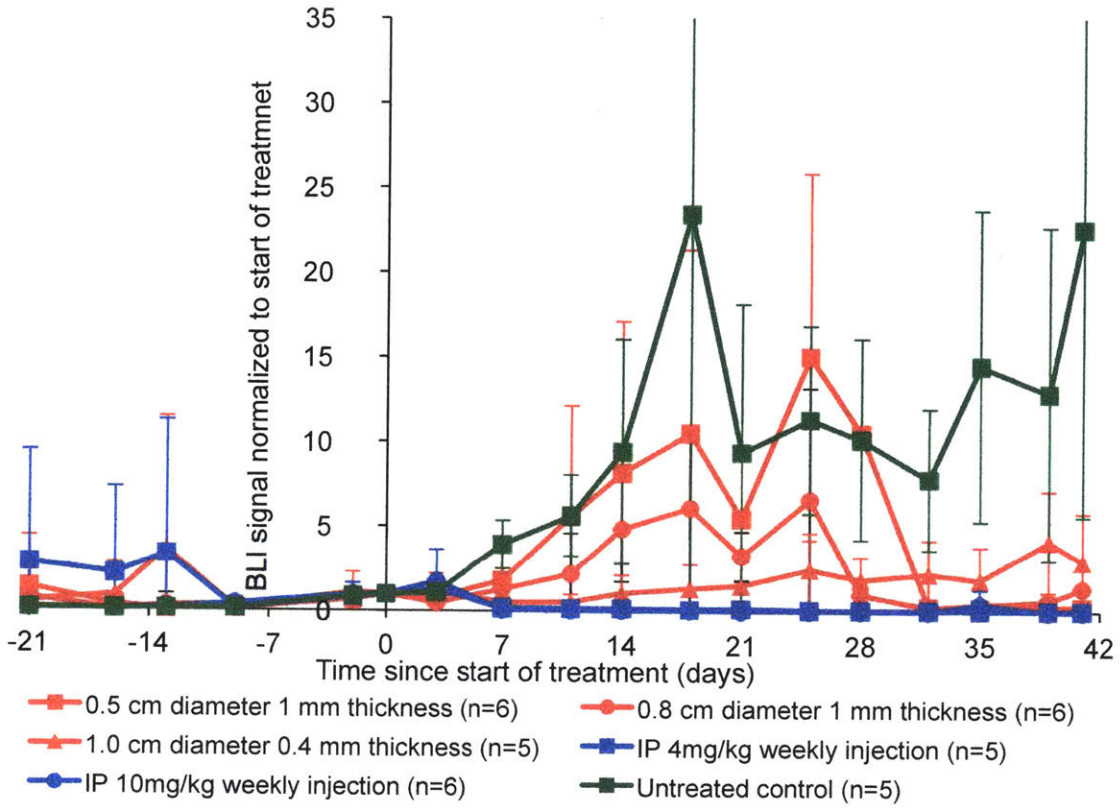
BLI signal normalized to start of treatmnet
35
30
25
20
15
10
5
0
-21
-14
-7
0
7
14
21
28
35
42
Time since start of treatment (days)
0.5 cm diameter 1 mm thickness (n=6)
0.8 cm diameter 1 mm thickness (n=6)
1.0 cm diameter 0.4 mm thickness (n=5)
IP 4mg/kg weekly injection (n=5)
IP 10mg/kg weekly injection (n=6)
Untreated control (n=5)

D

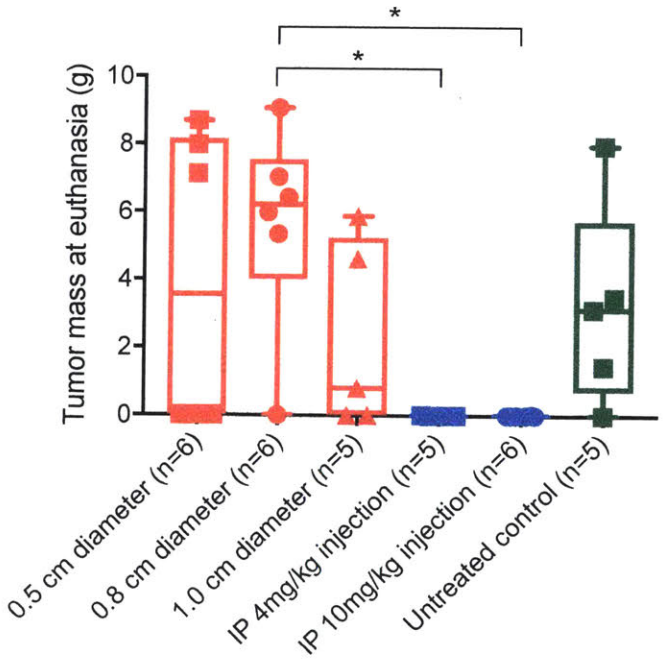
*
*
Tumor mass at euthanasia (g)
10
8
6
4
2
0
0.5 cm diameter (n=6)
0.8 cm diameter (n=6)
1.0 cm diameter (n=5)
IP 4mg/kg injection (n=5)
IP 10mg/kg injection (n=6)
Untreated control (n=5)

E

Figure 4.13: Antitumor efficacy pilot study results. (A) *In vitro* cisplatin release profile of extra CDDP25 disks prepared for the efficacy pilot but not implanted in mice. This *in vitro* release study was carried out over a 42-day time period to get an indirect metric of expected cisplatin release from the CDDP25 disks actually implanted in mice. All three CDDP25 disk types displayed relatively large standard deviations compared to previous studies. All three disk types released cisplatin at a rate slower than the one expected (83%, 76% and 87% respectively) and displayed a less linear release profile. (B) Animal survival is plotted for the six treatment groups. Multiple animals had to be euthanized before the 41-day intended final time point because of poor body condition either due to tumor load or, in the case of group (v) receiving 10 mg/kg weekly IP cisplatin injections, due to weight loss caused by cisplatin toxicity. (C) Average mouse weights normalized to the value at the start of treatment plotted for each of the six groups in the pilot. Groups (i)-(iii) lost weight immediately after surgical implantation of their CDDP25 disks but recovered within a week. Notable in this plot is the dramatic weight loss of group (v) animals receiving the mouse-scaled equivalent dose to IP cisplatin infusions given in the clinic. (D) BLI signal normalized to the value at the start of treatment is plotted as an average value for each treatment group at each imaging time point. Mice implanted with 1.0 cm-diameter 0.4 mm-thickness disks had the least increased BLI signal (the other two disk-implanted groups (i) and (ii) had lost most mice with high tumor burden before day 41). The two IP injection groups (iv) and (v) showed the most effective BLI signal reduction to less than 5% of its value at the start of treatment. (E) Tumor mass at euthanasia averaged for each treatment group and plotted as a box-and-whiskers plot. The ends of the box are the upper and lower quartiles of the data, the lines outside the box indicate the highest and lowest values and the median is marked by the vertical line inside the box. All individual data points are additionally shown. There was no statistically significant difference in average tumor mass between the two IP injection-treated groups and the untreated controls, suggesting that the findings of this pilot are unreliable since these were the two extreme control conditions. This lack of statistical significance is likely due to the large degree of variability in xenograft rejection and tumor growth between animals and the small n in each group. Values are plotted as means unless otherwise indicated and error bars show standard deviation from the mean.

4.3.8 Miura v-pleat origami prototypes

The Ecoflex 00-30 and LAC50 Miura v-pleat sheets cast using the machined Teflon mold measured approximately 44 mm in length by 44 mm in width. The individual pleat features on the partially pre-folded sheets measured approximately 2.5 mm in depth/height, 4 mm in width, 2 mm in length and 1 mm in thickness. The Ecoflex 00-30 and LAC50 Miura v-pleat sheets cast using the 3D-printed ABS*plus* mold measured approximately 70 mm in length by 70 mm in width. The individual pleat features on the

partially pre-folded sheets measured approximately 10 mm in depth/height, 8 mm in width, 4 mm in length and 1.5 mm in thickness (Figure 4.14). The prototypes did not exhibit any signs of air entrapment or other casting defects visible to the naked eye. No mechanical characterization of the origami prototypes was performed since they were intended for proof-of-concept demonstration of the feasibility of using an origami fold to drive collapse of a large thin composite sheet into a shape that can fit through laparoscopic tools and then be opened up once inside the body. The prototypes created were too thick to allow them to pass through laparoscopic tools at their compressed state but the work described in this chapter developing a thinner CDDP25 formulation can readily be translated to casting origami sheets that are thinner and/or have other optimized dimensions. These sheets will ultimately be required to reach a collapsed size that will allow them to be easily passed through a trocar with maximum diameter of 12 mm.

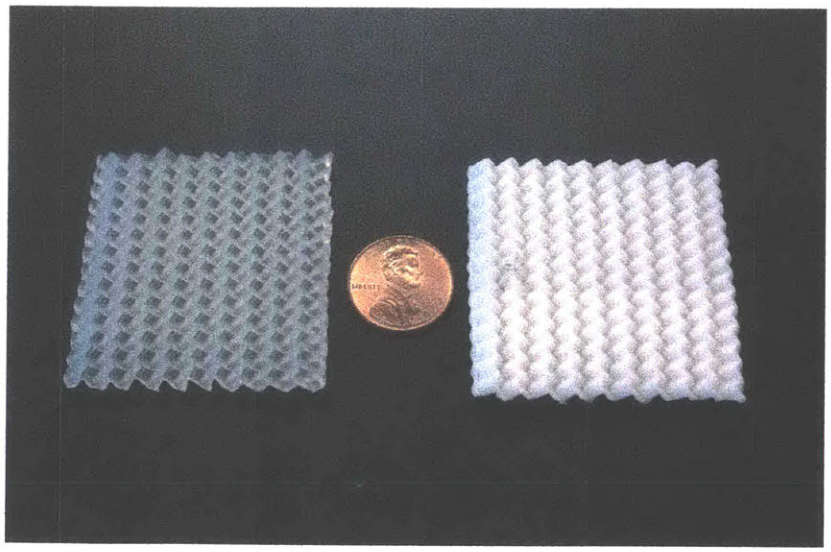

A

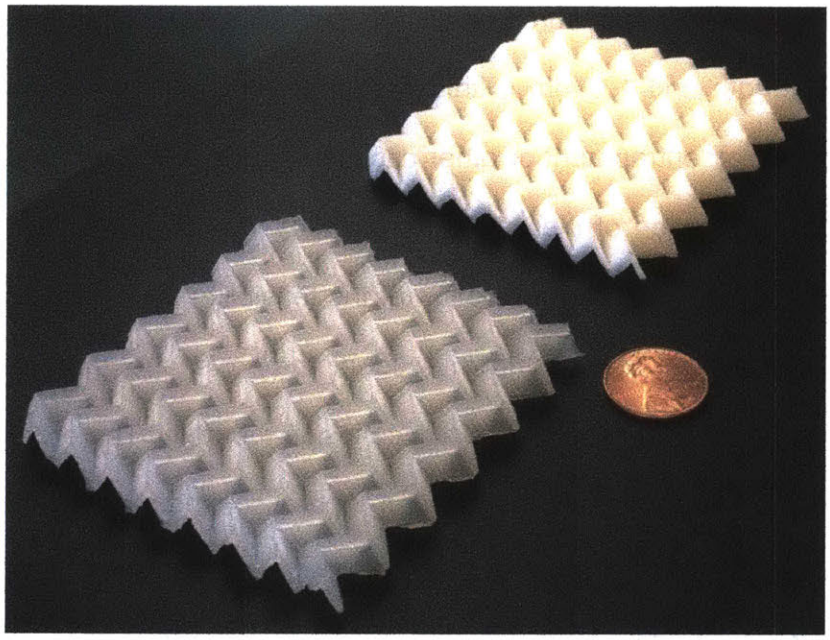

B

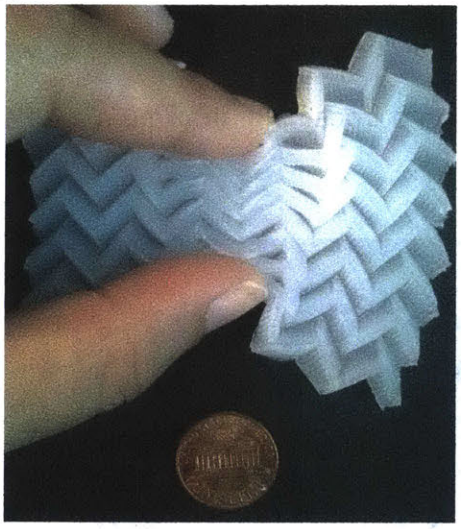

C D

Figure 4.14: Miura v-pleat origami sheet prototypes. The prototypes are made of Ecoflex 00-30 alone (left) or LAC50 (right). The prototypes were cast using a (A)-(B) machined Teflon and (C)-(D) 3D-printed ABS*plus* two-part mold. Scale bar 10 mm. (C)-(D): Application of force along the length or width of (C) Ecoflex 00-30 or (D) LAC50 origami prototypes allows compression to a smaller size to fit through a more narrow incision than the actual sheet dimensions. A US penny has been added for scale.

4.4 Discussion

The CDDP25 formulation developed previously for controlled, low-dose near-zero-order release of cisplatin over a prolonged period of time was optimized in this work to develop a material that is thinner and is a more viable candidate to create a laparoscopically deployable implant for IP cisplatin delivery. The material thickness was reduced by almost two thirds of its original value to 0.4-0.45 mm. This reduced-thickness material allowed dose escalation studies to be performed because it made implantation of much larger-diameter samples possible through a small incision on the mouse abdomen to minimize invasiveness of the surgery. The thinner disk-shaped samples can be easily rolled up for placement into the mouse abdomen through a small incision compared to the thicker ones. They can then be unrolled into their original dimensions once inside the abdomen. Thinner samples will have a lower bending stiffness since they will have a lower area moment of inertia I_c. The I_c of a rectangle with height h and width b when attempting to bend it about its centroid is expressed by:

$$I_c = \frac{bh^3}{12}$$

The height is raised to the third power in this expression, so any increase in sample thickness will dramatically increase I_c. The reduction in bending stiffness as a result of reducing the sample thickness is also expected to be beneficial for the safety of an implanted sample *in vivo*. A less rigid implant will more readily take on the shape of the space around it and is less likely to irritate the organs and tissues surrounding it compared to a more rigid implant.

Reducing the thickness of a composite elastomeric material can affect many of the properties influencing its behavior as a drug-eluting system *in vivo*. The manufacturing process for the material may have to change leading to better or worse performance in terms of defects in the structure. The composite comprises a silicone matrix impregnated with crystals of lactose and cisplatin. Confirmation of a homogeneous distribution of solid excipients in the silicone matrix is necessary to ensure that the material has not fundamentally changed due to this new manufacturing process. Reducing material thickness can additionally make it more prone to contain defects caused by crystal impregnation that can lead to failure under tension. A reduction in the material thickness under the disk sample preparation methods employed in this work – using a punch to cut out individual samples from a larger sheet of material – affects the surface area of the sides of a disk that was directly cut out from a bigger piece. This side surface area is likely to contain more exposed lactose and cisplatin crystals compared to the flat top and bottom surfaces that were in contact with the mold or the atmosphere during curing. A reduction in sample thickness will reduce this surface area and is likely to affect the release of lactose and cisplatin from the sample. The impact of such a change in release from the sides to the overall release profile of the sample will depend on the contribution of release from the sides to the overall release from the entire sample.

The structure, mechanical properties and *in vitro* release of this new CDDP25 thickness were assessed in order to compare them to those of the previously developed thicker CDDP25 formulation and confirm its appropriateness for manufacturing an IP implant. Secondary and backscatter electron SEM confirmed that this new thickness

contained uniformly distributed cisplatin and lactose crystals impregnated in the silicone matrix similar to what was observed in the thicker CDDP25 formulation (Figure 4.1). Mechanical characterization of the thin material revealed that its elastic modulus, ultimate tensile strength and elongation at break were all almost 80% of the values calculated for the thicker formulation and still well within ranges making them safe for presence inside the abdomen (Table 4.1). Evaluation of either formulation under mechanical tests simulating laparoscopic implantation and removal is outstanding and should be carried out as a next step to confirm safety for implantation in patients from a mechanical standpoint. The average *in vitro* cisplatin release rate of three different disk diameters cut out from the thinner CDDP25 formulation was close to the expected value with deviation increasing with increasing disk diameter. This trend is reasonable since sources of deviation, manufacturing or others, from the calculated surface area-normalized cisplatin release rate are expected for any sample batch. Such deviation will be amplified with increasing surface area of a sample. The surface area-normalized release rate displayed by all three disk sizes is plotted in Figure 4.4 and is in good agreement with the expected surface area-normalized release rate based on the thicker CDDP25 formulation. These findings confirmed that the thin CDDP25 formulation is releasing cisplatin as expected.

Thin CDDP25 disk sizes of different diameters were manufactured and implanted in the peritoneal cavity of mice to assess the toxicity of the cisplatin dose they delivered, the overall material biocompatibility and the concentration of platinum in tissues of the abdominal cavity accomplished by the disks as an indirect measure of their *in vivo* cisplatin release capacity. The two dose escalation studies performed compared weekly

4 mg/kg IP cisplatin injections – a regimen previously used in this project and found to be well tolerated *in vivo* – to 1.0-cm, 1.5-cm and 2.0-cm diameter disks expected to release cisplatin at a total dose that as 2.0X, 4.4X and 7.7X that of the injections respectively. The 2.0-cm disks were deemed too toxic for *in vivo* implantation most likely on the basis of their cisplatin release rate considering the acuteness of the toxicity that required euthanasia 3 days after implantation. The 1.5-cm disks were tolerated by two of the three mice and the cause leading to the toxicity that eliminated the third mouse has not yet been determined although it may be related to a more rapid cisplatin release observed on days 7-9 in this implant batch. The 1.0-cm disks appeared to be well tolerated in terms of animal weight, CBC and abdominal organ histology but were found to cause a more pronounced inflammatory foreign body response compared to the 1.5-cm disks and to the thicker CDDP25 formulation previously evaluated *in vivo*. This pronounced foreign body response may be associated with the increased mobility of 1.0-cm disks within the abdominal cavity observed *in vivo* and may point to a design component that must be optimized in the final implant dimensions selected for *in vivo* antitumor efficacy evaluation. The 1.5-cm disks may be considered representative of the maximum tolerated dose for this cisplatin-eluting material based on weight, CBC and histologic assessment and point to an implant size that may be most promising for future efficacy studies based also on the fibrotic response it induces.

The efficacy pilot study conducted using 1.0-cm disks of 0.4-mm thickness ('small implants' from the second dosing study described in this chapter) as well as 0.5-cm and 0.8-cm disks of 1.0-mm thickness suffered from critical drawbacks that compromised its outcome. Multiple animals in the study tested positive for a bacterial

infection that has been found to affect tumor growth, response to chemotherapeutics and immune cell populations. Animals receiving surgical implantation of CDDP25 disks additionally suffered large and infected abscesses at the site of subcutaneous analgesia infection at a very high incidence never observed before when performing such surgeries. These abscesses may likely be connected to the bacterial infection and may have further affected immune response to the xenografts inoculated in these animals as well as the administered cisplatin chemotherapy. A small number of mice were used in each treatment group and large variability in xenograft rejection and tumor growth were observed across the board. This led to lack of statistical significance in tumor mass difference between the two extreme controls (untreated vs. clinical standard of care equivalent) at euthanasia and further cast doubt to the validity of data from this pilot. Key takeaways were nevertheless obtained from this study: (1) a response to treatment was seen in all CDDP25 disk groups albeit transient in the two groups receiving the lowest continuous cisplatin dose; (2) 1.0-mm thick CDDP25 disks were primarily found embedded in the mouse fat pad near the bottom of the pelvis while 0.4-mm thin CDDP25 disks remained closer to the site of implantation; (3) xenograft rejection and tumor growth variability should be taken into account more conservatively moving forward, potentially using a BLI signal cutoff as an inclusion criterion for treatment group assignment; (4) diligent testing of animals upon arrival for infection with pathogens like C. bovis that can affect study outcomes should be performed to the extent possible every time; and (5) modifications in tumor inoculation technique should be carried out to prevent growth of subcutaneous lesions and only generate intraperitoneal tumors in mice. Next iterations of the efficacy study will involve only the thinner version of the

CDDP25 composite and will explore delivery of higher continuous cisplatin doses while targeting points (1) through (5) above.

The implant envisioned to deliver IP cisplatin to treat peritoneal metastasis in ovarian cancer patients must be able to expose as large a surface area as possible inside the abdomen to drug while allowing placement and removal via minimally invasive surgery to reduce postoperative complications and recovery time. Minimally invasive surgery, also known as laparoscopy, employs tools known as trocars to introduce and remove items intra-abdominally. Trocars exist in various diameters ranging from 2 to 12 mm.[154] Risk of complications both peri- and post-operatively such as tissue injury or herniation of the bowel or fat increases with increasing incision site.[154] It is desired therefore to design an implant that can fit through as small a laparoscopic incision as possible. The maximum trocar diameter is however assumed to be the upper bound to design a laparoscopically deployable implant since the implant must also optimize for maximal surface area of exposure to the drug. The Miura v-pleat origami tessellation was used to drive the shape of an Ecoflex 00-30 or LAC50 sheet by casting it in molds with three-dimensional features. The goal was to allow folding down of the origami sheet by pressing along either its length or width and so reduce that dimension to allow passing through a narrow opening. The origami sheets created with this approach maintain a partially folded shape even at their relaxed state and this is suboptimal in terms of implantation safety. The existence of peaks and troughs along the surface of the origami sheets can lead to accumulation of tissue or fluid in those features that may eventually cause infection inside the abdomen. The silicone-based composite materials developed in this work to deliver cisplatin are soft and stretchy and

so are challenging to fold down in a straightforward and repeatable manner without having some degree of pre-folding in their shape. Optimization of the dimensions of the Miura v-pleat shape used to produce the proof-of-concept prototypes shown in Figure 4.14 as well as reduction of the cast origami sheet to one third – one half of its current thickness are two starting points to enable creation of origami sheets that are more likely to fit through laparoscopic tools. Other origami tessellations such as a single v-pleat can be explored in case they are better suited to create sheets that can fit through a trocar. It is also important to note that the material developed in this work swells when immersed in an aqueous medium as part of its cisplatin and lactose release process. The degree of swelling was not quantified in this work but is an important next quantity to understand since it will impact the feasibility of laparoscopic removal of a composite implant at the end of the treatment period using a trocar.

Chapter 5: Assessment of Technology Adoption Potential in Low- and Middle-Income Countries

5.1 Introduction

Gynecologic and gastrointestinal cancers, affecting more than 2 million patients and killing more than 1 million patients in low- and middle-income countries (LMICs) annually, metastasize intraperitoneally with a very poor prognosis. IP chemotherapy can increase survival but is not an option in LMICs because of its high cost, complicated technology and debilitating toxicity. The sustained-release implants for IP delivery of cisplatin described in this work are well suited for use in resource-constrained environments. They are made of readily accessible materials, deliver off-patent chemotherapy at low doses to reduce side effects and do not require repeat visits to the hospital beyond placement and removal. They hold promise for improving accessibility, cost effectiveness and tolerability of IP chemotherapy particularly in LMICs. A clinician survey deployed across India reveals eagerness for early adoption of new technologies and dosing regimens to treat peritoneal metastasis and shows potential for utilization of the sustained-release implants developed in this project.

5.2 Materials and Methods

5.2.1 Online clinician survey

Exemption from institutional board review was granted by the MIT Committee on the Use of Humans as Experimental Subjects (COUHES) to the survey protocol. The Qualtrics platform was used to create an online survey targeted at healthcare providers in India. The survey was designed to be adaptable to participant input and direct participants to different question blocks depending on their answers. The survey response duration was kept to < 5 min in order to maximize successful completion. Question content focused on five key areas: (i) participant background, affiliation and experience caring for cancer patients; (ii) incidence and management of peritoneal metastasis; (iii) use and challenges of IP chemotherapy both catheter-based and HIPEC/PIPAC; (iv) use of metronomic chemotherapy particularly for patients with peritoneal metastasis; and (v) outlook on adopting new technologies for IP chemotherapy. The survey collected data in an anonymous fashion but allowed participants to provide their email address for follow-up if desired. Participants were informed of the purpose of the survey and potential use of their responses for presentations in scientific meetings, conferences and publications via an introductory consent section before starting the survey. Participants had the option of opting out of the survey at any point during its completion.

5.2.2 Survey dissemination

The clinician database of the National Cancer Grid of India was used to disseminate the survey electronically. Access to the database was given by the National Cancer Grid

Director. Clinicians were contacted via electronic messages containing a link to the anonymous survey.

5.2.3 Data representation and analysis

Data from survey participants were exported as .csv files from the Qualtrics platform and further analyzed and represented graphically. Incomplete, duplicate or invalid responses were removed prior to further analysis.

5.3 Results

5.3.1 Participant background, affiliation and cancer care experience

The clinician survey has collected responses from 40 participants to date representing 10 specialties and 35 hospitals across India (Figure 5.1A-B). The hospitals affiliated with the survey responders represent both public (35%) and private (65%) institutions and are mostly tertiary centers (94%) with a small number of secondary centers (6%) (Figure 5.1C-D).

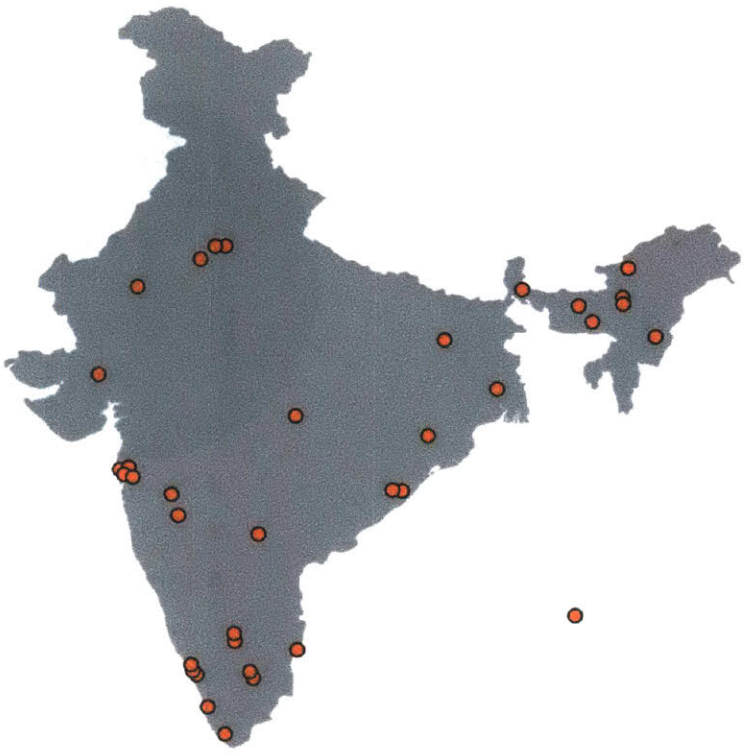

A

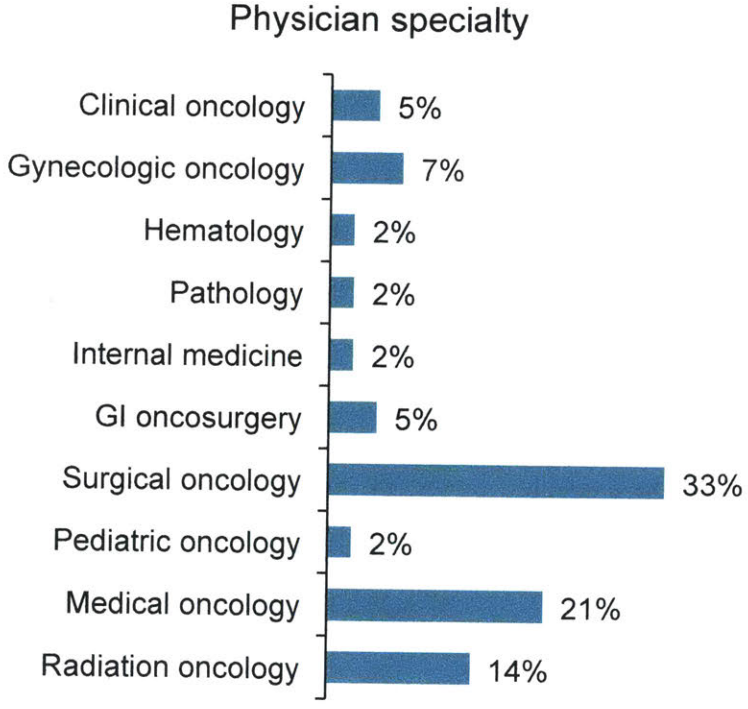
Physician specialty
Clinical oncology
5%
Gynecologic oncology
7%
Hematology
2%
Pathology
2%
Internal medicine
2%
GI oncosurgery
5%
Surgical oncology
33%
Pediatric oncology
2%
Medical oncology
21%
Radiation oncology
14%

B

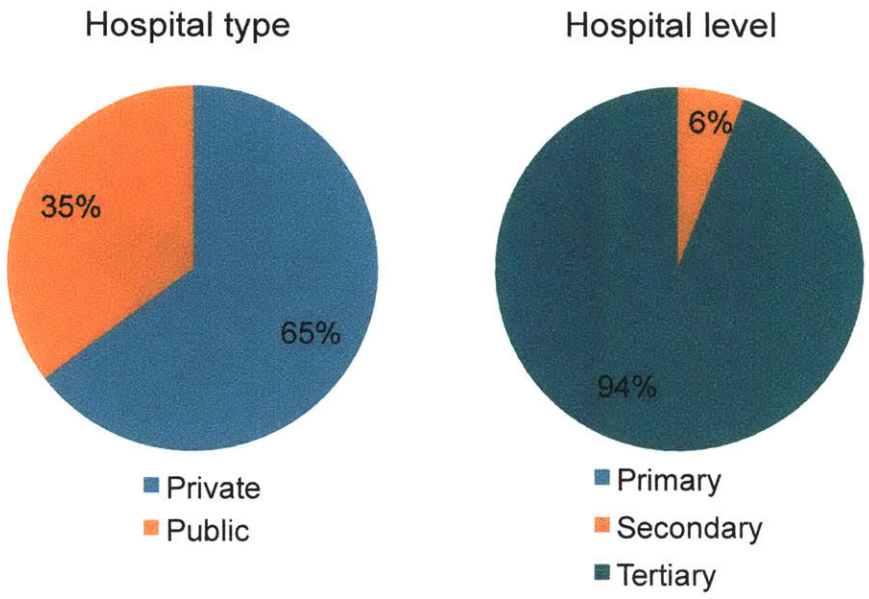

C D

Figure 5.1: Responder location, background, specialty and affiliation results of the Indian clinician survey to date. (A) Map representing the locations of hospital affiliations of survey responders to date. The locations include major urban centers like Mumbai and New Delhi as well as remote locations like the Andaman and Nicobar Islands and Assam. (B) Responders to date represent 10 specialties and all provide care to patients with cancer. (C)-(D) The hospitals affiliated with the survey responders represent both public (35%) and private (65%) institutions and are almost entirely tertiary centers (94%) with a few responses originating from secondary centers (6%).

5.3.2 Incidence and management of peritoneal metastasis

More than three quarters of responders reported the incidence of peritoneal metastasis among the cancer patients they treated to be between 1% and 25% and more than 90% of responders placed that number between 1% and 50% (Figure 2A). This number is lower than what would be expected based on the incidence of peritoneal metastasis at advanced stages of disease and the proportion of patients diagnosed late according to epidemiological data from India. This discrepancy may be related to the fact that responders belong to 10 specialties many of which treat multiple types of cancer (e.g. surgical oncology, medical oncology, radiation oncology). These specialists provide

incidence estimates taking into consideration their entire cancer patient pool. Many of their patients would face a very low probability of peritoneal metastasis given the origin and type of their cancer therefore skewing the peritoneal metastasis incidence estimates to lower numbers.

The percentage of cancer patients with peritoneal metastasis that undergo surgical debulking was reported to be between 1% and 25% by almost half of the survey responders (Figure 5.2B). Surgical debulking is a cornerstone of advanced ovarian cancer treatment but is less commonly used to treat other malignancies with peritoneal involvement. This low percentage is not surprising since the survey did not differentiate between patients with peritoneal metastasis of ovarian origin and others. Surgical debulking will also not be performed if the procedure is not deemed to be beneficial to the patient either because their disease is too advanced or because they should first undergo neoadjuvant chemotherapy to shrink down their tumors. These considerations of peritoneal metastasis care are reflected in the survey responses: the main reason for not performing surgical debulking cited in the survey was patient eligibility (24%) followed by cost (15%), lack of trained staff (13%) and resources (13%) and lack of benefit to the patient (12%) (Figure 5.2C).

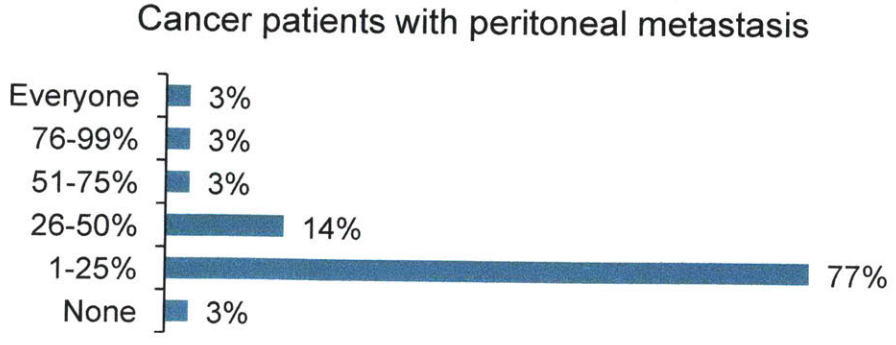

A

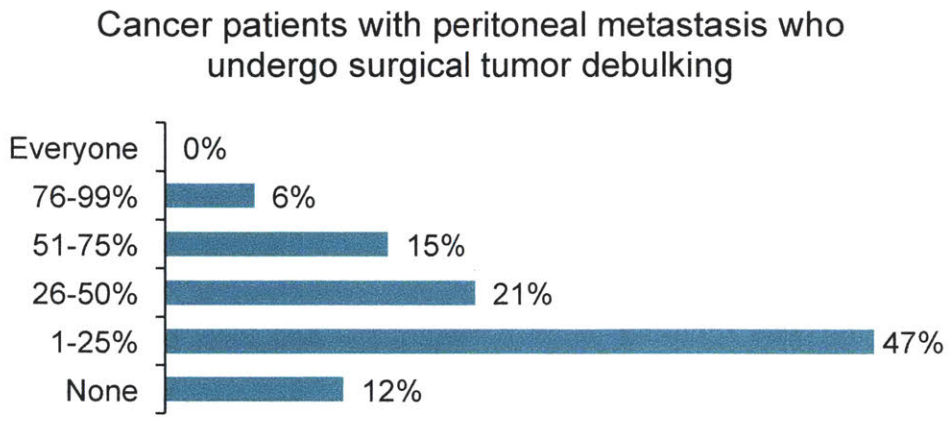

B

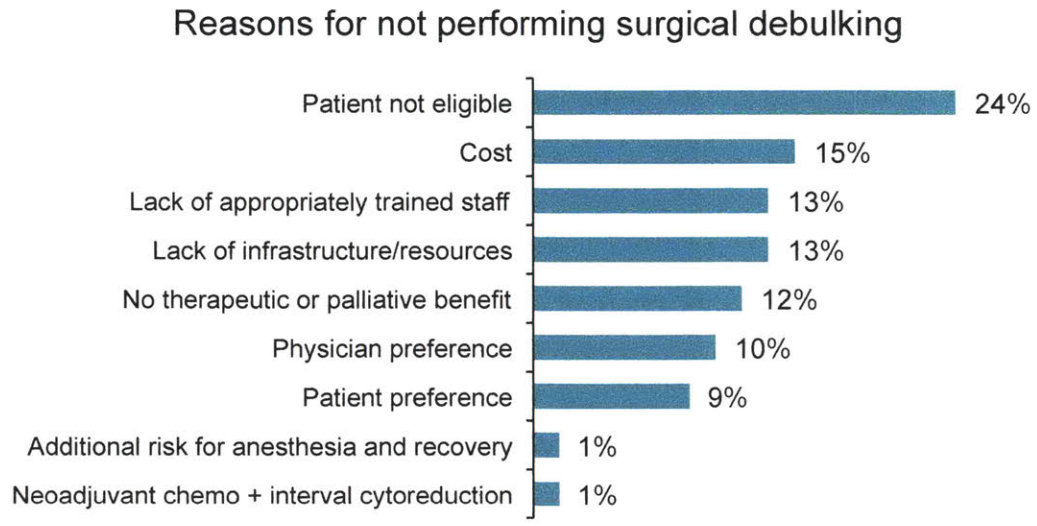

C

Figure 5.2: Incidence and management of peritoneal metastasis in India. (A) Incidence of peritoneal metastasis among cancer patients seen by responders. More than three quarters of responders reported this value to lie between 1% and 25% of patients. This low number may be explained by the fact that many responders represent specialties treating patients with various types of cancer, many of whom face a very low probability of developing peritoneal metastasis. (B) Proportion of patients with peritoneal metastasis undergoing surgical tumor debulking. Almost half of survey responders reported this number to lie between 1% and 25% of patients and the reasons for not performing surgical debulking ranked in (C) may help shed some light to this low number. Lack of patient eligibility for debulking (24%) and no benefit from the surgery (12%) are both common reasons to not perform debulking in the US as well while cost (15%) and access to trained staff (13%) and resources (13%) are likely reasons more applicable to the LMIC setting.

5.3.3 Use and challenges of IP chemotherapy

The majority of responders (74%) reported being familiar with IP chemotherapy but described limited use of this route of administration (Figure 5.3A, B). More than half (54%) reported not using IP chemotherapy at all with peritoneal metastasis patients while almost all remaining responders (42%) reported using IP chemotherapy only with 1-25% of their peritoneal metastasis patients (Figure 5.3B). IP chemotherapy when used is overwhelmingly performed in the operating room as HIPEC (73%) while only 27% of responders indicated using traditional catheter-and-port IP chemotherapy administration (Figure 5.3C). They cited the reasons for not performing catheter-and-port IP chemotherapy as primarily lack of infrastructure and resources (72%) and lack of appropriately trained nursing staff (59%) while cost (48%), infections (38%) and catheter or port complications (31%) and loss to follow-up (24%) were also ranked high. They also pointed to the importance of surgical debulking, citing it as the fifth reason for not performing catheter-and-port IP chemotherapy.

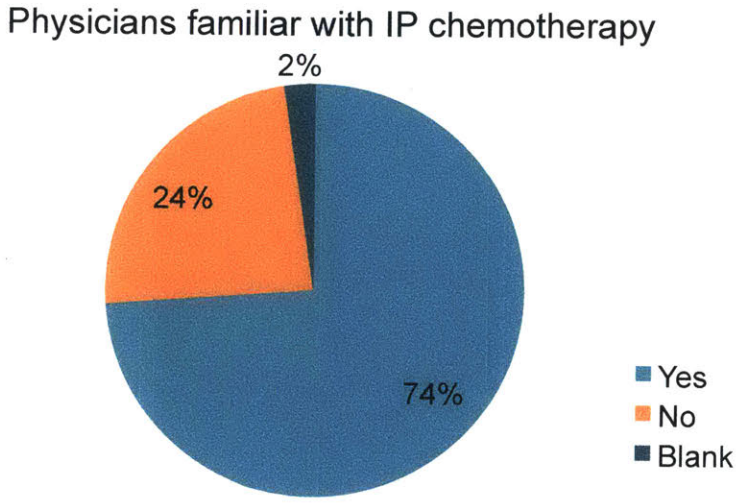

A

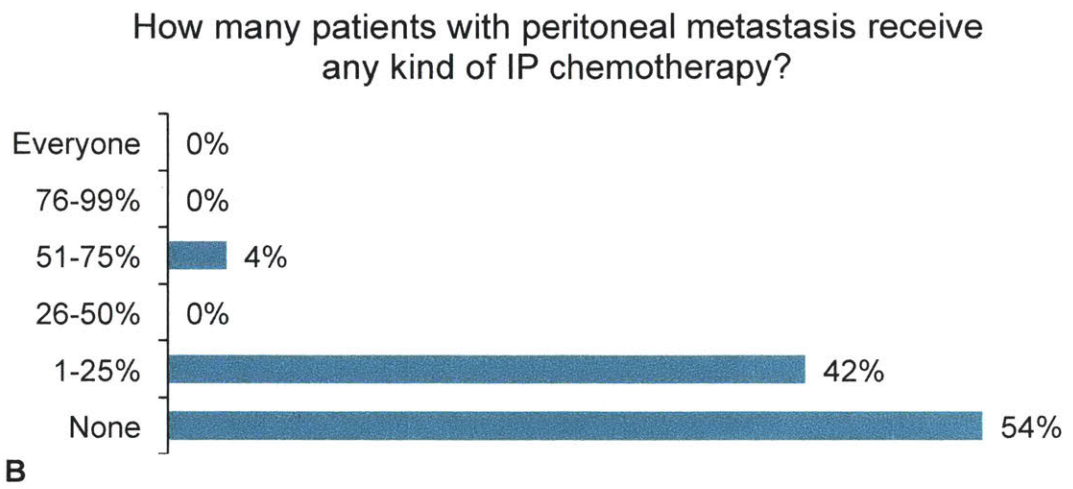
How many patients with peritoneal metastasis receive any kind of IP chemotherapy?
Everyone
76-99%
51-75%
26-50%
1-25%
None
0%
0%
4%
0%
42%
54%

B

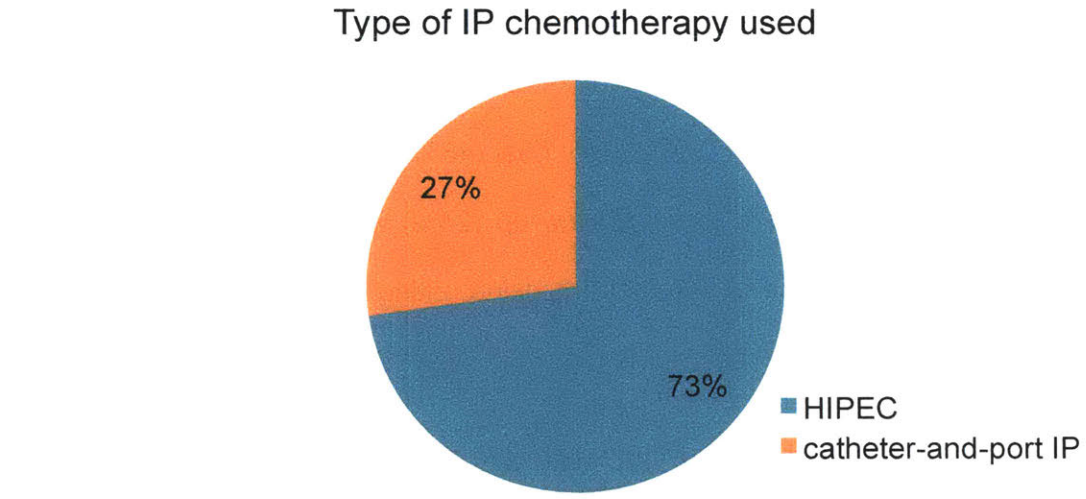
Type of IP chemotherapy used
27%
73%
HIPEC
catheter-and-port IP

C

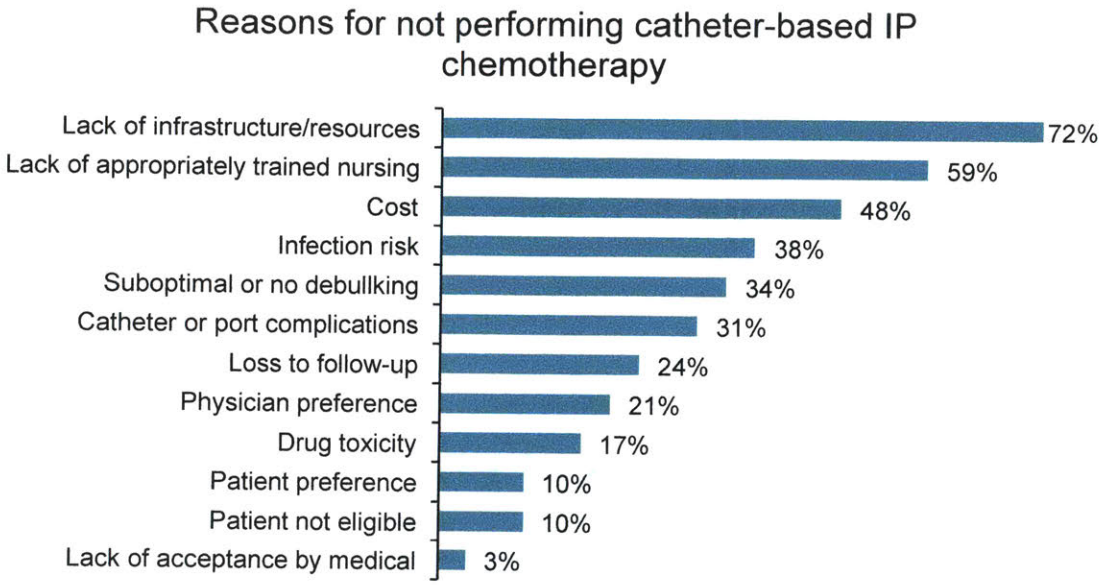

D

Figure 5.3: Use and challenges of IP chemotherapy in India. (A) Almost three quarters (77%) of survey responders described being familiar with IP chemotherapy but (B) more than half (54%) reported not giving it to any peritoneal metastasis patients. Most of the remaining responders (42%) reported giving IP chemotherapy to 1-25% of peritoneal metastasis patients. (C) When given, IP chemotherapy is overwhelmingly HIPEC (73%) and only 27% of responders reported using catheter-and-port IP chemotherapy for their patients. (D) Responders rank lack of infrastructure and resources (72%), lack of appropriately trained nurses (59%) and cost (48%) as the top three reasons for not performing catheter-and-port IP chemotherapy. Infections (38%) and catheter or port complications (31%) are also cited as important reasons for lack of use of this IP chemotherapy modality.

5.3.4 Use of metronomic chemotherapy

Metronomic or dose-dense chemotherapy is an attractive approach for cancer treatment in LMICs because it leads to fewer side effects for patients who cannot afford being unable to earn a livelihood during their treatment. This dosing regimen is similar in principle to the sustained low-dose chemotherapy administration described in this project. Use of metronomic chemotherapy is therefore promising for adoption of a sustained low-dose chemotherapy regimen.

Almost all survey responders (92%) reported being familiar with metronomic chemotherapy (Figure 5.4A) and described some use of this dosing regimen to treat peritoneal metastasis. Almost half of responders (42%) specifically reported using metronomic chemotherapy to treat 1-25% of their peritoneal metastasis patients.

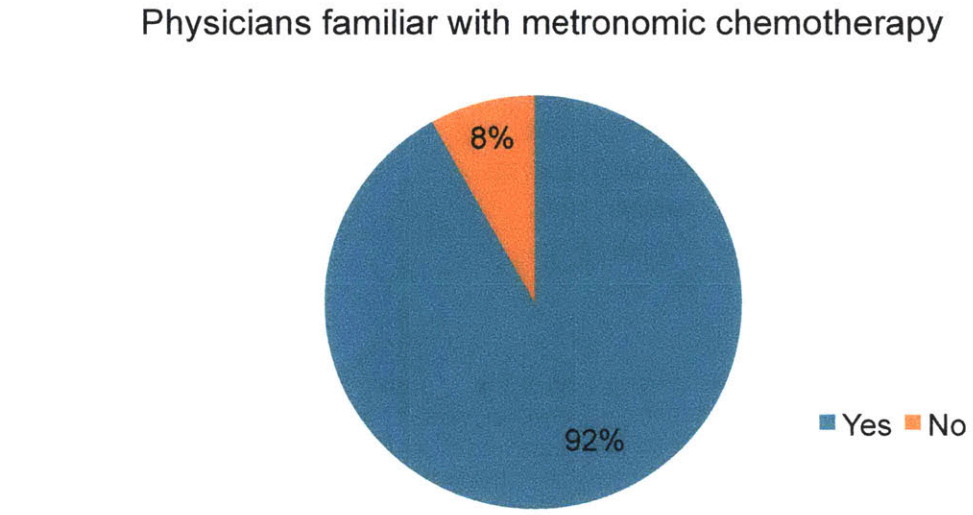

A

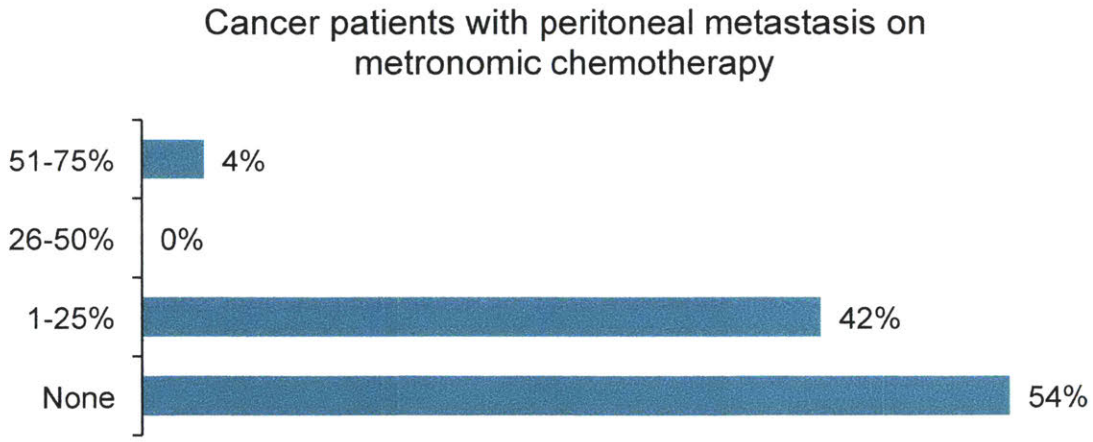

B

Figure 5.4: Use of metronomic chemotherapy against peritoneal metastasis in India. (A) Almost all responders indicated familiarity with metronomic chemotherapy. (B) Some use of metronomic chemotherapy in peritoneal metastasis treatment was reported with 42% of survey responders indicating that they use it for 1-25% of their peritoneal metastasis patients.

5.3.5 Outlook on adopting new technologies for IP chemotherapy

The responses regarding adoption of a new technology for IP chemotherapy were overwhelmingly positive. More than half of responders (56%) would definitely try a new technology whereas another 33% would probably try it. The remaining 11% indicated ambiguity about trying a new technology for IP chemotherapy and there were no negative responses.

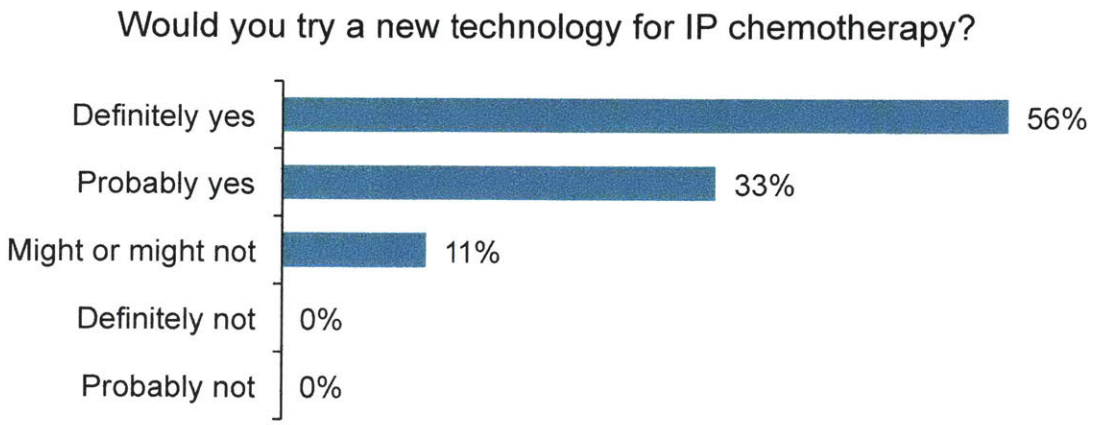

Figure 5.5: Adoption of new technologies for IP chemotherapy in India. More than half of responders (56%) would definitely try a new technology for IP chemotherapy while more than 30% would probably try it. The remaining 11% were ambiguous. This outlook is promising for use of the sustained-release chemotherapy implants developed in this project.

5.4 Discussion

Low-income countries face 56% of the global disease burden while accounting for only 2% of global health spending according to the World Bank.[155] Cancer care in resource-constrained settings in particular suffers from a tremendous mismatch between supply of trained personnel and resources and demand for services by a growing population of cancer patients. Approximately 70% of deaths from cancer occur in LMICs according to the World Health Organization.[156] The majority of patients in LMICs lack healthcare insurance and are expected to pay out of pocket for medical costs. Costs of care as well as missed wages and travel expenses to seek specialized treatment in major urban centers can have a major financial impact on families. Close to 100 million people are being pushed into extreme poverty annually because of out-of-pocket healthcare expenses according to a 2017 joint report by the World Health Organization and the World Bank.[157] These financial and access considerations underline the importance of solutions that improve accessibility and cost-effectiveness of healthcare options for patients in resource-constrained settings. The sustained-release chemotherapy implants for treatment of peritoneal metastasis described in this thesis are well suited for improving cancer care in LMICs. They can give patients the freedom to receive a single implantation procedure and avoid follow-up care often requiring extensive travel, while experiencing reduced toxicity that may allow them to still participate in the workforce. They also give clinicians the freedom to control treatment in their setting and not rely on patient follow-up to complete treatment courses.

India is particularly unique and well positioned for adoption of this proposed technology. It has the clinician expertise and resources required for deployment of this

technology in specialized cancer hospitals across the country and is a setting with a long tradition of pioneering medical innovations to improve access to better healthcare.[158,159]

The clinician survey deployed via the National Cancer Grid network led to accrual of cancer care information relevant to this project from across the country. Responses reflected care in public and private hospitals in many Indian states but came almost entirely from specialized cancer centers. This is not surprising as cancer cases are referred to specialty hospitals and clinics by primary and secondary care providers. Multiple physician specialties involved in treating cancer patients were represented in the survey allowing it to capture a more complete spectrum of cancer care across the country. The survey was at the same time designed to pose peritoneal metastasis-specific questions only to responders treating this patient population and so paint a more detailed picture of this area of cancer care in the Indian setting.

The survey revealed that the decision to not perform surgical debulking in India is driven by factors both resource-agnostic (patient ineligibility, no therapeutic or palliative benefit) and specific to limited-resource environments (lack of access to expertise and resources, cost). It is known that surgical debulking of patients with peritoneally metastasized ovarian cancer prior to start of IP chemotherapy is critical for optimal treatment outcome. Surgical debulking will likely be of similar importance if the implant described in this thesis is used to treat patients with peritoneal metastasis of non-ovarian origin with sustained low-dose local chemotherapy. The advanced ovarian cancer patient population seen by Indian clinicians could be the focus of a follow-up

survey attempting to quantify the frequency and quality of surgical debulking in these patients.

The use of IP chemotherapy by Indian clinicians was found to mirror the situation in the US and other high-resource countries. Catheter-and-port IP chemotherapy faces poor clinical adoption and hospitals are building up capacity to perform new IP techniques like HIPEC and PIPAC that are still under active research and development.[142] The reasons for not performing catheter-and-port IP chemotherapy in India also capture the access and financing obstacles faced by patients in LMICs: lack of expertise, resources and infrastructure as well as high cost are the top three reasons on the list.

Indian physicians are not only adopting cutting-edge experimental IP chemotherapy techniques like HIPEC and PIPAC but also making use of alternative dosing regimens to minimize patient toxicity and increase adherence to treatment. More than 90% of survey responders indicated awareness about metronomic chemotherapy. Use of this regimen for peritoneal metastasis treatment was reported by 42% of responders who indicated using metronomic chemotherapy in 1-25% of their peritoneal metastasis patients. Use of metronomic chemotherapy in cancer care generally and in peritoneal metastasis management specifically is very encouraging for adoption of the sustained-release chemotherapy implant described in this project because its dosing regimen is based on similar principles of toxicity minimization and drug-free period reduction.

Chapter 6: Conclusions and Future Work

6.1 Composite Material Development and Evaluation

The composite material developed in this thesis can form the basis for a cisplatin-eluting implant that can be safe for IP placement and effective in releasing cisplatin in the peritoneal cavity. The mechanical properties of CDDP25 make it well suited for creating implants shaped like large thin sheets that can be folded down for placement inside the patient's peritoneal cavity and still maximize surface area for drug release *in vivo*. This work is still preliminary but the findings are promising for the creation of an implant for continuous low-dose IP cisplatin delivery to treat residual tumors in ovarian cancer patients following optimal surgical debulking. This implant can be used as a platform to treat patients with peritoneal metastasis of different origin (gastrointestinal, primary peritoneal etc.) and to incorporate other chemotherapeutic agents already established or as those become available. Chemotherapeutics like carboplatin, gemcitabine, topotecan and possibly mitomycin are already established attractive possible candidates to attempt incorporating into the composite. Future work should focus on such expansion of incorporated agents to make these implants true platforms for sustained low-dose IP chemotherapy.

6.2 Spheroid-based Ovarian Cancer Models

The *in vitro* component of this section helps shed light to the question of the mechanism controlling drug distribution into tumors following IP administration of chemotherapy. The findings described in this thesis support the hypothesis that intratumoral drug

distribution in nodules without access to vasculature is diffusion-controlled and that continuous low-dose IP cisplatin treatment would be most effective againts microscopic tumors.

The *in vivo* findings of this work taken together demonstrate that an *in vivo* human ovarian cancer orthotopix xenograft model based on injection of size-controlled multicellular spheroids is a viable approach to accelerate tumor growth and achieve more widely distributed disease in mice. There exists an upper limit to the size of spheroids that can be successfully injected in mice for practical and safety considerations but smaller spheroids in fact appear to result in more diffuse disease and fewer off-site lesions compared to larger spheroids.

This work paves the way for development of a robust animal model to evaluate continuous low-dose IP chemotherapy developed at optimal doses in clinically relevant preclinical models of ovarian cancer that capture the debulked subcentimeter disease in patients. The next step in developing these models is to more systematically characterize the size and distribution of tumor nodules over time after spheroid injection and use the information to determine the appropriate time point for start of continuous low-dose treatment using cisplatin-eluting IP implants such that it captures this subcentimeter diffuse disease.

Another component of developing this spheroid *in vivo* model approach is to attempt establishing a spheroid model in immunocompetent animals bearing mouse-derived ovarian tumors. The immune system is hypothesized to play a critical role in the antitumor outcome of sustained low-dose chemotherapy. It is important to reveal any antitumor immunomodulatory effect of sustained low-dose chemotherapy and so work

to harness it alongside the cytotoxic capacity of the chemotherapeutic agent.[46,160] A pilot study pioneering the use of mouse-derived MOC-1 ovarian cancer cells to create orthotopic allografts in immunocompetent C57BL/6 wildtype mice revealed challenges in *in vitro* spheroid formation with these cells as well as difficulties in successfuly inoculating mice with MOC-1 tumors. Studies exploring optimization of MOC-1 spheroid formation by co-culturing MOC-1 cells with mouse fibroblasts to promote ECM production or including matrigel in the spheroid formation process in order to promote cell aggregation into spheroids are planned and underway.

6.3 Composite Material Optimization for *In Vivo* Use, Dosing Studies and Efficacy Pilot

The behavior of the thinner CDDP25 formulation considered on the basis of structure, mechanical properties, cisplatin release and biocompatibility was well predicted by the previously developed thick CDDP25 formulation. This behavior makes the thinner composite material well suited for *in vivo* IP implantation to deliver cisplatin as a chemotherapeutic agent regimen against peritoneal metastases of ovarian cancer. The thinner formulation allows straightforward dose calibration by modifying its surface area for release and enables implantation through a small abdominal incision in mice to minimize surgical trauma and complications. Preliminary antitumor efficacy findings from a study that suffered serious drawbacks nonetheless support the hypothesis that the thinner CDDP25 formulation is better suited for *in vivo* tumor treatment. The proof-of-concept origami sheet prototypes created out of Ecoflex 00-30 or LAC50 illustrated the potential of this approach to create deployable structures that can be folded down and introduced to the peritoneal cavity through a laparoscopic trocar and opened up

once inside the abdomen. Further shape design optimization and research into appropriate origami tessellations to reach the desired minimum dimension that would allow introduction through a 12-mm trocar are needed. A full mechanical characterization of the material both as a sheet and in its final three-dimensional shape as an implant is needed to ensure safety for laparoscopic implantation, manipulation, *in vivo* presence and removal. Testing criteria applied to indwelling catheters and other peritoneal implants can be used to ensure the developed materials and implants can withstand the expected forces with safety for the patient. Assessment of the tolerability and functionality of large-scale implants sized for human patients can be carried out in large animals such as pigs as a next step closer to a patient clinical trial. A patient trial comparing dose-dense to high-dose intermittent IP/IV therapy in ovarian cancer as described by Tanenbaum will also help promote clinical translation of these implants.[46]

6.4 Potential for Technology Adoption in LMICs

The critical role of accessibility and cost-effectiveness in providing treatment to patients and the overwhelmingly positive attitude toward adoption of new technologies for IP chemotherapy and of different dosing regimens (e.g. metronomic therapy) are very encouraging for the future of this work in the LMIC setting. Collaboration with centers currently performing cutting-edge IP chemotherapy treatments like HIPEC or PIPAC can help reveal potential synergies between those treatments and the proposed implant or otherwise help shape the implant use scenario in a resource-constrained setting. Adoption of the technology described in this thesis by physicians in LMICs like India can affect the life of millions of cancer patients in the developing world.

References

1 Flessner, M. F. Peritoneal transport physiology: insights from basic research. *Journal of the American Society of Nephrology : JASN* **2**, 122-135 (1991).

2 Cima, M. J. *et al.* Single compartment drug delivery. *Journal of controlled release : official journal of the Controlled Release Society*, doi:10.1016/j.jconrel.2014.04.049 (2014).

3 Koninckx, P. R., Kennedy, S. H. & Barlow, D. H. Endometriotic disease: the role of peritoneal fluid. *Human reproduction update* **4**, 741-751 (1998).

4 Jacquet, P. & Sugarbaker, P. H. in *Peritoneal Carcinomatosis: Principles of Management* 53-63 (Springer, 1996).

5 Howell, S. B. Pharmacologic principles of intraperitoneal chemotherapy for the treatment of ovarian cancer. *International journal of gynecological cancer : official journal of the International Gynecological Cancer Society* **18 Suppl 1**, 20-25, doi:10.1111/j.1525-1438.2007.01099.x (2008).

6 Flessner, M. F. The transport barrier in intraperitoneal therapy. *American journal of physiology. Renal physiology* **288**, F433-442, doi:10.1152/ajprenal.00313.2004 (2005).

7 Flessner, M. F. & Dedrick, R. L. in *The textbook of peritoneal dialysis* 769-789 (Springer, 1994).

8 van Dijk, P. R. *et al.* Report of a 7 year case-control study of continuous intraperitoneal insulin infusion and subcutaneous insulin therapy among patients with poorly controlled type 1 diabetes mellitus: Favourable effects on hypoglycaemic episodes. *Diabetes research and clinical practice* **106**, 256-263, doi:10.1016/j.diabres.2014.08.018 (2014).

9 Hedman, C. A., Frystyk, J., Lindstrom, T., Oskarsson, P. & Arnqvist, H. J. Intraperitoneal insulin delivery to patients with type 1 diabetes results in higher serum IGF-I bioactivity than continuous subcutaneous insulin infusion. *Clinical endocrinology* **81**, 58-62, doi:10.1111/cen.12296 (2014).

10 Hasovits, C. & Clarke, S. Pharmacokinetics and pharmacodynamics of intraperitoneal cancer chemotherapeutics. *Clinical pharmacokinetics* **51**, 203-224, doi:10.2165/11598890-000000000-00000 (2012).

11 Armstrong, D. K. & Bookman, M. A. in *Controversies in the Management of Gynecological Cancers* 145-153 (Springer, 2014).

12 Markman, M. Intraperitoneal antineoplastic drug delivery: rationale and results. *The lancet oncology* **4**, 277-283 (2003).

13 Levy, A. D., Shaw, J. C. & Sobin, L. H. Secondary tumors and tumorlike lesions of the peritoneal cavity: imaging features with pathologic correlation. *Radiographics : a review publication of the Radiological Society of North America, Inc* **29**, 347-373, doi:10.1148/rg.292085189 (2009).

14 Jayson, G. C., Kohn, E. C., Kitchener, H. C. & Ledermann, J. A. Ovarian cancer. *Lancet* **384**, 1376-1388, doi:10.1016/S0140-6736(13)62146-7 (2014).

15 NCI. *Cancer Stat Facts: Ovarian Cancer*, <https://seer.cancer.gov/statfacts/html/ovary.html> (2018).

16 *SEER Cancer Statistics Factsheets: Ovary Cancer*, <http://seer.cancer.gov/statfacts/html/ovary.html> (2018).

17 Cancer Facts & Figures 2015. (American Cancer Society, Atlanta, 2015).

18 Armstrong, D. K. *et al.* Intraperitoneal cisplatin and paclitaxel in ovarian cancer. *The New England journal of medicine* **354**, 34-43, doi:10.1056/NEJMoa052985 (2006).

19 Wright, A. A. *et al.* Use and Effectiveness of Intraperitoneal Chemotherapy for Treatment of Ovarian Cancer. *Journal of clinical oncology : official journal of the American Society of Clinical Oncology* **33**, 2841-2847, doi:10.1200/JCO.2015.61.4776 (2015).

20 Grady, D. in *The New York Times* (2015).
21 Grady, D. in *The New York Times* (2013).
22 Edwards, R. P. The legacy of intraperitoneal therapy in ovarian cancer: why are we never satisfied with the answer? *Oncology* **29**, 705-705 (2015).
23 Fujiwara, K., Armstrong, D., Morgan, M. & Markman, M. Principles and practice of intraperitoneal chemotherapy for ovarian cancer. *International journal of gynecological cancer : official journal of the International Gynecological Cancer Society* **17**, 1-20, doi:10.1111/j.1525-1438.2007.00809.x (2007).
24 Walker, J. L. *et al.* Intraperitoneal catheter outcomes in a phase III trial of intravenous versus intraperitoneal chemotherapy in optimal stage III ovarian and primary peritoneal cancer: a Gynecologic Oncology Group Study. *Gynecologic oncology* **100**, 27-32, doi:10.1016/j.ygyno.2005.11.013 (2006).
25 Helm, C. W. Ports and complications for intraperitoneal chemotherapy delivery. *BJOG* **119**, 150-159, doi:10.1111/j.1471-0528.2011.03179.x (2012).
26 Twardowski, Z. J. History of peritoneal access development. *The International journal of artificial organs* **29**, 2-40 (2006).
27 Rubin, H. R. *et al.* Patient ratings of dialysis care with peritoneal dialysis vs hemodialysis. *Jama* **291**, 697-703, doi:10.1001/jama.291.6.697 (2004).
28 Sennfalt, K., Magnusson, M. & Carlsson, P. Comparison of hemodialysis and peritoneal dialysis--a cost-utility analysis. *Peritoneal dialysis international : journal of the International Society for Peritoneal Dialysis* **22**, 39-47 (2002).
29 Cristea, M., Han, E., Salmon, L. & Morgan, R. J. Review: Practical considerations in ovarian cancer chemotherapy. *Therapeutic advances in medical oncology* **2**, 175-187 (2010).
30 Scharovsky, O., Mainetti, L. & VR, R. Metronomic chemotherapy: changing the paradigm that more is better. *Current Oncology* **16**, 7-15 (2009).
31 Zhidkov, N., De Souza, R., Ghassemi, A., Allen, C. & Piquette-Miller, M. Continuous Intraperitoneal Carboplatin Delivery for the Treatment of Late-Stage Ovarian Cancer. *Molecular Pharmaceutics* **10**, 3315-3322 (2013).
32 Colombo, P. E. *et al.* Intraperitoneal administration of novel doxorubicin loaded polymeric delivery systems against peritoneal carcinomatosis: experimental study in a murine model of ovarian cancer. *Gynecologic oncology* **122**, 632-640, doi:10.1016/j.ygyno.2011.05.032 (2011).
33 Araki, H., Tani, T. & Kodama, M. Antitumor effect of cisplatin incorporated into polylactic acid microcapsules. *Artificial organs* **23**, 161-168 (1999).
34 Ding, D. *et al.* Nanospheres-incorporated implantable hydrogel as a trans-tissue drug delivery system. *ACS nano* **5**, 2520-2534, doi:10.1021/nn102138u (2011).
35 Armstrong, D. K., Fleming, G. F., Markman, M. & Bailey, H. H. A phase I trial of intraperitoneal sustained-release paclitaxel microspheres (Paclimer) in recurrent ovarian cancer: a Gynecologic Oncology Group study. *Gynecologic oncology* **103**, 391-396, doi:10.1016/j.ygyno.2006.02.029 (2006).
36 De Souza, R., Zahedi, P., Allen, C. J. & Piquette-Miller, M. Biocompatibility of injectable chitosan-phospholipid implant systems. *Biomaterials* **30**, 3818-3824, doi:10.1016/j.biomaterials.2009.04.003 (2009).
37 Vassileva, V., Grant, J., De Souza, R., Allen, C. & Piquette-Miller, M. Novel biocompatible intraperitoneal drug delivery system increases tolerability and therapeutic efficacy of paclitaxel in a human ovarian cancer xenograft model. *Cancer chemotherapy and pharmacology* **60**, 907-914, doi:10.1007/s00280-007-0449-0 (2007).
38 Zhidkov, N., De Souza, R., Ghassemi, A. H., Allen, C. & Piquette-Miller, M. Continuous intraperitoneal carboplatin delivery for the treatment of late-stage ovarian cancer. *Molecular pharmaceutics* **10**, 3315-3322, doi:10.1021/mp400345h (2013).

39 Zahedi, P., Stewart, J., De Souza, R., Piquette-Miller, M. & Allen, C. An injectable depot system for sustained intraperitoneal chemotherapy of ovarian cancer results in favorable drug distribution at the whole body, peritoneal and intratumoral levels. *Journal of controlled release : official journal of the Controlled Release Society* **158**, 379-385, doi:10.1016/j.jconrel.2011.11.025 (2012).

40 Dang, W. Methods for treating ovarian cancer, poly (phosphoester) compositions, and biodegradable articles for same. US6641833 B2 (2002).

41 Vook, N. C. *et al.* Sustained release hydrophobic bioactive PLGA microspheres. US6447796 B1 (2002).

42 Werner, M. E. *et al.* Folate-targeted nanoparticle delivery of chemo- and radiotherapeutics for the treatment of ovarian cancer peritoneal metastasis. *Biomaterials* **32**, 8548-8554, doi:10.1016/j.biomaterials.2011.07.067 (2011).

43 Kohane, D. S. *et al.* Biodegradable polymeric microspheres and nanospheres for drug delivery in the peritoneum. *Journal of biomedical materials research. Part A* **77**, 351-361, doi:10.1002/jbm.a.30654 (2006).

44 De Souza, R. *et al.* Continuous docetaxel chemotherapy improves therapeutic efficacy in murine models of ovarian cancer. *Molecular cancer therapeutics* **9**, 1820-1830, doi:10.1158/1535-7163.MCT-10-0249 (2010).

45 Ye, H. *et al.* Sustained, low-dose intraperitoneal cisplatin improves treatment outcome in ovarian cancer mouse models. *Journal of controlled release : official journal of the Controlled Release Society* **220**, 358-367, doi:10.1016/j.jconrel.2015.11.001 (2015).

46 Tanenbaum, L. M. *Design of an intraperitoneal drug-release device for advanced ovarian cancer therapy*, Massachusetts Institute of Technology, (2016).

47 Scharovsky, O. G., Mainetti, L. E. & Rozados, V. R. Metronomic chemotherapy: changing the paradigm that more is better. *Current oncology* **16**, 7-15 (2009).

48 Sugarbaker, P. H., Stuart, O. A., Vidal-Jove, J., Pessagno, A. M. & DeBruijn, E. A. Pharmacokinetics of the peritoneal-plasma barrier after systemic mitomycin C administration. *Cancer treatment and research* **82**, 41-52 (1996).

49 Markman, M. Intraperitoneal chemotherapy in the management of ovarian cancer: focus on carboplatin. *Ther Clin Risk Manag* **5**, 161-168 (2009).

50 Ho, G. Y., Woodward, N. & Coward, J. I. Cisplatin versus carboplatin: comparative review of therapeutic management in solid malignancies. *Critical reviews in oncology/hematology* **102**, 37-46, doi:10.1016/j.critrevonc.2016.03.014 (2016).

51 Bouchard-Fortier, G. *et al.* A comparison of the toxicity and tolerability of two intraperitoneal chemotherapy regimens for advanced-stage epithelial ovarian cancer. *Gynecologic oncology* **140**, 36-41, doi:10.1016/j.ygyno.2015.11.005 (2016).

52 Los, G., van Vugt, M. J. & Pinedo, H. M. Response of peritoneal solid tumours after intraperitoneal chemohyperthermia treatment with cisplatin or carboplatin. *British journal of cancer* **69**, 235-241 (1994).

53 Markman, M. *et al.* Evidence supporting the superiority of intraperitoneal cisplatin compared to intraperitoneal carboplatin for salvage therapy of small-volume residual ovarian cancer. *Gynecologic oncology* **50**, 100-104, doi:10.1006/gyno.1993.1171 (1993).

54 Vermorken, J. B. Intraperitoneal chemotherapy in advanced ovarian cancer: recognition at last. *Ann Oncol* **17 Suppl 10**, x241-246, doi:10.1093/annonc/mdl267 (2006).

55 Padmakumar, S. *et al.* Intraperitoneal chemotherapy for ovarian cancer using sustained-release implantable devices. *Expert opinion on drug delivery* **15**, 481-494, doi:10.1080/17425247.2018.1446938 (2018).

56 Gamblin, T. C. *et al.* Intraperitoneal gemcitabine pharmacokinetics: a pilot and pharmacokinetic study in patients with advanced adenocarcinoma of the pancreas. *Cancer chemotherapy and pharmacology* **62**, 647-653, doi:10.1007/s00280-007-0647-9 (2008).

57 Sabbatini, P. *et al.* Intraperitoneal cisplatin with intraperitoneal gemcitabine in patients with epithelial ovarian cancer: results of a phase I/II Trial. *Clinical cancer research : an official journal of the American Association for Cancer Research* **10**, 2962-2967 (2004).
58 Ridwelski, K., Meyer, F., Hribaschek, A., Kasper, U. & Lippert, H. Intraoperative and early postoperative chemotherapy into the abdominal cavity using gemcitabine may prevent postoperative occurence of peritoneal carcinomatosis. *J Surg Oncol* **79**, 10-16 (2002).
59 Sugarbaker, P. H. Strategies to improve local control of resected pancreas adenocarcinoma. *Surgical oncology* **26**, 63-70, doi:10.1016/j.suronc.2017.01.002 (2017).
60 Sugarbaker, P. H., Stuart, O. A. & Bijelic, L. Intraperitoneal gemcitabine chemotherapy treatment for patients with resected pancreatic cancer: rationale and report of early data. *International journal of surgical oncology* **2011**, 161862, doi:10.1155/2011/161862 (2011).
61 Hofstra, L. S. *et al.* A phase I and pharmacokinetic study of intraperitoneal topotecan. *British journal of cancer* **85**, 1627-1633, doi:10.1054/bjoc.2001.2161 (2001).
62 McGonigle, K. *et al.* Phase II prospective study of weekly topotecan and bevacizumab in platinum refractory ovarian cancer or peritoneal cancer (OC). *Journal of Clinical Oncology* **26**, 5551-5551 (2008).
63 Muntz, H. G., Malpass, T. W., McGonigle, K. F., Robertson, M. D. & Weiden, P. L. Phase 2 study of intraperitoneal topotecan as consolidation chemotherapy in ovarian and primary peritoneal carcinoma. *Cancer* **113**, 490-496, doi:10.1002/cncr.23576 (2008).
64 Previs, R. A. *et al.* Dual Metronomic Chemotherapy with Nab-Paclitaxel and Topotecan Has Potent Antiangiogenic Activity in Ovarian Cancer. *Molecular cancer therapeutics* **14**, 2677-2686, doi:10.1158/1535-7163.MCT-14-0630 (2015).
65 Van der Speeten, K., Stuart, O. A., Chang, D., Mahteme, H. & Sugarbaker, P. H. Changes induced by surgical and clinical factors in the pharmacology of intraperitoneal mitomycin C in 145 patients with peritoneal carcinomatosis. *Cancer chemotherapy and pharmacology* **68**, 147-156, doi:10.1007/s00280-010-1460-4 (2011).
66 Sugarbaker, P. H., Mora, J. T., Carmignani, P., Stuart, O. A. & Yoo, D. Update on chemotherapeutic agents utilized for perioperative intraperitoneal chemotherapy. *The oncologist* **10**, 112-122 (2005).
67 Chi, D. S. *et al.* What is the optimal goal of primary cytoreductive surgery for bulky stage IIIC epithelial ovarian carcinoma (EOC)? *Gynecol Oncol* **103**, 559-564, doi:10.1016/j.ygyno.2006.03.051 (2006).
68 Winter, W. E., 3rd *et al.* Tumor residual after surgical cytoreduction in prediction of clinical outcome in stage IV epithelial ovarian cancer: a Gynecologic Oncology Group Study. *Journal of clinical oncology : official journal of the American Society of Clinical Oncology* **26**, 83-89, doi:10.1200/JCO.2007.13.1953 (2008).
69 Bristow, R. E., Tomacruz, R. S., Armstrong, D. K., Trimble, E. L. & Montz, F. J. Survival effect of maximal cytoreductive surgery for advanced ovarian carcinoma during the platinum era: a meta-analysis. *Journal of clinical oncology : official journal of the American Society of Clinical Oncology* **20**, 1248-1259, doi:10.1200/JCO.2002.20.5.1248 (2002).
70 Landrum, L. M. *et al.* Prognostic factors for stage III epithelial ovarian cancer treated with intraperitoneal chemotherapy: a Gynecologic Oncology Group study. *Gynecol Oncol* **130**, 12-18, doi:10.1016/j.ygyno.2013.04.001 (2013).
71 Walker, J. L., Brady, M. F. & Wenzel, L. in *Annual Meeting on Women's Cancer.*
72 Lee, J. *et al.* Timing is everything: intraperitoneal chemotherapy after primary or interval debulking surgery for advanced ovarian cancer. *Cancer chemotherapy and pharmacology* **82**, 55-63, doi:10.1007/s00280-018-3591-y (2018).

73 Monk, B. J. & Chan, J. K. Is intraperitoneal chemotherapy still an acceptable option in primary adjuvant chemotherapy for advanced ovarian cancer? *Ann Oncol* **28**, viii40-viii45, doi:10.1093/annonc/mdx451 (2017).

74 Markman, M. *et al.* Phase III trial of standard-dose intravenous cisplatin plus paclitaxel versus moderately high-dose carboplatin followed by intravenous paclitaxel and intraperitoneal cisplatin in small-volume stage III ovarian carcinoma: an intergroup study of the Gynecologic Oncology Group, Southwestern Oncology Group, and Eastern Cooperative Oncology Group. *Journal of clinical oncology : official journal of the American Society of Clinical Oncology* **19**, 1001-1007 (2001).

75 Alberts, D. S. *et al.* Intraperitoneal cisplatin plus intravenous cyclophosphamide versus intravenous cisplatin plus intravenous cyclophosphamide for stage III ovarian cancer. *The New England journal of medicine* **335**, 1950-1955, doi:10.1056/NEJM199612263352603 (1996).

76 Walker, J. L. *Bevacizumab and Intravenous or Intraperitoneal Chemotherapy in Treating Patients With Stage II-III Ovarian Epithelial Cancer, Fallopian Tube Cancer, or Primary Peritoneal Cancer*, <https://clinicaltrials.gov/ct2/show/NCT00951496?term=NCT00951496&rank=1> (2016).

77 Schorge, J. O., Bradford, L. S. & del Carmen, M. G. Primary cytoreductive surgery for advanced ovarian cancer: is it the past, present, or future? *Clin Adv Hematol Oncol* **9**, 912-918 (2011).

78 Walker, J. *et al.* A phase III trial of bevacizumab with IV versus IP chemotherapy for ovarian, fallopian tube, and peritoneal carcinoma: An NRG Oncology Study. *Gynecologic oncology* **141**, 208 (2016).

79 Jandial, D. D., Messer, K., Farshchi-Heydari, S., Pu, M. & Howell, S. B. Tumor platinum concentration following intraperitoneal administration of cisplatin versus carboplatin in an ovarian cancer model. *Gynecol Oncol* **115**, 362-366, doi:10.1016/j.ygyno.2009.08.028 (2009).

80 Helland, O. *et al.* First in-mouse development and application of a surgically relevant xenograft model of ovarian carcinoma. *PLoS One* **9**, e89527, doi:10.1371/journal.pone.0089527 (2014).

81 Ye, H. *et al.* Sustained, low-dose intraperitoneal cisplatin improves treatment outcome in ovarian cancer mouse models. *Journal of controlled release : official journal of the Controlled Release Society*, doi:10.1016/j.jconrel.2015.11.001 (2015).

82 Minchinton, A. I. & Tannock, I. F. Drug penetration in solid tumours. *Nature reviews. Cancer* **6**, 583-592, doi:10.1038/nrc1893 (2006).

83 Tanenbaum, L. M., Mantzavinou, A., Subramanyam, K. S., Del Carmen, M. G. & Cima, M. J. Ovarian cancer spheroid shrinkage following continuous exposure to cisplatin is a function of spheroid diameter. *Gynecologic oncology* **146**, 161-169, doi:10.1016/j.ygyno.2017.04.014 (2017).

84 Brenner, D. E. Intraperitoneal chemotherapy: a review. *Journal of clinical oncology : official journal of the American Society of Clinical Oncology* **4**, 1135-1147 (1986).

85 Dong, Y. *et al.* Paclitaxel resistance and multicellular spheroid formation are induced by kallikrein-related peptidase 4 in serous ovarian cancer cells in an ascites mimicking microenvironment. *PLoS One* **8**, e57056, doi:10.1371/journal.pone.0057056 (2013).

86 Shield, K., Ackland, M. L., Ahmed, N. & Rice, G. E. Multicellular spheroids in ovarian cancer metastases: Biology and pathology. *Gynecologic oncology* **113**, 143-148, doi:10.1016/j.ygyno.2008.11.032 (2009).

87 Rizvi, I. *et al.* Synergistic enhancement of carboplatin efficacy with photodynamic therapy in a three-dimensional model for micrometastatic ovarian cancer. *Cancer research* **70**, 9319-9328, doi:10.1158/0008-5472.CAN-10-1783 (2010).

88 Loessner, D. *et al.* Bioengineered 3D platform to explore cell-ECM interactions and drug resistance of epithelial ovarian cancer cells. *Biomaterials* **31**, 8494-8506, doi:10.1016/j.biomaterials.2010.07.064 (2010).
89 White, E. A., Kenny, H. A. & Lengyel, E. Three-dimensional modeling of ovarian cancer. *Advanced drug delivery reviews* **79-80**, 184-192, doi:10.1016/j.addr.2014.07.003 (2014).
90 Sirenko, O. *et al.* High-content assays for characterizing the viability and morphology of 3D cancer spheroid cultures. *Assay Drug Dev Technol* **13**, 402-414, doi:10.1089/adt.2015.655 (2015).
91 Lin, R. Z. & Chang, H. Y. Recent advances in three-dimensional multicellular spheroid culture for biomedical research. *Biotechnol J* **3**, 1172-1184, doi:10.1002/biot.200700228 (2008).
92 Kunz-Schughart, L. A., Freyer, J. P., Hofstaedter, F. & Ebner, R. The use of 3-D cultures for high-throughput screening: the multicellular spheroid model. *J Biomol Screen* **9**, 273-285, doi:10.1177/1087057104265040 (2004).
93 Lengyel, E. *et al.* Epithelial ovarian cancer experimental models. *Oncogene* **33**, 3619-3633, doi:10.1038/onc.2013.321 (2014).
94 Andre, N., Banavali, S., Snihur, Y. & Pasquier, E. Has the time come for metronomics in low-income and middle-income countries? *The lancet oncology* **14**, e239-248, doi:10.1016/S1470-2045(13)70056-1 (2013).
95 Knaul, F. M., Frenk, J. & Shulman, L. Closing the cancer divide: a blueprint to expand access in low and middle income countries. *Harvard Global Equity Initiative, Boston, MA* (2011).
96 Knaul, F. M. & Bhadelia, A. *Closing the cancer divide*. Vol. 2 (Harvard University Press, 2012).
97 Barbolosi, D. *et al.* Metronomics chemotherapy: time for computational decision support. *Cancer chemotherapy and pharmacology* **74**, 647-652, doi:10.1007/s00280-014-2546-1 (2014).
98 Keskar, V., Mohanty, P. S., Gemeinhart, E. J. & Gemeinhart, R. A. Cervical cancer treatment with a locally insertable controlled release delivery system. *Journal of controlled release : official journal of the Controlled Release Society* **115**, 280-288, doi:10.1016/j.jconrel.2006.08.014 (2006).
99 Park, Y.-L., Chen, B.-R. & Wood, R. J. Design and fabrication of soft artificial skin using embedded microchannels and liquid conductors. *Sensors Journal, IEEE* **12**, 2711-2718 (2012).
100 Boonvisut, P., Jackson, R. & Cavusoglu, M. C. Estimation of Soft Tissue Mechanical Parameters from Robotic Manipulation Data. *IEEE Int Conf Robot Autom* **2012**, 4667-4674, doi:10.1109/ICRA.2012.6225071 (2012).
101 Tepáyotl-Ramírez, D., Lu, T., Park, Y.-L. & Majidi, C. Collapse of triangular channels in a soft elastomer. *Applied Physics Letters* **102**, 044102 (2013).
102 Smooth-On. *Ecoflex 00-30*, <https://www.smooth-on.com/products/ecoflex-00-30/> (
103 Takeda, T. *et al.* A novel ultrasound technique to study the biomechanics of the human esophagus in vivo. *Am J Physiol Gastrointest Liver Physiol* **282**, G785-793, doi:10.1152/ajpgi.00394.2001 (2002).
104 Egorov, V. I., Schastlivtsev, I. V., Prut, E. V., Baranov, A. O. & Turusov, R. A. Mechanical properties of the human gastrointestinal tract. *J Biomech* **35**, 1417-1425 (2002).
105 Lim, Y. J., Deo, D., Singh, T. P., Jones, D. B. & De, S. In situ measurement and modeling of biomechanical response of human cadaveric soft tissues for physics-based surgical simulation. *Surgical endoscopy* **23**, 1298-1307, doi:10.1007/s00464-008-0154-z (2009).

106 Carter, F. J., Frank, T. G., Davies, P. J., McLean, D. & Cuschieri, A. Measurements and modelling of the compliance of human and porcine organs. *Med Image Anal* **5**, 231-236 (2001).
107 Vaezy, S. *et al.* Liver hemostasis using high-intensity focused ultrasound. *Ultrasound in medicine & biology* **23**, 1413-1420 (1997).
108 Johnson, L. A. *et al.* Matrix stiffness corresponding to strictured bowel induces a fibrogenic response in human colonic fibroblasts. *Inflamm Bowel Dis* **19**, 891-903, doi:10.1097/MIB.0b013e3182813297 (2013).
109 Christensen, M. B., Oberg, K. & Wolchok, J. C. Tensile properties of the rectal and sigmoid colon: a comparative analysis of human and porcine tissue. *Springerplus* **4**, 142, doi:10.1186/s40064-015-0922-x (2015).
110 Wang, J. C. Young's modulus of porous materials. *Journal of materials science* **19**, 801-808 (1984).
111 Knudsen, F. Effect of porosity on Young's modulus of alumina. *Journal of the American Ceramic Society* **45**, 94-95 (1962).
112 Currey, J. D. The effect of porosity and mineral content on the Young's modulus of elasticity of compact bone. *Journal of biomechanics* **21**, 131-139 (1988).
113 Molina, E. F., Pulcinelli, S. H., Santilli, C. V., Blanchandin, S. & Briois, V. Controlled cisplatin delivery from Ureasil-PEO1900 hybrid matrix. *J Phys Chem B* **114**, 3461-3466, doi:10.1021/jp9097638 (2010).
114 Santilli, C. V., Chiavacci, L., Lopes, L., Pulcinelli, S. H. & Oliveira, A. G. d. Controlled Drug Release from Ureasil− Polyether Hybrid Materials. *Chemistry of Materials* **21**, 463-467 (2009).
115 Golomb, G., Fisher, P. & Rahamim, E. The relationship between drug release rate, particle size and swelling of silicone matrices. *Journal of controlled release* **12**, 121-132 (1990).
116 Ashworth, J., Best, S. M. & Cameron, R. E. Quantitative architectural description of tissue engineering scaffolds. *Materials Technology* **29**, 281-295 (2014).
117 Zieske, P. A. *et al.* Characterization of cisplatin degradation as affected by pH and light. *Am J Hosp Pharm* **48**, 1500-1506 (1991).
118 El-Kareh, A. W. & Secomb, T. W. A theoretical model for intraperitoneal delivery of cisplatin and the effect of hyperthermia on drug penetration distance. *Neoplasia* **6**, 117-127, doi:10.1593/neo.03205 (2004).
119 Andersson, A. & Ehrsson, H. Stability of cisplatin and its monohydrated complex in blood, plasma and ultrafiltrate--implications for quantitative analysis. *Journal of pharmaceutical and biomedical analysis* **13**, 639-644 (1995).
120 Moller, C., Tastesen, H. S., Gammelgaard, B., Lambert, I. H. & Sturup, S. Stability, accumulation and cytotoxicity of an albumin-cisplatin adduct. *Metallomics : integrated biometal science* **2**, 811-818, doi:10.1039/c0mt00046a (2010).
121 Pinato, D. J., Graham, J., Gabra, H. & Sharma, R. Evolving concepts in the management of drug resistant ovarian cancer: dose dense chemotherapy and the reversal of clinical platinum resistance. *Cancer treatment reviews* **39**, 153-160, doi:10.1016/j.ctrv.2012.04.004 (2013).
122 Chang, C.-L. *et al.* Dose-dense chemotherapy improves mechanisms of antitumor immune response. *Cancer research* **73**, 119-127 (2013).
123 Kamat, A. A. *et al.* Metronomic chemotherapy enhances the efficacy of antivascular therapy in ovarian cancer. *Cancer research* **67**, 281-288, doi:10.1158/0008-5472.CAN-06-3282 (2007).
124 Kuter, D. J. Managing thrombocytopenia associated with cancer chemotherapy. *Oncology (Williston Park)* **29**, 282-294 (2015).

125 Herrmann, A. & De Wilde, R. L. Adhesions are the major cause of complications in operative gynecology. *Best Pract Res Clin Obstet Gynaecol* **35**, 71-83, doi:10.1016/j.bpobgyn.2015.10.010 (2016).
126 Liakakos, T., Thomakos, N., Fine, P. M., Dervenis, C. & Young, R. L. Peritoneal adhesions: etiology, pathophysiology, and clinical significance. Recent advances in prevention and management. *Digestive surgery* **18**, 260-273, doi:50149 (2001).
127 ten Broek, R. P., Bakkum, E. A., Laarhoven, C. J. & van Goor, H. Epidemiology and Prevention of Postsurgical Adhesions Revisited. *Ann Surg* **263**, 12-19, doi:10.1097/SLA.0000000000001286 (2016).
128 Dawson, S. J. *et al.* Intraperitoneal distribution imaging in ovarian cancer patients. *Internal medicine journal* **41**, 167-171, doi:10.1111/j.1445-5994.2009.02112.x (2011).
129 Coccolini, F. *et al.* Hyperthermic intraperitoneal chemotherapy with cisplatin and paclitaxel in advanced ovarian cancer: a multicenter prospective observational study. *J Gynecol Oncol* **26**, 54-61, doi:10.3802/jgo.2015.26.1.54 (2015).
130 Stafford, N. FDA finds breast implants to be safe but calls for better follow-up. *BMJ* **343**, d5664, doi:10.1136/bmj.d5664 (2011).
131 Dieterich, M., Stubert, J., Gerber, B., Reimer, T. & Richter, D. U. Biocompatibility, cell growth and clinical relevance of synthetic meshes and biological matrixes for internal support in implant-based breast reconstruction. *Arch Gynecol Obstet* **291**, 1371-1379, doi:10.1007/s00404-014-3578-9 (2015).
132 Teo, A. J. *et al.* Polymeric biomaterials for medical implants and devices. *ACS Biomaterials Science & Engineering* **2**, 454-472 (2016).
133 Tang, L., Wu, Y. & Timmons, R. B. Fibrinogen adsorption and host tissue responses to plasma functionalized surfaces. *Journal of biomedical materials research* **42**, 156-163 (1998).
134 Park, G. *et al.* Immunologic and tissue biocompatibility of flexible/stretchable electronics and optoelectronics. *Advanced healthcare materials* **3**, 515-525, doi:10.1002/adhm.201300220 (2014).
135 Platts, J. A. *et al.* The RP-HPLC measurement and QSPR analysis of logP(o/w) values of several Pt(II) complexes. *J Inorg Biochem* **100**, 1199-1207, doi:10.1016/j.jinorgbio.2006.01.035 (2006).
136 Tewari, D. *et al.* Long-Term Survival Advantage and Prognostic Factors Associated With Intraperitoneal Chemotherapy Treatment in Advanced Ovarian Cancer: A Gynecologic Oncology Group Study. *Journal of clinical oncology : official journal of the American Society of Clinical Oncology*, doi:10.1200/JCO.2014.55.9898 (2015).
137 Giger-Pabst, U., Solass, W., Buerkle, B., Reymond, M. A. & Tempfer, C. B. Low-dose pressurized intraperitoneal aerosol chemotherapy (PIPAC) as an alternative therapy for ovarian cancer in an octogenarian patient. *Anticancer research* **35**, 2309-2314 (2015).
138 Girshally, R. *et al.* Pressurized intraperitoneal aerosol chemotherapy (PIPAC) as a neoadjuvant therapy before cytoreductive surgery and hyperthermic intraperitoneal chemotherapy. *World J Surg Oncol* **14**, 253, doi:10.1186/s12957-016-1008-0 (2016).
139 Tempfer, C. B., Rezniczek, G. A., Ende, P., Solass, W. & Reymond, M. A. Pressurized Intraperitoneal Aerosol Chemotherapy with Cisplatin and Doxorubicin in Women with Peritoneal Carcinomatosis: A Cohort Study. *Anticancer research* **35**, 6723-6729 (2015).
140 Tempfer, C. B., Solass, W. & Reymond, M. A. Pressurized intraperitoneal chemotherapy (PIPAC) in women with gynecologic malignancies: a review. *Wien Med Wochenschr* **164**, 519-528, doi:10.1007/s10354-014-0312-y (2014).
141 Tempfer, C. B. *et al.* Pressurized intraperitoneal aerosol chemotherapy in women with recurrent ovarian cancer: A phase 2 study. *Gynecologic oncology* **137**, 223-228, doi:10.1016/j.ygyno.2015.02.009 (2015).

142 van Driel, W. J. *et al.* Hyperthermic Intraperitoneal Chemotherapy in Ovarian Cancer. *The New England journal of medicine* **378**, 230-240, doi:10.1056/NEJMoa1708618 (2018).
143 Polterauer, S. *et al.* Prognostic value of residual tumor size in patients with epithelial ovarian cancer FIGO stages IIA-IV: analysis of the OVCAD data. *International journal of gynecological cancer : official journal of the International Gynecological Cancer Society* **22**, 380-385, doi:10.1097/IGC.0b013e31823de6ae (2012).
144 Winter, W. E., 3rd *et al.* Prognostic factors for stage III epithelial ovarian cancer: a Gynecologic Oncology Group Study. *Journal of clinical oncology : official journal of the American Society of Clinical Oncology* **25**, 3621-3627, doi:10.1200/JCO.2006.10.2517 (2007).
145 du Bois, A. *et al.* Role of surgical outcome as prognostic factor in advanced epithelial ovarian cancer: a combined exploratory analysis of 3 prospectively randomized phase 3 multicenter trials: by the Arbeitsgemeinschaft Gynaekologische Onkologie Studiengruppe Ovarialkarzinom (AGO-OVAR) and the Groupe d'Investigateurs Nationaux Pour les Etudes des Cancers de l'Ovaire (GINECO). *Cancer* **115**, 1234-1244, doi:10.1002/cncr.24149 (2009).
146 Moss, N. M. *et al.* Ovarian cancer cell detachment and multicellular aggregate formation are regulated by membrane type 1 matrix metalloproteinase: a potential role in I.p. metastatic dissemination. *Cancer research* **69**, 7121-7129, doi:10.1158/0008-5472.CAN-08-4151 (2009).
147 Sodek, K. L., Ringuette, M. J. & Brown, T. J. Compact spheroid formation by ovarian cancer cells is associated with contractile behavior and an invasive phenotype. *International journal of cancer. Journal international du cancer* **124**, 2060-2070, doi:10.1002/ijc.24188 (2009).
148 Black, P. C. *et al.* Validating bladder cancer xenograft bioluminescence with magnetic resonance imaging: the significance of hypoxia and necrosis. *Bju Int* **106**, 1799-1804, doi:10.1111/j.1464-410X.2010.09424.x (2010).
149 Tannock, I. F., Lee, C. M., Tunggal, J. K., Cowan, D. S. & Egorin, M. J. Limited penetration of anticancer drugs through tumor tissue: a potential cause of resistance of solid tumors to chemotherapy. *Clin Cancer Res* **8**, 878-884 (2002).
150 Zanoni, M. *et al.* 3D tumor spheroid models for in vitro therapeutic screening: a systematic approach to enhance the biological relevance of data obtained. *Sci Rep* **6**, 19103, doi:10.1038/srep19103 (2016).
151 Mehta, G., Hsiao, A. Y., Ingram, M., Luker, G. D. & Takayama, S. Opportunities and challenges for use of tumor spheroids as models to test drug delivery and efficacy. *Journal of controlled release : official journal of the Controlled Release Society* **164**, 192-204, doi:10.1016/j.jconrel.2012.04.045 (2012).
152 Nishikawa, T. *et al.* Using size-controlled multicellular spheroids of murine adenocarcinoma cells to efficiently establish pulmonary tumors in mice. *Biotechnol J* **12**, doi:10.1002/biot.201600513 (2017).
153 Besselsen, D. G., Franklin, C. L., Livingston, R. S. & Riley, L. K. Lurking in the shadows: emerging rodent infectious diseases. *ILAR J* **49**, 277-290 (2008).
154 la Chapelle, C. F. *et al.* Trocar types in laparoscopy. *Cochrane Database Syst Rev*, CD009814, doi:10.1002/14651858.CD009814.pub2 (2015).
155 Ch. Health Financing Revisited, (World Bank Group).
156 *Cancer: Key Facts*, <http://www.who.int/news-room/fact-sheets/detail/cancer> (2018).
157 Tracking Universal Health Coverage: 2017 Global Monitoring Report. (The World Bank; The World Health Organization, 2017).

158 Govindarajan, V. & Ramamurti, R. What India can teach the U.S. about driving down the cost of health care. *STAT News First Opinion* (2018). <https://www.statnews.com/2018/07/10/reducing-health-care-costs-india-us/>.

159 Mantzavinou, A. *et al.* Global health innovations can be game-changers at home, too. *STAT News First Opinion* (2017).

160 de Biasi, A. R., Villena-Vargas, J. & Adusumilli, P. S. Cisplatin-Induced Antitumor Immunomodulation: A Review of Preclinical and Clinical Evidence. *Clinical Cancer Research* **20**, 5384-5391 (2014).

Appendix

A.1 Indian Clinician Survey

Tata Project IP Chemotherapy Survey

Start of Block: Background Info

Info: This survey is part of an MIT research project. It should take approximately 5 minutes to complete.
Your decision to complete this survey is voluntary and you may stop at any time. This is an anonymous survey, unless if you choose to share your email with us. The results of the research may be presented at scientific meetings or published in scientific journals. Clicking on the 'SUBMIT' button at the end of this survey indicates that you are at least 18 years of age and agree to complete this survey voluntarily.

*

1 What is your primary hospital/clinic affiliation? Please also indicate location. *(If none, please answer NA)*

_____

*

1b What is your email address? *(Optional)*

_____

2 What best describes your role?

- ○ Physician (1)
- ○ Other healthcare provider (nurse, nurse assistant etc.) (2)
- ○ Other: please specify (3) _____

3 Are you involved in the care of cancer patients?

- ○ Yes (1)
- ○ No (2)

End of Block: Background Info

Start of Block: Physicians

1.1 What is your specialty?

_____

End of Block: Physicians

Start of Block: Physicians with cancer patients

2.1 Approximately what percentage of your cancer patients suffer from peritoneal metastasis?

- ○ None (1)
- ○ 1-25% (2)
- ○ 26-50% (3)
- ○ 51-75% (4)
- ○ 76-99% (5)
- ○ Everyone (6)

2.2 Are you familiar with intraperitoneal (IP) chemotherapy, either given through a catheter into the patient's abdomen every few weeks or done during surgery as HIPEC?

- ○ Yes (1)
- ○ No (2)

Display This Question:

If Are you familiar with intraperitoneal (IP) chemotherapy, either given through a catheter into the... = Yes

2.2.1 In your opinion, what are the chief challenges with performing catheter-and-port intraperitoneal (IP) chemotherapy? *(You can select more than one)*

- ☐ Lack of appropriate infrastructure/hospital resources (1)
- ☐ Lack of appropriately trained nursing staff (2)
- ☐ Cost (3)
- ☐ Patient not eligible for IP chemotherapy (age, health status) (4)
- ☐ Suboptimal or no surgical debulking (5)
- ☐ Catheter or port complications (6)
- ☐ Drug toxicity (7)
- ☐ Loss to follow-up or poor patient adherence (12)
- ☐ Infection risk due to poor catheter or port maintenance (8)
- ☐ Physician preference (9)
- ☐ Patient preference (10)
- ☐ Other: please specify (11)

_____

Display This Question:

If Are you familiar with intraperitoneal (IP) chemotherapy, either given through a catheter into the... = Yes

2.2.2 Would you consider trying a new technology to deliver IP chemotherapy using an implant that reduces toxicity and side effects for patients, is less complicated and requires fewer resources?

- ○ Definitely yes (1)
- ○ Probably yes (2)
- ○ Might or might not (3)
- ○ Probably not (4)
- ○ Definitely not (5)

2.3 Are you familiar with metronomic chemotherapy, given at a lower dose more frequently to reduce toxicity and improve patient adherence to the treatment?

- ○ Yes (1)
- ○ No (2)

End of Block: Physicians with cancer patients

Start of Block: Physicians with peritoneal metastasis patients

3.1 Approximately what portion of your patients with peritoneal metastasis undergo surgical tumor debulking?

- ○ None (1)
- ○ 1-25% (2)
- ○ 26-50% (3)
- ○ 51-75% (4)
- ○ 76-99% (5)
- ○ Everyone (6)

3.2 In your opinion, what are the chief reasons why surgical debulking will not be performed on a patient with peritoneal metastasis? *(You can select more than one)*

- ☐ Cost (1)
- ☐ Lack of appropriate infrastructure/hospital resources (2)
- ☐ Lack of appropriately trained staff (3)
- ☐ No therapeutic or palliative benefit (4)
- ☐ Patient not eligible (5)
- ☐ Patient preference (6)
- ☐ Physician preference (7)
- ☐ Other: please specify (8)

_____

3.3 Approximately how many of your patients with peritoneal metastasis undergo chemotherapy?

	None (1)	1-25% (2)	26-50% (3)	51-75% (4)	76-99% (5)	Everyone (6)
Chemotherapy before surgical debulking (1)	○	○	○	○	○	○
Chemotherapy after surgical debulking (2)	○	○	○	○	○	○
Chemotherapy without surgical debulking (3)	○	○	○	○	○	○

End of Block: Physicians with peritoneal metastasis patients

Start of Block: Physicians with peritoneal metastasis patients + chemotherapy

Display This Question:

If Are you familiar with intraperitoneal (IP) chemotherapy, either given through a catheter into the... = Yes

4.1 Approximately how many of your patients with peritoneal metastasis receive any kind of intraperitoneal (IP) chemotherapy while under your care (incl. HIPEC, IP/IV combo etc.)?

- ○ None (1)
- ○ 1-25% (2)
- ○ 26-50% (5)
- ○ 51-75% (6)
- ○ 76-99% (7)
- ○ Everyone (8)

Display This Question:

If Approximately how many of your patients with peritoneal metastasis receive any kind of intraperit... = 1-25%

Or Approximately how many of your patients with peritoneal metastasis receive any kind of intraperit... = 26-50%

Or Approximately how many of your patients with peritoneal metastasis receive any kind of intraperit... = 51-75%

Or Approximately how many of your patients with peritoneal metastasis receive any kind of intraperit... = 76-99%

Or Approximately how many of your patients with peritoneal metastasis receive any kind of intraperit... = Everyone

4.2 What is the most common type of IP chemotherapy that these patients receive?

- ○ catheter-and-port IP infusions (1)
- ○ HIPEC (2)
- ○ Other: please specify (3) _____

Display This Question:

If Are you familiar with metronomic chemotherapy, given at a lower dose more frequently to reduce to... = Yes

4.3 Approximately what percentage of patients with peritoneal metastasis get treated with metronomic chemotherapy?

- ○ None (1)
- ○ 1-25% (2)
- ○ 26-50% (3)
- ○ 51-75% (4)
- ○ 76-99% (5)
- ○ Everyone (6)

End of Block: Physicians with peritoneal metastasis patients + chemotherapy

Start of Block: Other healthcare providers

5.1 Approximately what portion of the cancer patients you care for receive chemotherapy?

- ○ None (1)
- ○ 1-25% (2)
- ○ 26-50% (3)
- ○ 51-75% (4)
- ○ 76-99% (5)
- ○ Everyone (6)

5.2 Are you familiar with intraperitoneal (IP) chemotherapy, either given through a catheter into the patient's abdomen every few weeks or done during surgery as HIPEC to treat peritoneal metastasis?

- ○ Yes (1)
- ○ No (2)

5.3 Are you familiar with metronomic chemotherapy, given at a lower dose more frequently to reduce toxicity and improve patient adherence to the treatment?

- ○ Yes (1)
- ○ No (2)

Display This Question:

If Are you familiar with metronomic chemotherapy, given at a lower dose more frequently to reduce to... = Yes

5.3.1 In your opinion, how frequently is metronomic chemotherapy used to treat the cancer patients you care for?

- ○ Never (1)
- ○ Rarely (2)
- ○ Sometimes (3)
- ○ Often (4)
- ○ Always (5)

Display This Question:

If Are you familiar with intraperitoneal (IP) chemotherapy, either given through a catheter into the... = Yes

5.4 Approximately how many of the cancer patients you care for receive any kind of IP chemotherapy while under your care (incl. HIPEC, IP/IV combo etc.)?

- ○ None (1)
- ○ 1-25% (2)
- ○ 26-50% (5)
- ○ 51-75% (6)
- ○ 76-99% (7)
- ○ Everyone (8)

Display This Question:

If Approximately how many of the cancer patients you care for receive any kind of IP chemotherapy wh... = 1-25%

Or Approximately how many of the cancer patients you care for receive any kind of IP chemotherapy wh... = 26-50%

Or Approximately how many of the cancer patients you care for receive any kind of IP chemotherapy wh... = 51-75%

Or Approximately how many of the cancer patients you care for receive any kind of IP chemotherapy wh... = 76-99%

Or Approximately how many of the cancer patients you care for receive any kind of IP chemotherapy wh... = Everyone

5.4.1 What is the most common type of IP chemotherapy that these patients receive?

- ○ catheter-and-port IP infusions (1)
- ○ HIPEC (2)
- ○ Other: please specify (3)

_____

Display This Question:

If Are you familiar with intraperitoneal (IP) chemotherapy, either given through a catheter into the... = Yes

5.5 In your opinion, what are the chief challenges with performing catheter-and-port intraperitoneal (IP) chemotherapy? *(You can select more than one)*

- ☐ Lack of appropriate infrastructure/hospital resources (1)
- ☐ Lack of appropriately trained nursing staff (2)
- ☐ Cost (3)
- ☐ Patient not eligible for IP chemotherapy (age, health status) (4)
- ☐ Suboptimal or no surgical debulking (5)
- ☐ Catheter or port complications (6)
- ☐ Drug toxicity (7)
- ☐ Loss to follow-up or poor patient adherence (12)
- ☐ Infection risk due to poor catheter or port maintenance (8)
- ☐ Physician preference (9)
- ☐ Patient preference (10)
- ☐ Other: please specify (11)

_____

Display This Question:

If Are you familiar with intraperitoneal (IP) chemotherapy, either given through a catheter into the... = Yes

5.6 Would you consider trying a new technology to deliver IP chemotherapy using an implant that reduces toxicity and side effects for patients, is less complicated and requires fewer resources?

- ○ Definitely yes (1)
- ○ Probably yes (2)
- ○ Might or might not (3)
- ○ Probably not (4)
- ○ Definitely not (5)

End of Block: Other healthcare providers

Start of Block: Other

6.1 Are you familiar with intraperitoneal (IP) chemotherapy, either given through a catheter into the patient's abdomen every few weeks or done in the OR as HIPEC?

- ○ Yes (1)
- ○ No (2)

Display This Question:

If Are you familiar with intraperitoneal (IP) chemotherapy, either given through a catheter into the... = Yes

6.1.1 In your opinion, what are the chief challenges with performing catheter-and-port intraperitoneal (IP) chemotherapy? *(You can select more than one)*

- ☐ Lack of appropriate infrastructure/hospital resources (1)
- ☐ Lack of appropriately trained nursing staff (2)
- ☐ Cost (3)
- ☐ Patient not eligible for IP chemotherapy (age, health status) (4)
- ☐ Suboptimal or no surgical debulking (5)
- ☐ Catheter or port complications (6)
- ☐ Drug toxicity (7)
- ☐ Loss to follow-up or poor patient adherence (12)
- ☐ Infection risk due to poor catheter or port maintenance (8)
- ☐ Physician preference (9)
- ☐ Patient preference (10)
- ☐ Other: please specify (11)

_____

6.2 Are you familiar with metronomic chemotherapy, given at a lower dose more frequently to reduce toxicity and improve patient adherence to the treatment?

- ○ Yes (1)
- ○ No (2)

Display This Question:

If Are you familiar with metronomic chemotherapy, given at a lower dose more frequently to reduce to... = Yes

6.2.1 In your opinion, how frequently is metronomic chemotherapy used to treat cancer patients?

- ○ Never (1)
- ○ Rarely (2)
- ○ Sometimes (3)
- ○ Often (4)
- ○ Always (5)

End of Block: Other